International School Niccolò Cabeo on Hadronic Physics

## May 23-28, 2011 - Ferrara

# Hadron Electromagnetic Form Factors

# CONTENTS

# RADIATIVE CORRECTIONS TO LEPTON-HADRON INTERACTIONS

A. B. Arbuzov

*Bogoliubov Laboratory of Theoretical Physics,*
*Joint Institute for Nuclear Research,*
*Joliot-Curie 6, Dubna, 141980, Russia*

A brief review of the present status of radiative corrections to processes of particle interaction is presented. Examples are given for QED corrections to processes of lepton–hadron and lepton–lepton interactions at intermediate and low energies. The method of electron structure function in the leading logarithmic approximation is described. The origin of Coulomb singularity in the final state interactions of charged particles is demonstrated. A relativized version of the Sommerfeld-Gamow-Sakharov factor is proposed. The vacuum polarization effect is discussed. General recommendations on application of radiative corrections in data analysis are given.

*Keywords*: .

## 1. Introduction

The aim of these lectures to review the effects due to QED *Radiative Corrections* (RC) being relevant for lepton-hadron interactions at (relatively) low energies. We will discuss typical contributions like vacuum polarization, Coulomb singularity in the final state interactions, the leading logarithmic approximation *etc*. Concrete examples on RC calculation well be given. The main attention will be paid to the features of the corrections themselves and on the application of them to the analysis of experimental data. So, we will not go into details of step-by-step calculations of the corrections. Instead we will concentrate on the discussion of particular features of RC which are relevant for construction of high-precision theoretical predictions and experimental data analysis.

By *radiative corrections* we mean quantum effects which contribute to observable quantities in higher orders in a coupling constant. In other words, RC are the effects which appear beyond the lowest order which will be called here the *Born approximation*. So the first step in treatment of any type of radiative corrections is the definition of the zeroth level. Typically the latter corresponds to a very limited number of tree-level Feynman diagrams describing the given process. But in certain cases we use the so-called *improved Born approximation* in which some simple more or less factorizable effects of higher orders are already included. In this case to avoid double counting one should exclude them from the RC contributions.

Sometimes radiative corrections can be confused with background processes which contribute to the same observable. Typically RC are just some modifications of the basic process, while background corresponds to other processes which only look similar to the basic one in the detector. But in a general situation one should solve a complex problem, where both RC and backgrounds are taken into account. Then the definition of each effect within the given problem should be done explicitly.

By corrections we usually mean small modifications. It is really so concerning RC in the bulk of realistic problems. But that is not *always* so. There are many examples of radiative corrections which are not small in comparison with the Born contribution. Sometimes we even have corrections of the order of several hundred percent. And below we will discuss a particular case in which the correction is infinitely large while the observable remains finite.

It is worth to mention also that radiative corrections is a subjects where interests of theoreticians and experimentalists are strongly connected. In order to improve the resulting precision in analysis of concrete experimental data, they should work in a tight collaboration. In many cases the numerical contribution of RC depends very much on the experimental conditions of particle registration.

The studies of radiative corrections are of ultimate importance for the modern elementary particles physics. In fact physics is a *natural science*, so it unifies experimental and theoretical investigations. On the other hand, physics belongs to *exact sciences* and now we deal with very accurate experiments and theoretical predictions. Let us assume that a pure experimental uncertainty

$$\delta^{exp} \; = \; \delta^{syst} \, \oplus \, \delta^{stat} \tag{1}$$

is the proper sum of systematical and statistical errors. Then the final result of the study, *i.e.* some physical quantity, would contain also a contribution due to theoretical uncertainties which always enter the game at a certain stage of the data analysis. In order not to spoil the accuracy of the experiment which has been obtained by considerable human and material investments, one should provide the theoretical error as small as possible. In practice it is highly desirable that the latter should satisfy the condition

$$\delta^{theor} \; \lesssim \; \delta^{exp}/3. \tag{2}$$

If the theoretical error would be of the same size as the experimental one then the resulting uncertainty will be $\delta^{theor \oplus exp} \; \approx \; 1.4 \cdot \delta^{exp}$ which will mean that that a huge part of the investments has been spent just for nothing. We see also that the precision of modern experiments is continuously growing up due to new hardware, improvement of analysis techniques, increasing of exposition time and so on.

All these facts show that the theoretical accuracy should be adequate to the experimental one. So we need more and more precise theoretical predictions which should include radiative corrections.

One could say that precise studies are required only for tests of the Standard Model (SM), while in searches for *New Physics* radiative corrections are not important at all. That is not true, of course. Really, we are always looking for new physical effects as a difference of an observable and the corresponding theoretical prediction. We are doing that at the edges of the explored field of physical phenomena. In this case theoretical predictions should be also as accurate as possible. This requirement is valid as for the new physics searches at very high energies of the Large Hadron Collider (LHC) as well as *e.g.* for studies of neutrinoless double beta decays at low energies.

There are two extreme possible scenarios of physical studies at the LHC: i) the most exiting case would be the discovery of many particles and new interactions; ii) nothing new is discovered besides the SM-like Higgs boson. Let us imagine the first situation. Very soon after the experimental discovery of new particles we will see in the literature a whole bunch of theoretical models pretending to describe the new phenomena. In this case only having very precise theoretical predictions received within the SM and in its extensions[a] could help to choose the most adequate model of the new physics. In other words, the knowledge of radiative corrections will be required to discriminate different models of new physics. In the second case (which is obviously very unpleasant for the whole fundamental science) the physical program of experimental studies at the LHC will be

[a]Many accurate predictions with one-loop RC have been already developed within minimal supersymmetric extensions of the SM.

shifted to the continuation of precision tests of the Standard Model and looking for possible (small) deviations from its predictions. In this case calculation of RC will be again of ultimate importance.

## 2. Types of Radiative Corrections

Let us discuss the typical types of radiative corrections. First of all, we subdivide RC into perturbative (computed order-by-order by means of expansion in a coupling constant) and non-perturbative which are found either phenomenologically from experimental data or from an exact solution of some equations in the quantum field theory, *e.g.* the Bethe-Salpeter ones. Sometimes we can also perform a resummation of a certain class of perturbative corrections, for example, that is usually done with the vacuum polarization effect in the propagator of a virtual photon, see Sect. 5. The main method in calculation of radiative corrections is expansion in a small parameter which can be: a coupling constant, transverse momentum, mass ratio *etc.*.

RC are also usually separated according to the relevant type of interactions. So we can have QED, QCD and electroweak corrections. Note that separation of electroweak RC into pure QED and pure weak in the frames of the Standard Model is not always possible in a gauge invariant way. What is important that in practice we *always* have a mixture of RC of all types due to quantum effects. One of the primary problems in treatment of radiative corrections is to disentangle the mixture. Only in some extreme cases like the one of the electron anomalous magnetic moment we have almost a pure QED interaction.

There is a common statement that all relevant one-loop radiative corrections to any process being of interest for phenomenology have been computed long ago. That is not really so. Of course there is a lot of results in the literature. But for application for any new experiment we usually have to reconsider the evaluation of corrections in order to take into account concrete specific conditions.

As an example of radiative correction, let us look at the fit of the Higgs boson mass from LEP data, see Fig. 1 taken from Ref.[1]

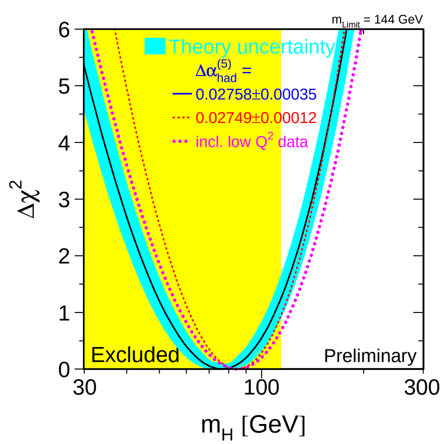


Fig. 1. Fit of the Higgs boson mass from LEP data.

One can see that even so the the Higgs boson has not been observed at LEP (shadowed (yellow) region means $m_h > 114.4$ GeV), the data are sensitive to the Higgs mass value via radiative corrections (quantum loop effects). And if the Higgs boson is SM-like (no valuable contributions of new physics affected the data) than its mass is limited from above, $m_h < 144$ GeV, with a very large confidence level. With this respect one can remind the situation with the discovery of the top quark: well before the direct observation of this particle, its mass was fitted from the LEP data with high precision: $m_t(LEP) \approx 172$ GeV[b]. We hope that the LHC will soon find the Higgs boson and check whether its mass lies in the region allowed by the LEP data fit.

## 3. QED radiative corrections

Let us discuss the general features of QED RC. Firs of all those are the most typical corrections which are relevant for almost all observables in particle physics. It is well known that the main method of their calculation is the perturbative expansion in the fine structure constant $\alpha \approx \frac{1}{137}$. Looking at the details of this procedure one can conclude that the actual small parameter of the expansion is actually $\alpha/(2\pi)$. Numerical values of the first terms in this expansion

$$\frac{\alpha}{2\pi} \approx 0.12\,\%, \qquad \left(\frac{\alpha}{2\pi}\right)^2 \approx 1.3\cdot 10^{-4} \tag{3}$$

admit a fast convergence of the perturbative series. But in practice the situation is not so simple: in actual calculations there could be other important small and large parameters. For instance, at large energies we usually expand also in the series over the small ration $m/E$, where $m$ is the charged particle mass and $E$ is its energy[c]. An example of a large parameter in QED is the large logarithm $\ln(E^2/m^2)$, it will be discussed in detail in Sect. 6.

As an example of QED RC we can look at the small–angle Bhabha scattering process

$$e^-(k_1)\ +\ e^+(k_2)\ \to\ e^-(p_1)\ +\ e^+(p_2), \tag{4}$$

which was used for luminosity measurement at LEP. Table 1 shows values of various RC contributions $\delta_i$ in percent for different values of experimental cut $x_c$ (see details of the set-up in Ref.[2]). The contribution of vacuum polarization (see Sect. 5) $\delta_{\rm VP}$ depends on the momentum transferred in the process $\sqrt{Q^2} = \sqrt{-(p_1-k_1)^2} \approx$ 1 GeV. One-photon contribution $\delta^\gamma$ (together with a part of $\delta_{\rm VP}$) correspond to $O\left(\alpha^1\right)$ term of the QED perturbative expansion. One can see that its numerical value is much more than the one expected from Eq. (3). The same observation can be done from the order of magnitude of the $O\left(\alpha^2\right)$ contributions $\delta^{2\gamma}_{\rm LLA,\,NLO}$ and $\delta^{e^+e^-}$ due to photonic and pair corrections, respectively. The third order leading logarithmic photonic contribution $\delta^{3\gamma}$ is small compared to the experimental precision tag $\sim 0.03$, but it is required to establish the theoretical uncertainty unambiguously. In spite of efforts of several groups of theoreticians, the latter was not reduced to the level adequate to the very accurate experimental measurement of small-angle Bhabha at LEP.[3] Only recently complete two-loop results (neglecting small terms $\sim m_e^2/Q^2$) for RC to Bhabha scattering were obtained.[4–6] Those hopefully will be used at the future $e^+e^-$ International Linear Collider (ILC).

### 3.1. *First order QED corrections*

The first order QED radiative corrections is nowadays a rather standard ingredient in phenomenological applications of particle physics. Usually we decompose them into three parts: i) virtual (loop) corrections; ii) the ones due to a soft photon emission, and iii) the ones due to a single hard photon radiation:

$$\sigma^{\text{1−loop corrected}} = \sigma^{\rm Born} + \sigma^{\rm Virt}(\lambda) + \sigma^{\rm Soft}(\lambda,\bar{\omega}) + \sigma^{\rm Hard}(\bar{\omega}). \tag{5}$$

---
[b]Due to specific features of the SM, radiative corrections are much more sensitive to the top quark mass than to the Higgs boson one.
[c]In many (but not all) cases this ratio is squared.

| $x_c$ | $\delta_{\rm VP}$ | $\delta^{\gamma}$ | $\delta^{2\gamma}_{\rm LLA}$ | $\delta^{2\gamma}_{\rm NLO}$ | $\delta^{e^+e^-}$ | $\delta^{e^+e^-\gamma}$ | $\delta^{3\gamma}$ | $\sum\delta^i$ |
|---|---|---|---|---|---|---|---|---|
| 0.1 | 4.120 | −8.918 | 0.657 | 0.162 | −0.016 | −0.017 | −0.019 | −4.031±0.006 |
| 0.3 | 4.120 | −9.626 | 0.615 | 0.148 | −0.033 | −0.008 | −0.013 | −4.797±0.006 |
| 0.5 | 4.120 | −10.850 | 0.539 | 0.129 | −0.044 | −0.003 | −0.006 | −6.115±0.006 |
| 0.7 | 4.120 | −13.770 | 0.379 | 0.130 | −0.057 | −0.001 | 0.005 | −9.194±0.006 |
| 0.9 | 4.120 | −25.269 | 1.952 | −0.085 | −0.085 | 0.005 | 0.017 | −19.379±0.006 |

First of all this is done because analytically and numerically each part is calculated separately.

Decomposition (5) involves introduction of two auxiliary parameters: $\lambda$ which regularizes the infrared singularity and $\bar{\omega}$ which separates the phase spaces of the hard and soft photons. The latter should be defined in a concrete reference frame, then the energy of a hard photon should be greater than $\bar{\omega}$:

$$\omega_{\rm hard} > \bar{\omega}, \qquad \omega_{\rm soft} < \bar{\omega}, \qquad \bar{\omega} \ll E. \tag{6}$$

Choosing the value of the soft-hard separator being small compared with the typical energy scale $E$ (of the given process) we gain considerable simplifications in the calculations of the soft photon contribution to RC. For the infrared regulator $\lambda$ we can take a fictitious photon mass with the conditions $\lambda \ll m$ and $\lambda \ll \bar{\omega}$.

Results for one loop QED corrections are known for very many processes. But sometimes in order to perform a concrete experimental study we have to re-compute the corrections taking into account specific experimental conditions. As an example we can take the classical process of bremsstrahlung off charged leptons, *e.g.* muons in collisions with heavy atoms:

$$\mu \,+\, A \,\to\, \mu \,+\, \gamma \,+\, A. \tag{7}$$

Some representatives of the relevant Feynman diagrams are given in Figs. 2 and 3. It appeared that existing calculations for RC to this process (known for about 50 years) are not suited for the COMPASS experiment conditions and we had to re-consider them.[7]

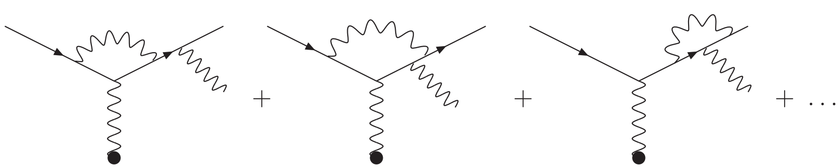


Fig. 2. Representatives of Feynman diagrams for virtual 1-loop RC to muon bremsstrahlung.

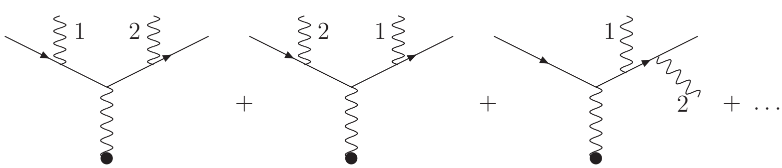


Fig. 3. Representatives of Feynman diagrams for real photon emission RC to muon bremsstrahlung.

The results of the calculations separated according to Eq. (5) are given in Table 2 and in Fig. 4.

| $\omega/E_1$ | Born | Virtual | Soft$_1$ | Hard$_1$ | $\delta_1$, % | Soft$_2$ | Hard$_2$ | $\delta_2$, % |
|---|---|---|---|---|---|---|---|---|
| 0.3 | 15677(1) | 76.8(4) | - 260.1(1) | 226.9(3) | +0.28 | -307.0(1) | 273.7(3) | +0.28 |
| 0.5 | 10836(1) | 77.9(2) | - 319.0(1) | 280.0(3) | +0.36 | -377.4(1) | 338.1(3) | +0.36 |
| 0.7 | 7337.7(1) | 76.9(2) | - 363.3(1) | 297.1(2) | +0.15 | -430.9(1) | 364.8(2) | +0.15 |
| 0.9 | 1267.4(1) | 20.5(1) | - 111.1(2) | 65.9(1) | −1.95 | -132.4(2) | 87.2(1) | −1.95 |

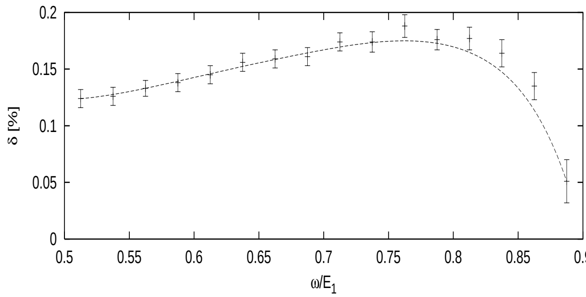


Fig. 4. Relative contribution of one-loop corrections for realistic set-up *vs.* the photon energy fraction.

In Fig. 4 one can see a peculiar feature: the size of the correction is rapidly increasing at large values of the observed photon energy fraction $\omega/E_1$. Emission of extra hard photons in this region is suppressed: we have an effective cut-off from above on the extra photon energy. In other words here we meet the typical situation: “the more we cut, the more we get” (when we cut-off a considerable part of hard radiation and get a large correction).

Another example of incompleteness of the RC studies is the calculation of the complete one-loop QED correction to the muon decay spectrum which was apparently finished only recently.[8,9] The one-loop contribution to the spectrum reads (see[8] for notation):

$$\frac{\mathrm{d}^2\Gamma^{(1)}}{\mathrm{d}x\mathrm{d}c} = \Gamma_0\, x^2\beta\frac{\alpha}{2\pi}\left(f_1(x) + c\xi g_1(x)\right), \qquad \beta = \sqrt{1 - \frac{m_e^2}{E_e^2}}, \tag{8}$$

$$
\begin{aligned}
f_1(x) = {} & f^{\mathrm{Born}}(x)\biggl(\frac{2}{\beta}A + \frac{x^2(1-\beta^2)-4(1+x\beta)}{2x\beta}\ln\frac{q^2}{m_\mu^2} \\
& + \frac{4-x^2(1-\beta^2)}{x\beta}\ln\frac{2-x(1-\beta)}{2}\biggr) + \frac{1}{\beta}\biggl(L + 2\ln x + 2\ln\frac{1+\beta}{2}\biggr)\biggl\{\frac{5x^4}{384}(1-\beta^2)^3 \\
& - \frac{x^3}{4}(1-\beta^2)^2 + \frac{3x^2}{32}(3-12\beta+\beta^2)(1-\beta^2) + x\biggl[\frac{2}{3} + 2\beta + (1-\beta^2)\biggl(\frac{3}{2}+\beta\biggr)\biggr] \\
& + \frac{1}{8}[-20-12\beta-19(1-\beta^2)] + \frac{2}{x} + \frac{5}{6x^2}\biggr\} + \biggl(\ln x + \ln\frac{1+\beta}{2}\biggr)\biggl[\frac{9}{4}x^2(1-\beta^2) \\
& + 2x(\beta^2-3) + 3\biggr] + f^{\mathrm{Born}}(x)\biggl[-\frac{11}{18}x(1-\beta^2) + \frac{22}{27}\beta^2 - \frac{2}{9}\biggr] \\
& + x\biggl(-\frac{22}{27}\beta^4 + \frac{\beta^2}{2} - \frac{11}{6}\biggr) + \frac{22}{9}(3-\beta^2) - \frac{22}{3x}, \\
A = {} & L\biggl(\ln\frac{q^2}{m_\mu^2} - \ln x + \ln\frac{1+\beta}{2\beta} + \ln\frac{2-x(1-\beta)}{2\beta}\biggr) + \biggl[\ln\frac{q^2}{m_\mu^2} - 2\ln x + 2\ln\frac{1+\beta}{2} \\
& + 4\ln\frac{2-x(1-\beta)}{2\beta}\biggr]\biggl(\ln x + \ln\frac{1+\beta}{2}\biggr) + 2\mathrm{Li}_2\left(\frac{(1-\beta)(2-x(1+\beta))}{(1+\beta)(2-x(1-\beta))}\right) \\
& - 2\mathrm{Li}_2\left(\frac{2-x(1+\beta)}{2-x(1-\beta)}\right), \qquad L \equiv \ln\frac{m_\mu^2}{m_e^2}, \\
f^{\mathrm{Born}}(x) = {} & 3 - 2x + \frac{x}{4}(3x-4)(1-\beta^2), \qquad \mathrm{Li}_2\,(x) \equiv -\int_0^x \frac{\mathrm{d}y}{y}\ln(1-y).
\end{aligned}
\tag{9}
$$

Here $x = 2E_e/m_\mu$ is the electron energy fraction and $c$ is the cosine between the electron 3-momentum and the muon spin. Expression for $g_1(x)$ is similar, it can be found in Ref.[8] In the above formula, one can find a large logarithm. Here the energy scale of the process is the muon mass, so the large log takes the form $L = \ln(m_\mu^2/m_e^2) \approx 11$. Numerically the terms enhanced by the large log give the bulk of the total one-loop correction.

Modern techniques of one-loop RC calculations involve automatized computer systems, *e.g.*: the Mathematica package for generation and visualization of Feynman diagrams `FeynArts`;[10] the Mathematica package for algebraic calculations in elementary particle physics `FeynCalc`;[11] the package for evaluation of scalar and tensor one-loop integrals `LoopTools`;[12] the generic automated package for the calculation of Feynman diagrams at one-loop `GRACE-loop`;[13] and other.

Among the computer systems used for one-loop correction calculations, there is the SANC project.[14] The project is devoted to Support of Analytic and Numeric Calculations for experiments at colliders. It is accessible via the Internet [http://sanc.jinr.ru] and allows automatic computation of pseudo- and realistic observables with the one-loop precision for various processes of elementary particle interactions in the frames of the Standard Model. The theoretical basis of SANC is given by book,[15] where one can find the detailed presentation of a consistent procedure of one-loop SM radiative correction calculations. The computer system computes SM predictions for a large number of processes of particle interactions and decays taking into account one-loop QED, QCD and electroweak RC.

### 3.2. *Soft photon emission*

Let us look at the process

$$p + \bar{p} \to e^+ + e^- + \gamma, \tag{10}$$

where the energy of the photon in the center-of-mass system is small $\omega < \bar{\omega} \ll E = \sqrt{s}/2$, where $E$ is the total c.m.s. energy. Then the cross section of this process takes the factorized form: the Born level cross section of the non-radiative process $p + \bar{p} \to e^+ + e^-$ is multiplied by the so-called accompanying radiation factor:

$$\frac{\mathrm{d}\sigma^{\mathrm{Soft}}}{\mathrm{d}\sigma^{\mathrm{Born}}} = -\frac{4\pi\alpha}{(2\pi)^3}\int\frac{\mathrm{d}^3k}{2\omega}\left(\frac{p_+}{p_+k} - \frac{p_-}{p_-k} + \frac{q_-}{q_-k} - \frac{q_+}{q_+k}\right)^2 = \frac{\mathrm{d}\sigma^{\mathrm{Soft}}_{\mathrm{even}}}{\mathrm{d}\sigma^{\mathrm{Born}}} + \frac{\mathrm{d}\sigma^{\mathrm{Soft}}_{\mathrm{odd}}}{\mathrm{d}\sigma^{\mathrm{Born}}}, \tag{11}$$

$$\begin{aligned}
\frac{\mathrm{d}\sigma^{\mathrm{Soft}}_{\mathrm{even}}}{\mathrm{d}\sigma^{\mathrm{Born}}} &= \frac{\alpha}{\pi}\Bigg\{-2\left[\ln\left(\frac{2\bar{\omega}}{\lambda}\right) - \frac{1}{2\beta}L_\beta\right] - 2\ln\left(\frac{\bar{\omega}\cdot m}{\lambda E}\right) \\
&\quad + 2\frac{1+\beta^2}{2\beta}\left[\ln\left(\frac{2\bar{\omega}}{\lambda}\right)L_\beta - \frac{1}{4}L_\beta^2 + \Phi(\beta)\right] + 2\left[\ln\left(\frac{2\bar{\omega}}{\lambda}\right)L_e - \frac{1}{4}L_e^2 - \frac{\pi^2}{6}\right]\Bigg\}, \\
\Phi(\beta) &= \frac{\pi^2}{12} + L_\beta\ln\frac{1+\beta}{2\beta} + \ln\frac{2}{1+\beta}\ln(1-\beta) + \frac{1}{2}\ln^2(1+\beta) - \frac{1}{2}\ln^2 2 \\
&\quad - \mathrm{Li}_2(\beta) + \mathrm{Li}_2(-\beta) - \mathrm{Li}_2\left(\frac{1-\beta}{2}\right), \qquad L_e \equiv \ln\frac{s}{m_e^2}, \\
\beta &= \frac{|\vec{p}_+|}{p_+^0} = \frac{|\vec{p}_-|}{p_-^0}, \qquad L_\beta \equiv \ln\left(\frac{1+\beta}{1-\beta}\right).
\end{aligned}$$

The P-odd contribution $\mathrm{d}\sigma^{\mathrm{Soft}}_{\mathrm{odd}}$ and detailed notation can be found in Ref.[16] In the formula above one can find the soft-hard separator $\bar{\omega}$ and the fictitious photon mass $\lambda$ used to regularize the infrared singularity. Both parameters appear under the logarithm. We meet here again the large logarithm $L_e$ which is about 16 at the threshold and grows logarithmically with the c.m.s. energy.

Factorization of the factor corresponding to the soft photon emission happens due to the difference of the energy scale of the two sub-processes: the hard non-radiative one and the one of the photon emission (from all charged particles in the initial and final states). An analytical calculation of a soft radiation factor is relatively simple. Moreover, going to higher order one can use the general result of the Yennie–Frautchi-Suura theorem.[17] The latter claims that the factorization of multiple soft photon emission sub-processes happens not only with respect to the hard sub-process but also between different photon contributions. That allows to exponentiate the factor and thus find the effect re-summed in all orders of the perturbation theory.

Meanwhile, cancellation of the dependence on the auxiliary parameters $\lambda$ and $\bar{\omega}$ should be provided. Cancellation of the terms containing $\ln\lambda$ happens in all orders in the sum of virtual (loop) and real soft photon emission contributions. That was proven in the well known Bloch-Nordsieck theorem. The dependence on the soft-hard separator should disappear after adding the hard photon contribution. The latter can be either calculated analytically or computed numerically. The numerical approach is nowadays the most appropriate because in this case it is possible to take into account all specific experimental conditions.

### 3.3. *Hard photon emission*

As an example of hard photon emission we can take the process

$$e^+(p_+) + e^-(p_-) \to \mu^+(q_+) + \mu^-(q_-) + \gamma(k). \tag{12}$$

Its differential cross section has the form[18]

$$\mathrm{d}\sigma = \frac{\alpha^3}{2\pi^2 s^2} R \mathrm{d}\Gamma, \qquad \mathrm{d}\Gamma = \frac{\mathrm{d}^3 k \mathrm{d}^3 q_- \mathrm{d}^3 q_+}{q_+^0 q_-^0 k^0} \delta(p_+ + p_- - q_- - q_+ - k),$$

$$R = \frac{s}{16}(4\pi\alpha)^{-3} \sum_{spins} |M|^2 = R_e + R_\mu + R_{e\mu}\,,$$

where we separated the contributions due to the initial state radiation (ISR) $R_e$, the final state radiation (FSR) $R_\mu$, and their interference $R_{e\mu}$. Let us first look at the ISR part:

$$\begin{aligned}
R_e = \frac{s}{s_1^2}\Bigg\{&\Big[-\frac{m_e^2}{\chi_+^2} - \frac{m_e^2}{\chi_-^2} + \frac{s}{\chi_+\chi_-}\Big]\left(\frac{1}{2}tt_1 + \frac{1}{2}uu_1 + sm_\mu^2\right)\\
&+ \frac{1}{\chi_-}(2m_\mu^2\chi_+ - u_1\chi_+' - t_1\chi_-') + \frac{1}{\chi_+}(2m_\mu^2\chi_- - u\chi_-' - t\chi_+')\\
&+ P\Big[q_-(u - t_1) + q_+(t - u_1) + 2m_\mu^2(p_+ - p_-) - \frac{p_-}{\chi_-}(2m_\mu^2\chi_+ - u_1\chi_+' - t_1\chi_-')\\
&+ \frac{p_+}{\chi_+}(2m_\mu^2\chi_- - u\chi_-' - t\chi_+')\Big]\Bigg\}, \qquad P = \frac{p_+}{\chi_+} - \frac{p_-}{\chi_-}\,,
\end{aligned}$$

$$s = 2p_+p_-, \quad s_1 = (q_+ + q_-)^2, \quad t = -2p_-q_-, \quad u = -2p_-q_+,$$

$$u_1 = -2p_+q_-, \quad t_1 = -2p_+q_+, \quad \chi_\pm = p_\pm k, \quad \chi_\pm{}' = q_\pm k.$$

The FSR and initial-final state radiation interference part are

$$R_\mu = A_\mu + B_\mu, \qquad R_{e\mu} = A_{e\mu} + B_{e\mu},$$

$$A_\mu = -\frac{tt_1 + uu_1 + 2sm_\mu^2}{2s}\left(\frac{m_\mu^2}{(\chi_+')^2} + \frac{m_\mu^2}{(\chi_-')^2} - \frac{2q_-q_+}{\chi_+'\chi_-'}\right),$$

$$A_{e\mu} = -\frac{tt_1 + uu_1 + 2sm_\mu^2}{2s_1}\left(\frac{t}{\chi_-\chi_-'} + \frac{t_1}{\chi_+\chi_+'} - \frac{u}{\chi_-\chi_+'} - \frac{u_1}{\chi_+\chi_-'}\right),$$

$$\begin{aligned}
B_\mu = \frac{1}{s}\Bigg\{&-\frac{4m_\mu^2\chi_+\chi_-}{\chi_+'\chi_-'} - \frac{t_1\chi_- + u\chi_+}{\chi_-'} - \frac{u_1\chi_- + t\chi_+}{\chi_+'}\\
&+ Q[p_+(t-u) + p_-(u_1 - t_1) + \frac{q_-}{\chi_-'}(t_1\chi_- + u\chi_+) - \frac{q_+}{\chi_+'}(u_1\chi_- + t\chi_+)]\Bigg\},
\end{aligned}$$

$$\begin{aligned}
B_{e\mu} = -\frac{2}{s_1}\Bigg\{&-t - t_1 + u + u_1 - \frac{1}{2}u_1(\frac{p_-}{\chi_-} - \frac{q_+}{\chi_+'})(Q\chi_+' + P\chi_-)\\
&- \frac{1}{2}t_1(\frac{p_-}{\chi_-} - \frac{q_-}{\chi_-'})(Q\chi_-' - P\chi_-) - m_\mu^2(\chi_+ + \chi_-)(QP)\\
&+ \left(\frac{m_\mu^2}{\chi_+'} - \frac{m_\mu^2}{\chi_-'}\right)(\chi_- - \chi_+) - \frac{1}{2}t(\frac{q_+}{\chi_+'} - \frac{p_+}{\chi_+})(Q\chi_+' - P\chi_+)\\
&- \frac{1}{2}u(\frac{q_-}{\chi_-'} - \frac{p_+}{\chi_+})(Q\chi_-' + P\chi_+)\Bigg\},
\end{aligned}$$

$$P = \frac{p_+}{\chi_+} - \frac{p_-}{\chi_-}\,, \qquad Q = \frac{q_-}{\chi_-'} - \frac{q_+}{\chi_+'}\,.$$

Note that the so-called *collinear singularities* appear in the denominators $\chi_\pm$ and $\chi_\pm'$. They are regularized by the fermion masses. In fact, $\chi_- = p_-k = p_-^0\omega[1 - \beta_- \cos(\widehat{\vec{p}_-\vec{k}})]$, where $\beta_- = \sqrt{1 - m_e^2/(p_-^o)^2} < 1$ and so on.

## 4. The Coulomb Singularity

It is well known that the electromagnetic interaction between charged particles in the final state can considerably affect the observable reaction rate. For example, the cross section of electron-positron annihilation into a proton–anti-proton pair becomes different from zero at the threshold due to the final state interactions.[19] Another observable effect is the difference in energy behavior at the threshold of the annihilation channels with production of charged and neutral mesons, see e.g. Ref.[20]

If the relative velocity of the charged particles is small ($v \ll 1$), then the effect of of multiple photon exchange between them becomes significant. This fact has been discussed in the literature for a long time. It was shown already in the textbook by A. Sommerfeld[21] that the correction due to re-scattering of charged particles in the final state is proportional to the bound state wave function at the origin squared, $|\Psi(0)|^2$, see also book.[22] So that the scattering (or annihilation) channel acquires some features of the corresponding bound state. G. Gamow has shown[23] that the same factor is relevant for the description of the Coulomb barrier in nuclear interactions. Using the non-relativistic Schrödinger equation, A. Sakharov derived this factor for the case of charged pair production[24] in the form

$$T(v) = \frac{\eta(v)}{1 - e^{-\eta(v)}}, \qquad \eta(v) = \frac{2\pi\alpha}{v}, \tag{13}$$

where $v$ is the non-relativistic relative velocity of the particles in the created pair, and $\alpha \approx 1/137$ is the fine structure constant. This function will be called below as the Sommerfeld-Gamow-Sakharov (SGS) factor.

For practical applications of the factor for modern experiments, it is highly desirable to have a relativized version of the SGS factor. This problem and some other ways of generalization of the factor, *e.g.* for non-equal masses and $P$-waves, is under discussion in the literature for a long time, see papers[25–28,30,31] and references therein.

Let us look at the explicit formula[6] for the FSR correction to the processes $e^+ + e^- \to \pi^+ + \pi^-$:

$$\begin{aligned}
\sigma^0_{\pi\pi(\gamma)} &= \frac{\pi\alpha^2}{3s}\beta_\pi^3\,|F_\pi(s)|^2\,|1-\Pi(s)|^2\left(1+\frac{\alpha}{\pi}\Lambda(s)\right),\\
\Lambda(s) &= \frac{1+\beta_\pi^2}{\beta_\pi}\Bigg\{4\mathrm{Li}_2\Big(\frac{1-\beta_\pi}{1+\beta_\pi}\Big) + 2\mathrm{Li}_2\Big(-\frac{1-\beta_\pi}{1+\beta_\pi}\Big) - \left[3\ln\Big(\frac{2}{1+\beta_\pi}\Big) + 2\ln\beta_\pi\right]\ln\frac{1+\beta_\pi}{1-\beta_\pi}\Bigg\}\\
&\quad -3\ln\Big(\frac{4}{1-\beta_\pi^2}\Big) - 4\ln\beta_\pi + \frac{1}{\beta_\pi^3}\left[\frac{5}{4}(1+\beta_\pi^2)^2 - 2\right]\ln\frac{1+\beta_\pi}{1-\beta_\pi} + \frac{3}{2}\frac{1+\beta_\pi^2}{\beta_\pi^2},
\end{aligned}$$

where $\beta_\pi$ is the pion velocity in the c.m.s. frame. Some Feynman diagrams for $O(\alpha)$ corrections to this process are shown in Fig. 5. One can see that the radiative correction $\Lambda(s)$ is proportional to the inverse power of $\beta_\pi$. It is important that this Coulomb singularity appears only in the correction, but the total corrected cross section is not singular for $\beta_\pi \to 0$.

Let us consider the case of the final state interaction of charged particles produced close to the threshold, *e.g.* in electron-positron annihilation

$$e^-(k_1) \;+\; e^+(k_2) \;\to\; a^-(p_1) \;+\; a^+(p_2), \tag{14}$$

$$s = (k_1+k_2)^2 = (p_1+p_2)^2 \gtrsim (m_1+m_2)^2, \tag{15}$$

where $a^\pm$ can be scalar, spinor, or vector particles. The Born-level cross section $\sigma^{\mathrm{Born}}$ of this process depends on the type of interaction and the spin. But in any case in the center-of-mass system, it is proportional to the first

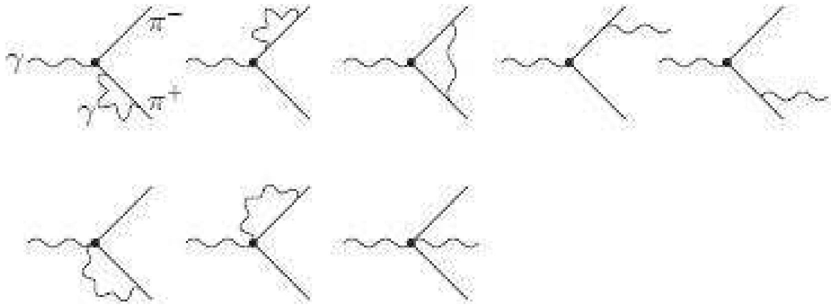


Fig. 5. Representatives of Feynman diagrams contribution to one-loop QED FSR corrections in $e^+e^-\pi\pi^+\pi^-$.

power of factor $\beta_{1,2}$ which comes from the phase space volume and vanish at the threshold $s \to (m_1 + m_2)^2$,

$$\beta_{1,2} = \frac{2p}{p_1^0 + p_2^0}, \qquad p \equiv |\vec{p}_1| = |\vec{p}_2| = \frac{\sqrt{\Lambda(s, m_1^2, m_2^2)}}{2\sqrt{s}},$$
$$p_1^0 + p_2^0 = 2\sqrt{s}, \qquad \Lambda(x, y, z) = x^2 + y^2 + z^2 - 2xy - 2xz - 2yz. \tag{16}$$

For the case of equal masses this factor takes the usual form of the relativistic velocity $\beta = \sqrt{1 - m^2/(p^0)^2}$ of the final state particles.

The relativistic relative velocity of our particles is

$$v_{\text{rel}} = \frac{\sqrt{\Lambda(s, m_1^2, m_2^2)}}{s - m_1^2 - m_2^2} = \frac{\sqrt{[s - (m_1^2 + m_2^2)^2][s - (m_1^2 - m_2^2)^2]}}{s - m_1^2 - m_2^2}, \tag{17}$$

which is a relativistic invariant, $0 < v_{\text{rel}} < 1$ (we work in the natural units $\hbar = c = 1$).

In the one-loop approximation the QED radiative correction to the annihilation cross section gets contributions from virtual and real photon emission:

$$\sigma^{1-\text{loop}} = \sigma^{\text{Born}}\Big(1 + \delta^{\text{Virt}} + \delta^{\text{Real}}\Big). \tag{18}$$

The last term in the parentheses is proportional to $\beta^2$, it is strongly suppressed at the threshold. Explicit expressions for different contributions with the exact dependence on the final state particle mass (for the equal mass case) can be found *e.g.* in Ref.[32] for fermions and in Ref.[33] for scalars. The final state one-loop virtual correction (in the on-mass-shell renormalization scheme) is described by the triangle diagram shown in Fig. 6. There are three types of integrals over the loop momentum: the scalar, the vector and the tensor ones:

$$\left\{I_S,\, I_V^{\mu},\, I_T^{\mu\nu}\right\} = \int \frac{d^4k}{i\pi^2}\, \frac{\{1,\ k^{\mu},\ k^{\mu\nu}\}}{((p_1 + k)^2 - m_1^2 + i\varepsilon)((p_2 - k)^2 - m_2^2 + i\varepsilon)(k^2 + i\varepsilon)}\,.$$

The tensor one contains an ultraviolet divergence, which has to be removed by the standard renormalization procedure. The vector integral $I_V^{\mu}$ is finite. The scalar integral $I_S$ contains an infrared divergence, which cancels out in the sum with the contribution of the real final state radiation.

Direct calculations show that the contributions of the vector and tensor integrals are proportional at least to the second power of final state particle velocities. While the scalar integral reveals at the threshold the well known Coulomb singularity, it is proportional to $1/\sqrt{\Lambda(s, m_1^2, m_2^2)}$. The coefficients before the integrals depend

Fig. 6. Feynman diagram for one-loop virtual correction in the final state.

in general on the type of the particles, but the one standing at the scalar one is *universal*, it is the same for scalar, spinor and vector final state particles. The contributions of the one-loop scalar integral to the cross section can be presented in the form

$$\delta\sigma_S^{1-\text{loop}} = \sigma^{\text{Born}}\frac{\alpha}{2\pi}(s - m_1^2 - m_2^2)C_0(m_1^2, m_2^2, s, m_1^2, m_\gamma^2, m_2^2), \tag{19}$$

where the triangular scalar one-loop integral $C_0$ is written in the LoopTools package[12] notation. So, by comparison of the first order of the perturbation theory in the limit $s \to (m_1 + m_2)^2$ with the corresponding term in the expansion of the SGS factor, we can adjust the parameter of the latter. It appears that the proper choice is just the substitution of the non-relativistic relative velocity by the relativistic one, see also Ref.[34] This choice is also supported by studies performed within relativistic quasipotential models.[28,35]

There is one important point here. In the description of the final state interactions we meet the situation when we have both perturbative and non-perturbative contributions. In such a case it is easy to get the so-called *double counting*. Really, the expansion in $\alpha$ of the SGS factor gives a part of the terms which are also included in the perturbative results. To avoid the double counting we introduce a scheme of *matching* between the two results. Here it can be done in the following way:

$$\sigma^{\text{Corr.}} = \sigma^{\text{Born}}\Big(T(v) - \frac{\pi\alpha}{v} - \frac{\pi^2\alpha^2}{3v^2} - \ldots\Big) + \Delta\sigma^{1-loop} + \Delta\sigma^{2-loop} + \ldots \tag{20}$$

where $\Delta\sigma^{n-loop}$ is the $n$-th order perturbative contribution to the observed corrected cross section $\sigma^{\text{Corr.}}$.

## 5. Vacuum polarization

A photon in QED can create a pair of charged particle and anti-particle. This pair can be either virtual (it annihilates soon after the creation) or real if the photon is off mass-shell and energy-momentum conservation law permits the ”photon decay”. The effect arising due to virtual pair creation is called in QED as *vacuum polarization* (VP), see Fig. 7.

Perturbative QED describes this effect for the case of lepton pairs. Results up to the fourth order in $\alpha$ are known. Let us look at the first order contributions. In the space like region (when the photon 4-momentum squared is negative: $q^2 < 0$)

$$\Pi_\ell(q^2) = -\frac{\alpha}{9\pi}\Big(5 - 12\eta + 3(-1 + 2\eta)\sqrt{1 + 4\eta}\,\ln\frac{\sqrt{1 + 4\eta} + 1}{\sqrt{1 + 4\eta} - 1}\Big) + O\big(\alpha^2\big),$$

where $\eta \equiv m_\ell^2/(-q^2)$ and $m_\ell$ is the lepton mass. In the time-like region below the threshold of real pair production ($4m_\ell^2 > q^2 > 0$) we have

$$\Pi_\ell(q^2) = -\frac{\alpha}{9\pi}\Big(5 - 12\eta + 3(-1 + 2\eta)\sqrt{-1 - 4\eta}\,\arctan\frac{\sqrt{-1 - 4\eta}}{-1 - 2\eta}\Big) + O\big(\alpha^2\big).$$

Above the threshold ($q^2 > 4m_\ell^2$) we get a nonzero imaginary part:

$$\Pi_\ell(q^2) = -\frac{\alpha}{9\pi}\Big(5 - 12\eta + 3(-1+2\eta)\sqrt{1+4\eta}\,\ln\frac{1+\sqrt{1+4\eta}}{1-\sqrt{1+4\eta}}\Big)$$
$$-i\,\frac{\alpha}{3}(1-2\eta)\sqrt{1+4\eta} + \mathcal{O}\left(\alpha^2\right).$$

So the leptonic contribution to VP is under control, the uncertainty in its calculation is negligible.

For high energies ($q^2 \gg m_\ell^2$) we get

$$\Pi(q^2) \approx -\frac{\alpha}{3\pi}\sum_f Q_f^2 N_c^f\Big(\ln\frac{q^2}{m_\ell^2} - \frac{5}{3}\Big), \tag{21}$$

where we sum over all fermions ($f$) with electric charge $Q_f$ and number of colors $N_c^f$. The above formula describes both lepton and quark contributions. For the latter we require also $q^2 \gg \Lambda_{QCD}$.

Resummation of the geometric progression

$$1 + \Pi(q^2) + \Pi^2(q^2) + \ldots = \frac{1}{1-\Pi(q^2)} \tag{22}$$

gives us the conventional expression for the running QED coupling constant

$$\alpha(q^2) = \frac{\alpha}{1 - \mathrm{Re}\Pi(q^2)}. \tag{23}$$

Here $\alpha(0) \equiv \alpha = 137.035999084(51)$ is the value of the fine structure constant extracted from experimental data at $q^2 \to 0$. The condition $\Pi(0) = 0$ is just the choice of the renormalization point within the so called *on-mass-shell scheme*. It is not unique, remind that at high energies we often use schemes where the point is shifted, for example in the $\alpha(M_Z^2)$ scheme we fix the value of the coupling constant at the $Z$ boson mass. The latter scheme was convenient for applications at LEP experiments. Another popular choice is the $G_{\mathrm{Fermi}}$ (or $G_\mu$) scheme in which the coupling constant is (re)normalized from very accurate measurements of the muon lifetime.[36]

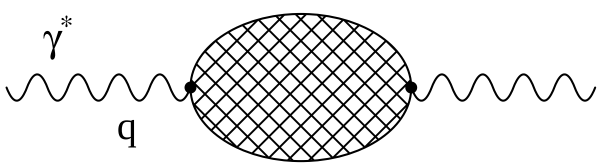


Fig. 7. Vacuum polarization in photon propagator.

Hadronic contribution to vacuum polarization $\Pi_{had}$ is hard to compute starting the QCD Lagrangian (lattice simulations are far from the required precision). However, it is possible to use the optical theorem to obtain the real part of $\Pi_{had}(q^2)$ from the imaginary part. In fact in the time like region

$$\mathrm{Im}\Pi_{\mathrm{had}}(q^2) \sim \sigma(e^+e^- \to hadrons) \tag{24}$$

The dispersion integral is then given by

$$\Delta\alpha_{\mathrm{had}}^{(5)}(q^2) \;=\; -\frac{q^2}{4\pi^2\alpha}\,\mathrm{P}\int_{m_\pi^2}^{\infty}\frac{\sigma_{\mathrm{had}}^0(s)\,\mathrm{d}s}{s-q^2}$$

Five quark flavors are taken into account (we include $e^+e^-$ annihilation channels into the corresponding mesons and baryons)[d]. The lower limit of the integral corresponds to the lowest energy channel of hadron production: $e^+ + e^- \to \pi^0\gamma$. This process has a rather small cross section, but we should take it into account to reach the required high precision in the description of vacuum polarization. In general, VP contributes to practically all observables in particle physics. Knowing it is very important for construction of theoretical predictions for the anomalous magnetic moment of muon, to extract the Higgs boson mass, see Fig. 1, *etc.*

For practical applications we use a combination of analytical results for leptonic contributions with phenomenological parameterizations of the hadronic effects. Several different computer codes are available (for a discussion and comparison see Ref.[37]): `REPI`[38]
[`http://hbu.web.cern.ch/hbu/aqed/aqed.html`]
(only for the space-like region); function `HADR5N` by F. Egerlehner[39]
[`http://www-com.physik.hu-berlin.de/~fjeger/`];
parametrization by the CMD collaboration (Novosibirsk)
[`http://cmd.inp.nsk.su/~ignatov/vpl/`];
and the `HNMT` routine.[40] Fig. 8 shows the dependence of the quantity $|1+\Pi(s)|^2$ as a function of $\sqrt{s} = \sqrt{|q^2|}$, where positive $\sqrt{s}$ correspond to the time-like region ($q^2 > 0$) and negative $\sqrt{s}$ formally define the space like case ($q^2 < 0$). In the time like region one can clearly see resonance peaks of vector mesons: $\rho$, $\omega$, $\phi$, $J/\Psi$ and so on. The solid line shows the sum of leptonic and hadronic contributions. The dotted one represents the pure leptonic effect.

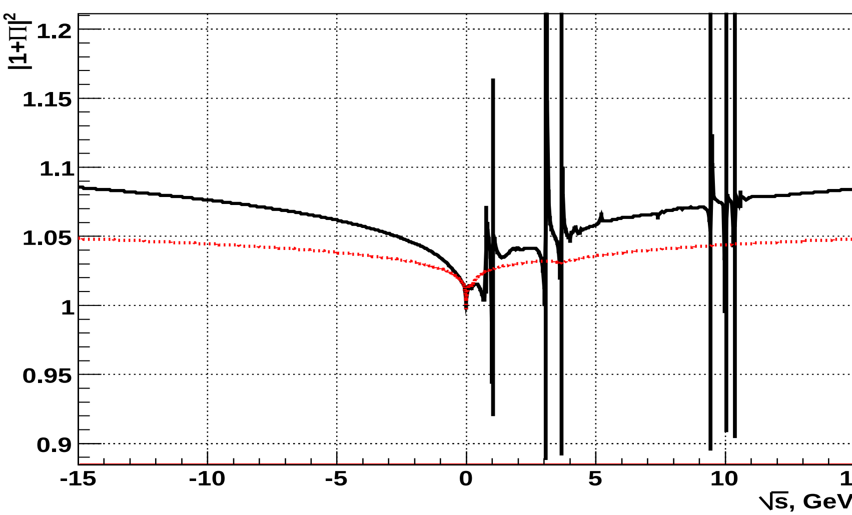


Fig. 8. $|1+\Pi|^2$ from CMD-2 compilation for space- and time-like momenta (labelled $\sqrt{s}$); solid (black) lines: leptonic plus hadronic contributions, dotted (red) lines: only leptonic contributions.

[d]The top quark and $W^\pm$ boson contributions are computed separately.

## 6. The Leading Logarithmic Approximation

Calculations of radiative corrections in QED for processes with characteristic energies being large compared with the electron mass, $E \gg m_e$, reveal the following peculiar property. It appears that besides the expansion in $\alpha$ it becomes very useful to expand also in the small parameter $m_e^2/E^2$ and in the large parameter $L \equiv \ln(E^2/m_e^2)$. Usually the terms suppressed by the small parameter can be neglected in RC (it is sufficient to keep them only in the Born level cross section). And the terms enhanced by the so called *large logarithm* $L$ give the bulk of the correction value. Calculation of these terms can be performed by specific methods which are much simpler than the general ones (see Sect. 3) developed for complete calculations of perturbative corrections. Moreover, higher order leading logarithmic (*leading log*) corrections can be re-summed.

Let us discuss the expansion in $\mathcal{O}(\alpha^n L^n)$, $n = 0, 1, 2, \ldots$, where

$$L \equiv \ln(\Lambda^2/m_e^2) \tag{25}$$

and $\Lambda$ is the so-called *factorization scale*, $\Lambda^2 \gg m_e^2$. Typical values of $\Lambda$ will be the center-of-mass energy for annihilation processes and the momentum transfer for scattering one. But in general this quantity is an parameter which can be varied.

The construction of the leading log approximation is based on the fundamental feature of quantum mechanics: interference of amplitudes which happen at different energy scales (or distances) is suppressed. In other words, we know that amplitudes of small-distance and large-distance sub-processes factorize with respect to each other. And neglecting their interference we get the final result for an observable quantity as a product of corresponding probabilities.

Let us look at the process $a + b \to c + d + \gamma$ with emission of a hard photon at a small angle with respect to the momentum of the initial particle $a$. Direct calculations show that its cross section can be presented, see Ref.[18] for details, in the form

$$\begin{aligned}
&\mathrm{d}\sigma[a(p_1) + b(p_2) \to c(q_1) + d(q_2) + \gamma(k \approx (1-z)p_1)] \\
&\quad \approx \mathrm{d}\hat{\sigma}[a(zp_1) + b(p_2) \to c(q_1) + d(q_2)] \otimes R_{\mathrm{H}}^{\mathrm{ISR}}(z) \\
&R_{\mathrm{H}}^{\mathrm{ISR}}(z) = \frac{\alpha}{2\pi}\left[\frac{1+z^2}{1-z}\left(\ln\frac{E^2}{m^2} - 1 + l_0\right) + 1 - z + \mathcal{O}\left(\frac{m^2}{E^2}\right) + \mathcal{O}\left(\vartheta_0^2\right)\right], \\
&\vartheta_\gamma = \widehat{\vec{p}_1\vec{k}} < \vartheta_0, \quad m/E \ll \vartheta_0 \ll 1, \quad l_0 = \ln(\vartheta_0^2/4),
\end{aligned} \tag{26}$$

where we integrated over the emission angles limited from above by the small parameter $\vartheta_0$. Here $\otimes$ denotes the so-called *convolution* operation, which is actually the integration over the photon energy fraction $z \equiv k^0/p_1^0$. The large logarithm appears in the *collinear radiation factor* $R_{\mathrm{H}}^{\mathrm{ISR}}$ as the logarithm of the initial particle energy $E = p_1^0$ over its mass $m$. Factorization in the above formula appeared as the result of direct calculations of Feynman diagrams where small terms proportional to $\vartheta^2$ and $m^2/E^2$ were neglected.

The amplitudes describing soft photon emission obviously do not interfere with the ones for hard radiation because their phase space do not overlap. So the one-loop correction to a differential cross section can be presented as

$$\mathrm{d}\sigma = \mathrm{d}\sigma^{\mathrm{Soft+Virt}}(\Delta) \; + \; \mathrm{d}\sigma^{\mathrm{Hard(coll)}}(\Delta, \vartheta_0) \; + \mathrm{d}\sigma^{\mathrm{Hard(non-coll)}}(\Delta, \vartheta_0), \tag{27}$$

where [Soft] and hard collinear [Hard(coll)] photon contributions are factorized at the Born cross section. The contribution $\mathrm{d}\sigma^{\mathrm{Hard(non-coll)}}$ takes into account radiation of photons at large angles ($\vartheta > \vartheta_0$) and does not contain any large log. The dependence on the auxiliary parameters $\Delta \ll 1$ and $\vartheta_0$ cancels out in the sum of contributions.

In this way, direct calculations in many cases explicitly demonstrate factorization properties of terms proportional to the large logs. What is important for us is that such observations can be generalized for a wide class of processes and for all orders of the perturbation theory. The *factorization theorems* were proved in QCD,[41,42] they can be easily adapted for QED.

The energy scale in the large log is an effective separator of the scales in the hard (short-distance) and soft (long-distance) sub-processes. In the example of collinear photon emission considered above changing of the large log scale corresponds to variation of the auxiliary parameter $\vartheta_0$, while the sum (27) remains unchanged. In the general case the total result should not depend on the *factorization scale*. This property is due to the conformal symmetry of the given theory. Of course particle masses (and $\Lambda_{\mathrm{QCD}}$) break the symmetry, but for large energies the conformal properties are restored. For this reason we can apply very powerful methods of the renormalization group approach, see review[43] and references therein.

So one can write renormalization group equations for application in QCD and QED at large energies. In particular the Dokshitzer–Gribov–Lipatov–Altarelli–Parisi (DGLAP)[44–48] evolution equation for the non–singlet electron structure function has the form

$$\mathcal{D}^{\mathrm{NS}}(z,Q^2) = \delta(1-z) + \int\limits_{m^2}^{Q^2} \frac{\alpha(q^2)}{2\pi}\,\frac{\mathrm{d}q^2}{q^2} \int\limits_{z}^{1} \frac{\mathrm{d}x}{x}\, P^{(0)}(x)\mathcal{D}^{\mathrm{NS}}\left(\frac{z}{x},q^2\right),$$

where $m$ is the electron mass; $P^{(0)}$ is the first order non–singlet *splitting function*; $\alpha(q^2)$ is the QED running coupling constant. Here we are going to consider only the electron contribution to vacuum polarization:

$$\alpha(q^2) = \frac{\alpha}{1-\frac{\alpha}{3\pi}\ln\frac{q^2}{m^2}}\,. \tag{28}$$

Structure function $\mathcal{D}^{\mathrm{NS}}(z,Q^2)$ is the probability density to find an electron with energy fraction $z$ in the given electron if the energy scale is limited by $\sqrt{Q^2}$ from above.

The splitting function

$$P^{(0)}(z) \equiv P_{ee}(z) = \left[\frac{1+z^2}{1-z}\right]_+ = \frac{1+z^2}{1-z} - \delta(1-z)\int\limits_0^1 \mathrm{d}x\,\frac{1+x^2}{1-x} \tag{29}$$

is used to describe the transition from an electron $e$ into another electron $e$ with energy fraction $z$ with respect to the initial one. The singularity in this function at $z \to 1$ is regularized by means of the so-called *plus prescription* which is defined by

$$\int\limits_{x_{\mathrm{min}}}^{1} \mathrm{d}x\,[f(x)]_+ g(x) = \int\limits_0^1 \mathrm{d}x\, f(x)[g(x)\Theta(x-x_{\mathrm{min}}) - g(1)]. \tag{30}$$

The complete set of evolution equations in the leading logarithmic approximation (LLA) of QED reads

$$\mathcal{D}_{ee}(x,s) = \delta(1-x) + \int\limits_{m^2}^{s} \frac{\mathrm{d}t\alpha(t)}{2\pi t}\Big[\int\limits_{x}^{1}\frac{\mathrm{d}y}{y}\mathcal{D}_{ee}(y,t)P_{ee}(\frac{x}{y}) + \int\limits_{x}^{1}\frac{\mathrm{d}y}{y}\mathcal{D}_{\gamma e}(y,t)P_{e\gamma}(\frac{x}{y})\Big],$$

$$\mathcal{D}_{\bar{e}e}(x,s) = \int\limits_{m^2}^{s} \frac{\mathrm{d}t\alpha(t)}{2\pi t}\Big[\int\limits_{x}^{1}\frac{\mathrm{d}y}{y}\mathcal{D}_{\bar{e}e}(y,t)P_{\bar{e}e}(\frac{x}{y}) + \int\limits_{x}^{1}\frac{\mathrm{d}y}{y}\mathcal{D}_{\gamma e}(y,t)P_{\bar{e}\gamma}(\frac{x}{y})\Big],$$

$$\mathcal{D}_{\gamma e}(x,s) = -\frac{2}{3}\int\limits_{m^2}^{s} \frac{\mathrm{d}t\alpha(t)}{2\pi t}\mathcal{D}_{\gamma e}(x,s)$$

$$+ \int\limits_{m^2}^{s} \frac{\mathrm{d}t\alpha(t)}{2\pi t}\Big[\int\limits_{x}^{1}\frac{\mathrm{d}y}{y}\mathcal{D}_{ee}(y,t)P_{\gamma e}(\frac{x}{y}) + \int\limits_{x}^{1}\frac{\mathrm{d}y}{y}\mathcal{D}_{\bar{e}e}(y,t)P_{\gamma\bar{e}}(\frac{x}{y})\Big].$$

Thanks to the smallness of $\alpha_{\mathrm{QED}}$, solutions of the evolution equations in QED can be obtained by iterations. The initial conditions for LLA QED are simple, for instance, one can take just the delta function as the zeroth approximation for $\mathcal{D}_{ee}(x,s)$. Note that in QCD the structure functions can not be computed analytically starting from the first principles and having only the parameters of the SM as input. Instead, we extract QCD structure function from experimental data. But the evolution of the functions with respect to the factorization scale is described by means of the DGLAP equations as in QED as well as in QCD.

Iteration and further application of the structure functions involves the *convolution* operation. Let us take two functions $f(x)$ and $g(y)$ defined for $0 \le x, y \le 1$. Their convolution is given by

$$[f\otimes g](z) = \int\limits_0^1 \mathrm{d}x \int\limits_0^1 \mathrm{d}y\delta(z-xy)f(x)g(y) = \int\limits_z^1 \frac{\mathrm{d}x}{x}f(x)g\left(\frac{z}{x}\right) \tag{31}$$

where $0 \le z \le 1$. This operation can be generalized for special functions regularized by plus-prescription:

$$\Big[[f]_+\otimes[g]_+\Big](z) = \lim_{\Delta\to 0}\Big\{\int\limits_{z/(1-\Delta)}^{1-\Delta}\frac{\mathrm{d}x}{x}f_\Theta(x)g_\Theta\left(\frac{z}{x}\right) + f_\Delta g_\Theta(z) + f_\Theta(z)g_\Delta\Big\},$$

$$f_\Delta = -\int\limits_0^{1-\Delta}\mathrm{d}x\ f(x), \qquad f_\Theta(x) = f(x)\Big|_{x<1}. \tag{32}$$

It is accepted to distinguish so-called *singlet* (S) and *non-singled* (NS) parts of the electron structure function $\mathcal{D}_{ee}$:

$$\mathcal{D}_{ee} = \mathcal{D}^S + \mathcal{D}^{NS}, \qquad \mathcal{D}^S = \mathcal{D}_{\bar{e}e}. \tag{33}$$

In the Feynman diagram language the non-singlet part corresponds to the graphs with continuous electron line, while in the singlet case the registered electron with energy fraction $z$ is a component of a created $e^+e^-$ pair (it is connected with the initial electron via a photon line).

Non-singlet structure functions have the properties

$$\int\limits_0^1 \mathcal{D}^{NS}(x,\beta)\mathrm{d}x = 1, \qquad \beta \equiv \frac{2\alpha}{\pi}L, \tag{34}$$

$$\int\limits_x^1 \frac{\mathrm{d}y}{y}\mathcal{D}^{NS,\gamma}(y,\beta_1)\,\mathcal{D}^{NS,\gamma}\left(\frac{x}{y},\beta_2\right) = \mathcal{D}^{NS,\gamma}(x,\beta_1+\beta_2)\,.$$

Let us now discuss the so-called *master formula* which shows how to apply the electron structure function method for evaluation of QED RC to a given process. Actually we take this formula from QCD. For concreteness let us take Bhabha scattering, where we have electrons and positrons both in the final and initial states. We will use the QCD-like massless partons. In QED there are three type of partons: electrons, positrons and photons. According to the factorization theorems, the corrected cross section of this process at high energies ($E \gg m_e$) can be presented in the form

$$\begin{aligned}
\mathrm{d}\sigma &= \sum_{a,b,c,d}\int_{\bar{z}_1}^1 \mathrm{d}z_1 \int_{\bar{z}_2}^1 \mathrm{d}z_2 \mathcal{D}^{\mathrm{str}}_{ae}(z_1)\mathcal{D}^{\mathrm{str}}_{b\bar{e}}(z_2)\left(\mathrm{d}\sigma^{\mathrm{Born}}_{ab\to cd}(z_1,z_2) + \mathrm{d}\bar{\sigma}^{(1)}(z_1,z_2) + \mathcal{O}\left(\alpha^2L^0\right)\right) \\
&\times \int_{\bar{y}_1}^1 \frac{\mathrm{d}y_1}{Y_1}\int_{\bar{y}_2}^1 \frac{\mathrm{d}y_2}{Y_2}\mathcal{D}^{\mathrm{frg}}_{ec}\left(\frac{y_1}{Y_1}\right)\mathcal{D}^{\mathrm{frg}}_{\bar{e}d}\left(\frac{y_2}{Y_2}\right), \\
\mathcal{D}^{\mathrm{str,frg}}_{ee}(z) &= \delta(1-z) + \frac{\alpha}{2\pi}d_1(z,\mu_0,m_e) + \frac{\alpha}{2\pi}LP^{(0)}(z) \\
&+\left(\frac{\alpha}{2\pi}\right)^2\left(\frac{1}{2}L^2P^{(0)}\otimes P^{(0)}(z) + LP^{(0)}\otimes d_1(z,\mu_0,m_e) + LP^{(1;\gamma,\mathrm{pair})\mathrm{str,frg}}_{ee}(z)\right) \\
&+\mathcal{O}\left(\alpha^2L^0,\alpha^3\right), \qquad L \equiv \ln\frac{Q^2}{\mu_0^2}, \qquad \mathrm{d}\bar{\sigma}^{(1)} = \mathrm{d}\sigma^{(1)}\Big|_{m_e=0,\ \overline{\mathrm{MS}}} \\
P^{(0)}(z) &= \left[\frac{1+z^2}{1-z}\right]_+, \quad d_1(z,\mu_0,m_e) = \left[\frac{1+z^2}{1-z}\left(\ln\frac{\mu_0^2}{m_e^2} - 2\ln(1-z) - 1\right)\right]_+.
\end{aligned}$$

Here $P^{(1;\gamma,\mathrm{pair})\mathrm{str,frg}}_{ee}(z)$ are the next-to-leading order (NLO) splitting functions, we also *borrow* them from QCD (by reduction to the abelian case), see Refs.[49,50] Function $d_1$ defines the initial condition for the evolution of electron structure and fragmentation functions, $\mu_0$ is the renormalization scale, in QED we choose it usually to be equal to the electron mass: $\mu_0 = m_e$.

The structure of the master formula is as follows. The electron structure functions $\mathcal{D}^{\mathrm{str}}_{ae}(z_1)$ and $\mathcal{D}^{\mathrm{str}}_{b\bar{e}}(z_2)$ give the probability density for transition of the initial massive electron and positron into massless partons of type $a$ and $b$, respectively. The differential cross sections $\mathrm{d}\sigma^{\mathrm{Born}}_{ab\to cd}$ and $\mathrm{d}\bar{\sigma}^{(1)}$ describe the parton-level process $a+b\to c+d$ at the Born and one-loop level, respectively. They are usually called *coefficient functions* which are dependent on the process, while all other elements of the master formula are universal (they are the same for a wide class of QED processes). The fragmentation functions $\mathcal{D}^{\mathrm{frg}}_{ec}$ and $\mathcal{D}^{\mathrm{frg}}_{\bar{e}d}$ give the probability density for conversion of the massless partons $c$ and $d$ into massive electron and positron, respectively. The one-loop cross section $\mathrm{d}\bar{\sigma}^{(1)}$ computed for massless particles is divergent. It should be regularized. Here we apply the modified minimal subtraction scheme[51] ($\overline{\mathrm{MS}}$). In this way the The sum over all possible intermediate parton reactions is taken. The master formula can be expanded in $\alpha$. The first two terms in this expansion reproduce the complete Born and one-loop expressions for the Bhabha scattering process (terms proportional to $m_e^2/E_e^2$ are neglected). Higher order corrections produced by this formula define the leading and next-to-leading log contributions.

It is worth to note that the above formula suppose integration over the angular phase space of secondary (emitted) particles. But experimental conditions do not allow perform such integration if certain cuts are imposed. In this case a more detailed study of kinematics should be performed,[52] see below Sect. 6.3.

### 6.1. *Logarithmic approximation: examples*

Let us return to the example of Bhabha scattering and look at the numerical effect in logarithmic corrections. Here we will look in the expansion the powers of the large log of the sum of virtual and soft photonic corrections in $\mathcal{O}\left(\alpha^2\right)$, where the analytic result is known.[4] So we can compare in Fig. 9 the LLA = $\mathcal{O}\left(\alpha^2 L^2\right)$ (solid lines), NLO = $\mathcal{O}\left(\alpha^2 L^1\right)$ and NNLO = $\mathcal{O}\left(\alpha^2 L^0\right)$ contributions for $\Delta = 1$ and $\sqrt{s} = 100$ GeV, see Ref.[53] for details. Relative contributions of the terms proportional to the large log to $i$-th power

$$r_i^{(2)}(\theta) = \frac{\mathrm{d}\sigma^{\mathrm{Soft+Virt}}[L^i]/\mathrm{d}\theta}{\mathrm{d}\sigma^{\mathrm{Born}}/\mathrm{d}\theta} \tag{35}$$

depend on the choice of the factorizations scale $\Lambda$. On the left plot we have $\Lambda = \sqrt{s}$, *i.e.* the scale is equal to the center-of-mass energy of the process. In this case the contributions have comparable magnitudes, even so that they are ordered according to the power of the large log. On the right plot we choose $\Lambda = \sqrt{-t}$, *i.e.* the scale is equal to the momentum transferred. It appears that in this case the hierarchy of the contributions is very strong: the LLA contributions dominates, the next-to-leading one is small, and the NNLO one is almost invisible. So we see that the proper choice of the factorization scale is very important. The choice $\Lambda = \sqrt{-t}$ for Bhabha scattering is justified by the fact that the $t$-channel exchange dominates in this process.

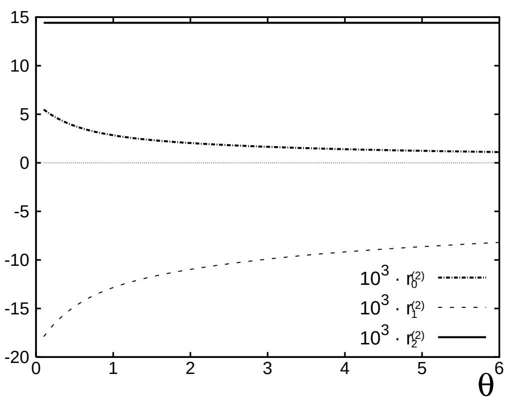


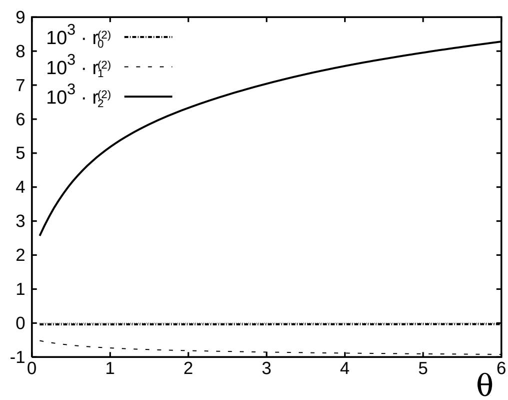


Fig. 9. The dependence on the choice of the factorization scale: $\Lambda = \sqrt{s}$ (left) and $\Lambda = \sqrt{-t}$ (right).

Let us look now at radiative corrections to the muon decay spectrum. In this process we have just one fast charged particle in the final state, so the application of the electron structure function method is simplified. The differential decay width of the anti-muon decay can be written as

$$\frac{\mathrm{d}^2\Gamma^{\mu^+\to e^+\nu\bar{\nu}}}{\mathrm{d}z\ \mathrm{d}\cos\theta} = \Gamma_0\left[F(z) - \cos\theta\, P_\mu G(z)\right] + \mathcal{O}\left(\frac{m_e^2}{m_\mu^2}\right),$$

$$\Gamma_0 \equiv \frac{G_\mu^2 m_\mu^5}{192\pi^3}\left(1 + \frac{3}{5}\ \frac{m_\mu^2}{m_W^2}\right), \qquad z \equiv \frac{2E}{m_\mu},$$

Function $F(z)$ and $G(z)$ cab be expanded in $\alpha$ and $L \equiv \ln(m_\mu^2/m_e^2)$ as

$$
\begin{aligned}
F(z) &= f_{\rm Born}(z) + \frac{\alpha}{2\pi} f_1(z) + \left(\frac{\alpha}{2\pi}\right)^2 f_2(z) + \mathcal{O}\left(\alpha^3\right), \\
f_1(z) &= L^1 \cdot f_1^{\rm LL}(z) + L^0 \cdot f_1^{\rm NLO}(z), \\
f_2(z) &= L^2 \cdot f_2^{\rm LL}(z) + L^1 \cdot f_2^{\rm NLO}(z) + L^0 \cdot f_2^{\rm NNLO}(z)
\end{aligned}
\tag{36}
$$

and so on. The Born level contributions are simple:

$$
f_{\rm Born}(z) \equiv f_0(z) = z^2(3-2z), \qquad g_{\rm Born}(z) \equiv g_0(z) = z^2(1-2z).
$$

The first order corrections enhanced by large logs can be obtained by convolution of the Born level functions with the lowest order splitting function:

$$
\begin{aligned}
f_1^{\rm LL}(z) &= P^{(0)}(\bullet) \otimes f_0(z) = \frac{5}{6} + 2z - 4z^2 + \frac{8}{3}z^3 + 2z^2(3-2z)\ln\frac{1-z}{z} P^{(0)}(\bullet) \otimes f_0(z), \\
g_1^{\rm LL}(z) &= P^{(0)}(\bullet) \otimes g_0(z) = -\frac{1}{6} - 4z^2 + \frac{8}{3}z^3 + 2z^2(1-2z)\ln\frac{1-z}{z}.
\end{aligned}
\tag{37}
$$

One can see that they agree with the corresponding terms received in the direct calculations,[8,54] see also Eq. (9).

Using the second order terms in the electron structure function we get the $\mathcal{O}\left(\alpha^2 L^2\right)$ photonic RC to the spectrum:[55]

$$
\begin{aligned}
f_2^{{\rm LL}(\gamma)}(z) &= P^{(0)}(\bullet) \otimes P^{(0)}(\bullet) \otimes f_0(z) \\
&= 4z^2(3-2z)\Phi(z) + \left(\frac{10}{3} + 8z - 16z^2 + \frac{32}{3}z^3\right)\ln(1-z) \\
&+ \left(-\frac{5}{6} - 2z + 8z^2 - \frac{32}{3}z^3\right)\ln z + \frac{11}{36} + \frac{17}{6}z + \frac{8}{3}z^2 - \frac{32}{9}z^3, \\
g_2^{{\rm LL}(\gamma)}(z) &= 4z^2(1-2z)\Phi(z) + \left(-\frac{2}{3} - 16z^2 + \frac{32}{3}z^3\right)\ln(1-z) \\
&+ \left(\frac{1}{6} + 8z^2 - \frac{32}{3}z^3\right)\ln z - \frac{7}{36} - \frac{7}{6}z + \frac{8}{3}z^2 - \frac{32}{9}z^3, \\
\Phi(z) &\equiv {\rm Li}_2\left(\frac{z-1}{z}\right) + \ln^2\frac{1-z}{z} - \frac{\pi^2}{6}.
\end{aligned}
\tag{38}
$$

By the second order photonic RC we mean here the contributions of Feynman diagrams with two photons. Each of them can be either real or virtual. Besides the photonic RC in the second order there are also pair corrections, their leading log contributions can be computed in the same way, see.[50,55]

## 6.2. *Kinoshita-Lee-Nauenberg theorem*

The large logs discussed above are divergent for $m_e \to 0$, in other words, they are a kind of *mass singularities*. Due to intrinsic (hidden) conformal properties of QED and QCD these mass singularities have a tendency to cancel out in inclusive observable quantities. The Kinoshita-Lee-Nauenberg (KLN) theorem[56,57] defines the conditions when the coefficients before the large logs do vanish. In practice we usually see that the large log terms from virtual loop corrections cancel out the corresponding terms coming from real radiation.

Let us formulate the theorem in the following way. If we *can not* or just *do not* distinguish the final states of a pure electron and of a combination of the electron with accompanying it photon(s), *i.e.* the energy and momentum of the *registered* electron is the sum of the energies and momenta of the bare electron and the photons $E_e^{\mathrm{observed}} = E_e + \Sigma E_\gamma$, then the large logarithm corresponding to collinear photon emission (see Eq. (26)) do not appear in the final answer. In the electron structure function approach the cancellation of the large logs is provided by the first property of the non-singlet function in Eq. (34).

In practice, cancellation of large logs happens for FSR corrections to (sufficiently) *inclusive observables* and for *calorimetric* electron registration. The large logs which come from the initial state radiation usually do not cancel out, since the KLN theorem conditions for them are not fulfilled. Also the large logs which appear in the correction due to vacuum polarization (in the QED running coupling constant) do not cancel out.

### 6.3. *Matching of LLA with $\mathcal{O}(\alpha)$ RC*

Having both complete $\mathcal{O}(\alpha)$ and LLA in $\mathcal{O}(\alpha^n L^n)$ $(n = 1, 2, \ldots)$ one should avoid the *double counting*. In fact, the first order correction already contains all terms of the order $\mathcal{O}\left(\alpha^1 L^1\right)$. The procedure which allows keep the correct first order result while adding the leading log corrections will be called here as *matching*. A possibility of such a matching is represented by the master formula (35). But as discussed above, the latter is valid only for sufficiently inclusive observables. Here we will show an example how to disentangle the double counting keeping at the same moment the possibility to impose experimental cuts on radiative events.

Let us consider the process of electron–positron annihilation into muons. First order corrections due to real hard photon emission in this process were discussed in Sect. 3.3. Adding of the higher order leading log terms provided by the electron structure function approach to the known Born and complete first order corrections can be done by the following formula:

$$
\begin{aligned}
\frac{\mathrm{d}\sigma^{e^+e^-\to\mu^+\mu^-(\gamma)}}{\mathrm{d}\Omega_-} &= \int\limits_{z_{\min}}^{1}\int\limits_{z_{\min}}^{1} \mathrm{d}z_1\mathrm{d}z_2\, \frac{\mathcal{D}(z_1,s)\mathcal{D}(z_2,s)}{|1-\Pi(sz_1z_2)|^2}\,\frac{\mathrm{d}\tilde{\sigma}_0(z_1,z_2)}{\mathrm{d}\Omega_-}\left(1+\frac{\alpha}{\pi}K\right) \\
&+\left\{\frac{\alpha^3}{2\pi^2 s^2}\int\limits_{\substack{k^0>\bar{\omega} \\ \widehat{kp_\pm}>\theta_0}} \frac{R_e|_{m_e=0}}{|1-\Pi(s_1)|^2}\,\frac{\mathrm{d}\Gamma}{\mathrm{d}\Omega_-} + \frac{D}{|1-\Pi(s_1)|^2}\right\} \\
&+\left\{\frac{\alpha^3}{2\pi^2 s^2}\int\limits_{k^0>\bar{\omega}}\left(\mathrm{Re}\,\frac{R_{e\mu}}{(1-\Pi(s_1))(1-\Pi(s))^*} + \frac{R_\mu}{|1-\Pi(s)|^2}\right)\frac{\mathrm{d}\Gamma}{\mathrm{d}\Omega_-}\right. \\
&\left.+\mathrm{Re}\,\frac{C_{e\mu}}{(1-\Pi(s_1))(1-\Pi(s))^*} + \frac{C_\mu}{|1-\Pi(s)|^2}\right\}, \qquad (39) \\
C_\mu &= \frac{2\alpha}{\pi}\frac{\mathrm{d}\sigma_0}{\mathrm{d}\Omega_-}\ln\frac{\bar{\omega}}{E}\left(\frac{1+\beta^2}{2\beta}\ln\frac{1+\beta}{1-\beta}-1\right), \qquad z_{\min} = \frac{2m_\mu}{2E-m_\mu}, \\
C_{e\mu} &= \frac{4\alpha}{\pi}\frac{\mathrm{d}\sigma_0}{\mathrm{d}\Omega_-}\ln\frac{\bar{\omega}}{E}\,\ln\frac{1-\beta c}{1+\beta c}, \qquad K = K_{\mathrm{odd}} + K_{\mathrm{even}},
\end{aligned}
$$

see notation and other details in Ref.[18] The condition $\widehat{kp_\pm} > \theta_0$ exclude the kinematical domain of collinear photon emission from the initial electron and positron. So, the corresponding large logs do not appear from the integral of the matrix element. They are coming, instead, from the structure functions. $K$ is the so-called *K-factor*, here it comes from virtual and soft photon corrections. The large logs which appear in this part of the correction are also removed. But it was explicitly demonstrated that the proper amount of large logs is restored by the structure functions also here.

## 7. General Remarks on RC

Let us summarize the present status of radiative correction calculations and discuss the general ways of their application.

1 Many analytical results are in the literature for QED, QCD and electroweak RC within the Standard Model. Radiative corrections have been studied in models beyond SM, like in the Minimal Supersymmetric SM or in the Chiral Perturbation Theory (an effective models for low energy strong interactions).
2 Advanced techniques of multi-loop and multi-leg diagrams calculation have been developed.
3 But still application of (even) well known results to a concrete case is rather non-trivial:
– old analytic calculations can have obsolete approximations,
– different effects should be combined properly,
– experimental conditions should be taken into account.
4 Semi-analytic codes like *e.g.* `ZFITTER`[58] and `HECTOR`[59] are well suited for inclusion of different effects.
5 But the best way is to incorporate RC into Monte Carlo event generators. This task is not simple because RC typically have kinematics (and dynamics) being much more complicated than the one of the Born approximation.
6 Dedicated Monte Carlo codes developed to describe a specific process are potentially more suitable for consistent inclusion of radiative corrections and interplay of other sub-leading effects that the General purpose MC programs like `PYTHIA, HERWIG, PHOTOS` *etc.*

So in these lectures, we have discussed general properties of radiative corrections. Most of the examples were given for the pure QED RC, but the QCD and electroweak corrections have very similar features. As we have seen above, radiative corrections could be as very small as well as very large. Only after a careful study of a particular process taking into account the conditions of the corresponding experiment one may get an idea about the magnitude of RC in the give case. We discussed also certain methods which help to extract the numerically most important contributions enhanced by large logarithms. Knowing the general features of radiative corrections should be also useful in application of existing ready-to-use solutions, *e.g.* computer codes or analytic formulae, to concrete problems in particle physics.

## References

1. J. Alcaraz *et al.* [LEP and ALEPH and DELPHI and L3 and OPAL and LEP Electroweak Working Group Collaborations], *Precision Electroweak Measurements and Constraints on the Standard Model*, [arXiv:0712.0929 [hep-ex]].
2. A. B. Arbuzov, V. S. Fadin, E. A. Kuraev, L. N. Lipatov, N. P. Merenkov, L. Trentadue, Nucl. Phys. B **485** (1997) 457.
3. A. Arbuzov, M. Bigi, H. Burkhardt *et al.*, Phys. Lett. B **383** (1996) 238.
4. A. A. Penin, Phys. Rev. Lett. **95** (2005) 010408.
5. R. Bonciani, A. Ferroglia, A. A. Penin, JHEP **0802** (2008) 080.
6. S. Actis, P. Mastrolia, G. Ossola, Phys. Lett. **B682** (2010) 419.
7. A.B. Arbuzov, JHEP **0801** (2008) 031.
8. A.B. Arbuzov, Phys. Lett. B **524** (2002) 99.
9. M. Fischer, S. Groote, J. G. Korner, M. C. Mauser, Phys. Rev. D **67** (2003) 113008.
10. T. Hahn, Comput. Phys. Commun. **140** (2001) 418.
11. R. Mertig, M. Bohm, A. Denner, Comput. Phys. Commun. **64** (1991) 345.
12. T. Hahn, M. Perez-Victoria, Comput. Phys. Commun. **118** (1999) 153.
13. G. Belanger, F. Boudjema, J. Fujimoto *et al.* Phys. Rept. **430** (2006) 117.
14. A. Andonov *et al.*, Comput. Phys. Commun. **174** (2006) 481; *ibid.* **181** (2010) 305.

15. D. Bardin, G. Passarino, *The Standard Model in the making: precision study of the electroweak interactions*, Clarendon Press, 1999.
16. A.I. Ahmadov, V.V. Bytev, E.A. Kuraev and E. Tomasi-Gustafsson, Phys. Rev. D **82** (2010) 094016.
17. D.R. Yennie, S.C. Frautschi, and H. Suura, Annals Phys. **13** (1961) 379.
18. A.B. Arbuzov, G.V. Fedotovich, E.A. Kuraev *et al.* JHEP **9710** (1997) 001.
19. R. Baldini, S. Pacetti, A. Zallo and A. Zichichi, Eur. Phys. J. A **39** (2009) 315.
20. M.B. Voloshin, Mod. Phys. Lett. A **18** (2003) 1783.
21. A. Sommerfeld, *Atmobau und Spektralinien*, F. Vieweg & Sohn: 1921.
22. J. Schwinger, *Particles, Sources, and Fields*, Perseus Books Publishing, Massachusetts, 1998, Vol.3.
23. G. Gamow, Z. Phys. **51** (1928) 204.
24. A.D. Sakharov, Sov. Phys. Usp. **34** (1991) 375.
25. V.S. Fadin, V.A. Khoze, Sov. J. Nucl. Phys. **48** (1988) 309.
26. V.S. Fadin, V.A. Khoze and T. Sjostrand, Z. Phys. C **48** (1990) 613.
27. D.Y. Bardin, W. Beenakker and A. Denner, Phys. Lett. B **317** (1993) 213.
28. A.B. Arbuzov, Nuovo Cim. A **107** (1994) 1263.
29. J.H. Yoon and C.Y. Wong, Phys. Rev. C **61** (2000) 044905.
30. J.H. Yoon and C.Y. Wong, J. Phys. G **31** (2005) 149.
31. O.P. Solovtsova, Yu.D. Chernichenko, Phys. Atom. Nucl. **73** (2010) 1612.
32. A.B. Arbuzov, D.Y. Bardin and A. Leike, Mod. Phys. Lett. A **7** (1992) 2029, *Erratum-ibid.* **9** (1994) 1515.
33. A.B. Arbuzov, V.A. Astakhov, A.V. Fedorov *et al.*, JHEP **9710** (1997) 006.
34. A. H. Hoang, Phys. Rev. D **56** (1997) 7276.
35. I.T. Todorov, Phys. Rev. D **3** (1971) 3251.
36. T. van Ritbergen, R.G. Stuart, Nucl. Phys. **B564** (2000) 343.
37. S. Actis, A. Arbuzov, G. Balossini *et al.* [ Working Group on Radiative Corrections and Monte Carlo Generators for Low Energies Collaboration ], Eur. Phys. J. C **66** (2010) 585.
38. H. Burkhardt, B. Pietrzyk, Phys. Rev. D **72** (2005) 057501.
39. F. Jegerlehner, Nucl. Phys. Proc. Suppl. **162** (2006) 22.
40. K. Hagiwara, R. Liao, A. D. Martin, D. Nomura, T. Teubner, J. Phys. G **G38** (2011) 085003.
41. S. J. Brodsky, L. Frankfurt, J. F. Gunion, A. H. Mueller and M. Strikman, Phys. Rev. D **50** (1994) 3134.
42. J.C. Collins, L. Frankfurt and M. Strikman, Phys. Rev. D **56** (1997) 2982.
43. D.V. Shirkov, “Evolution of the Bogoliubov renormalization group”, In Mitra, A.N. (ed.): *Quantum field theory*, 25-58 [arXiv:hep-th/9909024].
44. V.N. Gribov, L.N. Lipatov, Sov. J. Nucl. Phys. **15** (1972) 438.
45. V.N. Gribov and L.N. Lipatov, Sov. J. Nucl. Phys. **15** (1972) 675.
46. L.N. Lipatov, Sov. J. Nucl. Phys. **20** (1975) 94.
47. G. Altarelli and G. Parisi, Nucl. Phys. B **126** (1977) 298.
48. Y.L. Dokshitzer, Sov. Phys. JETP **46** (1977) 641.
49. F.A. Berends, W.L. van Neerven and G.J.H. Burgers, Nucl. Phys. B **297** (1988) 429 [Erratum-ibid. B **304** (1988) 921].
50. A. Arbuzov and K. Melnikov, Phys. Rev. D **66** (2002) 093003.
51. W.A. Bardeen, A.J. Buras, D.W. Duke, and T. Muta, Phys. Rev. D **18** (1978) 3998.
52. A.B. Arbuzov and E.S. Scherbakova, Phys. Lett. B **660** (2008) 37.
53. A.B. Arbuzov and E.S. Scherbakova, JETP Lett. **83** (2006) 427.
54. T. Kinoshita and A. Sirlin, Phys. Rev. **113** (1959) 1652.
55. A. Arbuzov, A. Czarnecki, and A. Gaponenko, Phys. Rev. D **65** (2002) 113006.
56. T. Kinoshita, J. Math. Phys. **3** (1962) 650-677.
57. T.D. Lee, M. Nauenberg, Phys. Rev. **133** (1964) B1549-B1562.
58. A. B. Arbuzov, M. Awramik, M. Czakon *et al.*, Comput. Phys. Commun. **174** (2006) 728.
59. A. Arbuzov, D.Y. Bardin, J. Blumlein, L. Kalinovskaya and T. Riemann, Comput. Phys. Commun. **94** (1996) 128-184.

# On the possibility and necessity of space-time unified descriptions for electromagnetic Form Factors

R. Baldini Ferroli

*Centro Studi e Ricerche e Museo Storico della Fisica "Enrico Fermi", Roma and INFN Laboratori Nazionali di Frascati, Frascati, Italy*

S. Pacetti

*Dipartimento di Fisica, Università di Perugia, and INFN, Sezione di Perugia, Italy*

Electromagnetic form factor represent the only experimental probe for non-perturbative quantum chromodynamics. They allow to access information on the parton structure of hadrons in terms of energy-dependent couplings to photons. New sets of data, mainly in time-like region, coming from flavor-factories, make possible more accurate analyses which require a deeper understanding of hadron structure and more sophisticated fitting techniques.

*Keywords*: .

## 1. Introduction

Electromagnetic form factors (FFs) describe modifications of pointlike photon-hadron vertices due to the structure of hadrons. The photon, interacting with single elementary charges, the quarks, represents a powerful probe for the internal structure of composite particles. Furthermore, being the electromagnetic leptonic interaction exactly calculable in QED, the dynamical content of each vertex can be easily extract from data.

### 1.1. *Nucleon Form Factors*

The elastic scattering of an electron by a nucleon $e^- N \to e^- N$ is represented, in Born approximation, by the diagram of fig. 1, in the vertical direction. In this kinematic region the four-momentum of the virtual photon is space-like and hence its squared value is negative: $q^2 = -2\omega_1\omega_2(1-\cos\theta_e) \leq 0$, being $\omega_{1(2)}$ the energy of the incoming (outgoing) electron and $\theta_e$ the scattering angle.
The same diagram of fig. 1, but in the horizontal direction, represents the annihilation $e^+e^- \to N\overline{N}$ or $N\overline{N} \to e^+e^-$. For these processes the four-momentum $q$ is time-like, in fact: $q^2 = (2\omega)^2 \geq 0$, where $\omega \equiv \omega_1 = \omega_2$ is the common value of the lepton energy in the $e^+e^-$ center of mass frame (CM).
The Feynman amplitude for the elastic scattering is

$$\mathcal{M} = \frac{1}{q^2}[e\,\overline{u}(k_2)\gamma^\mu u(k_1)][e\,\overline{U}(p_2)\Gamma_\mu(p_1,p_2)U(p_1)]\,, \tag{1}$$

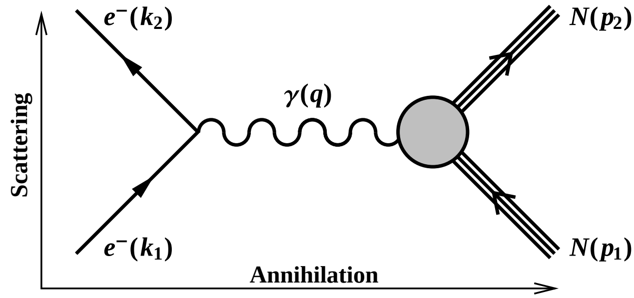


Fig. 1. One-photon exchange Feynman diagram for scattering $e^-N \to e^-N$ and annihilation $e^+e^- \to N\overline{N}$.

where the four-momenta follow the labelling of fig. 1, $u$ and $U$ are the electron and nucleon spinors, and $\Gamma^\mu$ is a non-constant matrix which describes the nucleon vertex. Using gauge and Lorentz invariance the most general form of such a matrix is[1]

$$\Gamma^\mu = \gamma^\mu F_1(q^2) + \frac{i\sigma^{\mu\nu}q_\nu}{2M} F_2(q^2)\,, \tag{2}$$

where $M$ is the nucleon mass. $\Gamma^\mu$ depends on two Lorentz scalar functions of $q^2$, $F_1(q^2)$ and $F_2(q^2)$ called Dirac and Pauli FFs, they describe the non-helicity-flip and the helicity-flip part of the hadronic current respectively. Normalizations at $q^2 = 0$ follow from total charge and magnetic moment conservation and are

$$F_1(0) = Q_N\,, \qquad F_2(0) = \kappa_N\,, \tag{3}$$

where $Q_N$ is the electric charge (in units of $e$) and $\kappa_N$ the anomalous magnetic moment (in units of the Bohr magneton $\mu_B$) of the nucleon $N$.
Other pairs of FFs can be defined as combinations of $F_1$ and $F_2$, of particular interest are the so-called Sachs FFs $G_E$ and $G_M$[2] that can be obtained from the hadronic current written in a special frame, i.e. the Breit frame. Indeed in such a frame the transferred four-momentum $q$ is purely space-like: $q = (0, \vec{q})$ and the nucleon momentum, during the scattering, passes from $-\vec{q}/2$ to $+\vec{q}/2$. Under these conditions the hadronic current gets the standard form of an electromagnetic four-current, i.e. the time and the space-component are Fourier transformations of a charge density and a current density respectively, i.e.:

$$\begin{cases} \rho_q = J^0 = e\left[F_1 + \dfrac{q^2}{4M^2}F_2\right] \\[2ex] \vec{J}_q = e\,\overline{U}(p_2)\vec{\gamma}U(p_1)\,[F_1 + F_2]\,. \end{cases} \tag{4}$$

As a consequence, Sachs electric and magnetic FFs are defined through the combinations

$$\begin{cases} G_E = F_1 + \dfrac{q^2}{4M^2}F_2 \\[2ex] G_M = F_1 + F_2\,. \end{cases} \tag{5}$$

At the time-like production threshold $q^2 = 4M^2$, assuming only $S$-wave contribution, that is, a non singular behavior for $F_1$ and $F_2$, the Sachs FFs are equal each other, i.e.:

$$G_E(4M^2) = G_M(4M^2)\,. \tag{6}$$

The normalization of the Sachs FFs at $q^2 = 0$ follows from their interpretation in terms of Fourier transformations of charge and magnetic moment distributions and it is

$$G_E(0) = Q_N\,, \qquad G_M(0) = \mu_N\,, \tag{7}$$

where $\mu_N = Q_N + \kappa_N$ is the nucleon magnetic moment in units of the Bohr magneton $\mu_B$.

### 1.2. *Time-like region, analytic properties and asymptotic behavior*

Analyticity of nucleon FFs as functions of $q^2$ is guaranteed by the microcausality[3] and the unitarity, implemented through the optical theorem,[4] defines discontinuities in the $q^2$ complex plane. Nucleon FFs are real in the space-like region, i.e. for $q^2 \leq 0$. In the time-like region, for positive $q^2$, the photon carries enough virtual mass to couple with intermediate, on-shell states.

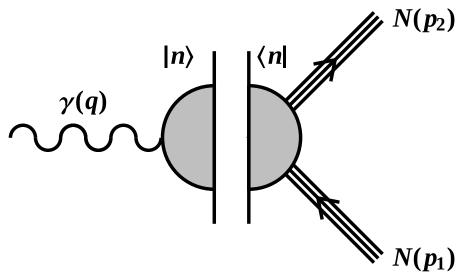


Fig. 2. Spectral decomposition of the time-like nucleon vertex.

Therefore, using the optical theorem as schematically represented in fig. 2, the imaginary part of the amplitude which describes the coupling of the photon to the nucleon-antinucleon pair can be decomposed as

$$\mathrm{Im}\left[\langle \overline{N}(p_1)N(p_2)|J|0\rangle\right] \sim \sum_n \langle \overline{N}(p_1)N(p_2)|J^\dagger|n\rangle\langle n|J|0\rangle\,, \tag{8}$$

where $n$ runs over all the hadronic intermediate states allowed by conservation laws. The lightest hadronic state to be considered, and hence the first that opens, is the $\pi^+\pi^-$ channel. It follows that the amplitude as well as the FFs, which characterize the $q^2$ dependence of the nucleon current, acquire an imaginary part different from zero starting from the so-called theoretical threshold $s_0 = (2M_\pi)^2$. The FFs are then analytic functions in the whole $q^2$ complex plane, shown in fig. 3, with a discontinuity cut, over the real axis (time-like region), from $s_0$ up to infinity.
Such a cut is the superposition of the infinite possible intermediate states that can couple with the virtual photon and produce the final nucleon-antinucleon pair.
In the framework of perturbative QCD (pQCD), the FF asymptotic behavior in the space-like region, i.e. as $q^2 \to -\infty$, is driven by two principles: the quark counting rule[5] and the hadronic helicity conservation.[6] At asymptotically large values of $-q^2$, the photon has sufficiently large virtuality to see the nucleon made of three collinear quarks, as sketched in fig. 4. To keep the nucleon intact, the momentum transferred by the photon has to be shared among the constituent quarks. The minimal action to be done in order to guarantee the partitioning of $q$ is represented by two gluon exchanges as shown in fig. 4. The corresponding two gluon propagators give the power low $(-q^2)^{-2}$ for the FF. More in detail, for the Dirac and Pauli FFs the asymptotic power laws are

$$\lim_{q^2\to-\infty} F_1(q^2) \sim \left(\frac{1}{-q^2}\right)^2\,, \qquad \lim_{q^2\to-\infty} F_2(q^2) \sim \left(\frac{1}{-q^2}\right)^3\,. \tag{9}$$

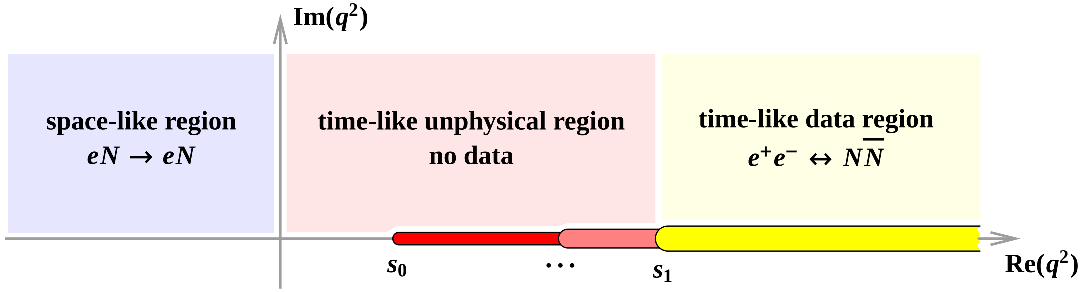


Fig. 3. The $q^2$ complex plane with the discontinuity on the real axis given by the superposition of all the intermediate-channel cuts.

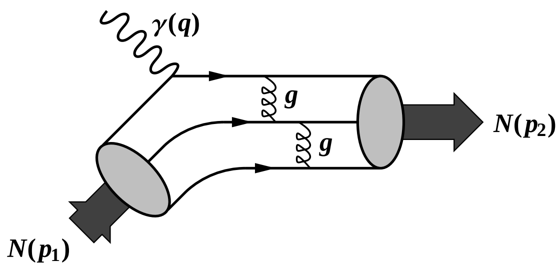


Fig. 4. A photon at large virtuality interacts with the nucleon.

The Pauli FF $F_2(q^2)$ is connected to the helicity-violating part of the hadronic current and, since the helicity flip involves, at leading order, a further gluon-exchange and hence an additional gluon propagator, the resulting power law is $(-q^2)^{-3}$, as reported in eq. (9). The Sachs FFs, defined in eq. (5), have the same asymptotic power law, i.e.

$$\lim_{q^2\to-\infty} G_{E,M}(q^2) \sim \left(\frac{1}{-q^2}\right)^2 . \tag{10}$$

The asymptotic behavior in the time-like region can be inferred from the space-like one invoking the Phragmén-Lindelöf theorem[a].[7] In fact, having that the FFs are regular and bounded in the whole upper half $q^2$-complex plane ($\mathrm{Im}\, q^2 \geq 0$), the limits along the two lines that define this region, the negative and positive real axes, must be equal, i.e.:

$$\underbrace{\lim_{q^2\to+\infty} G_{E,M}(q^2)}_{\text{time-like}} = \underbrace{\lim_{q^2\to-\infty} G_{E,M}(q^2)}_{\text{space-like}} \sim \left(\frac{1}{|q^2|}\right)^2 . \tag{11}$$

Since in the time-like region FFs are complex, the fact that they vanish as real functions means that the imaginary part vanishes faster than the real one or, in other words, that the phase, as $q^2 \to +\infty$, tends to integer multiples of $\pi$ radians.

[a]The Phragmén-Lindelöf theorem states that: given an analytic function $f(z)$, such that $f(z) \to a$ as $z \to \infty$ along a straight line, and $f(z) \to b$ as $z \to \infty$ along another straight line, if $f(z)$ is regular and bounded in the angle between these two lines, then $a = b$ and $f(z) \to a$ uniformly in this angle.

### 1.3. *Cross sections*

Data on nucleon FFs can be obtained studying angular distributions of differential cross sections for the scattering $e^-N \to e^-N$ and the annihilation $e^+e^- \leftrightarrow N\overline{N}$. In particular, as it is shown in the schematic representation of fig. 3:

- from elastic scattering we gain information on the real values of FFs in the space-like region ($q^2 \le 0$);
- from annihilation cross sections we extract the moduli of the FFs above the physical threshold $s_1 = (2M)^2$;
- in the remaining energy interval, from $q^2 = 0$ up to $q^2 = s_1$, the so-called "unphysical region", FFs are not experimentally accessible even though, thanks to the analyticity, they are still well defined.

The differential cross section for the elastic scattering $e^-N \to e^-N$ in the laboratory frame, i.e. $p_1 = (M, \vec{0})$, and in Born approximation is

$$\frac{d\sigma}{d\cos\theta_e} = \frac{\pi\alpha^2\omega_2\cos^2\frac{\theta_e}{2}}{2\,\omega_1^3\sin^4\frac{\theta_e}{2}}\left\{G_E(q^2)^2 - \tau\left[1 + 2(1-\tau)\tan^2\frac{\theta_e}{2}\right]G_M(q^2)^2\right\}\frac{1}{1-\tau}\,, \tag{12}$$

where: $\tau = q^2/(2M)^2$, $\theta_e$ is the lepton scattering angle and $\omega_{1(2)}$ is the energy of the incoming (outgoing) lepton. The expression of eq. (12) is known as the Rosenbluth formula.[8]

The differential cross section for the crossed process of the scattering, i.e. the annihilation $e^+e^- \to N\overline{N}$, in the CM is[9]

$$\frac{d\sigma}{d\cos\theta} = \frac{\pi\alpha^2}{2\,q^2}\beta C_{Q_N}\left[(1+\cos^2\theta)\left|G_M(q^2)\right|^2 + \frac{1}{\tau}\sin^2\theta\left|G_E(q^2)\right|^2\right],\quad \beta = \sqrt{1-\frac{1}{\tau}}\,, \tag{13}$$

where $\beta$ is the velocity of the outgoing nucleon and $C_{Q_N}$ is the so-called Coulomb factor[10]

$$C_{Q_N} = \begin{cases} \dfrac{\pi\alpha/\beta}{1-\exp(-\pi\alpha/\beta)} & Q_N = 1 \\[2ex] 1 & Q_N = 0\,. \end{cases} \tag{14}$$

It accounts for the electromagnetic $N\overline{N}$ final state interaction and corresponds to the squared value of the Coulomb scattering wave function at the origin.

## 2. Data and discoveries in the time-like region

The total cross section for production processes: $e^+e^- \to N\overline{N}$ can be obtained from eq. (13) via angular integration and it reads

$$\sigma(e^+e^- \to N\overline{N}) = \frac{4\pi\alpha^2}{3\,q^2}\beta C_{Q_N}\left[\left|G_M(q^2)\right|^2 + \frac{1}{2\tau}\left|G_E(q^2)\right|^2\right]. \tag{15}$$

The cross section of the time-reversed process $N\overline{N} \to e^+e^-$ is related to the previous one through the proportionality relation: $\sigma(N\overline{N} \to e^+e^-) = \sigma(e^+e^- \to N\overline{N})\frac{|\vec{k}_1|^2}{|\vec{p}_1|^2} = \frac{\sigma(e^+e^-\to N\overline{N})}{\beta^2}$, and hence

$$\sigma(N\overline{N} \to e^+e^-) = \frac{4\pi\alpha^2}{3\,q^2}\frac{C_{Q_N}}{\beta}\left[\left|G_M(q^2)\right|^2 + \frac{1}{2\tau}\left|G_E(q^2)\right|^2\right]. \tag{16}$$

Obviously the only difference between the expressions of eq. (15) and (16) lies in the phase-space factor, the dynamical content, represented by the quantity inside the square brackets, is the same.

### 2.1. *The $p\overline{p}$ case*

In order to have comparable data, what usually experiments give is an effective FF obtained under the working hypothesis $|G_E(q^2)| = |G_M(q^2)|$. This assumption is exactly true only at the threshold $q^2 = s_1 = 4M^2$ [see eq. (6)].

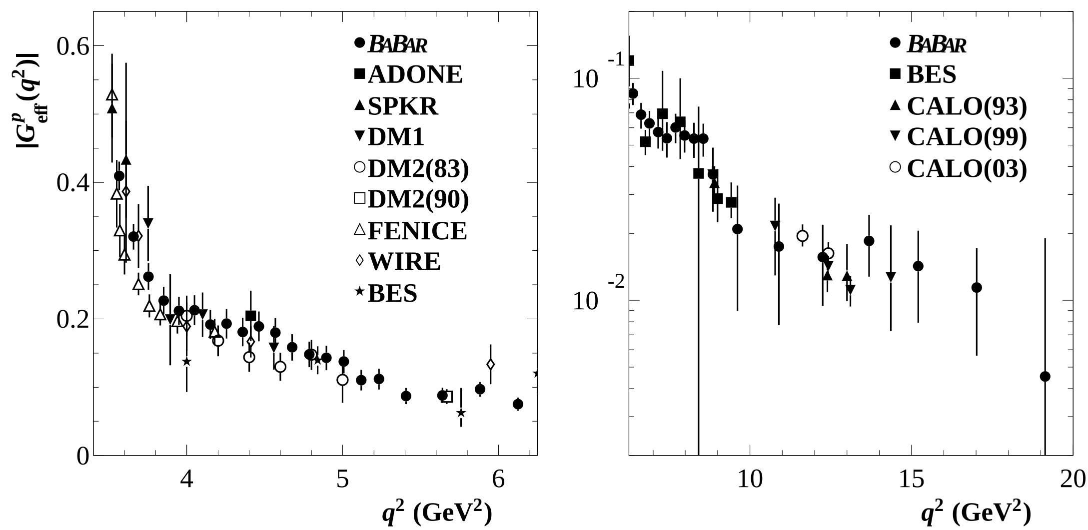


Fig. 5. Worldwide collection of data on $|G^p_{\rm eff}(q^2)|$. The experiments are: BABAR,[11] ADONE,[12] SPKR,[13] DM1,[14] DM2(83),[15] DM2(90),[16] FENICE,[17] WIRE,[18] BES,[19] CALO(93),[20] CALO(99),[21] CALO(03).[22]

Using the cross section $\sigma(e^+e^- \to p\overline{p})$ from eq. (15) and $\sigma(p\overline{p} \to e^+e^-)$ from eq. (16) in the proton case, i.e. with $N \equiv p$, such an effective FF can be extracted from data through

$$\left|G^p_{\rm eff}(q^2)\right| = \sqrt{\frac{\sigma(e^+e^- \to p\overline{p})}{\frac{4\pi\alpha^2}{3q^2}\beta C_1\left(1+\frac{1}{2\tau}\right)}} = \sqrt{\frac{\sigma(p\overline{p} \to e^+e^-)}{\frac{4\pi\alpha^2}{3q^2}\frac{C_1}{\beta}\left(1+\frac{1}{2\tau}\right)}}\,, \tag{17}$$

where the second identity holds under the assumption of time-reversal symmetry. In terms of Sachs FFs, $|G^p_{\rm eff}|$ corresponds to the following expression

$$\left|G^p_{\rm eff}(q^2)\right| = \sqrt{\frac{2\tau\left|G_M(q^2)\right|^2 + \left|G_E(q^2)\right|^2}{2\tau+1}}\,. \tag{18}$$

The worldwide collection of data on $|G^p_{\rm eff}|$ is shown in fig. 5. It is interesting to note that at large $q^2$, even though $|G^p_M| \to |G^p_E|$, the effective FF $|G^p_{\rm eff}|$ goes to $|G^p_M|$.

#### 2.1.1. *Production of $p\overline{p}$ at threshold*

BABAR has measured the cross section of the process

$$e^+e^- \to p\overline{p}$$

with unprecedented accuracy, collecting more then 4000 events in a wide rage of $p\overline{p}$ invariant mass: from threshold up to $\sim$ 4 GeV. The measurement has been performed by using the initial state radiation technique (ISR) and detecting the radiated photon.

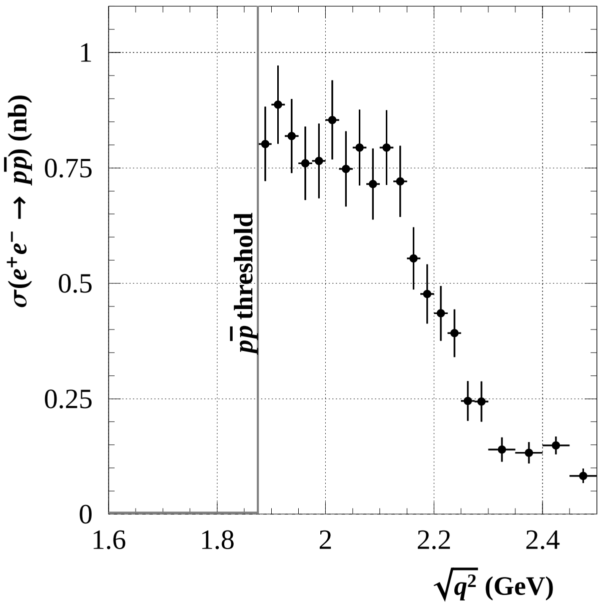


Fig. 6. Low-energy $e^+e^- \to p\overline{p}$ total cross section as measured by BABAR.[11] The gray vertical line indicates the production threshold.

Besides the unavoidable drawback to have a reduced luminosity by about a factor of $\alpha$, the main advantages in using this technique are:

- the detection efficiency is quite high even at the production threshold, i.e. when the $p\overline{p}$-system invariant mass is equal to $2M$. This is a consequence of the fact that the $p\overline{p}$ pair is produced together with a photon and hence it has always a boost in the laboratory frame which makes the detection possible for any $p\overline{p}$ invariant mass;
- an energy resolution of $\sim$ 1 MeV for the hadronic system;
- a full angular acceptance, even at $0^o$ and $180^o$, due to the detection of the radiated photon.

Figure 6 shows low-energy BABAR data on the $e^+e^- \to p\overline{p}$ total cross section. At the production threshold such a cross section is suddenly different from zero and then it maintains an almost constant values for about 200 MeV. At leading order, as $q^2 \to 4M^2$, the behavior of the cross section $\sigma(e^+e^- \to p\overline{p})$, reported in eq. (15), is guided by the phase-space factor and hence it should vanish like the velocity $\beta = \sqrt{1 - 4M^2/q^2}$. However, since we are producing a pair of charged particles, the Coulomb correction has to be considered. This correction is represented by the factor $C_1$ defined in eq. (14), that, close to threshold, when $\beta \to 0$, goes like $(\pi\alpha/\beta)$ and then *it compensates the vanishing of the phase-space*. In light of that, the threshold cross section can be computed in terms of the modulus of $G^p(4M^2)$, the common value of $G_E^p$ and $G_E^p$ at $q^2 = 4M^2$ [eq. (6)], and it is[23]

$$\sigma(e^+e^- \to p\overline{p})(4M^2) = \frac{\pi^2\alpha^3}{2M^2} \times \left|G^p(4M^2)\right|^2 = (0.85\,\text{nb}) \times \left|G^p(4M^2)\right|^2 , \tag{19}$$

that, compared with the *BABAR* threshold measurement[11]

$$\sigma(e^+e^- \to p\overline{p})(4M^2) = 0.85 \pm 0.05\,\mathrm{nb}\,,$$

gives the FF normalization:

$$|G^p(4M^2)| = 1.00 \pm 0.05\,. \tag{20}$$

This means that the proton and the antiproton, at the production threshold, *behave like a pointlike fermion pair*, i.e. their hadronic structure does not have any effect.

Even though, the identity of eq. (20) corresponds to the normalizations of $G_E^p(q^2)$ and $G_M^p(q^2)/\mu_p$ at $q^2 = 0$, as reported in eq. (7), the validity of similar constraints in the time-like region is completely unexpected. In fact, at that value of $q^2$, the interpretation of FFs as Fourier transformations of charge and magnetization distributions, which underlies the identities of eq. (7), does not make any sense. Micorscopic models[24] describing nucleon FFs in both space and time-like regions can be easily tuned to fulfil the normalization of eq. (20).

As already pointed out in § 1.1, the hadronic current can be parametrized in terms of different pairs of FFs. Besides $F_{1,2}^p$ and $G_{E,M}^p$, also a partial-wave decomposition can be considered. Indeed, parity conservation allows only $L = 0$ and $L = 2$ angular momentum for the $p\overline{p}$ system, hence we can use the $S$ and $D$-wave FFs $G_S^p$ and $G_D^p$. They can be defined as

$$G_S^p = \frac{2G_M^p\sqrt{\tau} + G_E^p}{3}\,, \qquad G_D^p = \frac{G_M^p\sqrt{\tau} - G_E^p}{3}\,, \tag{21}$$

and the total cross section of eq. (15), written in terms of $G_S^p$ and $G_D^p$, becomes

$$\sigma(e^+e^- \to p\overline{p}) = \frac{2\pi\alpha^2}{q^2}\,\frac{\beta}{\tau}\left[C_1\left|G_S^p(q^2)\right|^2 + 2\left|G_D^p(q^2)\right|^2\right]. \tag{22}$$

Here the Coulomb correction $C_1$ affects the only $S$ wave because the $D$ wave vanishes at the origin.

With a mild assumption on the relative phase between $G_E^p$ and $G_M^p$, and using the *BABAR* data on the ratio $|G_E^p|/|G_M^p|$ and total cross section[11] shown in fig. 7, time-like values of $|G_S^p|$ and $|G_D^p|$ can be extracted. Figure 8 shows moduli of $S$ and $D$-wave FFs, obtained with this procedure in Ref.,[25] and the function $1/\sqrt{\mathcal{R}}$, where $\mathcal{R}$ is the resummation factor of the Coulomb correction. More in detail, the function $C_1$ defined in eq. (14) is usually written as the product of an enhancement factor $\mathcal{E}$ and a resummation factor $\mathcal{R}$, with

$$\mathcal{E} = \frac{\pi\alpha}{\beta}\,, \qquad \mathcal{R} = \frac{1}{1 - \exp(-\pi\alpha/\beta)}\,. \tag{23}$$

*BABAR* data proved that

$$|G_S^p(q^2)| \simeq \frac{1}{\sqrt{\mathcal{R}}} = \sqrt{1 - \exp(-\pi\alpha/\beta)}\,, \qquad \text{for } q^2 \in (4M^2, \sim 4\,\mathrm{GeV}^2)\,,$$

i.e.: the $S$-wave FF, close to threshold, is in striking agreement with the function $1/\sqrt{\mathcal{R}}$, as it is shown in fig. 8. It follows that, a Coulomb correction, $\widetilde{C}_1$, with the only enhancement factor should imply an $S$-wave FF, $\widetilde{G}_S^p$, which remains almost constant and equal to one for about 200 MeV above threshold, i.e.

$$C_1 = \mathcal{E}\times\mathcal{R} \;\longrightarrow\; \widetilde{C}_1 = \mathcal{E} \;\Longrightarrow\; |\widetilde{G}_S^p(q^2)| \sim 1\,, \qquad \text{for } q^2 \in (4M^2, \sim 4\,\mathrm{GeV}^2)\,. \tag{24}$$

A naïve explanation[25] for the introduction of the “rescaled” factor $\widetilde{C}_1$ of eq. (24) could be the existence of a cutoff for the Coulomb dominance that, in case of baryons, is hundred times greater than that expected for pointlike charged fermions.

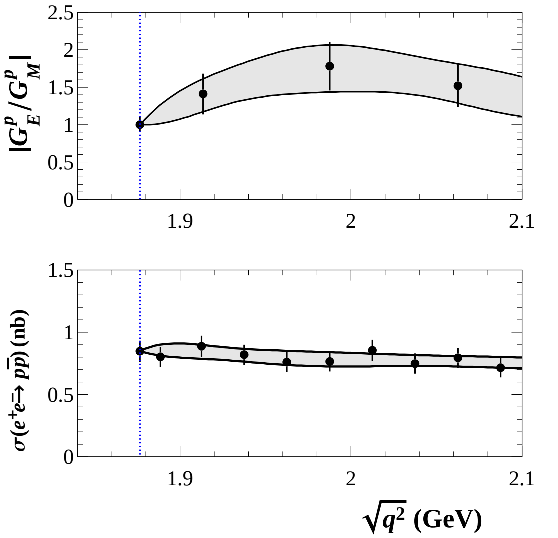


Fig. 7. Top figure: modulus of the ratio $|G_E^p/G_M^p|$; bottom figure: $e^+e^- \to p\bar{p}$ total cross section. The gray bands are the fits, while the dotted vertical line indicates the $p\bar{p}$ production threshold.

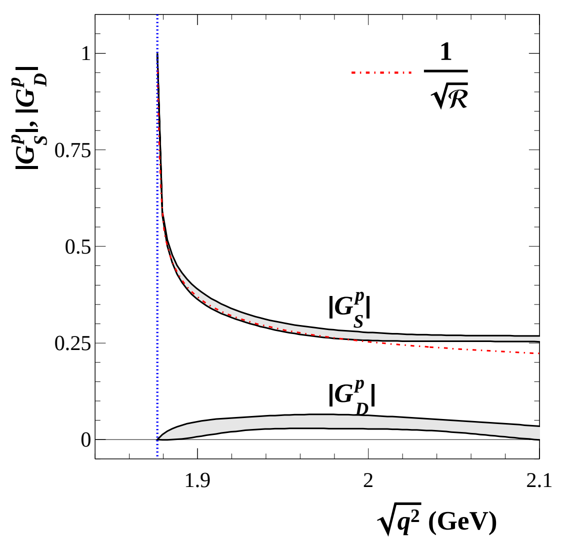


Fig. 8. $|G_S^p|$ and $|G_D^p|$ obtained using the ratio $|G_E^p/G_M^p|$, the total $p\bar{p}$ cross section. The dot-dashed curve is the inverse of the square root of the resummation factor of eq. (23), the dotted line is the $p\bar{p}$ production threshold.

### 2.2. *The ratio* $|G_E^p/G_M^p|$

For the first time BABAR has measured the modulus of the ratio between electric and magnetic FFs in the annihilation $e^+e^- \to p\bar{p}$. There exists only one previous attempt done by the WIRE Collaboration, but in the time-reversed process $p\bar{p} \to e^+e^-$.[18] Recently, performing a re-analysis of old data sets from; the $e^+e^-$ experiments FENICE and DM2, and the $p\bar{p}$ experiment E835, two new points have been added.[26] Figure 9 shows all available data in the time-like region for the modulus of the ratio

$$R(q^2) = \mu_p \, \frac{G_E^p(q^2)}{G_M^p(q^2)} \,. \tag{25}$$

The horizontal line represents the so called "scaling", i.e. the identity $|G_E^p| = |G_M^p|$, that, in principle, holds only at the threshold, see eq. (6), where not only moduli but also phases coincide. In particular the validity of the scaling above threshold has been definitively disproved by BABAR (fig. 9) that measured for the first time the inequality

$$|G_E^p(q^2)| > |G_M^p(q^2)| \,, \qquad \text{for } q^2 \sim 2\,\text{GeV}^2 \,. \tag{26}$$

From the theoretical point of view the ratio $R(q^2)$ is an analytic function in the whole $q^2$-complex plane with the cut $(s_0, \infty)$, as each single FFs (see § 1.2), it follows that its time-like and space-like values are intimately related. In particular, the time-like enhancement has been connected with the space-like data that show, instead, a decreasing behavior.[27]

Furthermore, time-like data on $|R|$ can be used to estimate the two-photon contribution in the process $e^+e^- \to p\bar{p}$. Indeed, the two-photon exchanged annihilation $e^+e^- \to \gamma^*\gamma^* \to p\bar{p}$ has positive charge conjugation, $C = +1$, hence its amplitude interferes with the $C = -1$ Born amplitude, originating terms with odd powers of $\cos\theta$ in the angular distribution. A study performed on the BABAR data gave an estimate for two-photon exchange contribution of the order of few %,[28] in agreement with natural expectations for radiative corrections.

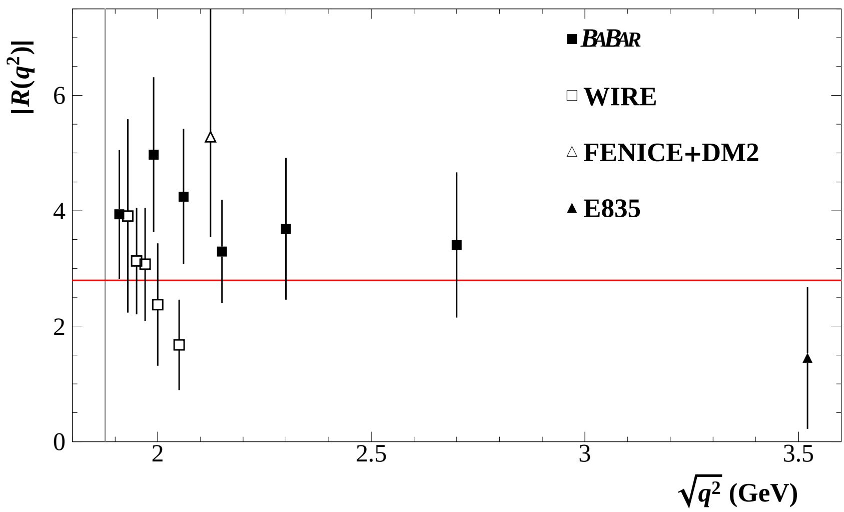


Fig. 9. Modulus of the ratio $R = \mu_p G_E^p / G_M^p$. BABAR data[11] (solid squares) are compared with WIRE[18] data (empty squares) and two other points obtained from reanalyses of old data sets (triangles). The horizontal line indicates the identity $|G_E^p| = |G_M^p|$, i.e. $R = \mu_p$, while the vertical line is the threshold.

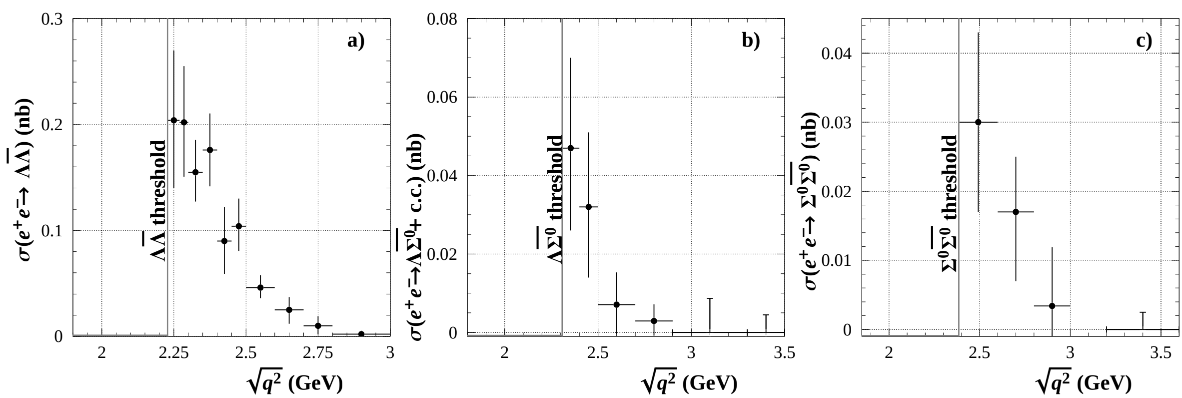


Fig. 10. $e^+e^- \to \Lambda\overline{\Lambda}$ (a), $e^+e^- \to \Lambda\overline{\Sigma^0} + \overline{\Lambda}\Sigma^0$ (b) and $e^+e^- \to \Sigma^0\overline{\Sigma^0}$ (c) total cross sections measured by the BABAR[29] experiment. The gray vertical lines indicate the production thresholds.

## 2.3. *Strange baryons*

The peculiar behavior shown by the $e^+e^- \to p\overline{p}$ process, i.e. a cross section which is suddenly different from zero at threshold where it reaches its maximum value and then decreases uniformly, has been observed also in other reactions where baryon-antibaryon pairs are produced via $e^+e^-$ annihilation. BABAR measured total cross sections for the processes: $e^+e^- \to \Lambda\overline{\Lambda}$, $e^+e^- \to \Lambda\overline{\Sigma^0} + \overline{\Lambda}\Sigma^0$ and $e^+e^- \to \Sigma^0\overline{\Sigma^0}$ using the ISR technique,[29] in particular $\sigma(e^+e^- \to \Lambda\overline{\Sigma^0} + \overline{\Lambda}\Sigma^0)$ and $\sigma(e^+e^- \to \Sigma^0\overline{\Sigma^0})$ have been measured for the first time, while for $\sigma(e^+e^- \to \Lambda\overline{\Lambda})$ there exists only one previous data point from the DM2 collaboration.[16] Figure 10 shows the cross section data that, even if with larger errors, have the same trend as the $p\overline{p}$ data. The interesting thing is that in all these processes the involved baryons are neutral and hence no "standard" Coulomb correction is expected. A possible explanation, still based on the copositness of the baryons, could be that threshold behaviors

are due to remnants of Coulomb interactions but at quark level.[25]
A study of these strange baryon FFs using $U$-spin[30] relationships, and hence flavor-$SU(3)$ invariance also in the low-$q^2$ region, could be justified by their small mass differences. In particular, assuming negligible electromagnetic transitions between $U$-spin triplet and singlet, one can set the following relation among magnetic moments

$$\mu_\Lambda = \mu_{\Sigma_0} + \frac{2}{\sqrt{3}}\mu_{\Lambda\overline{\Sigma^0}}$$

that could be interpreted as the FF normalization

$$G_\Lambda = G_{\Sigma_0} + \frac{2}{\sqrt{3}}G_{\Lambda\overline{\Sigma^0}}\,,$$

that should hold at least at some $q^2$ value. In the time-like region at the production threshold the electric and magnetic FFs coincide and are exactly proportional to the square root of the cross section, hence, at this momentum transferred, the previous relationship can be written in terms of masses and cross sections as

$$M_\Lambda\sqrt{\sigma_{\Lambda\overline{\Lambda}}} = M_{\Sigma_0}\sqrt{\sigma_{\Sigma^0\overline{\Sigma^0}}} + \frac{2}{\sqrt{3}}\overline{M}_{\Lambda\Sigma_0}\sqrt{\sigma_{\Lambda\overline{\Sigma^0}}}\,.$$

If we use threshold values extrapolated from the lowest energy point of the three BABAR data sets shown in fig. 10, we can check this identity by evaluating the ratio

$$\frac{\left|M_\Lambda\sqrt{\sigma_{\Lambda\overline{\Lambda}}} - M_{\Sigma_0}\sqrt{\sigma_{\Sigma^0\overline{\Sigma^0}}} - (2/\sqrt{3})\overline{M}_{\Lambda\Sigma_0}\sqrt{\sigma_{\Lambda\overline{\Sigma^0}}}\right|}{M_\Lambda\sqrt{\sigma_{\Lambda\overline{\Lambda}}} + M_{\Sigma_0}\sqrt{\sigma_{\Sigma^0\overline{\Sigma^0}}} + (2/\sqrt{3})\overline{M}_{\Lambda\Sigma_0}\sqrt{\sigma_{\Lambda\overline{\Sigma^0}}}} = 0.01 \pm 0.10\,. \tag{27}$$

Despite the large error due the low statistics of the data, this result is impressive. In fact, the connection among the threshold values of these quite different cross sections (the data are spread in a wide range, from tens to hundreds of picobarns) is incredibly good.
However, vanishing cross sections at threshold, raising according to the baryon velocity phase space factor, cannot be excluded by the present BABAR data.[25] More precise measurements are needed to settle this issue.
Furthermore, in the case of $\Lambda\overline{\Lambda}$ production there is the unique opportunity to access the complex structure of the $\Lambda$ electric and magnetic FFs. Indeed, studying the angular distribution of the decay $\Lambda \to p\pi^-$ ($\overline{\Lambda} \to \overline{p}\pi^+$) it is possible to measure the $\Lambda$ ($\overline{\Lambda}$) polarization, whose component perpendicular to the scattering plane is proportional to the sine of the relative phase between $G_E^\Lambda$ and $G_M^\Lambda$.[31] A first attempt to determine this phase has been done,[29] but the limited statistics did allow only a poor estimate.

Figure 11 shows data on the $e^+e^- \to n\overline{n}$ total cross section. There are only two measurements; the first one done in 1993 by the FENICE Collaboration in Frascati[32] and a more recent set obtained in 2011 by the SND experiment[33] at the VEPP-2000 collider in Novosibirsk. The red curve is a fit of the first four data points done using a dipole-type effective FF, with two free parameters.
Even though there are no well establish predictions for such a cross section, the obtained values appear quit high. Indeed, by using as $n\overline{n}$ effective FF the measured $p\overline{p}$ one, scaled by the ratio between $d$ and $u$ quark charges, we get an estimate for such a cross section, the blue curve of fig. 11, which, close to threshold, is at least a factor of four lower than the data.

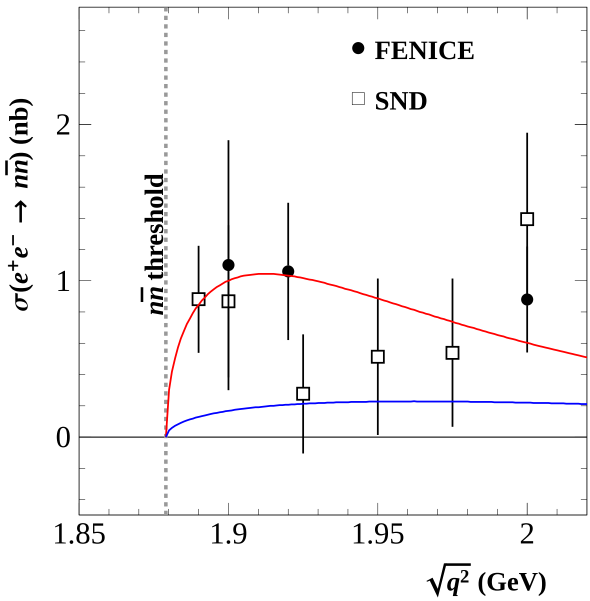


Fig. 11. Total cross section of $e^+e^- \to n\bar{n}$ measured by FENICE[32] and SND.[33] The gray vertical line indicates the production threshold, the red curve is the fit described in the text and the blue curve represents the naïve expectation driven from the $p\bar{p}$ data.

## 3. Conclusions

The knowledge, the study and the comprehension of baryon FFs are indispensable steps towards a deep understanding of the low-energy QCD dynamics. Nevertheless, even in case of nucleons, the available data are still quite incomplete. The experimental situation is twofold:

- many data sets in the space-like region where recently, with the increasingly common use of polarization techniques (see e.g.[34]), a great improvement of accuracy and hence of the capability to disentangle electric and magnetic FFs has been achieved;
- few measurements in the time-like region, with only two attempts, which actually gave incompatible results, to separate the moduli of $G_E$ and $G_M$ for the proton.

From the theoretical point of view, different interpretations have been proposed and the wide variety of attempts reflects the difficulty to connect the phenomenological properties of nucleons, parametrized by the FFs, to the underlying theory which is the QCD in non-perturbative (low-energy) regime.
Nevertheless, the analyticity requirement, which compels descriptions to be valid in both space- and time-like regions, drastically reduces the range of models to be considered. In particular, the more successful ones are the Vector-Meson-Dominance based models,[35] that not only are easily extensible from negative to positive $q^2$, but they were also able to make quite "unnatural" predictions then confirmed by the data. An example is the Iachello-Jackson-Landé model,[36] the authors predicted in 1973 the decreasing space-like behavior for the ratio $G_E^p/G_M^p$ well 30 years before its experimental observation.[37]
BABAR data gave a factual help in shedding light on the time-like behavior of proton FFs. Three very interesting aspects have been clarified:

- the threshold unitary normalization for the proton FF, see eq. (20);
- the need of a rescaled Coulomb correction accounting for the structure of baryons;
- the inequality of eq. (26): $|G_E^p(q^2)| > |G_M^p(q^2)|$, just above the production threshold.

Many other aspects of the time-like FFs, i.e.: a separate extraction of $|G_E|$ and $|G_M|$, the measurement of their relative phase, the explanation of the threshold normalization and the asymptotic behavior in connection with the space-like region, are still waiting for further experimental results and theoretical interpretations.

## Acknowledgments

We owe a special thanks to the Organizers of the “2011 Ferrara International School Niccolò Cabeo on Hadron Structure and Interactions” and, for suggestions and fruitful discussions on the topics of this work, we acknowledge Guido Altarelli, Giulia Pancheri, Yogendra Srivastava and Antonino Zichichi.

## References

1. L. L. Foldy, Phys. Rev. **87**, 688 (1952).
2. L. N. Hand, D. G. Miller and R. Wilson, Rev. Mod. Phys. **35**, 335 (1963).
3. M. Gell-Mann, M. L. Goldberger and W. E. Thirring, Phys. Rev. **95**, 1612 (1954); M. L. Goldberger, Phys. Rev. **97**, 508 (1955).
4. G. F. Chew, R. Karplus, S. Gasiorowicz, and F. Zachariasen, Phys. Rev. **110**, 265 (1958); P. Federbush, M. L. Goldberger, and S. B. Treiman, Phys. Rev. **112**, 642 (1958).
5. S. J. Brodsky and G. R. Farrar, Phys. Rev. Lett. **31**, 1153 (1973); V. Matveev *et al.*, Nuovo Cimento Lett. **7** (1973) 719.
6. G. P. Lepage and S. J. Brodsky, Phys. Rev. D **22**, 2157 (1980).
7. L. E. Phragmén, and E. Lindelöf, Acta Math. **31**, 381 (1908); E. C. Tichmarsch, *The Theory of Functions* (Oxford University Press, London, 1939).
8. M. N. Rosenbluth, Phys. Rev. **79**, 615 (1950).
9. A. Zichichi, S. M. Berman, N. Cabibbo and R. Gatto, Nuovo Cim. **24** (1962) 170.
10. A. D. Sakharov, Zh. Eksp. Teor. Fiz. **18**, 631 (1948) [Sov. Phys. Usp. **34**, 375 (1991)]; A. Sommerfeld, *Atombau und Spektralliniem* (Vieweg, Braunschweig, 1944), Vol. 2, p.130; J. Schwinger, *Particles, Sources, and Fields* (Addison-Wesley, Reading, Massachusetts, 1973), Vol. III, p. 80.
11. B. Aubert *et al.* [BABAR Collaboration], Phys. Rev. D **73**, 012005 (2006) [arXiv:hep-ex/0512023].
12. M. Castellano, G. Di Giugno, J. W. Humphrey, E. Sassi Palmieri, G. Troise, U. Troya and S. Vitale, Nuovo Cim. A **14**, 1 (1973).
13. G. Bassompierre *et al.*, Phys. Lett. B **64**, 475 (1976).
14. B. Delcourt *et al.*, Phys. Lett. B **86**, 395 (1979).
15. D. Bisello *et al.* [DM2 Collaboration], Nucl. Phys. B **224**, 379 (1983).
16. D. Bisello *et al.* [DM2 Collaboration], Z. Phys. C **48**, 23 (1990).
17. A. Antonelli *et al.*, Phys. Lett. B **334**, 431 (1994).
18. G. Bardin *et al.*, Nucl. Phys. B **411**, 3 (1994).
19. M. Ablikim *et al.* [BES Collaboration], Phys. Lett. B **630**, 14 (2005) [arXiv:hep-ex/0506059].
20. T. A. Armstrong *et al.* [E760 Collaboration], Phys. Rev. Lett. **70**, 1212 (1993).
21. M. Ambrogiani *et al.* [E835 Collaboration], Phys. Rev. D **60**, 032002 (1999).
22. M. Andreotti *et al.*, Phys. Lett. B **559**, 20 (2003).
23. R. Baldini, S. Pacetti, A. Zallo and A. Zichichi, Eur. Phys. J. A **39**, 315 (2009) [arXiv:0711.1725 [hep-ph]]; R. B. Baldini, S. Pacetti and A. Zallo, arXiv:0812.3283 [hep-ph].
24. E. A. Kuraev, E. Tomasi-Gustafsson and A. Dbeyssi, arXiv:1106.1670 [hep-ph].
25. R. B. Ferroli, S. Pacetti and A. Zallo, arXiv:1008.0542 [hep-ph].
26. R. Baldini, C. Bini, P. Gauzzi, M. Mirazita, M. Negrini and S. Pacetti, Nucl. Phys. Sec. A **755**, 286 (2005); R. Baldini, C. Bini, P. Gauzzi, M. Mirazita, M. Negrini and S. Pacetti, Eur. Phys. J. C **46**, 421 (2006).

27. S. Pacetti, Eur. Phys. J. A **32**, 421 (2007)
28. E. Tomasi-Gustafsson, E. A. Kuraev, S. Bakmaev and S. Pacetti, Phys. Lett. B **659**, 197 (2008) [arXiv:0710.0454 [hep-ph]].
29. B. Aubert *et al.* [BABAR Collaboration], Phys. Rev. D **76**, 092006 (2007) [arXiv:0709.1988 [hep-ex]].
30. D. Park, *Introduction to strong interactions* (W. A. Benjamin, Inc., New York, 1966).
31. A. Z. Dubničkova, S. Dubnička, M. P. Rekalo, Nuovo Cim. A **109**, 241 (1996).
32. A. Antonelli *et al.*, Nucl. Phys. B **517**, 3 (1998).
33. S. I. Serednyakov, "First results from SND at VEPP-2000", *International Workshop on $e^+e^-$ collisions from Phi to Psi*, BINP, Novosibirsk, 2011.
34. C. F. Perdrisat, V. Punjabi and M. Vanderhaeghen, Prog. Part. Nucl. Phys. **59**, 694 (2007) [arXiv:hep-ph/0612014].
35. See e.g. E. Tomasi-Gustafsson, F. Lacroix, C. Duterte and G. I. Gakh, Eur. Phys. J. A **24**, 419 (2005) [arXiv:nucl-th/0503001].
36. F. Iachello, A. D. Jackson and A. Landé, Phys. Lett. B **43** (1973) 191.
37. M. K. Jones *et al.* [Jefferson Lab Hall A Collaboration], Phys. Rev. Lett. **84**, 1398 (2000) [arXiv:nucl-ex/9910005];
O. Gayou *et al.*, Phys. Rev. C **64**, 038202 (2001);
O. Gayou *et al.* [Jefferson Lab Hall A Collaboration], Phys. Rev. Lett. **88**, 092301 (2002) [arXiv:nucl-ex/0111010];
A. J. R. Puckett *et al.*, Phys. Rev. Lett. **104**, 242301 (2010) [arXiv:1005.3419 [nucl-ex]];
B. D. Milbrath *et al.* [Bates FPP collaboration], Phys. Rev. Lett. **80**, 452 (1998) [Erratum-ibid. **82**, 2221 (1999)] [arXiv:nucl-ex/9712006].

# Experimental Search for Two Photon Exchange in *ep* Elastic Scattering

B. A. Raue
*Florida International University*
*Miami, FL, U.S.A.*

Two photon exchange (TPE) has been proposed as the primary source of the discrepancy between Rosenbluth and polarization-transfer methods of determining the electric-to-magnetic form-factor ratio of the proton. A direct measurement of the TPE contribution to elastic scattering is necessary to verify this hypothesis. In this proceeding I will briefly review the motivation for the TPE search, discuss how one experimentally obtains the real part of the TPE amplitude, and present some of the details of setting up such an experiment. I will also present some very preliminary results from Jefferson Lab and discuss what is expected to be measured in the very near future.

## 1. Introduction

Elastic scattering of electrons on protons is one of the simplest processes studied in nuclear physics. Under the assumption of single-photon exchange, known as the Born Approximation, the elastic cross section is given by

$$\left(\frac{d\sigma}{d\Omega}\right)_{lab} = \left(\frac{d\sigma}{d\Omega}\right)_{Mott} \frac{1}{\epsilon\,(1+\tau)} \left[\epsilon G_E^2(Q^2) + \tau G_M^2(Q^2)\right], \tag{1}$$

where the Mott cross section describes scattering from a point-like particle and $G_E^2(Q^2)$ and $G_M^2(Q^2)$ are the Sachs electric and magnetic form factors. The other variables are kinematic quantities that are defined in the appendix. The electromagnetic form factors, simplistically, describe the distribution of charge and current within the proton and are discussed extensively by Professor Tomasi elsewhere in these proceedings.

One way to determine the form factors is through what is known as a Rosenbluth separation.[1] In a Rosenbluth separation the cross section is measured as a function of $\epsilon$ at fixed $Q^2$. A linear fit of the reduced cross section, $\sigma_{red} = \left[\epsilon G_E^2(Q^2) + \tau G_M^2(Q^2)\right]$, then has a slope of $G_E^2$ and a y-intercept of $\tau G_M^2$. Two examples of Rosenbluth separations[2] are shown in Fig. 1 at $Q^2 = 2.75$ and 4.25 GeV$^2$. This was the predominant method of extracting the form factors for many years and the database for the elastic-scattering cross section is quite extensive. (See Ref.[3] and references therein.)

One can also determine the ratio $G_E/G_M$ through polarization transfer measurements.[4–7] For example, in the reaction of $\vec{e} + p \to e + \vec{p}$, one can measure the transverse ($P_T$) and longitudinal ($P_L$) polarizations of the outgoing protons. The ratio of the form factors is then given by

$$\frac{G_E}{G_M} = -\frac{P_T}{P_L}\frac{(E+E')}{2m_p}\tan\frac{\theta}{2}. \tag{2}$$

This technique was first used at MIT Bates[8] followed by a series of measurements at Jefferson Lab[9–11,13–17]

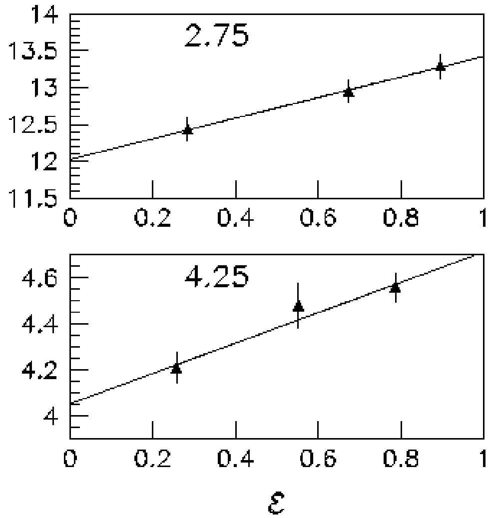


Fig. 1. Typical Rosenbluth separations[2] showing the reduced cross section ($\times 10^3$) vs. $\epsilon$ for $Q^2$ = 2.75 and 4.25 $GeV^2$, as indicated.

and Mainz.[12] One can also extract the form-factor ratio using a polarized electron beam on a polarized proton target.[19,20]

Fig. 2 shows the ratio $\mu_p G_E/G_M$ (where $\mu_p$ is the magnetic moment of the proton) as measured by the two methods. There is an obvious discrepancy between the Rosenbluth points (hollow) and the polarization results (solid) that grows with $Q^2$.

The most prevalent explanation that has been put forth to resolve this discrepancy is that two photon exchange (TPE) contributes to the elastic cross section at level larger than previously expected. Fig. 3 shows the various diagrams that contribute to elastic scattering. It is the Born diagram that we are interested in for determining the form factors. Diagrams (a)-(d) and (g) and (h) are generally accounted for by "standard" radiative corrections[24,25] while diagrams (e) and (f) are the two-photon exchange terms, which are ignored in the standard corrections. The motivation for ignoring the TPE diagrams has been the expectation that they must only contribute on the order of $\alpha^2$ ($\alpha$ being the fine structure constant) while the other terms contribute to order $\alpha$. However, since the intermediate state in the TPE diagrams can be not only a proton but any accessible baryon resonance or a continuum state, it is not hard to imagine that these diagrams may well sum up to a significant contribution.

It is the very fact that there are so many possible intermediate states–mostly with unknown photo-couplings–that make a reliable calculation of the TPE correction so difficult. Nonetheless, many such calculations* have been recently done, several of which do a remarkable job of reconciling the form-factor discrepancy. For example, the Hadronic Intermediate State model of Blunden, Melnitchouk, and Tjon[27] has been used to correct the Rosenbluth data as shown in Fig. 4. Further corrections have come even closer to reconciling the form-factor discrepancy.[3]

*For an excellent review of our current knowledge of TPE, including a summary of TPE calculations, see Ref.[26]

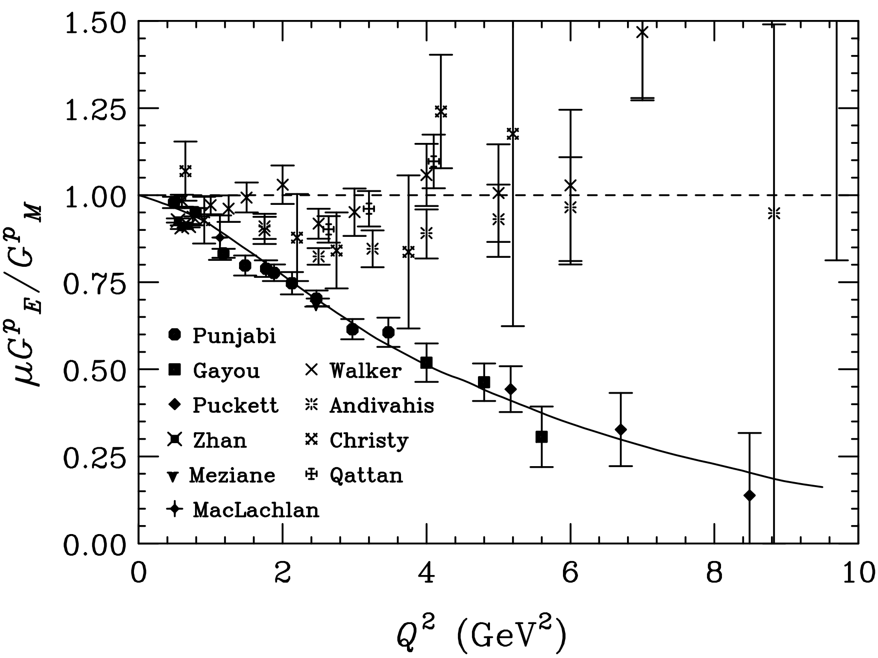


Fig. 2. Proton form factor ratio $\mu_p G_E^p/G_M^p$ from polarization-transfer measurements (filled symbols) of Puckett,[16] Punjabi and Jones,[9] Gayou[13] Zhan,[17] Meziane,[11] and MacLachlan,[14] as well as from Rosenbluth measurements of Walker,[21] Andivahis,[22] Christy,[2] and Qattan.[23] The solid curve is a global fit of polarization results from Ref.[18]

## 2. Direct Measurement of TPE

Though TPE is the most likely explanation for the form-factor discrepancy, a direct measure of the TPE amplitude is essential. A direct model-independent measurement of the TPE correction can be achieved experimentally by finding the ratio of the positron-proton to electron-proton elastic cross sections.

The amplitude of elastic $ep$-scattering with an accuracy of $\alpha_{em}^2$ can be written as

$$A_{total} = e_e e_p A_{Born} + e_e^2 e_p A_{e.br.} + e_e e_p^2 A_{p.br.} + e_e^2 e_p^2 A_{2\gamma}, \tag{3}$$

where the amplitudes $A_{Born}, A_{e.br.}, A_{p.br.}$ and $A_{2\gamma}$ respectively describe one-photon exchange, electron bremsstrahlung, proton bremsstrahlung and two-photon exchange. Note that radiative corrections such as vertex corrections and vacuum polarization do not contribute to the charge asymmetry and are therefore not included here. Squaring the above amplitude and keeping the corrections up to order $\alpha_{em}$ that have odd powers of electron charge, we have

$$|A_{ep\to ep}|^2_{odd} = e_e^2 e_p^2 [|A_{Born}|^2 + e_e e_p A_{Born} 2Re(A^*_{2\gamma}) + e_e e_p 2Re(A_{e.br.} A^*_{p.br.})], \tag{4}$$

where the notation $Re$ is used for the real part of the amplitude.

Corrections that have an even power of lepton charge, including the largest correction from electron bremsstrahlung, do not lead to any charge asymmetry. The last term in the above expression describes interference between electron and proton bremsstrahlung. Its infrared divergence exactly cancels the corresponding infrared divergence of the term $A_{Born} Re(A^*_{2\gamma})$. This interference effect for the standard kinematics of elastic $ep$-scattering experiments is dominated by soft-photon emission and results in a factorizable correction already included in the standard approach to radiative corrections.[24]

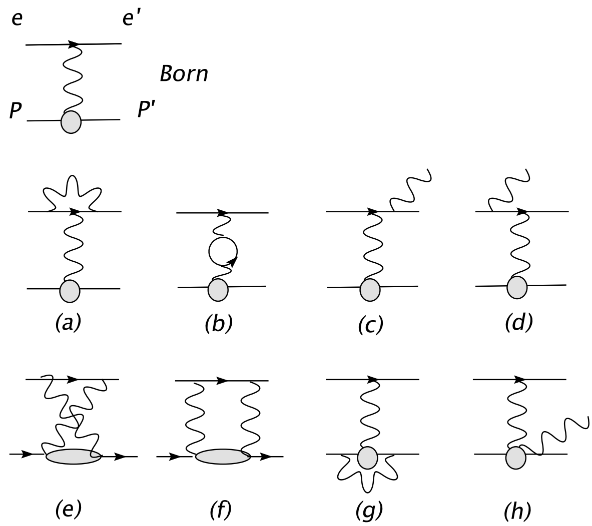


Fig. 3. Feynman diagrams for elastic electron-proton scattering, including the 1st-order QED radiative corrections. Diagrams (e) and (f) show the two-photon exchange e terms, where the intermediate state can be an unexcited proton, a baryon resonance or a continuum of hadrons.

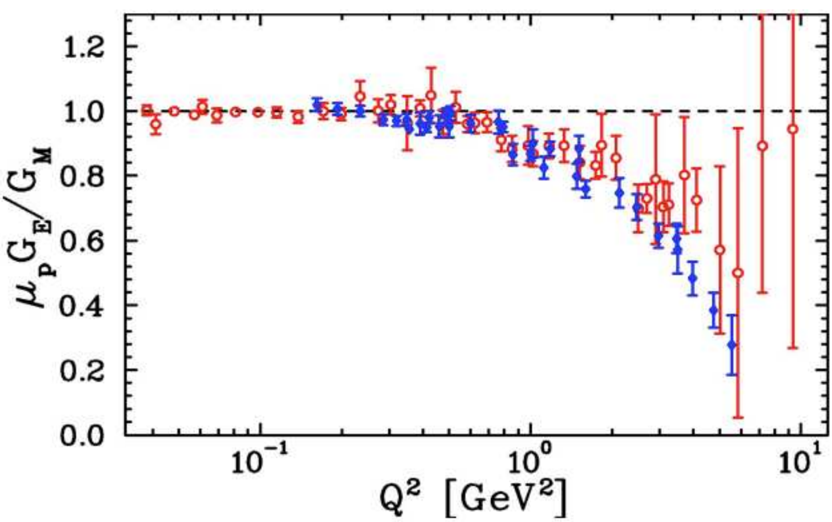


Fig. 4. Comparison of form-factor ratios for polarization transfer data (filled diamonds) and Rosenbluth data corrected for TPE effects (open circles) using the HIS calculation.[27]

Therefore, after correcting for the interference between electron and proton bremsstrahlung, one can isolate the TPE term by taking the ratio of positron- to electron-proton cross sections:

$$\sigma(e^{\pm}) = \sigma_{Born}(1 \mp \delta_{2\gamma}), \tag{5}$$

$$R_{2\gamma} = \frac{\sigma(e^{+})}{\sigma(e^{-})} \approx 1 - 2\delta_{2\gamma}, \tag{6}$$

where $\delta_{2\gamma}$ is the two photon exchange correction factor. Obviously, in the absence of TPE effects, $R$ is equal to one.

Since $\delta_{2\gamma}$ is expected to be of order 0.01, one needs to measure $R_{2\gamma}$ with to an uncertainty of no more that $\sim$ 1%. To do this with separate cross section measurements is very difficult. One must control factors such as the lepton flux, the target thickness, and the beam energy precisely, as well as maintaining a high degree of certainty on detector acceptance. Experiments can typically do no better than few percent for the systematic uncertainty.

### 2.1. *Previous Experimental Work*

Though it is difficult to measure $R_{2\gamma}$ precisely, there were several experiments in the 1960's to do just that.† The first experiment took place in 1962 at the Stanford Mark III Linac (a predecessor to SLAC).[29] This was followed by a series of seven other experiments through 1968. Fig. 5 shows these data plotted vs. $\epsilon$. These data span $0.01 < Q^2 < 5.0$ GeV$^2$ and the entire $\epsilon$ range. However, the size of the uncertainties and the relative lack of low $\epsilon$ make it impossible to discern any significant deviation from unity. In Ref.,[28] a linear fit to the data for $Q^2 < 2.0$ GeV$^2$ did find a large non-zero slope (0.057±0.018) but there is almost certainly some $Q^2$ dependence that has not been disentangled from the $\epsilon$ dependence.

At the time of these measurements, the large uncertainties on $R_{2\gamma}$ were enough to convince people that TPE was negligible, at least relative to the typical size of uncertainties on the cross section measurements available. Clearly, given the size of the form-factor discrepancy that now exists, that is no longer the case and more precise measurements of $R_{2\gamma}$ are now required.

## 3. The CLAS TPE Experiment

The CLAS TPE experiment[30] will measure $R_{2\gamma}$ for $Q^2 \leq 3.0$ GeV$^2$ and nearly the entire range of $\epsilon$ with small uncertainties. Systematic uncertainties of $\sim$ 1% will be achieved by using a novel technique of simultaneous measurements of electron and positron elastic scattering yields. In this way, factors that contribute to systematic uncertainties in cross section measurements–such as incident particle flux, target thickness, and detector acceptances–will largely cancel out.

### 3.1. *Experimental Details*

The experiment took place at the Thomas Jefferson National Accelerator Facility (Jefferson Lab) in Newport News, Virginia, U.S.A. At the heart of Jefferson Lab is the CEBAF superconducting electron accelerator capable of achieving continuous, high intensity beams with energies of almost 6 GeV. The beam can be simultaneously delivered to each of the three experimental halls–A, B, or C.

For this experiment, the CEBAF Large Acceptance Spectrometer (CLAS)[31] in Hall B was used. CLAS (shown in Fig. 6) is a nearly $4\pi$ detector. The magnetic field is provided by six superconducting coils, which

†See Ref.[28] for a summary of the early electron-positron ratio measurements.

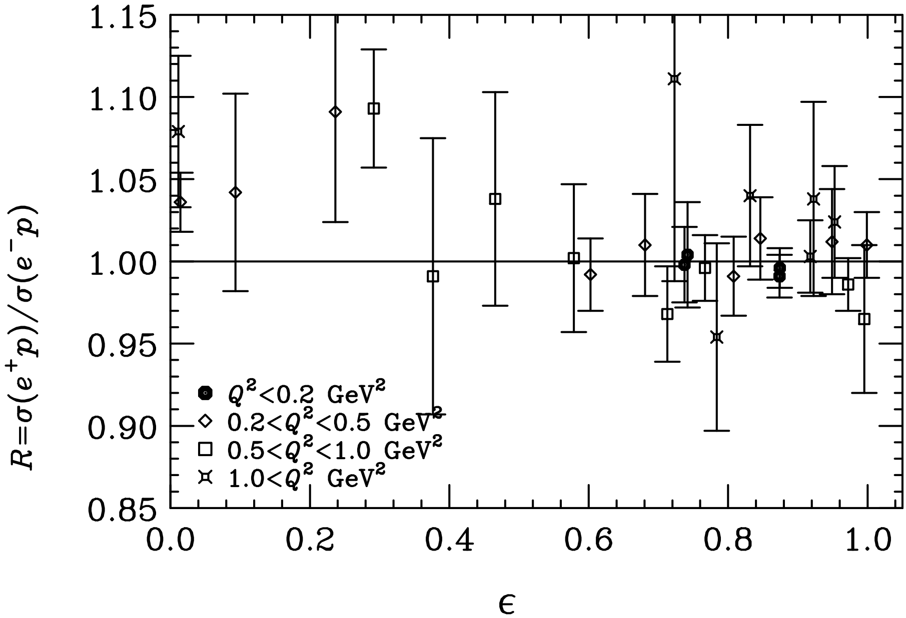


Fig. 5. Previous world data on $R_{2\gamma}$.[28] Data for different $Q^2$ ranges are indicated by different symbols as shown on the figure.

produce an approximately toroidal field in the azimuthal direction around the beam axis. The regions between the six magnet cryostats are instrumented with identical detector packages called sectors. Each sector consists of three regions of drift chambers (R1, R2, and R3) to determine the trajectories of charged particles, Cherenkov Counters (CC) for electron identification, Scintillation Counters (SC) for time of flight information, and Electromagnetic Calorimeters for electron identification and neutral particle detection. The R2 drift chambers are in the region of the magnetic field and provide tracking that is then used to determine particle momenta with $\delta p/p \sim 0.6\%$ In this experiment, the CC's were not used and the EC's were only used as a cross check.

In order to produce simultaneous positron and electron beams, the electron beam was first incident upon a gold radiator foil to produce a photon beam through Bremsstrahlung. The Hall B tagger magnet[32] was then used to divert the electrons into an underground beam dump. The photon beam then struck a gold converter to produce $e^+/e^-$ pairs. The beams then entered a three-dipole chicane to separate the lepton beams from the photon beam. The photon beam was stopped by a tungsten block, while the leptons were recombined into a single beam at the third dipole before proceeding to a liquid hydrogen target at the center of CLAS. Fig. 7 shows the layout of the beamline.

A feasibility test run of the experiment was conducted in 2006 in which most of the elements shown in Fig. 7 were in place. A primary electron-beam energy of 3.3 GeV and ~ 100 nA was used to produce a beam current $|I| \sim 20$ pA (each charge) of tertiary beam current with $0.5 \leq E \leq 3.3$ GeV on an 18-cm-long LH$^2$ target. While the run's primary goal was to study backgrounds and count rates, data useful extracting $R_{2\gamma}$ were taken for about $1\frac{1}{2}$ days. The CLAS torus polarity was flipped periodically, which cancels out lepton acceptance affects. The data acquisition was triggered on events with TOF hits in opposite CLAS sectors with one hit being at $\theta < 40°$.

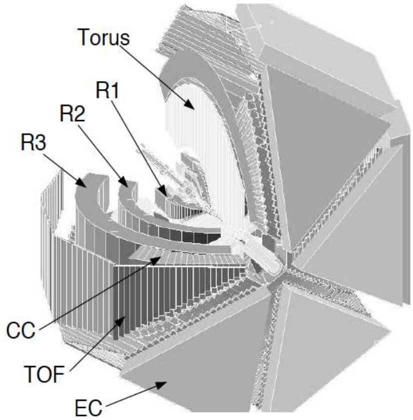


Fig. 6. Three dimensional view of CLAS showing various components as described in the text. In this view, the beam enters the picture from the upper left corner.

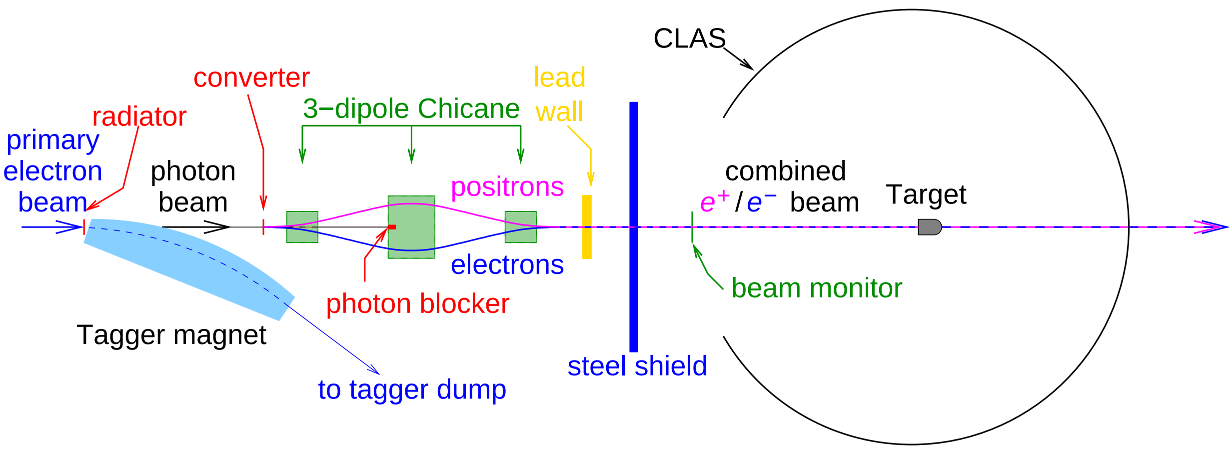


Fig. 7. Beamline sketch for the CLAS TPE experiment.

### 3.2. *Data Analysis*

In this analysis we were faced with a number of issues that are uncommon to the majority of CLAS experiments. For example, the energy of the incident lepton is not known and the standard methods of lepton identification cannot be applied because we do not have CC or EC information. The solution to this is to require the detection of the protons along with the leptons and exploit elastic-scattering kinematics and other cuts to identify events of interest and to match the detector acceptances for the two types of events (electron-proton and positron-proton). A description of the important analysis techniques is given below.

#### 3.2.1. *Elastic Event Identification*

The first step in event identification was to isolate the events with only two particles in the final state and require that these particles were in opposite sectors. A cut was also placed on the charge of these final state tracks, and only events with positive/negative or positive/positive charge combination were kept. In order to determine which particle was the proton and which was the positron in positive/positive events, a threshold of $\beta > 0.9$ was imposed to decide which particle was the positron. A $\beta > 0.9$ would require $p_p > 1.94$ GeV, which is well above our elastic acceptance limit of $p_p < 1.8$ GeV. For positive/positive events that did not subsequently satisfy the additional cuts listed below, we swapped the identities of the two positive particles and checked to see if they then satisfied the additional cuts. They did not.

The additional cuts included bad paddle removal, event vertex cuts, and range limitations applied to six individual kinematic variables that correspond to the elastic scattering interaction. These are summarized in the list below. As will be shown, these cuts were correlated in that any single cut has minimal effect when all of the other cuts are applied. This lead to a very clean elastic event distributions with minimal background contamination. Figs. 8-11 show some of the cut variables. Unless otherwise indicated, they show the combined data for both torus polarities.

(1) **Bad paddle removal.** As CLAS has aged, some of the TOF photomultiplier tubes (PMT) have deteriorated in performance and no longer give reliable information. Events that register hits in these paddles have been removed from the analysis.

(2) ***Z*-vertex.** Using the CLAS drift chambers to reconstruct the particle trajectories, the event origin along the beamline ($z$-vertex) can be identified. A cut was placed on $z$-vertex to ensure that events came from the $LH^2$ target.

(3) Azimuthal opening angle (co-planarity). Since there are only two particles in the final state, these events must be co-planar. Fig. 8 shows the azimuthal-angle difference between events before and after all other cuts.

(4) **Transverse momentum.** Because the beam travels along the $z$-axis, conservation of momentum requires the total transverse momentum of the final elastic scattering products to be zero. Therefore, good elastic events will result in a transverse momentum peaked near zero as shown in Fig. 9.

(5) **Beam energy difference.** Because we measured the energies and 3-momenta for both particles in the final state, our kinematics are over constrained. This allows us to reconstruct the unknown energy of the incident lepton (tertiary beam energy) in two different ways. Equation 7 finds the incident energy using the scattered lepton and proton angles, whereas equation 8 calculates this value from the total momentum along the $z$ direction.

$$E_{beam}^{angles} = m_p \left( \cot \frac{\theta_{e^\pm}}{2} \cot \theta_p - 1 \right) \tag{7}$$

$$E_{beam}^{mom.} = p_{e^\pm} \cos \theta_{e^\pm} + p_p \cos \theta_p \tag{8}$$

Assuming perfect momentum and angle reconstruction, these two quantities should be the same resulting in $\Delta E_{beam} \equiv E_{beam}^{angles} - E_{beam}^{mom.} = 0$. The $\Delta E_{beam}$ distribution is shown in Fig. 10. The 7 to 22 MeV shift in the centroids from zero is due to energy losses, which will reduce the value of $E_{beam}^{mom.}$. Events that fall outside of this cut include those in which the final state has three or more particles with one undetected. Note that in later calculations that depend on beam energy ($Q^2$, $W$, $\epsilon$), we have used $E_{beam}^{angles}$.

(6) **Beam polar angle.** The reconstructed incident lepton ($\vec{p}_l = \vec{p}_{l'} + \vec{p}_{p'}$) was required to travel along the $z$ axis. Any large deviations may be due to inelastic events, mis-reconstructed scattered particles, or multiple-scattered final particles. To discard these background events, the beam polar angle–from the reconstructed three-momenta of the detected particles–was required to be $\theta_{beam} < 5°$. The beam polar angle distribution is presented in Fig. 11. This cut also has the effect of removing events with a missing particle so it is largely redundant to the beam energy difference cut and the transverse momentum cut.

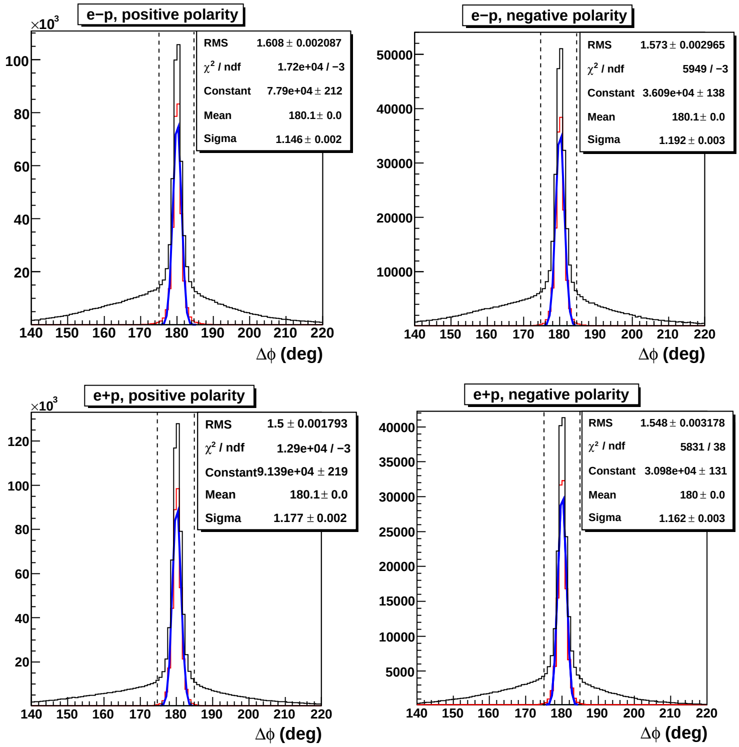


Fig. 8. Angle between lepton and proton ($\Delta\phi$) distributions for event type and torus polarity as indicated. The black histogram is the data before all cuts except the opposite sector cut. The red histogram is after all other cuts and the blue curve is its Gaussian fit. The dashed lines show the applied cut.

(7) **Distance of closest approach between lepton and proton candidates.** The distance of closest approach in this context is defined as the distance that two tracks (lepton and proton) come closest to one another. The shortest distance is found using an algorithm that draws a line perpendicular to both tracks and calculates the length of this line and a cut is placed on this distance to ensure the two tracks come from the same event.

(8) **Fiducial cuts.** Fiducial cuts are used to select the region of CLAS with uniform acceptance.

The cuts for above items 3,4,5,7 and 8 were determined by fitting a Gaussian to the peak of the combined distribution for that variable of both event types and torus polarities and setting the cut to $\pm 4\sigma$.

The cleanliness of the final data sample after these cuts were applied is show in Fig. 12, which is a $W = \sqrt{m_p + 2m_p\nu - Q^2}$ distribution for one of our bins in $\epsilon$. The peak is at the proton mass–as expected–and is completely without any hint of non-elastic background.

The distribution of events in $Q^2$ vs. $\epsilon$ after all cuts is shown in Fig. 13. The green boxes in the figure show the bins used for the final analysis, while the pink boxes show the binning used in our systematic uncertainty analysis. The final results cover a single $Q^2$ bin ($0.125 \leq Q^2 \leq 0.400$ GeV$^2$ with $\langle Q^2 \rangle = 0.206$ GeV$^2$) and seven bins in $\epsilon$ ($0.830 \leq \epsilon \leq 0.943$) such that we have similar statistical uncertainties in each $\epsilon$ bin. This allows direct comparison to previously existing data.

### 3.2.2. *Acceptance Corrections*

Clearly, the detector acceptances for electrons and positrons for a given kinematic bin are going to be different because one bends away from the beam line while the other bends toward the beam line in the CLAS magnetic field. We have accounted for this acceptance difference by using an acceptance-matching algorithm. This "swimming" algorithm calculates the trajectory of particles through the CLAS detector system and magnetic field. The acceptance matching was done by taking each event, say an $e^- p$ event, generating the conjugate lepton with the same kinematic quantities ($p$ and $\theta$), and swimming the hypothetical lepton through CLAS–an $e^+$ in this case. If the conjugate event remains in the CLAS acceptance, the original event is kept. If the conjugate event falls outside of the CLAS acceptance (either outside fiducial cuts or hits a bad paddle), the event is discarded, thus ensuring that the two types of events have the same kinematic acceptances.

The remaining differences between torus settings can be removed in the ratio cross sections as follows:

$$
\begin{aligned}
R &= \frac{\sigma(e^+ p)}{\sigma(e^- p)} = \sqrt{\frac{N_+^+ f_+^+}{N_+^- f_+^-}\frac{N_-^+ f_-^+}{N_-^- f_-^-}} \\
&= \sqrt{R_+ R_-}, \qquad (9)
\end{aligned}
$$

where $f_\pm^\pm$ represent unknown torus-polarity-related acceptance and detector efficiency functions. In all cases the subscript refers to the torus polarity and the superscript refers to the lepton charge. By charge symmetry,

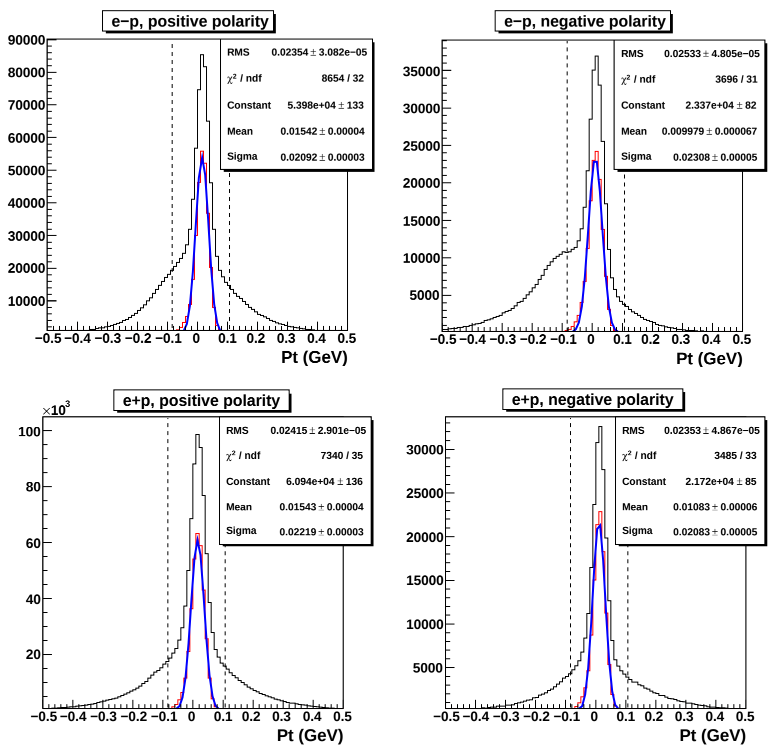


Fig. 9. Reconstructed transverse momentum distributions for event type and torus polarity as indicated. The black histogram is the data before all cuts except the opposite sector cut. The red histogram is after all other cuts and the blue curve is its Gaussian fit. The dashed lines show the applied cut.

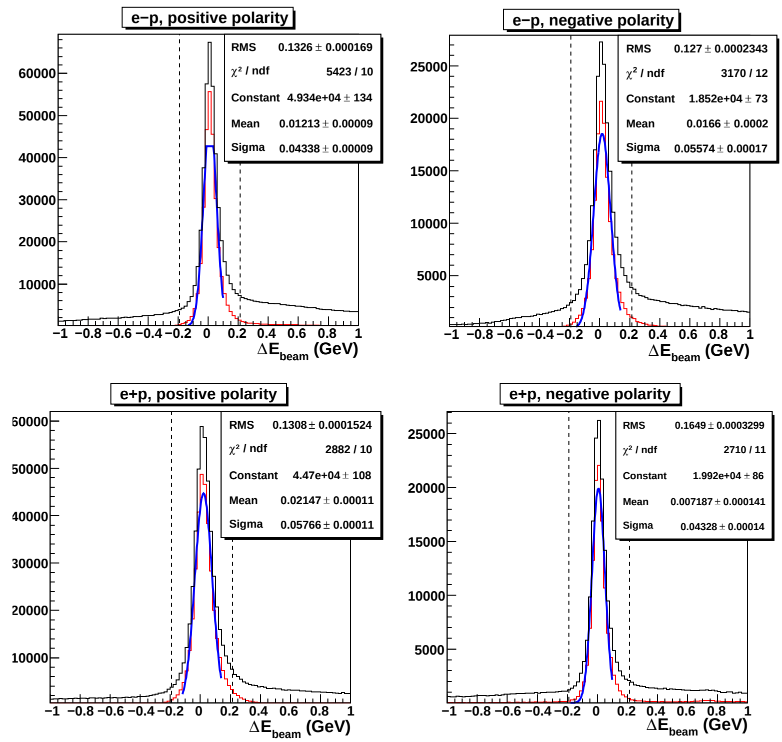


Fig. 10. $\Delta E_{beam}$ for event type and torus polarity as indicated. Black histogram is the data before all cuts except the opposite sector cut. The red histogram is after all other cuts and the blue curve is its Gaussian fit. The dashed lines show the applied cut.

one expects $f_+^+ = f_-^-$ and $f_-^+ = f_+^-$, thus canceling out in ratio.

We checked the quality of our acceptance corrections in two ways: 1) Doing a full Monte Carlo (MC) acceptance correction, and 2) calculating the double-ratio given in Eq. 9 with no corrections at all. We found that differences in $R$ to be smaller than the statistical uncertainty. We used the difference between our acceptance-matched results and our MC-corrected results to estimate the acceptance-related systematic uncertainty.

### 3.2.3. *Systematic Uncertainties*

The four major categories of systematic uncertainties that we have considered in this analysis are:

(1) **Luminosity differences between electrons and positrons.** This uncertainty was determined by a detailed MC study of the beam line that included all known lepton interactions. The MC study showed that the relative flux difference between positrons and electrons on the target was less than 0.01.
(2) **Effects of elastic event ID cuts.** This was studied by varying the widths of these cuts (from the nominal 4-$\sigma$ cut to a 3-$\sigma$ cut or removing the cut entirely). The differences in the final results between the nominal and the varied cuts result in an estimated absolute uncertainty of 0.0040.
(3) **Effects of fiducial cuts.** We also varied the cuts that define the good region of CLAS, again comparing the nominal results to those with the varied fiducial cuts. The estimated absolute uncertainty is 0.0071.
(4) **Acceptance effects.** As previously mentioned, this was done by comparing our nominal results (using acceptance matching) to results using a MC acceptance correction. The estimated absolute uncertainty is

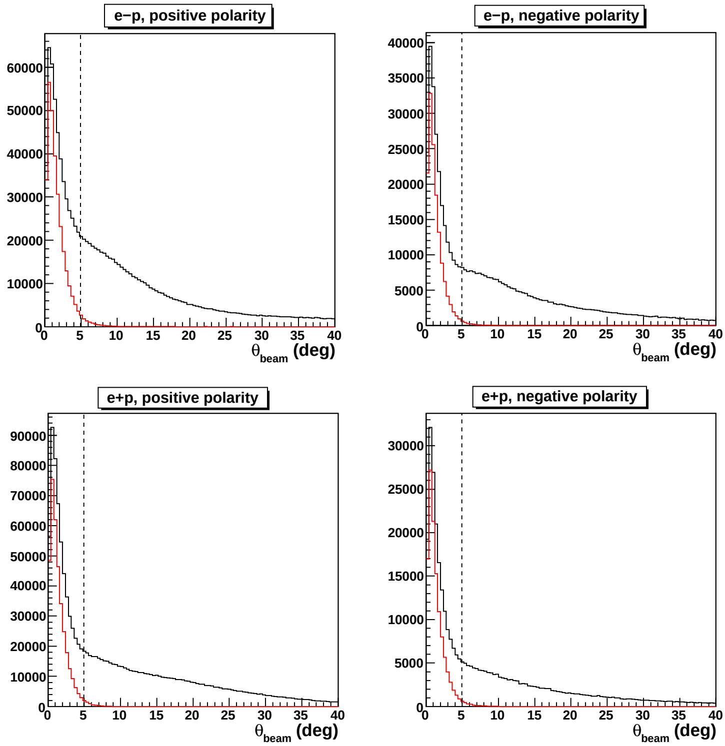


Fig. 11. Reconstructed polar angle of the beam for event type and torus polarity as indicated. Black histogram is the data before all cuts except the opposite sector cut and the red histogram is after all other cuts. The dashed lines show the applied cut.

0.0083 and is the largest of our systematic uncertainties.

### 3.3. *Early Results from CLAS*

Our final results are shown in Fig. 14 along with the previous world's data at a similar value of $Q^2$. A small radiative correction (< 0.0049) has been applied for lepton-proton bremsstrahlung interference. There are seven previous data points in this same range of $Q^2$ (blue points). The plot shows a fit linear in $\epsilon$ ($R = m\epsilon + b$) that includes our data (again including point-to-point systematic uncertainties) and the blue points. The fit at this $Q^2$ results in an $\epsilon$-dependence consistent with zero ($m = -0.005 \pm 0.020$) and $b = 1.028 \pm 0.017$ with $\chi^2/\nu = 0.70$. Essentially, there is no $\epsilon$ dependence at this $Q^2$ but there is a statistically significant deviation from unity. A constant fit of our data and the world data results in an average value of 1.024±0.0047, which is more than five standard deviations from unity, though systematic uncertainties do shrink the significance of this deviation. The figure also includes the BMT calculation.[27] There is a significant difference between our fit and the BMT calculation.

## 4. Conclusion and Future Prospects

During late 2010 and early 2011 we conducted the full CLAS TPE experiment using an incident beam energy of 5.5 GeV and with about a 50 times higher luminosity than for the 2006 run. The final results from the experiment will have statistical uncertainties of better than 1% for $Q^2 < 1.5$ GeV$^2$ and better than 2% for

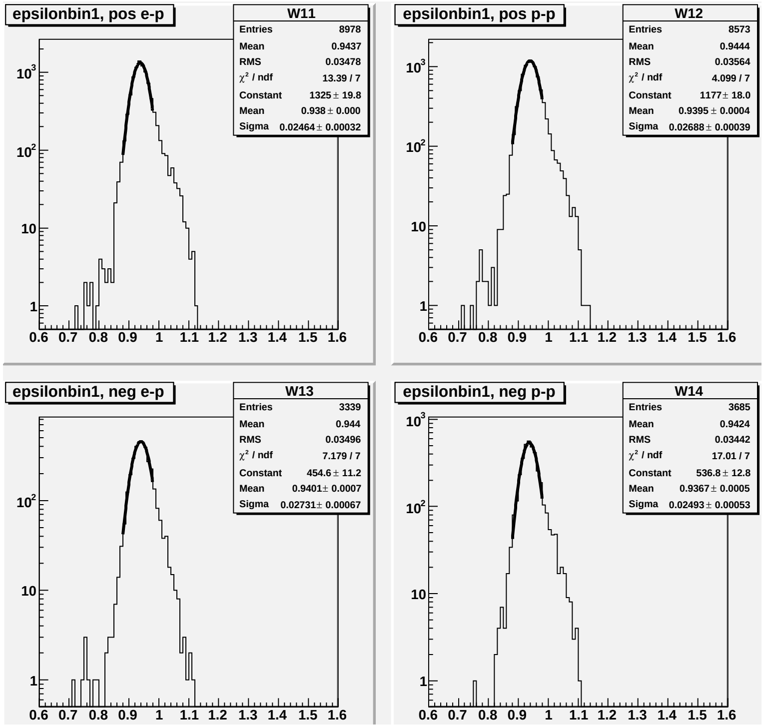


Fig. 12. Top two panels show the $W$ distributions (in GeV) for positive torus polarity electron (left) and positron (right) events for $0.820 \le \epsilon \le 0.840$ and $\langle Q^2 \rangle = 0.206$ GeV$^2$ with all cuts applied. The bottom two panels show the same for negative torus polarity events. A Gaussian fit is included in the region around the peak.

$Q^2 < 2.5$ GeV$^2$ over nearly the entire $\epsilon$ range. Analysis is underway and we expect preliminary results to be available in early 2012.

There are two other experiments that will also provide measurements of the TPE effect in much the same way as the CLAS experiment. In 2009, the Novosibirsk group[33] measured $R_{2\gamma}$ at $Q^2 = 1.5$ GeV$^2$ and in 2012, the OLYMPUS[34] collaboration will measure $R_{2\gamma}$ at $Q^2 < 2.5$ GeV$^2$. Both experiments should result in similar uncertainties as our CLAS experiment though with more limited coverage in $\epsilon$. Fig. 15 shows the expected uncertaintes and kinematic coverage once the analyses are completed.

These experiments will provide information that is vital to our understanding of the electon-scattering process as well as our understanding of the proton structure. We have heard the common mantra that “the electromagnetic probe is well understood.” However, the discrepancy between Rosenbluthe and polarization measurements of the form-factor ratio indicates otherwise. Indeed, if we don’t even understand elastic electron scattering, how well do we know anything we have measured with electron scattering? There are important implications for many of the nuclear physics quantities we study ranging from high-precision quasi-elastic experiments to strangeness and parity violation experiments to transition form factor exeperiments.

## 5. Appendix: Kinematics Definitions

Several kinematic quantities appear throughout this proceeding that require definition. Fig. 16 shows the scattering of an electron from a proton through the exchange of a single virtual photon (shown by $\gamma^*$). The incident

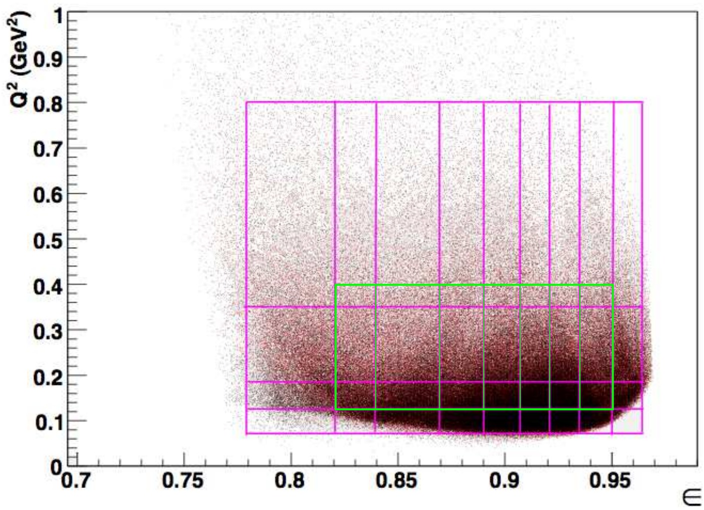


Fig. 13. Binning scheme, shown for negative polarity for electrons (black) and positrons (red). The green boxes show the binning for the final data and the pink boxes show the fine bins used in the systematics studies.

electron is described by the four vector $(E, \vec{p_e})$, the scattered electron by the four vector $(E, \vec{p_e}')$, and the scattered proton by the four vector $(E_p, \vec{p_p})$. The electron scattering angle is denoted by $\theta_e$ and the proton scattering angle is denoted by $\theta_p$. A quantity that we see frequently is the square of the four-momentum transfer of the virtual photon:

$$Q^2 = -q^2 = 4EE' \sin^2 \frac{\theta_e}{2}. \tag{10}$$

This quantity can be thought of as the resolution of the virtual photon or, more appropriately for our case, how deeply the virtual photon probes the proton.

The degree of the transverse polarization of the virtual photon is given by

$$\epsilon = \left[1 + 2\left(1 + \frac{\nu^2}{Q^2}\right) \tan \frac{\theta_e}{2}\right]^{-1}, \tag{11}$$

where $\nu = E - E'$ is the energy transfer by the virtual photon.

In our expression for the cross section we also saw the term $\tau$ which is defined as

$$\tau = \frac{Q^2}{4m_p}, \tag{12}$$

where $m_p$ is the proton mass.

Finally, the invariant mass of the intermediate hadronic state is given by

$$W = \sqrt{m_p^2 + 2m_p\nu - Q^2} = \sqrt{s}, \tag{13}$$

where $s$ is the Mandelstam variable. In the case of elastic scattering it is always the case that $W = m_p$.

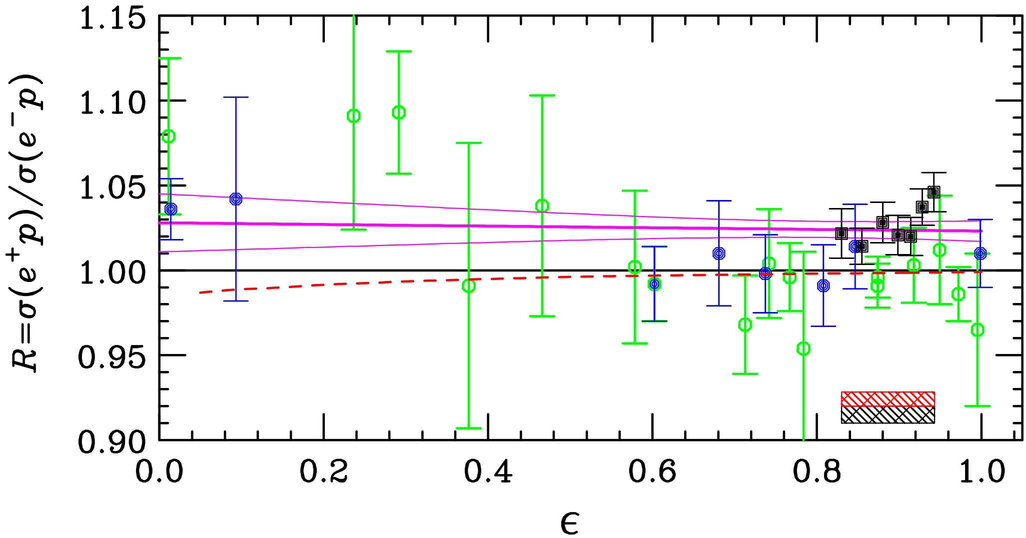


Fig. 14. Charge asymmetry ratio overlaid on the world data. Black filled squares are from this experiment at $\langle Q^2 \rangle = 0.206$ GeV$^2$ and have had radiative corrections applied, blue filled circles are previous world data at similar $Q^2$, and green hollow points the rest of the previous world data with $Q^2 < 2$ GeV$^2$.[28] The linear fit (heavy magenta line) includes the present data and the blue points while the light magenta lines indicate the $1\sigma$ uncertainty in the fit. The red shaded band indicates the point-to-point systematic uncertainty ($1\sigma$) and the black shaded band represents the scale-type systematic uncertainty (due to relative luminosity) on the present data. The red dashed curve is the BMT calculation[27] at $Q^2 = 0.2$ GeV$^2$.

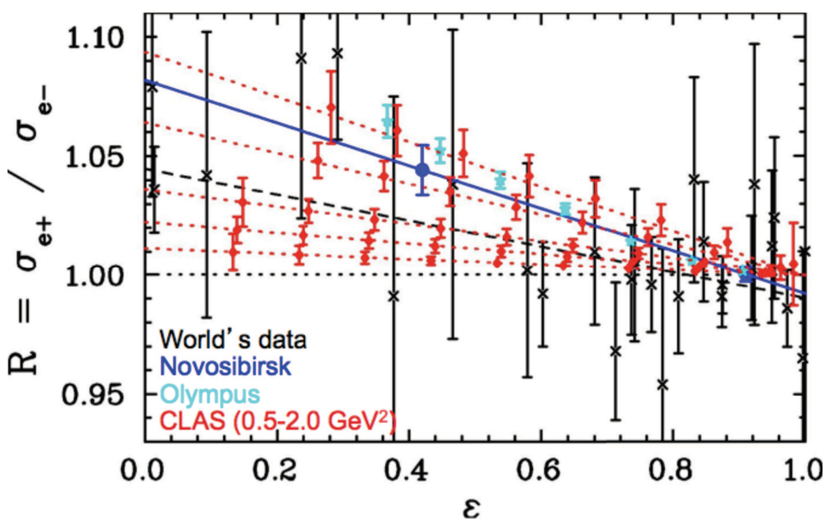


Fig. 15. Expected uncertainties and kinematic coverage for $R_{2\gamma}$ for the Novosibirsk VEPP-3 experiment (blue points), OLYMPUS (cyan points), and CLAS TPE (red points) compared to the previous world data.

## References


1. M. N. Rosenbluth, Phys. Rev. **79**, 615 (1950).
2. M. E. Christy *et al.*, Phys. Rev C**70**, 015206 (2004).

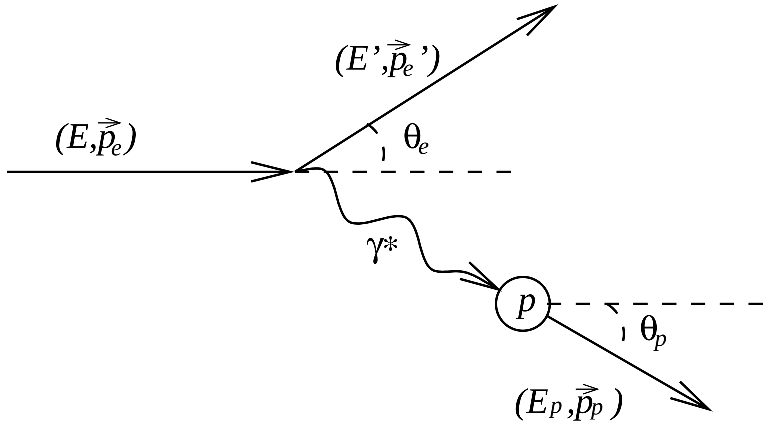


Fig. 16. Diagram of elastic scattering of an electron from a proton through the exchange of a virtual photon ($\gamma^*$).


3. J. Arrington, W. Melnitchouk, and J. A. Tjon, Phys. Rev. C**76**, 035205 (2007).
4. A. I. Akhiezer and M. P. Rekalo, Sov. Phys. Dokl. **13**, 572 (1968).
5. N. Dombrey, Rev. Mod. Phys. **41**, 236 (1969).
6. A. I. Akhiezer and M. P. Rekalo, Sov. J. Part. Nucl. **3**, 277 (1974).
7. R. G. Arnold, C. E. Carlson, and F. Gross, Phys. Rev. C **23**, 363 (1981).
8. B. Milbrath *et al.*, Phys. Rev. Lett. **80**, 452 (1998); **82**, 2221(E) (1999).
9. V. Punjabi *et al.*, Phys. Rev. C **71**, 055202 (2005); M. K. Jones *et al.*, Phys. Rev. Lett. **84**, 1398 (2000).
10. O. Gayou *et al.*, Phys. Rev. C **64**, 038202 (2001).
11. M. Meziane *et al.* Phys. Rev. Lett. **106**, 132501 (2011).
12. T. Pospischil *et al.*, Eur. Phys. J. A **12**, 125 (2001).
13. O. Gayou *et al.*, Phys. Rev. Lett. **88**, 092301 (2002); Revised analysis in Ref..[18]
14. G. MacLachlan *et al.*, Nucl. Phys. **A764**, 261 (2006).
15. G. Ron *et al.*, Phys. Rev. Lett. **99**, 202002 (2007); G. Ron *et al.*, arXiv:1103.5784 [nucl-ex].
16. A. J. R. Puckett *et al.*, Phys. Rev. Lett. **104**, 242301 (2010).
17. X. Zhan *et al.*, arXiv:1102.0318 [nucl-ex].
18. A. J. R. Puckett *et al.*, arXiv:1102.5737 [nucl-ex].
19. M. K. Jones *et al.*, Phys. Rev. C **74**, 035201 (2006).
20. C. B. Crawford *et al.*, Phys. Rev. Lett. **98**, 052301 (2007).
21. R. C. Walker *et al.*, Phys. Rev. D **49**,5671 (1994).
22. L. Andivahis *et al.*, Phys. Rev. D **50**, 5491 (1994).
23. L. A. Qattan *et al.*, Phys. Rev. Lett. **94**, 142301 (2005).
24. Y. S. Tsai, Phys. Rev. **122**, 1898 (1961); L. W. Mo and Y. S. Tsai, Rev. Mod. Phys. **41**, 205 (1969).
25. L. C. Maximon and J. A. Tjon, Phys. Rev. C **62**, 054320 (2000).
26. J. Arrington, P. G. Blunden, and W. Melnitchouk, arXiv:1105.0951 [nuclt-th] (2011).
27. P. G. Blunden, W. Melnitchouk, and J. A. Tjon, Phys. Rev. C **72**, 034612 (2005).
28. J. Arrington, Phys. Rev. C **69**, 032201 (2004).
29. D. Yount and J. Pine, Phys. Rev. **128**, 1842 (1962).
30. Jefferson Lab Experiment E07-005, *Beyond the Born approximation: A precise comparison of positron-proton and electron-proton elastic scattering in CLAS*, A. Afanasev *et al.*, spokespersons.
31. B. A. Mecking *et al.*, Nucl. Instr. and Meth. A **503**, 513 (2003).
32. D. I. Sober *et al.*, Nucl. Instr. and Meth. A **440**, 263 (2000).
33. J. Arrington *et al.*, VEPP-3 proposal, arXiv:nucl-ex/040802, (2004).
34. M. Kohl, API Conf. Proc. 1160, 19 (2009).

# HADRONIC FORM FACTOR MODELS AND SPECTROSCOPY WITHIN THE GAUGE/GRAVITY CORRESPONDENCE

G. F. de Teramond

*Universidad de Costa Rica, San José, Costa Rica*
*email: gdt@asterix.crnet.cr*

S. J. Brodsky

*SLAC National Accelerator Laboratory, Stanford University, Stanford, CA 94309, USA*
*email: sjbth@slac.stanford.edu*

We show that the nonperturbative light-front dynamics of relativistic hadronic bound states has a dual semiclassical gravity description on a higher dimensional warped AdS space in the limit of zero quark masses. This mapping of AdS gravity theory to the boundary quantum field theory, quantized at fixed light-front time, allows one to establish a precise relation between holographic wave functions in AdS space and the light-front wavefunctions describing the internal structure of hadrons. The resulting AdS/QCD model gives a remarkably good accounting of the spectrum, elastic and transition form factors of the light-quark hadrons in terms of one parameter, the QCD gap scale. The light-front holographic approach described here thus provides a frame-independent first approximation to the light-front Hamiltonian problem for QCD. This article is based on lectures at the Niccolò Cabeo International School of Hadronic Physics, Ferrara, Italy, May 2011.

## 1. Introduction

One of the most challenging problems in particle physics is to understand hadron dynamics and spectroscopy in terms of the confined quark and gluon quanta of quantum chromodynamics, the fundamental theory of the strong interactions. A central goal is to compute detailed hadronic properties, such as moments, structure functions, distribution amplitudes, transversity distributions, elastic and transition form factors, and the excitation dynamics of hadron resonances from first principles; *i.e.*, directly from the QCD Lagrangian. The most successful theoretical approach thus far has been to quantize QCD on discrete lattices in Euclidean space-time.[1] Lattice numerical results follow from the computation of frame-dependent moments of distributions in Euclidean space; however, dynamical observables in Minkowski space-time, such as the time-like hadronic form factors, are not obtained directly from Euclidean-space lattice computations. Dyson-Schwinger methods have led to many important insights, such as the infrared fixed-point behavior of the strong coupling constant;[2] however, in practice, these analyses are limited to ladder approximation in Landau gauge.

In principle, one could calculate hadronic spectroscopy and wavefunctions by solving for the eigenvalues and eigenfunctions of the QCD Hamiltonian: $H|\Psi\rangle = E|\Psi\rangle$ at fixed time $t$. However, this traditional method – called the "instant form" by Dirac,[3] is plagued by complex vacuum and relativistic effects. In contrast, quantization at fixed light-front (LF) time $\tau = t + z/c$ – the "front-form" of Dirac[3] – provides a powerful boost-invariant non-perturbative method for solving QCD and constitutes the ideal framework to describe the structure of hadrons in terms of their quark and gluon degrees of freedom. The simple structure of the light-front vacuum allows an unambiguous definition of the partonic content of a hadron in QCD and of hadronic light-front wavefunctions (LFWFs), the underlying link between large distance hadronic states and the constituent degrees of freedom at short distances. Thus, one can also solve QCD by diagonalizing the light-front QCD Hamiltonian $H_{LF}$. The spectrum and light-front Fock-state wavefunctions are obtained from the eigenvalues and eigensolutions of the Heisenberg problem $H_{LF}|\psi\rangle = M^2|\psi\rangle$, which becomes an infinite set of coupled integral equations for the light-front components $\psi_n = \langle n|\psi\rangle$ in the Fock expansion.[4,5] This nonperturbative method has the advantage that it is frame-independent, operates in physical Minkowski space-time, and has no fermion-doubling problem.[4] It has been applied successfully in lower space-time dimensions. In practice, however, the resulting large matrix diagonalization problem in 3 + 1 space-time has proven to be a daunting task, so alternative methods and approximations are necessary.

The AdS/CFT correspondence between gravity or string theory on a higher-dimensional anti–de Sitter (AdS) space and conformal field theories (CFT) in physical space-time,[6] has led to a semiclassical approximation for strongly-coupled quantum field theories which provides physical insights into its nonperturbative dynamics. The correspondence is holographic in the sense that it determines a duality between theories in different number of space-time dimensions. In practice, the duality provides an effective gravity description in a $(d + 1)$-dimensional AdS space-time in terms of a flat $d$-dimensional conformally-invariant quantum field theory defined at the AdS asymptotic boundary.[7,8] Thus, in principle, one can compute physical observables in a strongly coupled gauge theory in terms of a classical gravity theory.

Anti-de Sitter $AdS_5$ space is the maximally symmetric space-time with negative curvature and a four-dimensional space-time boundary. The most general group of transformations that leave the $AdS_{d+1}$ differential line element

$$ds^2 = \frac{R^2}{z^2}\left(\eta_{\mu\nu} dx^\mu dx^\nu - dz^2\right), \tag{1}$$

invariant, the isometry group, has dimensions $(d + 1)(d + 2)/2$ ($R$ is the AdS radius). Five-dimensional anti-de Sitter space $\mathrm{AdS}_5$ has 15 isometries, in agreement with the number of generators of the conformal group in four dimensions. Since the AdS metric (1) is invariant under a dilatation of all coordinates $x^\mu \to \lambda x^\mu$ and $z \to \lambda z$, it follows that the additional dimension, the holographic variable $z$, acts as a scaling variable in Minkowski space: different values of $z$ correspond to different energy scales at which the hadron is examined. As a result, a short space-like or time-like invariant interval near the light-cone, $x_\mu x^\mu \to 0$ maps to the conformal AdS boundary near $z \to 0$. This also corresponds to the $Q \to \infty$ ultraviolet (UV) zero separation distance. On the other hand, a large invariant four-dimensional interval of confinement dimensions $x_\mu x^\mu \sim 1/\Lambda^2_{\mathrm{QCD}}$ maps to the large infrared (IR) region of AdS space $z \sim 1/\Lambda_{\mathrm{QCD}}$.

QCD is fundamentally different from conformal theories since its scale invariance is broken by quantum effects. A gravity dual to QCD is not known, but the mechanisms of confinement can be incorporated in the gauge/gravity correspondence by modifying the AdS geometry in the large IR domain $z \sim 1/\Lambda_{\mathrm{QCD}}$, which also sets the scale of the strong interactions.[9] In this simplified approach, we consider the propagation of hadronic modes in a fixed effective gravitational background asymptotic to AdS space, which encodes salient properties of the QCD dual theory, such as the UV conformal limit at the AdS boundary, as well as modifications of the background geometry in the large-$z$ IR region to describe confinement.

The physical states in AdS space are represented by normalizable modes $\Phi_P(x, z) = e^{-iP\cdot x}\Phi(z)$, with plane waves along Minkowski coordinates $x^\mu$ and a profile function $\Phi(z)$ along the holographic coordinate $z$. The hadronic invariant mass states $P_\mu P^\mu = \mathcal{M}^2$ are found by solving the eigenvalue problem for the AdS wave equation. The modified theory generates the point-like hard behavior expected from QCD, instead of the soft behavior characteristic of extended objects.[9] It is rather remarkable that the QCD dimensional counting rules[10,11] are also a key feature of nonperturbative models[9] based on the gauge/gravity duality. Although the mechanisms are different, both the perturbative QCD and the AdS/QCD approaches depend on the leading-twist (dimension minus spin) interpolating operators of the hadrons and their structure at short distances.

The gauge/gravity duality leads to a simple analytical and phenomenologically compelling nonperturbative frame-independent first approximation to the light-front Hamiltonian problem for QCD – "Light-Front Holography".[12] Incorporating the AdS/CFT correspondence[6] as a useful guide, light-front holographic methods were originally introduced[13,14] by mapping the Polchinski-Strassler formula for the electromagnetic (EM) form factors in AdS space[15] to the corresponding Drell-Yan-West expression at fixed light-front time in physical space-time.[16,17] It was also shown that one obtains identical light-front holographic mapping for the gravitational form factor[18] – the matrix elements of the energy-momentum tensor, by perturbing the AdS metric (1) around its static solution.[19] In the usual "bottom-up" approach to the gauge/gravity duality,[20,21] fields in the bulk geometry are introduced to match the chiral symmetries of QCD and axial and vector currents become the primary entities as in effective chiral theory. In contrast, in light-front holography a direct connection with the internal constituent structure of hadrons is established using light-front quantization.[12–14,18,22]

The identification of higher dimensional AdS space with partonic physics in physical space-time is specific to the light front: the Polchinski-Strassler formula for computing transition matrix elements is a simple overlap of AdS amplitudes, which maps to a convolution of frame-independent light-front wavefunctions. This AdS convolution formula cannot be mapped to current matrix elements at ordinary fixed time $t$, since the instant-time wavefunctions must be boosted away from the hadron's rest frame – an intractable dynamical problem. In fact, the boost of a composite system at fixed time $t$ is only known at weak binding. Moreover, the form factors in instant time also require computing the contributions of currents which arise from the vacuum in the initial state and which connect to the hadron in the final state. Thus instant form wavefunctions alone are not sufficient to compute covariant current matrix elements in the instant form. There is no analog of such contributions in AdS. In contrast, there are no vacuum contributions in the light-front formulae for current matrix elements – in agreement with the AdS formulae.

Unlike ordinary instant-time quantization, the Hamiltonian equation of motion in the light-front is frame independent and has a structure similar to eigenmode equations in AdS space. This makes a direct connection of QCD with AdS/CFT methods possible. In fact, one can also study the AdS/CFT duality and its modifications starting from the LF Hamiltonian equation of motion for a relativistic bound-state system $H_{LF}|\psi\rangle = \mathcal{M}^2|\psi\rangle$ in physical space-time,[12] where the QCD light-front Hamiltonian $H_{LF} \equiv P_\mu P^\mu = P^+P^- - \mathbf{P}_\perp^2$, $P^\pm = P^0 \pm P^3$, is constructed from the QCD Lagrangian using the standard methods of quantum field theory.[4] To a first semiclassical approximation, where quantum loops and quark masses are not included, LF holography leads to a LF Hamiltonian equation which describes the bound-state dynamics of light hadrons in terms of an invariant impact kinematical variable $\zeta$ which measures the separation of the partons within the hadron at equal light-front time $\tau = x^+ = x^0 + x^3$. The transverse coordinate $\zeta$ is closely related to the invariant mass squared of the constituents in the LFWF and its off-shellness in the LF kinetic energy, and it is thus the natural variable to characterize the hadronic wavefunction. In fact $\zeta$ is the only variable to appear in the relativistic light-front Schr̈odinger equations predicted from holographic QCD in the limit of zero quark masses. The coordinate $z$ in AdS space is thus uniquely identified with a Lorentz-invariant coordinate $\zeta$ which measures the separation of the constituents within a hadron at equal light-front time. The AdS/CFT correspondence shows that the holographic coordinate $z$ in AdS space is related inversely to the internal relative momentum. In fact, light-front holography makes this identification precise.

Remarkably, the unmodified AdS equations correspond to the kinetic energy terms of the partons inside a hadron, whereas the interaction terms in the QCD Lagrangian build confinement and correspond to the truncation of AdS space in an effective dual gravity approximation.[12] Thus, all the complexities of the strong interaction dynamics are hidden in an effective potential $U(\zeta)$, and the central question – how to derive the effective color-confining potential $U(\zeta)$ directly from QCD, remains open. To circumvent this obstacle, the effective confinement potential can be introduced either with a sharp cut-off in the infrared region of AdS space, as in the "hard-wall" model,[9] or, more successfully, using a "dilaton" background in the holographic coordinate to produce a smooth cutoff at large distances as in the "soft-wall" model.[23] Furthermore, one can impose from the onset a correct phenomenological confining structure to determine the effective IR warping of AdS space, for example, by adjusting the dilaton background to reproduce the observed linear Regge behavior of the hadronic mass spectrum $\mathcal{M}^2$ as a function of the excitation quantum numbers[23,24] [a]. By using light-front holographic mapping techniques, one also obtains a connection between the mass parameter $\mu R$ of the AdS theory with the orbital angular momentum of the constituents in the light-front bound-state Hamiltonian equation.[12] The identification of orbital angular momentum of the constituents is a key element in our description of the internal structure of hadrons using holographic principles, since hadrons with the same quark content, but different orbital angular momenta, have different masses.

In our approach, the holographic mapping is carried out in the strongly coupled regime where QCD is almost conformal, corresponding to an infrared fixed-point. A QCD infrared fixed point arises since the propagators of the confined quarks and gluons in the loop integrals contributing to the $\beta$-function have a maximal wavelength;[14,26] thus, an infrared fixed point appears as a natural consequence of confinement. The decoupling of quantum loops in the infrared is analogous to QED dynamics where vacuum polarization corrections to the photon propagator decouple at $Q^2 \to 0$. Since there is a window where the QCD coupling is large and approximately constant, QCD resembles a conformal theory for massless quarks. One then uses the isometries of $AdS_5$ to represent scale transformations within the conformal window. We thus begin with a conformal approximation to QCD to model an effective dual gravity description in AdS space. The large-distance non-conformal effects are taken into account with the introduction of an effective confinement potential as described above.

Early attempts to derive effective one-body equations in light-front QCD are described in reference.[27] We should also mention previous work by 't Hooft, who obtained the spectrum of two-dimensional QCD in the large $N_C$ limit in terms of a Schrödinger equation as a function of the parton $x$-variable.[28] In the scale-invariant limit, this equation is equivalent to the equation of motion for a scalar field in $AdS_3$ space.[29] In this case, there is a mapping between the variable $x$ and the radial coordinate in $AdS_3$.

## 2. Light-front bound-state Hamiltonian equation of motion and light-front holography

A key step in the analysis of an atomic system, such as positronium, is the introduction of the spherical coordinates $r, \theta, \phi$ which separates the dynamics of Coulomb binding from the kinematical effects of the quantized orbital angular momentum $L$. The essential dynamics of the atom is specified by the radial Schrödinger equation whose eigensolutions $\psi_{n,L}(r)$ determine the bound-state wavefunction and eigenspectrum. In our recent work, we have shown that there is an analogous invariant light-front coordinate $\zeta$ which allows one to separate the essential dynamics of quark and gluon binding from the kinematical physics of constituent spin and internal orbital angular momentum. The result is a single-variable light-front Schrödinger equation for QCD which determines the eigenspectrum and the light-front wavefunctions of hadrons for general spin and orbital angular

[a]Using a mean-field mechanism, an effective harmonic confinement interaction was obtained in Ref.[25] in a constituent quark model.

momentum,[12] thus providing a description of the internal dynamics of hadronic states in terms of their massless constituents at the same LF time $\tau = x^+ = x^0 + x^3$, the time marked by the front of a light wave,[3] instead of the ordinary instant time $t = x^0$.

### 2.1. *Light-front quantization of QCD*

Our starting point is the $SU(3)_C$ invariant Lagrangian of QCD

$$\mathcal{L}_{\rm QCD} = \bar{\psi}\left(i\gamma^\mu D_\mu - m\right)\psi - \tfrac{1}{4}G^a_{\mu\nu}G^{a\mu\nu}, \tag{2}$$

where $D_\mu = \partial_\mu - ig_s A^a_\mu T^a$ and $G^a_{\mu\nu} = \partial_\mu A^a_\nu - \partial_\nu A^a_\mu + g_s c^{abc} A^b_\mu A^c_\nu$, with $\left[T^a, T^b\right] = ic^{abc}T^c$ and $a, b, c$ are $SU(3)_C$ color indices.

One can express the hadron four-momentum generator $P = (P^+, P^-, \mathbf{P}_\perp)$, $P^\pm = P^0 \pm P^3$, in terms of the dynamical fields, the Dirac field $\psi_+$, where $\psi_\pm = \Lambda_\pm \psi$, $\Lambda_\pm = \gamma^0\gamma^\pm$, and the transverse field $\mathbf{A}_\perp$ in the $A^+ = 0$ gauge[4] quantized on the light-front at fixed light-cone time $x^+$, $x^\pm = x^0 \pm x^3$

$$P^- = \frac{1}{2}\int dx^- d^2\mathbf{x}_\perp \bar{\psi}_+ \gamma^+ \frac{(i\nabla_\perp)^2 + m^2}{i\partial^+}\psi_+ + (\text{interactions}), \tag{3}$$

$$P^+ = \int dx^- d^2\mathbf{x}_\perp \bar{\psi}_+ \gamma^+ i\partial^+ \psi_+, \tag{4}$$

$$\mathbf{P}_\perp = \frac{1}{2}\int dx^- d^2\mathbf{x}_\perp \bar{\psi}_+ \gamma^+ i\nabla_\perp \psi_+, \tag{5}$$

where the integrals are over the null plane $\tau = x^+ = 0$, the hyper-plane tangent to the light cone. This is the initial-value surface for the fields where the commutation relations are fixed. The LF Hamiltonian $P^-$ generates LF time translations

$$\left[\psi_+(x), P^-\right] = i\frac{\partial}{\partial x^+}\psi_+(x), \tag{6}$$

to evolve the initial conditions to all space-time, whereas the LF longitudinal $P^+$ and transverse momentum $\mathbf{P}_\perp$ are kinematical generators. For simplicity we have omitted from (3-5) the contributions from the gluon field $\mathbf{A}_\perp$.

According to Dirac's classification of the forms of relativistic dynamics,[3] the fundamental generators of the Poincaré group can be separated into kinematical and dynamical generators. The kinematical generators act along the initial surface and leave the light-front plane invariant: they are thus independent of the dynamics and therefore contain no interactions. The dynamical generators change the light-front position and depend consequently on the interactions. In addition to $P^+$ and $\mathbf{P}_\perp$, the kinematical generators in the light-front frame are the $z$-component of the angular momentum $J^z$ and the boost operator $\mathbf{K}$. In addition to the Hamiltonian $P^-$, $J^z$ and $J^y$ are also dynamical generators. The light-front frame has the maximal number of kinematical generators.

### 2.2. *A semiclassical approximation to QCD*

A physical hadron in four-dimensional Minkowski space has four-momentum $P_\mu$ and invariant hadronic mass states $P_\mu P^\mu = \mathcal{M}^2$ determined by the Lorentz-invariant Hamiltonian equation for the relativistic bound-state system

$$H_{LF}|\psi(P)\rangle = \mathcal{M}^2|\psi(P)\rangle, \tag{7}$$

with $H_{LF} \equiv P_\mu P^\mu = P^- P^+ - \mathbf{P}_\perp^2$, where the hadronic state $|\psi\rangle$ is an expansion in multiparticle Fock eigenstates $|n\rangle$ of the free light-front Hamiltonian: $|\psi\rangle = \sum_n \psi_n |\psi\rangle$. The state $|\psi(P^+, \mathbf{P}_\perp, J^z)\rangle$ is an eigenstate of the total momentum $P^+$ and $\mathbf{P}_\perp$ and the total spin $J^z$. Quark and gluons appear from the light-front quantization of the excitations of the dynamical fields $\psi_+$ and $\mathbf{A}_\perp$, expanded in terms of creation and annihilation operators at fixed LF time $\tau$. The Fock components $\psi_n(x_i, \mathbf{k}_{\perp i}, \lambda_i)$ are independent of $P^+$ and $\mathbf{P}_\perp$ and depend only on relative partonic coordinates: the momentum fraction $x_i = k_i^+/P^+$, the transverse momentum $\mathbf{k}_{\perp i}$ and spin component $\lambda_i^z$. Momentum conservation requires $\sum_{i=1}^n x_i = 1$ and $\sum_{i=1}^n \mathbf{k}_{\perp i} = 0$. The LFWFs $\psi_n$ provide a *frame-independent* representation of a hadron which relates its quark and gluon degrees of freedom to their asymptotic hadronic state. Since for each constituent $k_i^+ = \sqrt{\mathbf{k}_i^2 + m_i^2} + k_i^z > 0$ there are no contributions from the vacuum. Thus, apart from possible zero modes, the light-front QCD vacuum is the trivial vacuum. The constituent spin and orbital angular momentum properties of the hadrons are also encoded in the LFWFs. Actually, the definition of quark and gluon angular momentum is unambiguous in Dirac's front form in light-cone gauge $A^+ = 0$, and the gluons have physical polarization $S_g^z = \pm 1$.

One can also derive light-front holography using a first semiclassical approximation to transform the fixed light-front time bound-state Hamiltonian equation of motion in QCD (7) to a corresponding wave equation in AdS space.[12] To this end we expand the initial and final hadronic states in terms of its Fock components. The computation is simplified in the frame $P = (P^+, \mathcal{M}^2/P^+, \vec{0}_\perp)$ where $P^2 = P^+ P^-$. We find

$$\mathcal{M}^2 = \sum_n \int [dx_i]\left[d^2\mathbf{k}_{\perp i}\right] \sum_q \left(\frac{\mathbf{k}_{\perp q}^2 + m_q^2}{x_q}\right) |\psi_n(x_i, \mathbf{k}_{\perp i})|^2 + (\text{interactions}), \tag{8}$$

plus similar terms for antiquarks and gluons ($m_g = 0$). The integrals in (8) are over the internal coordinates of the $n$ constituents for each Fock state

$$\int [dx_i] \equiv \prod_{i=1}^n \int dx_i \, \delta\Big(1 - \sum_{j=1}^n x_j\Big), \quad \int \left[d^2\mathbf{k}_{\perp i}\right] \equiv \prod_{i=1}^n \int \frac{d^2\mathbf{k}_{\perp i}}{2(2\pi)^3} \, 16\pi^3 \, \delta^{(2)}\Big(\sum_{j=1}^n \mathbf{k}_{\perp j}\Big), \tag{9}$$

with phase space normalization

$$\sum_n \int [dx_i] \left[d^2\mathbf{k}_{\perp i}\right] \, |\psi_n(x_i, \mathbf{k}_{\perp i})|^2 = 1. \tag{10}$$

Each constituent of the light-front wavefunction $\psi_n(x_i, \mathbf{k}_{\perp i}, \lambda_i)$ of a hadron is on its respective mass shell $k_i^2 = k_i^+ k_i^- - \mathbf{k}_{\perp i}^2 = m_i^2$, $i = 1, 2 \cdots n$. Thus $k_i^- = \left(\mathbf{k}_{\perp i}^2 + m_i^2\right)/x_i P^+$. However, the light-front wavefunction represents a state which is off the light-front energy shell: $P^- - \sum_i^n k_i^- < 0$, for a stable hadron. Scaling out $P^+ = \sum_i^n k_i^+$, the invariant mass of the constituents $\mathcal{M}_n$ is

$$\mathcal{M}_n^2 = \Big(\sum_{i=1}^n k_i^\mu\Big)^2 = \sum_i \frac{\mathbf{k}_{\perp i}^2 + m_i^2}{x_i}. \tag{11}$$

The functional dependence for a given Fock state is expressed in terms of the invariant mass, the measure of the off-energy shell of the bound state of the $n$-parton LFWF: $\mathcal{M}^2 - \mathcal{M}_n^2$.

The LFWF $\psi_n(x_i, \mathbf{k}_{\perp i}, \lambda_i)$ can be expanded in terms of $n - 1$ independent position coordinates $\mathbf{b}_{\perp j}$, $j = 1, 2, \ldots, n-1$, conjugate to the relative coordinates $\mathbf{k}_{\perp i}$, with $\sum_{i=1}^n \mathbf{b}_{\perp i} = 0$. We can also express Eq. (8) in terms of the internal impact coordinates $\mathbf{b}_{\perp j}$ with the result

$$\mathcal{M}^2 = \sum_n \prod_{j=1}^{n-1} \int dx_j \, d^2\mathbf{b}_{\perp j} \, \psi_n^*(x_j, \mathbf{b}_{\perp j}) \sum_q \left(\frac{-\nabla_{\mathbf{b}_{\perp q}}^2 + m_q^2}{x_q}\right) \psi_n(x_j, \mathbf{b}_{\perp j}) + (\text{interactions}). \tag{12}$$

The normalization is defined by

$$\sum_n \prod_{j=1}^{n-1} \int dx_j d^2\mathbf{b}_{\perp j} \left|\psi_n(x_j, \mathbf{b}_{\perp j})\right|^2 = 1. \tag{13}$$

If we want to simplify further the description of the multiple parton system and reduce its dynamics to a single variable problem, we must take the limit of quark masses to zero. Indeed, the underlying classical QCD Lagrangian with massless quarks is scale and conformal invariant,[30] and consequently only in this limit it is possible to map the equations of motion and transition matrix elements to their correspondent conformal AdS expressions.

To simplify the discussion we will consider a two-parton hadronic bound state. In the limit of zero quark mass $m_q \to 0$

$$\mathcal{M}^2 = \int_0^1 \frac{dx}{x(1-x)} \int d^2\mathbf{b}_\perp \, \psi^*(x, \mathbf{b}_\perp) \left(-\nabla^2_{\mathbf{b}_\perp}\right) \psi(x, \mathbf{b}_\perp) + (\text{interactions}). \tag{14}$$

For $n = 2$, the invariant mass is $\mathcal{M}^2_{n=2} = \frac{\mathbf{k}^2_\perp}{x(1-x)}$. Similarly, in impact space the relevant variable for a two-parton state is $\zeta^2 = x(1-x)\mathbf{b}^2_\perp$. Thus, to first approximation LF dynamics depend only on the boost invariant variable $\mathcal{M}_n$ or $\zeta$, and hadronic properties are encoded in the hadronic mode $\phi(\zeta)$ from the relation

$$\psi(x, \zeta, \varphi) = e^{iL\varphi} X(x) \frac{\phi(\zeta)}{\sqrt{2\pi\zeta}}, \tag{15}$$

thus factoring out the angular dependence $\varphi$ and the longitudinal, $X(x)$, and transverse mode $\phi(\zeta)$. This is a natural factorization in the light front since the corresponding canonical generators, the longitudinal and transverse generators $P^+$ and $\mathbf{P}_\perp$ and the $z$-component of the orbital angular momentum $J^z$ are kinematical generators which commute with the LF Hamiltonian generator $P^-$. We choose the normalization $\langle\phi|\phi\rangle = \int d\zeta \, |\langle\zeta|\phi\rangle|^2 = P_{q\bar{q}}$, where $P_{q\bar{q}}$ is the probability of finding the $q\bar{q}$ component in the pion light-front wavefunction. The longitudinal mode is thus normalized as $\int_0^1 \frac{X^2(x)}{x(1-x)} = 1$.

We can write the Laplacian operator in (14) in circular cylindrical coordinates $(\zeta, \varphi)$

$$\nabla^2_\zeta = \frac{1}{\zeta}\frac{d}{d\zeta}\left(\zeta \frac{d}{d\zeta}\right) + \frac{1}{\zeta^2}\frac{\partial^2}{\partial\varphi^2}, \tag{16}$$

and factor out the angular dependence of the modes in terms of the $SO(2)$ Casimir representation $L^2$ of orbital angular momentum in the transverse plane. Using (15) we find[12]

$$\mathcal{M}^2 = \int d\zeta \, \phi^*(\zeta) \sqrt{\zeta} \left(-\frac{d^2}{d\zeta^2} - \frac{1}{\zeta}\frac{d}{d\zeta} + \frac{L^2}{\zeta^2}\right) \frac{\phi(\zeta)}{\sqrt{\zeta}} + \int d\zeta \, \phi^*(\zeta) U(\zeta) \phi(\zeta), \tag{17}$$

where $L = |L^z|$. In writing the above equation we have summed the complexity of the interaction terms in the QCD Lagrangian by the introduction of the effective potential $U(\zeta)$, which is modeled to enforce confinement at some IR scale. The LF eigenvalue equation $P_\mu P^\mu |\phi\rangle = \mathcal{M}^2 |\phi\rangle$ is thus a light-front wave equation for $\phi$

$$\left(-\frac{d^2}{d\zeta^2} - \frac{1 - 4L^2}{4\zeta^2} + U(\zeta)\right) \phi(\zeta) = \mathcal{M}^2 \phi(\zeta), \tag{18}$$

a relativistic single-variable LF Schrödinger equation. Its eigenmodes $\phi(\zeta)$ determine the hadronic mass spectrum and represent the probability amplitude to find $n$-partons at transverse impact separation $\zeta$, the invariant separation between pointlike constituents within the hadron[13] at equal LF time. Thus the effective interaction potential is instantaneous in LF time $\tau$, not instantaneous in ordinary time $t$. The LF potential thus satisfies causality, unlike the instantaneous Coulomb interaction. Extension of the results to arbitrary $n$ follows from the $x$-weighted definition of the transverse impact variable of the $n-1$ spectator system[13]

$$\zeta = \sqrt{\frac{x}{1-x}}\Big|\sum_{j=1}^{n-1} x_j \mathbf{b}_{\perp j}\Big|, \tag{19}$$

where $x = x_n$ is the longitudinal momentum fraction of the active quark. One can also generalize the equations to allow for the kinetic energy of massive quarks using Eqs. (8) or (12).[31] In this case, however, the longitudinal mode $X(x)$ does not decouple from the effective LF bound-state equations.

### 2.3. *Higher spin hadronic modes in AdS space*

We now turn to the formulation of bound-state equations for mesons of arbitrary spin $J$ in AdS space [a]. As we shall show in the next section, there is a remarkable correspondence between the equations of motion in AdS space and the Hamiltonian equation for the relativistic bound-state system for the corresponding angular momentum in light-front theory.

The description of higher spin modes in AdS space is a notoriously difficult problem.[33–35] A spin-$J$ field in $\mathrm{AdS}_{d+1}$ is represented by a rank $J$ tensor field $\Phi(x^A)_{M_1\cdots M_J}$, which is totally symmetric in all its indices. Such a tensor contains also lower spins, which can be eliminated by imposing gauge conditions. The action for a spin-$J$ field in $\mathrm{AdS}_{d+1}$ space-time in presence of a dilaton background field $\varphi(z)$ (the string frame) is given by

$$S = \frac{1}{2}\int d^d x\, dz\, \sqrt{g}\, e^{\varphi(z)}\Big(g^{NN'} g^{M_1 M_1'} \cdots g^{M_J M_J'} D_N \Phi_{M_1\cdots M_J} D_{N'} \Phi_{M_1'\cdots M_J'} \\ - \mu^2 g^{M_1 M_1'} \cdots g^{M_J M_J'} \Phi_{M_1\cdots M_J} \Phi_{M_1'\cdots M_J'} + \cdots\Big), \tag{20}$$

where $M, N = 1, \cdots, d+1$, $\sqrt{g} = (R/z)^{d+1}$ and $D_M$ is the covariant derivative which includes parallel transport. The omitted terms in (20) refer to terms with different contractions. The coordinates of AdS are the Minkowski coordinates $x^\mu$ and the holographic variable $z$ labeled $x^M = (x^\mu, z)$. The d + 1 dimensional mass $\mu$ is not a physical observable and is *a priory* an arbitrary parameter. The dilaton background field $\varphi(z)$ in (20) introduces an energy scale in the five-dimensional AdS action, thus breaking its conformal invariance. It is a function of the holographic coordinate $z$ which vanishes in the conformal ultraviolet limit $z \to 0$. In the hard wall model $\varphi = 0$ and the conformality is broken by the IR boundary conditions at $z = z_0 \sim 1/\Lambda_{\rm QCD}$.

A physical hadron has plane-wave solutions and polarization indices $M$ along the 3 + 1 physical coordinates

$$\Phi_P(x, z)_{\mu_1\cdots\mu_J} = e^{-iP\cdot x}\Phi(z)_{\mu_1\cdots\mu_J}, \tag{21}$$

with four-momentum $P_\mu$ and invariant hadronic mass $P_\mu P^\mu = \mathcal{M}^2$. All other components vanish identically: $\Phi_{z\mu_2\cdots\mu_J} = \Phi_{\mu_1 z\cdots\mu_J} = \cdots = \Phi_{\mu_1\mu_2\cdots z} = 0$. One can then construct an effective action in terms of high spin modes $\Phi_J = \Phi_{\mu_1\mu_2\cdots\mu_J}$, with only physical degrees of freedom.[23] In this case the system of coupled differential equations which follow from (20) reduce to a homogeneous equation in terms of the physical field $\Phi_J$.

In terms of fields with tangent indices

$$\hat{\Phi}_{A_1 A_2\cdots A_J} = e^{M_1}_{A_1} e^{M_2}_{A_2} \cdots e^{M_J}_{A_J}\, \Phi_{M_1 M_2\cdots M_J} = \left(\frac{z}{R}\right)^J \Phi_{A_1 A_2\cdots A_J}, \tag{22}$$

[a]This section is based on our collaboration with Hans Guenter Dosch. A detailed discussion of higher integer and half-integer spin wave equations in modified AdS spaces will be given in Ref.[32] See also the discussion in Ref.[37]

we find the effective action[32] ($\hat\Phi_J \equiv \hat\Phi_{\mu_1\cdots\mu_J}$)

$$S = \frac{1}{2}\int d^d x\, dz\; \sqrt{g}\, e^{\varphi(z)}\Big(g^{NN'}\,\partial_N\hat\Phi_J\partial_{N'}\hat\Phi_J - \mu^2\hat\Phi_J^2\Big), \tag{23}$$

containing only the physical degrees of freedom and usual derivatives. Thus, the effect of the covariant derivatives in the effective action for spin-$J$ fields with polarization components along the physical coordinates is a shift in the AdS mass $\mu$. The vielbein $e^A_M$ is defined by $g_{MN} = e^A_M e^B_N \eta_{AB}$, where $A, B = 1, \cdots, d+1$ are tangent AdS space indices and $\eta_{AB}$ has diagonal components $(1, -1, \cdots, -1)$. In AdS the vielbein is $e^A_M = (R/z)\delta^A_M$.

In terms of the AdS field $\Phi_J \equiv \Phi_{\mu_1\cdots\mu_J}$ we can express the effective action (23)

$$S = \frac{1}{2}\int d^d x\, dz\; \sqrt{g_J}\, e^{\varphi(z)}\Big(g^{NN'}\,\partial_N\Phi_J\partial_{N'}\Phi_J - \mu^2\Phi_J^2\Big), \tag{24}$$

where we have defined an effective metric determinant

$$\sqrt{g_J} = (R/z)^{d+1-2J}, \tag{25}$$

and rescaled the AdS mass $\mu$ in (23). Variation of the higher-dimensional action (24) gives the AdS wave equation for the spin-$J$ mode $\Phi_J$

$$\left[-\frac{z^{d-1-2J}}{e^{\varphi(z)}}\partial_z\left(\frac{e^{\varphi}(z)}{z^{d-1-2J}}\partial_z\right) + \left(\frac{\mu R}{z}\right)^2\right]\Phi(z)_J = \mathcal{M}^2\Phi(z)_J, \tag{26}$$

where the eigenmode $\Phi_J$ is normalized according to

$$R^{d-1-2J}\int_0^\infty \frac{dz}{z^{d-1-2J}}\, e^{\varphi(z)}\Phi_J^2(z) = 1. \tag{27}$$

The AdS mass is $\mu$ obeys the relation

$$(\mu R)^2 = (\tau - J)(\tau - d + J), \tag{28}$$

which follows from the scaling behavior of the tangent AdS field near $z \to 0$, $\hat\Phi_J \sim z^\tau$.

We can also derive (26) by shifting dimensions for a $J$-spin mode.[12,38] To this end, we start with the scalar wave equation which follows from the variation of (20) for $J = 0$. This case is particularly simple as the covariant derivative of a scalar field is the usual derivative. We obtain the eigenvalue equation

$$\left[-\frac{z^{d-1}}{e^{\varphi(z)}}\partial_z\left(\frac{e^{\varphi(z)}}{z^{d-1}}\partial_z\right) + \left(\frac{\mu R}{z}\right)^2\right]\Phi = \mathcal{M}^2\Phi. \tag{29}$$

A physical spin-$J$ mode $\Phi_{\mu_1\cdots\mu_J}$ with all indices along 3+1 is constructed by shifting dimensions $\Phi_J(z) = (z/R)^{-J}\Phi(z)$. It is simple to show that the shifted field $\Phi_{\mu_1\mu_2\cdots\mu_J}$ obeys the wave equation (26) which follows from (29) upon mass rescaling $(\mu R)^2 \to (\mu R)^2 - J(d-J) + Jz\,\varphi'(z)$.

### 2.3.1. *Non-conformal warped metrics*

In the Einstein frame conformal invariance is broken by the introduction of an additional warp factor in the AdS metric in order to include confinement forces

$$\begin{aligned} ds^2 &= (g_E)_{MN} dx^M dx^N \\ &= \frac{R^2}{z^2} e^{\lambda(z)}\left(\eta_{\mu\nu}dx^\mu dx^\nu - dz^2\right). \end{aligned} \tag{30}$$

The action is

$$S = \frac{1}{2}\int d^d x\, dz\, \sqrt{g_E}\Big(g_E^{NN'} g_E^{M_1 M_1'} \cdots g_E^{M_J M_J'} D_N \Phi_{M_1\cdots M_J} D_{N'} \Phi_{M_1'\cdots M_J'} - \mu^2 g_E^{M_1 M_1'} \cdots g_E^{M_J M_J'} \Phi_{M_1\cdots M_J} \Phi_{M_1'\cdots M_J'} + \cdots\Big), \quad (31)$$

where $g_E^{MN} \equiv (g_E)^{MN}$ and $(g_E)_{MN} = \frac{R^2}{z^2} e^{\lambda(z)} \eta_{MN}$. The flat metric $\eta_{MN}$ has diagonal components $(1, -1, \cdots, -1)$.

The use of warped metrics is useful to visualize the overall confinement behavior as we follow an object in warped AdS space as it falls to the infrared region by the effects of gravity. The gravitational potential energy for an object of mass $m$ in general relativity is given in terms of the time-time component of the metric tensor $g_{00}$

$$V = mc^2 \sqrt{(g_E)_{00}} = mc^2 R\, \frac{e^{\lambda(z)/2}}{z}, \quad (32)$$

thus we may expect a potential that has a minimum at the hadronic scale $z_0$ and grows fast for larger values of $z$ to confine effectively a particle in a hadron within distances $z \sim z_0$. In fact, according to Sonnenscheim[39] a background dual to a confining theory should satisfy the conditions for the metric component $g_{00}$

$$\partial_z (g_{00})|_{z=z_0} = 0, \quad g_{00}|_{z=z_0} \neq 0, \quad (33)$$

to display the Wilson loop area law for confinement of strings.

To relate the results in the Einstein frame where hadronic modes propagate in the non-conformal warped metrics (30) to the results in the String-Jordan frame (20), we scale away the dilaton profile by a redefinition of the fields in the action. This corresponds to the multiplication of the metric determinant $\sqrt{g_E} = \left(\frac{R}{z}\right)^{d+1} e^{(d+1)\lambda(z)/2}$ by the contravariant tensor $(g_E)^{MN}$. Thus the result[32] $\varphi(z) \to \frac{d-1}{2}\lambda(z)$, or $\varphi \to \frac{3}{2}\lambda$ for $AdS_5$.

### 2.3.2. *Effective confining potentials in AdS*

For some applications it is convenient to scale away the dilaton factor in the action by a field redefinition.[40] For example, for a scalar field we can shift $\Phi \to e^{-\varphi/2}\Phi$, and the bilinear component in the action is transformed into the equivalent problem of a free kinetic part plus an effective confining potential $V(z)$ which breaks the conformal invariance. [a] For the spin-$J$ effective action (24) we find upon the field redefinition $\Phi_J \to e^{-\varphi/2}\Phi_J$

$$S = \frac{1}{2}\int d^d x\, dz\, \sqrt{g_J}\Big(g^{NN'} \partial_N \Phi_J \partial_{N'} \Phi_J - \mu^2 \Phi_J^2 - V(z) \Phi_J^2\Big) - \frac{1}{4}\lim_{\epsilon\to 0} \int d^d x \left(\frac{R}{z}\right)^{d-1-2J} \varphi'(z) \Phi_J^2\Big|_{\epsilon}^{\infty}, \quad (34)$$

with effective metric determinant (25) $\sqrt{g_J} = (R/z)^{d+1-2J}$ and effective potential $V(z) = \frac{z^2}{R^2} U(z)$, where

$$U(z) = \frac{1}{2}\varphi''(z) + \frac{1}{4}\varphi'(z)^2 + \frac{2J - d + 1}{2z}\varphi'(z). \quad (35)$$

The action (24) is thus equivalent, modulo a surface term, to the action (34) written in terms of the rotated fields $\Phi_J \to e^{-\varphi/2}\Phi_J$. The result (35) is identical to the result obtained in Ref.[37] As we will show in the

[a] In fact, for fermions the conformality cannot be broken by the introduction of a dilaton background or by explicitly deforming the AdS metric as discussed above, since the additional warp factor is scaled away by a field redefinition. In this case the breaking of the conformal invariance and the generation of the fermion spectrum can only be accomplished by the introduction of an effective potential. This is further discussed in Sec. 5.2.

following section, the effective potential (35), for $d = 4$, is precisely the effective light-front potential which appears in Eq. (18), where the LF transverse impact variable $\zeta$ is identified with the holographic variable $z$.

A different approach is discussed in Ref.[41] where the infrared physics is introduced by a back-reaction model to the AdS metric. See also Refs.[42–45]

### 2.4. *Light-front holographic mapping*

The structure of the QCD light-front Hamiltonian equation (7) for the state $|\psi(P)\rangle$ is similar to the structure of the wave equation (26) for the $J$-mode $\Phi_{\mu_1 \cdots \mu_J}$ in AdS space; they are both frame-independent and have identical eigenvalues $\mathcal{M}^2$, the mass spectrum of the color-singlet states of QCD. This provides the basis for a profound connection between physical QCD formulated in the light-front and the physics of hadronic modes in AdS space. However, important differences are also apparent: Eq. (7) is a linear quantum-mechanical equation of states in Hilbert space, whereas Eq. (26) is a classical gravity equation; its solutions describe spin-$J$ modes propagating in a higher dimensional warped space. Physical hadrons are composite, and thus inexorably endowed of orbital angular momentum. Thus, the identification of orbital angular momentum is of primary interest in establishing a connection between both approaches. In fact, to a first semiclassical approximation, light-front QCD is formally equivalent to the equations of motion on a fixed gravitational background[12] asymptotic to $AdS_5$, where the prominent properties of confinement are encoded in a dilaton profile $\varphi(z)$.

As shown in Sect. 2.2, one can indeed systematically reduce the LF Hamiltonian eigenvalue Eq. (7) to an effective relativistic wave equation (18), analogous to the AdS equations, by observing that each $n$-particle Fock state has an essential dependence on the invariant mass of the system and thus, to a first approximation, LF dynamics depend only on $\mathcal{M}_n^2$. In impact space the relevant variable is the boost invariant variable $\zeta$, which measures the separation of quarks and gluons, and which also allows one to separate the bound state dynamics of the constituents from the kinematics of their internal angular momentum.

Upon the substitution $z \to \zeta$ and

$$\phi_J(\zeta) = (\zeta/R)^{-3/2+J} \, e^{\varphi(z)/2} \, \Phi_J(\zeta), \tag{36}$$

in (26), we find for $d = 4$ the QCD light-front wave equation (18) with effective potential[38]

$$U(\zeta) = \frac{1}{2}\varphi''(\zeta) + \frac{1}{4}\varphi'(\zeta)^2 + \frac{2J-3}{2z}\varphi'(\zeta), \tag{37}$$

provided that the fifth dimensional mass $\mu$ is related to the internal orbital angular momentum $L = max|L^z|$ and the total angular momentum $J^z = L^z + S^z$ of the hadron. Light-front holographic mapping thus implies that the fifth dimensional AdS mass $\mu$ is not a free parameter but scales as

$$(\mu R)^2 = -(2-J)^2 + L^2. \tag{38}$$

The angular momentum projections in the light-front $\hat{z}$ direction $L^z, S^z$ and $J^z$ are kinematical generators in the front form, so they are the natural quantum numbers to label the eigenstates of light-front physics. In general, a hadronic eigenstate with spin $J^z$ in the front form corresponds to an eigenstate of $J^2 = j(j+1)$ in the rest frame in the conventional instant form. It thus has $2j+1$ degenerate states with $J^z = -j, -j+1, \cdots j-1, +j$,[4] thus $J$ represents the maximum value of $|J^z|$, $J = max|J^z|$.

If $L^2 < 0$, the LF Hamiltonian defined in Eq. (7) is unbounded from below $\langle\phi|H_{LF}|\phi\rangle < 0$ and the spectrum contains an infinite number of unphysical negative values of $\mathcal{M}^2$ which can be arbitrarily large. As $\mathcal{M}^2$ increases in absolute value, the particle becomes localized within a very small region near $\zeta = 0$, since the effective potential is conformal at small $\zeta$. For $\mathcal{M}^2 \to -\infty$ the particle is localized at $\zeta = 0$, the particle "falls towards the center".[46] The critical value $L = 0$ corresponds to the lowest possible stable solution, the ground state of the light-front Hamiltonian. For $J = 0$ the five dimensional mass $\mu$ is related to the orbital momentum of the hadronic bound state by $(\mu R)^2 = -4 + L^2$ and thus $(\mu R)^2 \geq -4$. The quantum mechanical stability condition $L^2 \geq 0$ is thus equivalent to the Breitenlohner-Freedman stability bound in AdS.[47] The scaling dimensions are $2+L$ independent of $J$, in agreement with the twist-scaling dimension of a two-parton bound state in QCD. It is important to notice that in the light-front the $SO(2)$ Casimir for orbital angular momentum $L^2$ is a kinematical quantity, in contrast to the usual $SO(3)$ Casimir $L(L+1)$ from non-relativistic physics which is rotational, but not boost invariant. The $SO(2)$ Casimir form $L^2$ corresponds to the group of rotations in the transverse LF plane. Indeed, the Casimir operator for $SO(N) \sim S^{N-1}$ is $L(L+N-2)$.

## 3. Mesons in light-front holography

Considerable progress has recently been achieved in the study of the meson excitation spectrum in QCD from discrete lattices which is a first-principles method.[48] In practice, lattice gauge theory computations of eigenvalues beyond the ground-state are very challenging. Furthermore, states at rest are not classified according to total angular momentum $J$ and $J_z$, but according to the irreducible representation of the lattice, and thus a large basis of interpolating operators is required for the extraction of meaningful data.[48] In contrast, the semiclassical light-front holographic wave equation (18) obtained in the previous section describes relativistic bound states at equal light-front time with a simplicity comparable to the Schrödinger equation of atomic physics at equal instant time. It thus provides a framework for a first-order analytical exploration of the spectrum of mesons. In the limit of zero-quark masses, the light-front wave equation has a geometrical equivalent to the equation of motion in a warped AdS space-time.

### 3.1. *A hard-wall model for mesons*

As the simplest example we consider a truncated model where quarks propagate freely in the hadronic interior up to the confinement scale $1/\Lambda_{\rm QCD}$. The interaction terms in the QCD Lagrangian effectively build confinement, here depicted by a hard wall potential

$$U(\zeta) = \begin{cases} 0 & \text{if} \quad \zeta \leq \frac{1}{\Lambda_{\rm QCD}}, \\ \infty & \text{if} \quad \zeta > \frac{1}{\Lambda_{\rm QCD}}. \end{cases} \tag{39}$$

This provides an analog of the MIT bag model[49] where quarks are permanently confined inside a finite region of space. In contrast to bag models, boundary conditions are imposed on the boost-invariant variable $\zeta$, not on the bag radius at fixed time. The wave functions have support for longitudinal momentum fraction $0 < x < 1$. The resulting model is a manifestly Lorentz invariant model with confinement at large distances, while incorporating conformal behavior at small physical separation.

The eigenvalues of the LF wave equation (18) for the potential (39) are determined by the boundary conditions $\phi(z = 1/\Lambda_{\rm QCD}) = 0$, and are given in terms of the roots of the Bessel functions: $\mathcal{M}_{L,k} = \beta_{L,k}\Lambda_{\rm QCD}$. Light-front eigenmodes $\phi(\zeta)$ are normalized according to

$$\int_0^{\Lambda_{\rm QCD}^{-1}} d\zeta\, \phi^2(\zeta) = 1, \tag{40}$$

and are given by

$$\phi_{L,k}(\zeta) = \frac{\sqrt{2}\Lambda_{QCD}}{J_{1+L}(\beta_{L,k})} \sqrt{\zeta} J_L(\zeta\beta_{L,k}\Lambda_{QCD})\,. \tag{41}$$

Individual hadron states can be identified by their interpolating operators, which are defined at the $z \to 0$ asymptotic boundary of AdS space, and couple to the AdS field $\hat{\Phi}(x,z)$ (22) at the boundary limit (See Appendix 9). The short-distance behavior of a hadronic state is characterized by its twist (canonical dimension minus spin) $\tau = \Delta - \sigma$, where $\sigma$ is the sum over the constituent's spin $\sigma = \sum_{i=1}^{n} \sigma_i$. The twist of a hadron is also equal to the number of its constituent partons $n$. [a]

Pion interpolating operators are constructed by examining the behavior of bilinear covariants $\overline{\psi}\Gamma\psi$ under charge conjugation and parity transformation. Thus, for example, a pion interpolating operator $\overline{q}\gamma^+\gamma_5 q$ creates a state with quantum numbers $J^{PC} = 0^{-+}$, and a vector meson interpolating operator $\overline{q}\gamma_\mu q$ a state $1^{--}$. Likewise the operator $\overline{q}\gamma_\mu\gamma_5 q$ creates a state with $1^{++}$ quantum numbers, for example the $a_1(1260)$ positive parity meson. If we include orbital excitations, the pion interpolating operator is $\mathcal{O}_{2+L} = \overline{q}\gamma^+\gamma_5 D_{\{\ell_1} \cdots D_{\ell_m\}} q$. This is an operator with total internal orbital momentum $L = \sum_{i=1}^{m} \ell_i$, twist $\tau = 2 + L$ and canonical dimension $\Delta = 3 + L$. Similarly the vector-meson interpolating operator is given by $\mathcal{O}^\mu_{2+L} = \overline{q}\gamma^\mu D_{\{\ell_1} \cdots D_{\ell_m\}} q$. The scaling of the AdS field $\hat{\Phi}$ (22) near $z \to 0$, $\hat{\Phi}(z) \sim z^\tau$, is precisely the scaling required to match the scaling dimension of the local meson interpolating operators.

| $L$ | $S$ | $n$ | $J^{PC}$ | Meson State |
|---|---|---|---|---|
| 0 | 0 | 0 | $0^{-+}$ | $\pi(140)$ |
| 0 | 0 | 1 | $0^{-+}$ | $\pi(1300)$ |
| 0 | 0 | 2 | $0^{-+}$ | $\pi(1800)$ |
| 0 | 1 | 0 | $1^{--}$ | $\rho(770)$ |
| 0 | 1 | 1 | $1^{--}$ | $\rho(1450)$ |
| 0 | 1 | 2 | $1^{--}$ | $\rho(1700)$ |
| 1 | 0 | 0 | $1^{+-}$ | $b_1(1235)$ |
| 1 | 1 | 0 | $0^{++}$ | $a_0(980)$ |
| 1 | 1 | 1 | $0^{++}$ | $a_0(1450)$ |
| 1 | 1 | 0 | $1^{++}$ | $a_1(1260)$ |
| 1 | 1 | 0 | $2^{++}$ | $a_2(1320)$ |
| 2 | 0 | 0 | $2^{-+}$ | $\pi_2(1670)$ |
| 2 | 0 | 1 | $2^{-+}$ | $\pi_2(1880)$ |
| 2 | 1 | 0 | $3^{--}$ | $\rho_3(1690)$ |
| 3 | 1 | 0 | $4^{++}$ | $a_4(2040)$ |

We list in Table 1 the confirmed (4-star and 3-star) isospin $I = 1$ mesons states from the updated Particle Data Group (PDG),[50] with their assigned internal spin, orbital angular momentum and radial quantum numbers. The $I = 1$ mesons have quark content $|u\overline{d}\rangle$, $\frac{1}{\sqrt{2}}|u\overline{u} - d\overline{d}\rangle$ and $|d\overline{u}\rangle$. The $I = 1$ mesons are the $\pi$, $b$, $\rho$ and $a$ mesons. We have not listed in Table 1 the $I = 0$ mesons which are a mix of $u\overline{u}$, $d\overline{d}$ and $s\overline{s}$, thus more complex entities. The light $I = 0$ mesons are $\eta$, $\eta'$, $h$, $h'$ $\omega$, $\phi$, $f$ and $f'$. This list comprises the puzzling $I = 0$ scalar $f$-mesons, which may be interpreted as a superposition of tetra-quark states with a $q\overline{q}$, $L = 1$, $S = 1$, configuration which couple to a $J = 0$ state.[51] [a]

[a]To include orbital $L$-dependence we make the substitution $\tau \to n + L$.

[a]The interpretation of the $\pi_1(1400)$ is not very clear[51] and is not included in Table 1. Likewise we do not include the $\pi_1(1600)$ in the present

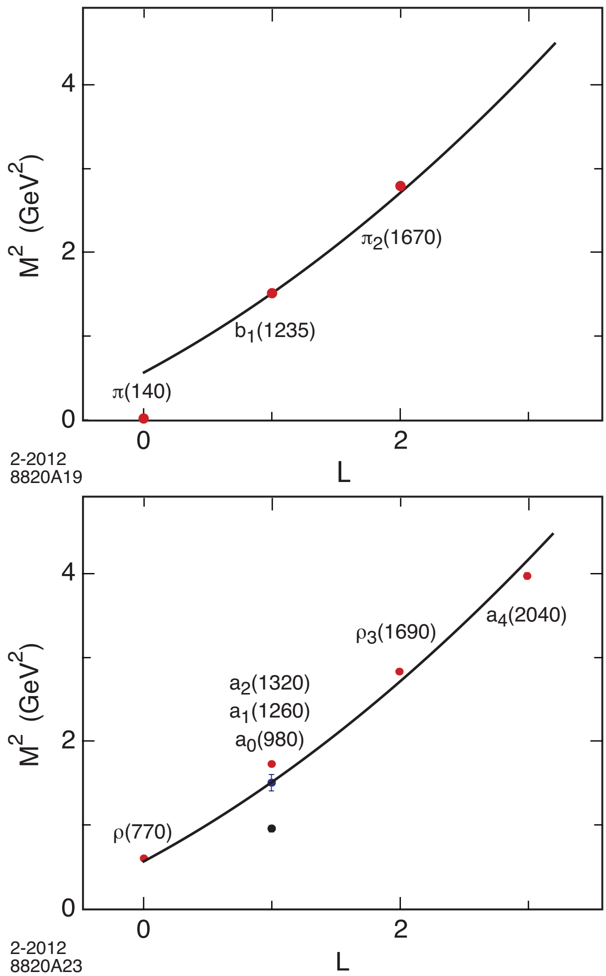


Fig. 1. $I = 1$ light-meson orbital states in the hard wall model for $\Lambda_{QCD} = 0.32$ GeV: pseudoscalar mesons (left) and vector mesons (right).

The light $I = 1$ orbital meson spectrum is compared in Fig. 1 with the truncated-space model for $n = 0$. The data is from PDG.[50] The predictions for the lower mass mesons are in better agreement with data as compared with Ref.,[52] where naive conformal dimensions were used instead. However the model fails to account for the pion as a chiral $\mathcal{M}_\pi = 0$ state. The hard-wall model for mesons is degenerate with respect to the orbital quantum number $L$, and thus fails to account for the important $L = |L^z| = 1$ triplet splitting shown in Fig. 1 (right); the $a_0(980)$, $a_1(1260)$ and $a_2(1320)$ states, which corresponds to $J = |J^z| = 0, 1, 2$ respectively. Using the asymptotic expansion of the Bessel function for large arguments we find that $\mathcal{M} \sim 2n + L$, in contrast to the usual Regge dependence $\mathcal{M}^2 \sim n + L$ found experimentally.[51] As a consequence, the radial modes are not well described in the truncated-space model. For example the first radial AdS eigenvalue has a mass 1.77 GeV, which is too high compared to the mass of the observed first radial excitation of the meson, the $\pi(1300)$.

analysis.

The shortcomings of the hard-wall model described in this section are evaded in the soft wall model discussed below, where the sharp cutoff is modified.

### 3.2. *A soft-wall model for mesons*

As we discussed in Sec. 2.4, the conformal metric of AdS space can be modified within the gauge/gravity framework to include confinement by the introduction of an additional warp factor or, equivalently, with a dilaton background $\varphi(z)$, which breaks the conformal invariance of the theory. A particularly interesting case is a dilaton profile $\exp\left(\pm\kappa^2 z^2\right)$ of either sign, since it leads to linear Regge trajectories[23] and avoids the ambiguities in the choice of boundary conditions at the infrared wall. The corresponding modified metric can be interpreted in the higher dimensional warped AdS space as a gravitational potential in the fifth dimension

$$V(z) = mc^2 \sqrt{g_{00}} = mc^2 R \frac{e^{\pm 3\kappa^2 z^2/4}}{z}. \tag{42}$$

In the case of the negative solution, the potential decreases monotonically, and thus an object located in the boundary of AdS space will fall to infinitely large values of $z$. This is illustrated in detail by Klebanov and Maldacena in Ref.[53] For the positive solution, the potential is nonmonotonic and has an absolute minimum at $z_0 \sim 1/\kappa$. Furthermore, for large values of $z$ the gravitational potential increases exponentially, thus confining any object to distances $\langle z\rangle \sim 1/\kappa$.[54,55]

From (37) we obtain for the positive sign confining solution $\varphi = \exp\left(\kappa^2 z^2\right)$ the effective potential[55]

$$U(\zeta) = \kappa^4 \zeta^2 + 2\kappa^2 (J-1), \tag{43}$$

which corresponds to a transverse oscillator in the light-front. For the effective potential (43) equation (18) has eigenfunctions

$$\phi_{n,L}(\zeta) = \kappa^{1+L} \sqrt{\frac{2n!}{(n+L)!}}\, \zeta^{1/2+L} e^{-\kappa^2 \zeta^2/2} L_n^L(\kappa^2 \zeta^2), \tag{44}$$

and eigenvalues [a]

$$\mathcal{M}^2_{n,J,L} = 4\kappa^2 \left(n + \frac{J+L}{2}\right). \tag{45}$$

The meson spectrum (45) has a string-theory Regge form $\mathcal{M}^2 \sim n + L$: the square of the eigenmasses are linear in both the angular momentum $L$ and radial quantum number $n$, where $n$ counts the number of nodes of the wavefunction in the radial variable $\zeta$. The LFWFs (44) for different orbital and radial excitations are depicted in Fig. 2. Constituent quark and antiquark separate from each other as the orbital and radial quantum numbers increase. The number of nodes in the light-front wave function depicted in Fig. 2 (b) correspond to the radial excitation quantum number $n$.

For the $J = L + S$ meson families Eq. (45) becomes

$$\mathcal{M}^2_{n,L,S} = 4\kappa^2 \left(n + L + \frac{S}{2}\right). \tag{46}$$

The lowest possible solution for $n = J = 0$ has eigenvalue $\mathcal{M}^2 = 0$. This is a chiral symmetric bound state of two massless quarks with scaling dimension 2 and size $\langle\zeta^2\rangle \sim 1/\kappa^2$, which we identify with the lowest state, the pion. Thus one can compute the corresponding Regge families by simply adding $4\kappa^2$ for a unit change in

[a] Similar results are found in Ref.[37]

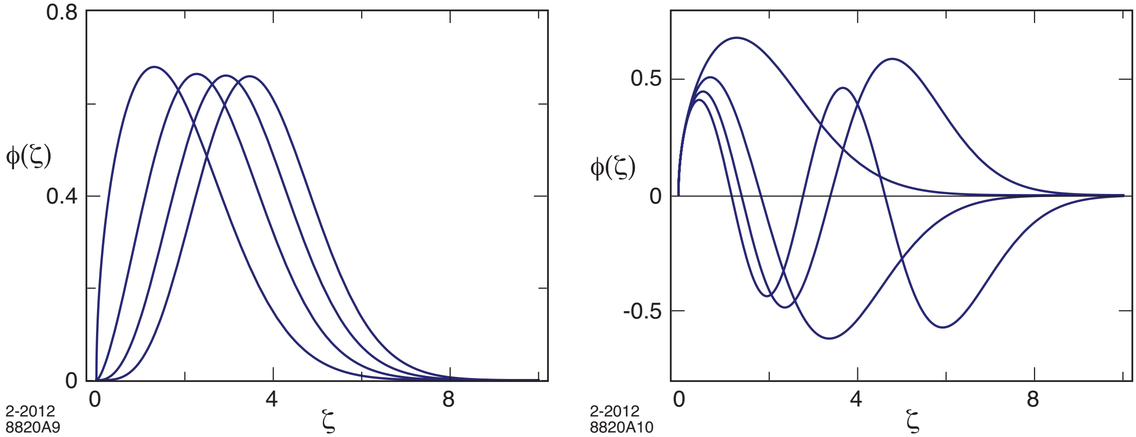


Fig. 2. Light-front wavefunctions $\phi_{n,L}(\zeta)$ in physical spacetime corresponding to a dilaton profile $\exp(\kappa^2 z^2)$: (left) orbital modes ($n = 0$) and (right) radial modes ($L = 0$).

the radial quantum number, $4\kappa^2$ for a change in one unit in the orbital quantum number and $2\kappa^2$ for a change of one unit of spin to the ground state value of $\mathcal{M}^2$. The spectral predictions for the $J = L + S$ light pseudoscalar and vector meson states, listed in Table. 1, are compared with experimental data in Fig. 3 for the positive sign dilaton model discussed here. The data is from PDG.[50]

It is important to notice that in contrast to the hard-wall model, the soft-wall model with positive dilaton accounts for the mass pattern observed in radial excitations, as well as for the triplet splitting for the $L = 1$, $J = 0, 1, 2$, vector meson $a$-states. Using the spectral formula (45) we find

$$\mathcal{M}_{a_2(1320)} > \mathcal{M}_{a_1(1260)} > \mathcal{M}_{a_0(980)}. \tag{47}$$

The predicted values are 0.76, 1.08 and 1.32 GeV for the masses of the $a_0(980)$, $a_1(1260)$ and $a_2(1320)$ vector mesons, compared with the experimental values 0.98, 1.23 and 1.32 GeV respectively. The prediction for the mass of the $L = 1$, $n = 1$ state $a_0(1450)$ is 1.53 GeV, compared with the observed value 1.47 GeV. For other calculations of the hadronic spectrum in the framework of AdS/QCD, see Refs.[56–73] [a]

## 4. Meson form factors

A form factor in QCD is defined by the transition matrix element of a local quark current between hadronic states. The great advantage of the front form – as emphasized by Dirac – is that boost operators are kinematic. Unlike the instant form, the boost operators in the front form have no interaction terms. The calculation of a current matrix element $\langle P + q|J^\mu|P\rangle$ requires boosting the hadronic eigenstate from $|P\rangle$ to $|P + q\rangle$, a task which becomes hopelessly complicated in the instant form. In addition, the virtual photon couples to connected currents which arise from the instant form vacuum.

In AdS space form factors are computed from the overlap integral of normalizable modes with boundary currents which propagate in AdS space. The AdS/CFT duality incorporates the connection between the twist scaling dimension of the QCD boundary interpolating operators to the falloff of the normalizable modes in AdS near its conformal boundary. If both quantities represent the same physical observable for any value of

[a]For recent reviews see, for example, Refs.[74,75]

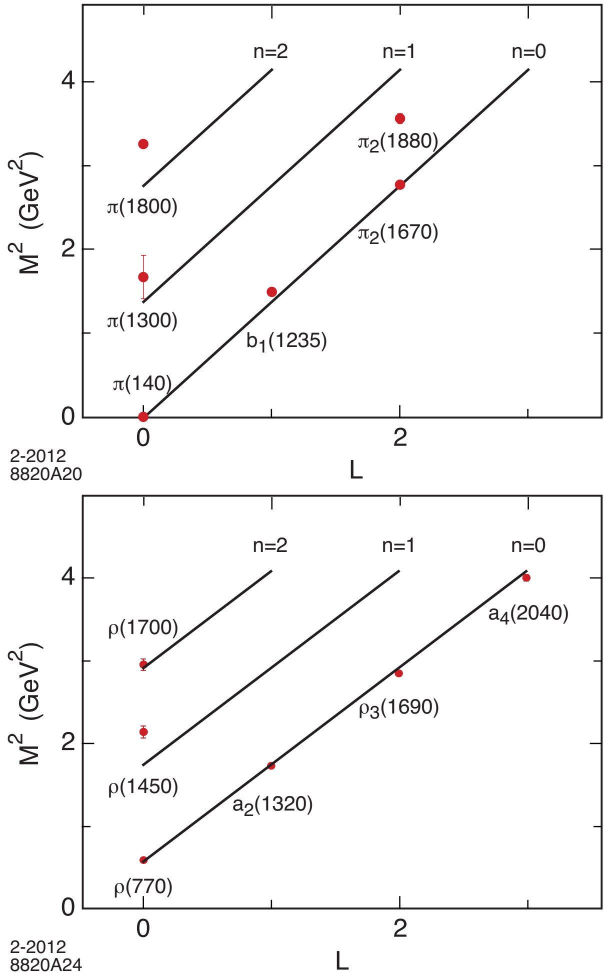


Fig. 3. $I = 1$ parent and daughter Regge trajectories for the $\pi$-meson family (left) with $\kappa = 0.59$ GeV; and the $\rho$-meson family (right) with $\kappa = 0.54$ GeV.

the transferred momentum squared $q^2$, a precise correspondence can be established between the string modes $\Phi$ in AdS space and the light front wavefunctions of hadrons $\psi_n$ in physical four dimensional space-time.[13] In fact, Light-Front Holography was originally derived by observing the correspondence between matrix elements obtained in AdS/CFT with the corresponding formula using the light-front representation.[13] The same results follow from comparing the relativistic light-front Hamiltonian equation describing bound states in QCD with the wave equations describing the propagation of modes in a warped AdS space, as shown in the previous section.[12]

### 4.1. *Meson electromagnetic form factor*

In the higher dimensional gravity theory, the hadronic transition matrix element corresponds to the coupling of an external electromagnetic field $A^M(x, z)$, for a photon propagating in AdS space, with the extended field

$\Phi_P(x,z)$ describing a meson in AdS is[15]

$$\int d^4x\, dz\, \sqrt{g}\, A^M(x,z)\Phi^*_{P'}(x,z)\overleftrightarrow{\partial}_M\Phi_P(x,z) \sim (2\pi)^4\delta^4\left(P'-P-q\right)\epsilon_\mu(P+P')^\mu F_M(q^2). \tag{48}$$

To simplify the discussion we will first describe a model with a wall at $z \sim 1/\Lambda_{\rm QCD}$ – the hard wall model – which limits the propagation of the string modes in AdS space beyond the IR separation $z \sim 1/\Lambda_{\rm QCD}$ and also sets the gap scale.[9] We recall from Sec. 2.3 that the coordinates of AdS$_5$ are the Minkowski coordinates $x^\mu$ and $z$ labeled $x^M = (x^\mu, z)$, with $M, N = 1, \cdots 5$, and $g$ is the determinant of the metric tensor. The pion has initial and final four momentum $P$ and $P'$ respectively and $q$ is the four-momentum transferred to the pion by the photon with polarization $\epsilon_\mu$. The expression on the right-hand side of (48) represents the space-like QCD electromagnetic transition amplitude in physical space-time

$$\langle P'|J^\mu(0)|P\rangle = (P+P')^\mu F_M(q^2). \tag{49}$$

It is the EM matrix element of the quark current $J^\mu = e_q\bar{q}\gamma^\mu q$, and represents a local coupling to pointlike constituents. Although the expressions for the transition amplitudes look very different, one can show that a precise mapping of the matrix elements can be carried out at fixed light-front time.[13,14]

The form factor is computed in the light front from the matrix elements of the plus-component of the current $J^+$ in order to avoid coupling to Fock states with different numbers of constituents. Expanding the initial and final meson states $|\psi_M(P^+, \mathbf{P}_\perp)\rangle$ in terms of Fock components, $|\psi_M\rangle = \sum_n \psi_{n/M}|n\rangle$, we obtain the DYW expression[16,17] upon the phase space integration over the intermediate variables in the $q^+ = 0$ frame:

$$F_M(q^2) = \sum_n \int [dx_i]\left[d^2\mathbf{k}_{\perp i}\right]\sum_j e_j\psi^*_{n/M}(x_i, \mathbf{k}'_{\perp i}, \lambda_i)\psi_{n/M}(x_i, \mathbf{k}_{\perp i}, \lambda_i), \tag{50}$$

where the phase space factor $[dx_i]\left[d^2\mathbf{k}_{\perp i}\right]$ is given by (9) and the variables of the light cone Fock components in the final-state are given by $\mathbf{k}'_{\perp i} = \mathbf{k}_{\perp i} + (1-x_i)\,\mathbf{q}_\perp$ for a struck constituent quark and $\mathbf{k}'_{\perp i} = \mathbf{k}_{\perp i} - x_i\,\mathbf{q}_\perp$ for each spectator. The formula is exact if the sum is over all Fock states $n$. The form factor can also be conveniently written in impact space as a sum of overlap of LFWFs of the $j = 1, 2, \cdots, n-1$ spectator constituents[76]

$$F_M(q^2) = \sum_n \prod_{j=1}^{n-1}\int dx_j d^2\mathbf{b}_{\perp j}\exp\!\Big(i\mathbf{q}_\perp\cdot\sum_{j=1}^{n-1}x_j\mathbf{b}_{\perp j}\Big)\left|\psi_{n/M}(x_j, \mathbf{b}_{\perp j})\right|^2, \tag{51}$$

corresponding to a change of transverse momentum $x_j\mathbf{q}_\perp$ for each of the $n-1$ spectators with $\sum_{i=1}^n \mathbf{b}_{\perp i} = 0$.

For definiteness we shall consider the $\pi^+$ valence Fock state $|u\bar{d}\rangle$ with charges $e_u = \frac{2}{3}$ and $e_{\bar{d}} = \frac{1}{3}$. For $n = 2$, there are two terms which contribute to Eq. (51). Exchanging $x \leftrightarrow 1-x$ in the second integral we find

$$F_{\pi^+}(q^2) = 2\pi\int_0^1\frac{dx}{x(1-x)}\int\zeta d\zeta\, J_0\!\left(\zeta q\sqrt{\frac{1-x}{x}}\right)\left|\psi_{u\bar{d}/\pi}(x,\zeta)\right|^2, \tag{52}$$

where $\zeta^2 = x(1-x)\mathbf{b}_\perp^2$ and $F_{\pi^+}(q\!=\!0) = 1$.

We now compare this result with the electromagnetic form factor in AdS space-time. The incoming electromagnetic field propagates in AdS according to $A_\mu(x^\mu, z) = \epsilon_\mu(q)e^{-iq\cdot x}V(q^2, z)$ in the gauge $A_z = 0$ (no physical polarizations along the AdS variable $z$). The bulk-to-boundary propagator $V(q^2, z)$ is the solution of the AdS wave equation given by ($Q^2 = -q^2 > 0$)

$$V(Q^2, z) = zQK_1(zQ), \tag{53}$$

with boundary conditions[15]

$$V(Q^2 = 0, z) = V(Q^2, z = 0) = 1. \tag{54}$$

The propagation of the pion in AdS space is described by a normalizable mode $\Phi_P(x^\mu, z) = e^{-iP\cdot x}\Phi(z)$ with invariant mass $P_\mu P^\mu = \mathcal{M}^2$ and plane waves along Minkowski coordinates $x^\mu$. Extracting the overall factor $(2\pi)^4\delta^4(P' - P - q)$ from momentum conservation at the vertex which arises from integration over Minkowski variables in (48), we find[15]

$$F(Q^2) = R^3 \int \frac{dz}{z^3}\, V(Q^2, z)\, \Phi^2(z), \tag{55}$$

where $F(Q^2 = 0) = 1$. Using the integral representation of $V(Q^2, z)$

$$V(Q^2, z) = \int_0^1 dx\, J_0\!\left(zQ\sqrt{\frac{1-x}{x}}\right), \tag{56}$$

we write the AdS electromagnetic form-factor as

$$F(Q^2) = R^3 \int_0^1 dx \int \frac{dz}{z^3}\, J_0\!\left(zQ\sqrt{\frac{1-x}{x}}\right)\Phi^2(z). \tag{57}$$

To compare with the light-front QCD form factor expression (52) we use the expression of the LFWF (15) in the transverse LF plane, where we factor out the longitudinal and transverse modes $\phi(\zeta)$ and $X(x)$ respectively. If both expressions for the form factor are to be identical for arbitrary values of $Q$, we obtain $\phi(\zeta) = (\zeta/R)^{3/2}\Phi(\zeta)$ and $X(x) = \sqrt{x(1-x)}$,[13] where we identify the transverse impact LF variable $\zeta$ with the holographic variable $z$, $z \to \zeta = \sqrt{x(1-x)}|\mathbf{b}_\perp|$. [a] Thus, in addition of recovering the expression found in Sec. 2.4 which relates the transverse mode $\phi(\zeta)$ in physical space-time to the field $\Phi$ in AdS space, we find a definite expression for the longitudinal LF mode $X(x)$. Identical results follow from mapping the matrix elements of the energy-momentum tensor.[18]

### 4.2. *Elastic form factor with a dressed current*

The results for the elastic form factor described above correspond to a ÒfreeÓ current propagating on AdS space. It is dual to the electromagnetic point-like current in the Drell-Yan-West light-front formula[16,17] for the pion form factor. The DYW formula is an exact expression for the form factor. It is written as an infinite sum of an overlap of LF Fock components with an arbitrary number of constituents. This allows one to map state-by-state to the effective gravity theory in AdS space. However, this mapping has the shortcoming that the multiple pole structure of the time-like form factor does not appear in the time-like region unless an infinite number of Fock states is included. Furthermore, the moments of the form factor at $Q^2 = 0$ diverge term-by-term; for example one obtains an infinite charge radius.[77] This could have been expected, as we are dealing with a massless quark approximation. In fact, infinite slopes also occur in chiral theories when coupling to a massless pion.

Alternatively, one can use a truncated basis of states in the LF Fock expansion with a limited number of constituents and the nonperturbative pole structure can be generated with a dressed EM current as in the Heisenberg picture, *i.e.*, the EM current becomes modified as it propagates in an IR deformed AdS space to simulate confinement. The dressed current is dual to a hadronic EM current which includes any number of virtual $q\bar{q}$ components. The confined EM current also leads to finite moments at $Q^2 = 0$, as illustrated in Fig. 4 for the EM pion form factor.

---

[a]Extension of the results to arbitrary $n$ follows from the $x$-weighted definition of the transverse impact variable of the $n-1$ spectator system given by Eq. (19). In general the mapping relates the AdS density $\Phi^2(z)$ to an effective LF single particle transverse density.[13]

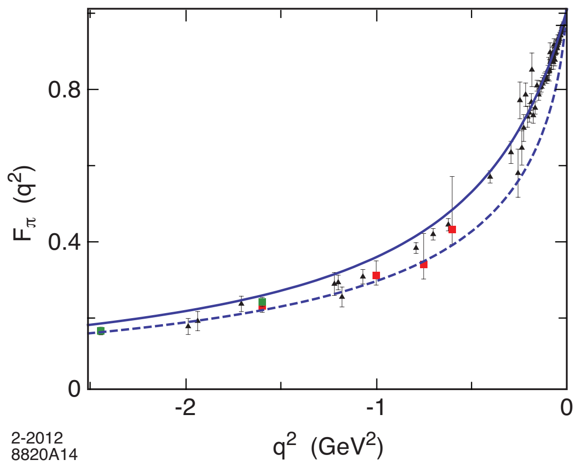


Fig. 4. Space-like electromagnetic pion form factor $F_\pi(q^2)$. Continuous line: confined current, dashed line free current. Triangles are the data compilation from Baldini,[78] boxes are JLAB data.[79]

We describe briefly below how to compute a form factor for a confined current in AdS space using a soft wall example. However, the actual computation of a form factor in AdS has several caveats which we will discuss in Sec. 4.4.

The effective potential corresponding to a dilaton profile $\exp(\pm\kappa^2 z^2)$ has the form of a harmonic oscillator confining potential $\kappa^4 z^2$. The normalizable solution for a meson of twist $\tau$ (the number of constituents for a given Fock component) corresponding to the lowest radial $n = 0$ and orbital $L = 0$ state is given by

$$\Phi^\tau(z) = \sqrt{\frac{2P_\tau}{\Gamma(\tau-1)}}\,\kappa^{\tau-1} z^\tau e^{-\kappa^2 z^2/2}, \tag{58}$$

with normalization

$$\langle \Phi^\tau | \Phi^\tau \rangle = \int \frac{dz}{z^3}\, e^{-\kappa^2 z^2}\, \Phi^\tau(z)^2 = P_\tau, \tag{59}$$

where $P_\tau$ is the probability for the twist $\tau$ mode (58). This agrees with the fact that the field $\Phi^\tau$ couples to a local hadronic interpolating operator of twist $\tau$ defined at the asymptotic boundary of AdS space (See Appendix 9), and thus the scaling dimension of $\Phi^\tau$ is $\tau$.

In the case of a soft-wall potential the EM bulk-to-boundary propagator is[14,80]

$$V(Q^2, z) = \Gamma\left(1 + \frac{Q^2}{4\kappa^2}\right) U\left(\frac{Q^2}{4\kappa^2}, 0, \kappa^2 z^2\right), \tag{60}$$

where $U(a, b, c)$ is the Tricomi confluent hypergeometric function

$$\Gamma(a) U(a, b, z) = \int_0^\infty e^{-zt} t^{a-1} (1+t)^{b-a-1} dt. \tag{61}$$

The modified current $V(Q^2, z)$, Eq. (60), has the same boundary conditions (54) as the free current (53), and reduces to (53) in the limit $Q^2 \to \infty$.[14] Eq. (60) can be conveniently written in terms of the integral representation[80]

$$V(Q^2, z) = \kappa^2 z^2 \int_0^1 \frac{dx}{(1-x)^2}\, x^{\frac{Q^2}{4\kappa^2}}\, e^{-\kappa^2 z^2 x/(1-x)}. \tag{62}$$

Substituting in (55) the expression for the hadronic state (58) with twist $\tau$ and the bulk-to-boundary propagator (62), we find that the corresponding elastic form factor for a twist $\tau$ Fock component $F_\tau(Q^2)$ $(Q^2 = -q^2 > 0)$[14]

$$F_\tau(Q^2) = \frac{P_\tau}{\left(1 + \frac{Q^2}{\mathcal{M}^2_\rho}\right)\left(1 + \frac{Q^2}{\mathcal{M}^2_{\rho'}}\right)\cdots\left(1 + \frac{Q^2}{\mathcal{M}^2_{\rho^{\tau-2}}}\right)}, \tag{63}$$

which is expressed as a $\tau - 1$ product of poles along the vector meson Regge radial trajectory. For a pion, for example, the lowest Fock state – the valence state – is a twist-2 state, and thus the form factor is the well known monopole form.[14] Thus the mean-square charge radius of the pion $\langle r_\pi^2 \rangle = 6/\mathcal{M}_\rho^2$ in the valence approximation. For $\mathcal{M}_\rho \simeq 770$ MeV we find $\langle r_\pi \rangle \simeq 0.63$ fm, compared with the experimental value $\langle r_\pi \rangle = 0.672 \pm 0.008$ fm.[50] In contrast, the computation with a free current gives the logarithmically divergent result [a].

$$\langle r_\pi^2 \rangle = \frac{3}{2} \ln\left(\frac{4\kappa^2}{Q^2}\right)\Big|_{Q^2 \to 0}. \tag{64}$$

The remarkable analytical form of (63), expressed in terms of the $\rho$ vector meson mass and its radial excitations, incorporates the correct scaling behavior from the constituent's hard scattering with the photon and the mass gap from confinement.

### 4.3. *Effective wave function from holographic mapping of a confined current*

It is also possible to find a precise mapping of a confined EM current propagating in a warped AdS space to the light-front QCD Drell-Yan-West expression for the form factor. In this case we we find an effective LFWF, which corresponds to a superposition of an infinite number of Fock states generated by the "dressed" confined current. For the soft-wall model this mapping can be done analytically.

The form factor in light-front QCD can be expressed in terms of an effective single-particle density[76]

$$F(Q^2) = \int_0^1 dx\, \rho(x, Q), \tag{65}$$

where

$$\rho(x, Q) = 2\pi \int_0^\infty b\, db\, J_0(bQ(1-x))|\psi(x, b)|^2, \tag{66}$$

for a two-parton state ($b = |\mathbf{b}_\perp|$).

We can also compute an effective density on the gravity side corresponding to a twist $\tau$ hadronic mode $\Phi_\tau$ in a modified AdS space. For the soft-wall model the expression is[14]

$$\rho(x, Q) = (\tau - 1)\,(1-x)^{\tau-2}\, x^{\frac{Q^2}{4\kappa^2}}. \tag{67}$$

To compare (67) with the QCD expression (66) for twist-two we use the integral

$$\int_0^\infty u\, du\, J_0(\alpha u)\, e^{-\beta u^2} = \frac{1}{2\beta}\, e^{-\alpha^2/4\beta}, \tag{68}$$

[a] The logarithmically divergent result does not appear in the hard-wall model if one uses Neumann boundary conditions. In this case the EM current is confined and $\langle r_\pi^2 \rangle \sim 1/\Lambda^2_{\rm QCD}$. A discussion of the pion form factor including chiral symmetry breaking effects in the hard-wall model is given in Refs.[81] and.[82]

and the relation $x^\gamma = e^{\gamma \ln(x)}$. We find the effective two-parton LFWF

$$\psi(x, \mathbf{b}_\perp) = \kappa \frac{(1-x)}{\sqrt{\pi \ln(\frac{1}{x})}}\, e^{-\frac{1}{2}\kappa^2 \mathbf{b}_\perp^2 (1-x)^2/\ln(\frac{1}{x})}, \tag{69}$$

in impact space. The momentum space expression follows from the Fourier transform of (69) and it is given by

$$\psi(x, \mathbf{k}_\perp) = 4\pi \frac{\sqrt{\ln\left(\frac{1}{x}\right)}}{\kappa(1-x)}\, x^{\mathbf{k}_\perp^2/2\kappa^2(1-x)^2} \tag{70}$$

$$= 4\pi \frac{\sqrt{\ln\left(\frac{1}{x}\right)}}{\kappa(1-x)}\, e^{-\mathbf{k}_\perp^2/2\kappa^2(1-x)^2 \ln\left(\frac{1}{x}\right)}. \tag{71}$$

The effective LFWF encodes nonperturbative dynamical aspects that cannot be learned from a term-by-term holographic mapping, unless one includes an infinite number of terms. Furthermore, it has the right analytical properties to reproduce the bound state vector meson pole in the time-like EM form factor. Unlike the "true" valence LFWF, the effective LFWF, which represents a sum of an infinite number of Fock components, is not symmetric in the longitudinal variables $x$ and $1 - x$ for the active and spectator quarks, respectively.

### 4.4. *Some caveats computing matrix elements in AdS/QCD*

The positive dilaton background $\exp(+\kappa^2 z^2)$ used in Sec. 3.2 leads to a successful description of the meson spectrum in terms of the internal quantum numbers $n$, $L$ and $S$, and has been preferred for computations in the framework of light-front holography, where the internal structure of hadrons is encoded in the wave function. The positive dilaton background has been discussed in the literature[37,54,55,83,84] since it has the expected behavior of a model dual to a confining theory.[39,53] This solution was studied in Ref.[23] but discarded in the same paper, as it leads to a spurious massless scalar mode in the two-point correlation function for vector mesons,[85] and a dilaton field with opposite sign, $\exp(-\kappa^2 z^2)$, was adopted instead.[23] However, using the results of Sec. 2.3.2, one can readily show that the difference in the effective potential $U(z)$ corresponding to positive and negative dilaton factors $\exp(\pm\kappa^2 z^2)$ simply amounts to a $z$-independent shift in the light-front effective potential $U$, which in fact vanishes in the vector meson $J = 1$ channel. From (35)

$$\Delta U(z) = U_\varphi(z) - U_{-\varphi}(z) = \varphi''(z) + \frac{2J - d + 1}{z}\varphi'(z), \tag{72}$$

in agreement with the results found in Ref.[37]

For the dilaton profile $\varphi = k^2 z^2$ we find for $d = 4$

$$\Delta U = 4(J-1)\kappa^2. \tag{73}$$

Therefore, from the point of view of light-front physics, plus and minus dilaton soft-wall solutions are equivalent upon a redefinition of the eigenvalues for $J \neq 1$. For $J = 1$ the effective potential is $U = \kappa^4 z^2$, identical for the plus and minus solutions.[40] Thus, the five-dimensional effective AdS action for a conserved EM current $V_M$ in presence of a confining potential $U = \kappa^4 z^2$[40]

$$S = \int d^4x\, dz\, \sqrt{g}\left(\frac{1}{4} F_{MN} F^{MN} - \frac{\kappa^4 z^4}{2R^2} V_M V^M\right), \tag{74}$$

where $F_{MN} = \partial_M V_N - \partial_N V_M$, only differs by a surface term from the action corresponding to plus or minus dilaton profiles. Equivalently, one can start from the five-dimensional action (74). Upon the field redefinition

$V_M \to e^{\pm\kappa^2 z^2/2} V_M$ one obtains the five-dimensional actions corresponding to plus or minus dilaton solutions, which differ from (74) only by a surface term. Consequently, essential physics cannot dependent on the particular choice of the dilaton sign.

Another difficulty found in the holographic approach to QCD is that the vector meson masses obtained from the spin-1 equation of motion do not match the poles of the dressed current when computing a form factor. The discrepancy, in the case of the pion, is an overall factor of $\sqrt{2}$ between the value of the gap scale which follows from the spectrum or from the computation of the pion form factor in the valence state approximation.[a] This is quite puzzling, since the same discrepancy is also found, for example, when computing a space-like form factor using the Drell-Yan-West expression, which is an exact expression if all Fock states are included. In AdS conserved currents are not renormalized and correspond to five dimensional massless fields propagating in AdS according to the relation $(\mu R)^2 = (\Delta - p)(\Delta + p - 4)$ for a $p$ form. In the usual AdS/QCD framework[20,21] this corresponds for $p = 1$ to $\Delta = 3$ or 1, the canonical dimensions of an EM current and the massless gauge field respectively. Normally, one uses a hadronic interpolating operator with minimum twist $\tau$ to identify a hadron and to predict the power-law fall-off behavior of its form factors and other hard scattering amplitudes;[9] *e.g.*, for a two-parton bound state $\tau = 2$. However, in the case of a current, one needs to use an effective field operator with dimension $\Delta = 3$. The apparent inconsistency between twist (28) and canonical dimension is removed by noticing that in the light-front one chooses to calculate the matrix element of the twist-3 plus component of the "good" current $J^+$,[13,14] in order to avoid coupling to Fock states with different numbers of constituents.[16,17]

As described in Sec. 2.4, light front holography provides a precise relation of the fifth-dimensional mass $\mu$ with the total and orbital angular momentum of a hadron in the transverse LF plane $(\mu R)^2 = -(2 - J)^2 + L^2$ (38). Thus the poles computed from the AdS wave equations for a conserved current $\mu R = 0$, correspond to a $J = L = 1$ twist-3 state. Following this, we can compute the mass of the radial excitations of the twist-3 vector family $J = L = 1$ using Eq. (45). The result is

$$\mathcal{M}^2_{n,J=1,L=1} = 4\kappa^2(n + 1), \tag{75}$$

which is identical with the results obtained in Ref.,[23] since, as explained above, the meson spectrum computed with positive or negative dilaton solutions is indistinguishable for $J = 1$.

The twist-3 computation of the space-like form factor, involves the current $J^+$, and the poles given by (75) do not correspond to the physical poles of the twist-2 transverse current $\mathbf{J}_\perp$ present in the annihilation channel, namely the $J = 1, L = 0$ state. In this case Eq. (45) gives for the twist-2, $J = 1$, $L = 0$ vector family the result

$$\mathcal{M}^2_{n,J=1,L=0} = 4\kappa^2\left(n + \frac{1}{2}\right). \tag{76}$$

Thus, to compare with physical data one must shift in (63) the twist-2 poles given by (75) to their physical positions (76). When the vector meson masses are shifted to their physical values the agreement of the predictions with observed data is very good.[86] We presume that the problem arises because of the specific truncation used.

### 4.5. *Meson transition form factors*

The photon-to-meson transition form factors [a] (TFFs) $F_{M\gamma}(Q^2)$ measured in $\gamma\gamma^* \to M$ reactions have been of intense experimental and theoretical interest. The pion transition form factor between a photon and pion

[a]This discrepancy is also present in the gap scale if one computes the spectrum and form factors without recourse to holographic methods, for example using the semi-classical approximation of Ref.[12] In this case a discrepancy of a factor factor $\sqrt{2}$ is also found between the spectrum and the computation of space-like form factors.

[a]This section is based on our collaboration with Fu-Guang Cao. Further details are given in.[87,88]

measured in the $e^-e^- \to e^-e^-\pi^0$ process, with one tagged electron, is the simplest bound-state process in QCD. It can be predicted from first principles in the asymptotic $Q^2 \to \infty$ limit.[89] More generally, the pion TFF at large $Q^2$ can be calculated at leading twist as a convolution of a perturbative hard scattering amplitude $T_H(\gamma\gamma^* \to q\bar{q})$ and a gauge-invariant meson distribution amplitude (DA), which incorporates the nonperturbative dynamics of the QCD bound-state.[89]

The BaBar Collaboration has reported measurements of the transition form factors from $\gamma^*\gamma \to M$ process for the $\pi^0$,[90] $\eta$, and $\eta'$[91,92] pseudoscalar mesons for a momentum transfer range much larger than previous measurements.[93,94] Surprisingly, the BaBar data for the $\pi^0$-$\gamma$ TFF exhibit a rapid growth for $Q^2 > 15$ GeV$^2$, which is unexpected from QCD predictions. In contrast, the data for the $\eta$-$\gamma$ and $\eta'$-$\gamma$ TFFs are in agreement with previous experiments and closer in agreement with theoretical predictions. Many theoretical studies have been devoted to explaining BaBar's experimental results.[95–111]

The pion transition form factor $F_{\pi\gamma}(Q^2)$ can be computed from first principles in QCD. To leading leading order in $\alpha_s(Q^2)$ and leading twist the result is[89] ($Q^2 = -q^2 > 0$)

$$Q^2 F_{\pi\gamma}(Q^2) = \frac{4}{\sqrt{3}} \int_0^1 \mathrm{d}x \frac{\phi(x, \bar{x}Q)}{\bar{x}} \left[1 + O\left(\alpha_s, \frac{m^2}{Q^2}\right)\right], \tag{77}$$

where $x$ is the longitudinal momentum fraction of the quark struck by the virtual photon in the hard scattering process and $\bar{x} = 1 - x$ is the longitudinal momentum fraction of the spectator quark. The pion distribution amplitude $\phi(x, Q)$ in the light-front formalism[89] is the integral of the valence $q\bar{q}$ LFWF in light-cone gauge $A^+ = 0$

$$\phi(x, Q) = \int_0^{Q^2} \frac{d^2\mathbf{k}_\perp}{16\pi^3} \psi_{q\bar{q}/\pi}(x, \mathbf{k}_\perp), \tag{78}$$

and has the asymptotic form[89] $\phi(x, Q \to \infty) = \sqrt{3} f_\pi x(1 - x)$; thus the leading order QCD result for the TFF at the asymptotic limit is obtained,[89]

$$Q^2 F_{\pi\gamma}(Q^2 \to \infty) = 2 f_\pi. \tag{79}$$

To describe the two-photon processes $\gamma\gamma^* \to M$, using light-front holographic methods similar to those described in Sec. 4, we need to explore the mathematical structure of higher-dimensional forms in the five dimensional action, since the amplitude (48) can only account for the elastic form factor $F_M(Q^2)$.[88] For example, in the five-dimensional AdS action there is an additional Chern-Simons (CS) term in addition to the usual Yang-Mills term $F^2$.[8] In the case of a $U(1)$ gauge theory the CS action is of the form $\epsilon^{LMNPQ} A_L \partial_M A_N \partial_P A_Q$. The CS action is not gauge invariant: under a gauge transformation it changes by a total derivative which gives a surface term. The CS form is the product of three fields at the same point in five-dimensional space corresponding to a local interaction. Indeed the five-dimensional CS action is responsible for the anomalous coupling of mesons to photons and has been used to describe, for example, the $\omega \to \pi\gamma$[112] decay as well as the $\gamma\gamma^* \to \pi^0$[113,114] and $\gamma^*\rho^0 \to \pi^0$[115] processes. [a]

The hadronic matrix element for the anomalous electromagnetic coupling to mesons in the higher gravity theory is given by the five-dimensional CS amplitude

$$\int d^4x \int dz\, \epsilon^{LMNPQ} A_L \partial_M A_N \partial_P A_Q \sim (2\pi)^4 \delta^{(4)}\left(P + q - k\right) F_{\pi\gamma}(q^2) \epsilon^{\mu\nu\rho\sigma} \epsilon_\mu(q) P_\nu \epsilon_\rho(k) q_\sigma, \tag{80}$$

[a]The anomalous EM couplings to mesons in the Sakai and Sugimoto model is described in Ref.[116]

which includes the pion field as well as the external photon fields by identifying the fifth component of $A$ with the meson mode in AdS space.[117] In the right-hand side of (80) $q$ and $k$ are the momenta of the virtual and on-shell incoming photons respectively with corresponding polarization vectors $\epsilon_\mu(q)$ and $\epsilon_\mu(k)$ for the amplitude $\gamma\gamma^* \to \pi^0$. The momentum of the outgoing pion is $P$.

We now compare the QCD expression on the right-hand side of (80) with the AdS transition amplitude on the left-hand side. As for the elastic form factor discussed in Sec. 4.1, the incoming off-shell photon is represented by the propagation of the non-normalizable electromagnetic solution in AdS space, $A_\mu(x^\mu, z) = \epsilon_\mu(q) e^{-iq\cdot x} V(q^2, z)$, where $V(q^2, z)$ is the bulk-to-boundary propagator with boundary conditions (54) $V(q^2 = 0, z) = V(q^2, z = 0) = 1$. Since the incoming photon with momentum $k$ is on its mass shell, $k^2 = 0$, its wave function is $A_\mu(x^\mu, z) = \epsilon_\mu(k) e^{ik\cdot x}$. Likewise, the propagation of the pion in AdS space is described by a normalizable mode $\Phi_P(x^\mu, z) = e^{-iP\cdot x}\Phi_\pi(z)$ with invariant mass $P_\mu P^\mu = \mathcal{M}_\pi^2 = 0$ in the chiral limit for massless quarks. The normalizable mode $\Phi_\pi(z)$ scales as $\Phi_\pi(z) \to z^2$ in the limit $z \to 0$, since the leading interpolating operator for the pion has twist two. A simple dimensional analysis implies that $A_z \sim \Phi_\pi(z)/z$, matching the twist scaling dimensions: two for the pion and one for the EM field. Substituting in (80) the expression given above for the the pion and the EM fields propagating in AdS, and extracting the overall factor $(2\pi)^4\delta^4\left(P' - q - k\right)$ upon integration over Minkowski variables, we find ($Q^2 = -q^2 > 0$)

$$F_{\pi\gamma}(Q^2) = \frac{1}{2\pi}\int_0^\infty \frac{dz}{z}\,\Phi_\pi(z) V\big(Q^2, z\big), \tag{81}$$

where the normalization is fixed by the asymptotic QCD prediction (79). We have defined our units such that the AdS radius $R = 1$.

Since the LF mapping of (81) to the asymptotic QCD prediction (79) only depends on the asymptotic behavior near the boundary of AdS space, the result is independent of the particular model used to modify the large $z$ IR region of AdS space. At large enough $Q$, the important contribution to (79) only comes from the region near $z \sim 1/Q$ where $\Phi(z) = 2\pi f_\pi z^2 + \mathcal{O}(z^4)$. Using the integral $\int_0^\infty dx\, x^\alpha K_1(x) = 2^{\alpha-2}\alpha\left[\Gamma\left(\frac{\alpha}{2}\right)\right]^2$, $\mathrm{Re}(\alpha) > 1$, we recover the asymptotic result (79)

$$Q^2 F_{\pi\gamma}(Q^2 \to \infty) = 2 f_\pi + \mathcal{O}\left(\frac{1}{Q^2}\right), \tag{82}$$

with the pion decay constant $f_\pi$[88]

$$f_\pi = \frac{1}{4\pi}\frac{\partial_z \Phi^\pi(z)}{z}\Big|_{z=0}. \tag{83}$$

A simple analytical expression for the pion TFF can be obtained from the "soft-wall" holographic model described in Sec. 4.2. Using (58) to describe the twist-two pion valence wave function in AdS space we find

$$Q^2 F_{\pi\gamma}(Q^2) = \frac{4}{\sqrt{3}}\int_0^1 dx \frac{\phi(x)}{1-x}\left[1 - \exp\left(-\frac{(1-x)P_{q\bar q}Q^2}{4\pi^2 f_\pi^2 x}\right)\right], \tag{84}$$

where $\phi(x) = \sqrt{3} f_\pi x(1-x)$ is the asymptotic QCD distribution with $f_\pi$ the pion decay constant and $P_{q\bar q}$ is the probability for the valence state. Remarkably, the holographic result for the pion TFF factor given by (84) for $P_{q\bar q} = 1$ is identical to the results for the pion TFF obtained with the exponential light-front wave function model of Musatov and Radyushkin[118] consistent with the leading order QCD result.[89] Since the pion field is identified as the fifth component of $A_M$, the CS form $\epsilon^{LMNPQ} A_L \partial_M A_N \partial_P A_Q$ is similar in form to an axial current; this correspondence can explain why the resulting pion distribution amplitude has the asymptotic form. [a]

[a] In Ref.[113] the pion TFF was studied in the framework of a CS extended hard-wall AdS/QCD model with $A_z \sim \partial_z \Phi(z)$. The expression for

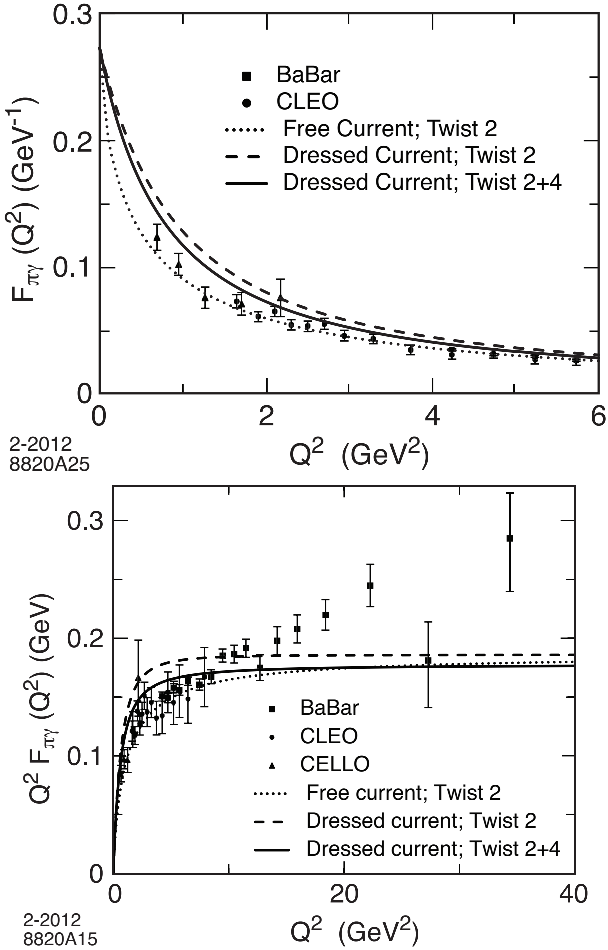


Fig. 5. The $\gamma\gamma^* \to \pi^0$ transition form factor $F_{\pi\gamma}(Q^2)$ (left) and $Q^2F_{\pi\gamma}(Q^2)$ (right). The dotted curve is the asymptotic result. The dashed and solid curves include the effects of using a confined EM current for twist-two and twist-two plus twist-four respectively. The data are from.[90,93,94]

Taking $P_{q\bar{q}} = 0.5$ in (84) one obtains a result in agreement with the Adler, Bell and Jackiw anomaly result which agrees within a few percent with the observed value obtained from the the decay $\pi^0 \to \gamma\gamma$. This suggests that the contribution from higher Fock states vanishes at $Q = 0$ in this simple holographic confining model. Thus (84) represents a description of the pion TFF which encompasses the low-energy nonperturbative and the high-energy hard domains, but includes only the asymptotic distribution amplitude of the $q\bar{q}$ component of the pion wave function at all scales. The results from (84) for $P_{q\bar{q}} = 0.5$ are shown in Fig. 5. Also shown in Fig. 5 are the results for the free current approximation (which corresponds to the asymptotic result) with $P_{q\bar{q}} = 0.5$ and a twist-two plus twist-four model[88] with $P_{q\bar{q}} = 0.915$, and $P_{q\bar{q}q\bar{q}} = 0.085$. The calculations[88]

---

the TFF which follows from (80) then vanishes at $Q^2 = 0$, and has to be corrected by the introduction of a surface term at the IR wall.[113] However, this procedure is only possible for a model with a sharp cutoff.

agree reasonably well with the experimental data at low- and medium-$Q^2$ regions ($Q^2 < 10$ GeV$^2$), but disagree with BaBar's large $Q^2$ data.

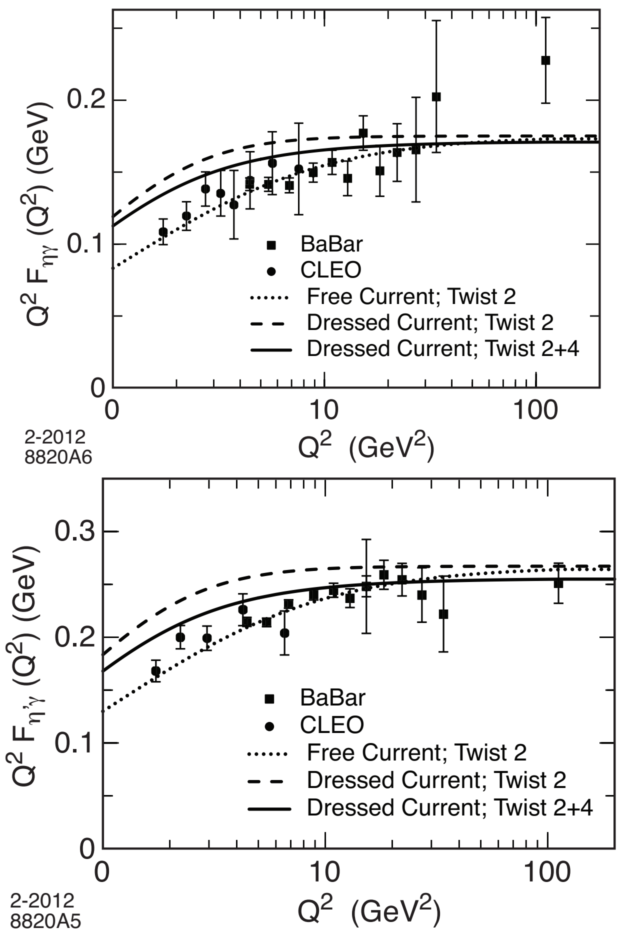


Fig. 6. The $\gamma\gamma^* \to \eta$ transition form factor $Q^2 F_{\eta\gamma}(Q^2)$ (left). The dotted curve is the asymptotic result. The dashed and solid curves include the effects of using a confined EM current for twist-two plus twist-two plus twist-four respectively. Same for the $\gamma\gamma^* \to \eta'$ transition form factor $Q^2 F_{\eta'\gamma}(Q^2)$ (right). The data are from.[90,93,94]

The $\eta$ and $\eta'$ mesons result from the mixing of the neutral states $\eta_8$ and $\eta_1$ of the SU(3)$_F$ quark model. The TFFs for the $\eta$ and $\eta'$ mesons have the same expression as the pion transition form factor, except for an overall multiplying factor $c_P = 1, \frac{1}{\sqrt{3}}$, and $\frac{2\sqrt{2}}{\sqrt{3}}$ for the $\pi^0$, $\eta_8$ and $\eta_1$, respectively.[88] The results for the $\eta$ and $\eta'$ transitions form factors are shown in Fig. 6. The calculations agree very well with available experimental data over a large range of $Q^2$. The rapid growth of the large $Q^2$ data for the pion-photon transition form factor reported by the BaBar Collaboration is difficult to explain within the current framework of QCD. The analysis presented here thus indicates the importance of additional measurements of the pion-photon transition form factor at large $Q^2$.

## 5. Baryons in light-front holography

The study of the excitation spectrum of baryons is one of the most challenging aspects of particle physics. In fact, dedicated experimental programs are in place to determine the spectrum of nucleon excitations and its internal structure. Important computational efforts in lattice QCD aim to the reliable extraction of the excited nucleon eigenstates. Lattice calculations of the ground state light hadron masses agree with experimental values within 5%.[48] However, the excitation spectrum of the nucleon represents a formidable challenge to lattice QCD due to the enormous computational complexity required beyond the leading ground state configuration.[119] Moreover, a large basis of interpolating operators is required since excited nucleon states are classified according to irreducible representations of the lattice, not the total angular momentum.

As we shall discuss below, the analytical exploration of the baryon spectrum and nucleon form factors, using light-front gauge/gravity duality ideas, leads, in contrast, to simple formulas and rules which describe quite well the systematics of the established light-baryon resonances and elastic and transition nucleon form factors, which can be tested against new experimental findings. The gauge/gravity duality can give us important insights into the strongly coupled dynamics of nucleons using simple analytical methods.

We can extended the holographic ideas to spin-$\frac{1}{2}$ hadrons by considering the propagation of spin-$\frac{1}{2}$ Dirac modes in AdS space.[15] The action for a Dirac field in AdS$_{d+1}$ is

$$S_F = \int d^d x\, dz\, \sqrt{g}\left(\frac{i}{2}\bar{\Psi} e^M_A \Gamma^A D_M \Psi - \frac{i}{2}(D_M\bar{\Psi}) e^M_A \Gamma^A \Psi - \mu\bar{\Psi}\Psi\right), \tag{85}$$

where $\sqrt{g} = \left(\frac{R}{z}\right)^{d+1}$ and $e^M_A$ is the inverse vielbein, $e^M_A = \left(\frac{z}{R}\right)\delta^M_A$. The covariant derivative of the spinor field is $D_M = \partial_M - \frac{i}{2}\omega^{AB}_M \Sigma_{AB}$ where $\Sigma_{AB}$ are the generators of the Lorentz group in the spinor representation, $\Sigma_{AB} = \frac{i}{4}[\Gamma_A, \Gamma_B]$, and the tangent space Dirac matrices obey the usual anti-commutation relation $\left\{\Gamma^A, \Gamma^B\right\} = \eta^{AB}$. For $d$ even we can choose the set of gamma matrices $\Gamma_A = \left(\Gamma_\mu, \Gamma_z\right)$ with $\Gamma_z = -\Gamma^z = \Gamma_0\Gamma_1 \cdots \Gamma_{d-1}$. For $d = 4$ we have $\Gamma_A = \left(\gamma_\mu, -i\gamma_5\right)$, where $\gamma_\mu$ and $\gamma_5$ are the usual 4-dimensional Dirac matrices with $\gamma_5 = i\gamma_0\gamma_1\gamma_2\gamma_3$ and $\gamma_5^2 = +1$. The spin connection in AdS is $w^{AB}_M = \left(\eta^{Az}\delta^B_M - \eta^{Bz}\delta^A_M\right)/z$, thus the equation of motion $\left(ie^M_A\Gamma^A D_M - \mu\right)\Psi = 0$ leads to the Dirac equation in AdS space

$$\left[i\left(z\eta^{MN}\Gamma_M\partial_N + \frac{d}{2}\Gamma_z\right) - \mu R\right]\Psi = 0, \tag{86}$$

where the $d+1$ dimensional mass $\mu$ is a priory an arbitrary parameter. [a]

One can also take as starting point the construction of light-front wave equations in physical space-time for baryons by studying the LF transformation properties of spin 1/2 states.[122] The light-front wave equation describing baryons is a matrix eigenvalue equation $D_{LF}|\psi\rangle = \mathcal{M}|\psi\rangle$ with $H_{LF} = D_{LF}^2$. In a $2\times 2$ spinor component representation

$$\begin{aligned} \frac{d}{d\zeta}\psi_+ + \frac{\nu+\frac{1}{2}}{\zeta}\psi_+ &= \mathcal{M}\psi_-, \\ -\frac{d}{d\zeta}\psi_- + \frac{\nu+\frac{1}{2}}{\zeta}\psi_- &= \mathcal{M}\psi_+. \end{aligned} \tag{87}$$

As shown below, we can identify $\nu$ with the orbital angular momentum $L$: $\nu = L + 1$.

---

[a]The spinor action (85) is often complemented by an additional surface term in the UV boundary[120] $\lim_{\epsilon\to 0}\int d^d x\, \sqrt{g_\epsilon}\bar{\Psi}\Psi$ where $g_\epsilon$ is the metric induced in the boundary surface by the metric $g$ of AdS$_{d+1}$. The additional term is required to preserve the $O(d+1,1)$ isometry group of AdS$_{d+1}$ and to compute a two-point correlation function in the conformal boundary theory.[121] The equation of motion (86) is not modified by the surface term.

Upon the substitution $z \to \zeta$ and

$$\Psi(x,z) = e^{-iP\cdot x} z^2 \psi(z) u(P), \tag{88}$$

in (86) we recover for $d = 4$ its LF expression (87), provided that $|\mu R| = \nu + \frac{1}{2}$. The baryon invariant mass is $P_\mu P^\mu = \mathcal{M}^2$ and the spinor $u(P)$ is a four-dimensional spinor which obeys the Dirac equation $(\not{P} - \mathcal{M})u(P) = 0$. Thus the eigenvalue equation $H_{LF}\psi_\pm = \mathcal{M}^2 \psi_\pm$ for the upper and lower components leads to the wave equation

$$\left(-\frac{d^2}{d\zeta^2} - \frac{1-4\nu^2}{4\zeta^2}\right)\psi_+(\zeta) = \mathcal{M}^2 \psi_+(\zeta), \tag{89}$$

and

$$\left(-\frac{d^2}{d\zeta^2} - \frac{1-4(\nu+1)^2}{4\zeta^2}\right)\psi_-(\zeta) = \mathcal{M}^2 \psi_-(\zeta), \tag{90}$$

with solutions

$$\psi_+ \sim \sqrt{\zeta} J_\nu(\zeta \mathcal{M}), \qquad \psi_- \sim \sqrt{\zeta} J_{\nu+1}(\zeta \mathcal{M}). \tag{91}$$

The solution of the spin-$\frac{3}{2}$ Rarita-Schwinger equation for the field $\Psi_M$ in AdS space is more involved, but considerable simplification occurs in the $\Psi_z = 0$ gauge for physical polarization along Minkowski coordinates $\Psi_\mu$, where it becomes similar to the spin-$\frac{1}{2}$ solution.[123,124]

### 5.1. *A hard-wall model for baryons*

The hermiticity of the LF Dirac operator $D_{LF}$ in the eigenvalue equation $D_{LF}|\psi\rangle = \mathcal{M}|\psi\rangle$ implies that the surface term $\psi_+^*(\zeta)\psi_-(\zeta) - \psi_-^*(\zeta)\psi_+(\zeta)$ should vanish at the boundary. Thus in a truncated space holographic model, the light front modes $\psi_+$ or $\psi_-$ should vanish at the boundary $\zeta = 0$ and $\zeta = \zeta_0$. This condition fixes the boundary conditions and determine the baryon spectrum in the truncated hard-wall model. A similar surface term arises when one computes the equation of motion from the action (85). In fact, integrating by parts (85) and using the equation of motion we find

$$S_F = -\lim_{\epsilon \to 0} \int \frac{d^d x}{2z^d} \left(\bar{\Psi}_+ \Psi_- - \bar{\Psi}_- \Psi_+\right)\Big|_\epsilon^{z_0}, \tag{92}$$

where $\Psi_\pm = \frac{1}{2}(1 \pm \gamma_5)\Psi$, and $R$ has units $R = 1$. The baryon mass spectrum thus follows from the LF "bag" boundary conditions $\psi_\pm(\zeta_0) = 0$ or the AdS boundary conditions $\Psi_\pm(z_0) = 0$ at the IR value, $z_0 = 1/\Lambda_{\rm QCD}$, where the LF invariant impact variable $\zeta$ (19) is identified with the AdS holographic coordinate $z$, $z \to \zeta$. We find

$$\mathcal{M}^+ = \beta_{\nu,k}\,\Lambda_{\rm QCD}, \qquad \mathcal{M}^- = \beta_{\nu+1,k}\,\Lambda_{\rm QCD}, \tag{93}$$

with a scale-independent mass ratio determined by the zeros of Bessel functions $\beta_{\nu,k}$.

In the usual AdS/CFT correspondence the baryon is an $SU(N_C)$ singlet bound state of $N_C$ quarks in the large $N_C$ limit. Since there are no quarks in this theory, quarks are introduced as external sources at the AdS asymptotic boundary.[125,126] The baryon is constructed as an $N_C$ baryon vertex located in the interior of AdS. In this top-down string approach baryons are usually described as solitons or Skyrmion-like objects.[127,128] In contrast, the bottom-up light-front holographic approach described here is based on the precise mapping of AdS expressions to light-front QCD. Consequently, we construct baryons corresponding to $N_C = 3$ not $N_C \to \infty$. The corresponding interpolating operator for an $N_C = 3$ physical baryon $\mathcal{O}_{3+L} = \psi D_{\{\ell_1} \ldots D_{\ell_q} \psi D_{\ell_{q+1}} \ldots D_{\ell_m\}} \psi$, $L = \sum_{i=1}^m \ell_i$, is a twist-3, dimension $9/2 + L$ with scaling behavior given by its twist-dimension $3 + L$. We thus require $\nu = L + 1$ to match the short distance scaling behavior. One can interpret $L$ as the maximal value of $|L^z|$ in a given LF Fock state.

In the case of massless quarks, the nucleon eigenstate ($u_\pm = \frac{1}{2}(1 \pm \gamma_5)\,u$)

$$\begin{aligned}\psi(\zeta) &= \psi_+(\zeta)u_+ + \psi_-(\zeta)u_- \\ &= C\sqrt{\zeta}\left(J_\nu(\zeta\mathcal{M})u_+ + J_{\nu+1}(\zeta\mathcal{M})u_-\right), \end{aligned} \tag{94}$$

has components $\psi_+$ and $\psi_-$ with different orbital angular momentum, $L^z = 0$ and $L^z = +1$, combined with spin components $S^z = +1/2$ and $S^z = -1/2$ respectively, but with equal probability [a]

$$\int d\zeta |\psi_+(\zeta)|^2 = \int d\zeta |\psi_-(\zeta)|^2, \tag{95}$$

a manifestation of the chiral invariance of the theory for massless quarks. Thus in light-front holography, the spin of the proton is carried by the quark orbital angular momentum: $J^z = \langle L^z \rangle = \pm 1/2$ since $\langle \sum S_q^z \rangle = 0$,[129] and not by its gluons.

An important feature of bound-state relativistic theories is that hadron eigenstates have in general Fock components with different $L$ components. In the holographic example discussed above, the proton has $S$ and P components with equal probability. In the case of QED, the ground state $1S$ state of the Dirac-Coulomb equation has both $L = 0$ and $L = 1$ components. By convention, in both light-front QCD and QED, one labels the eigenstate with its minimum value of $L$. For example, the symbol $L$ in the light-front AdS/QCD spectral prediction for mesons (46) refers to the *minimum* $L$ (which also corresponds to the leading twist) and $S$ is the total internal spin of the hadron.

We list in Table 2 the confirmed (3-star and 4-star) baryon states from the updated Particle Data Group.[50] [a] To determine the internal spin, internal orbital angular momentum and radial quantum number assignment of the $N$ and $\Delta$ excitation spectrum from the total angular momentum-parity PDG assignment, it is convenient to use the conventional $SU(6) \supset SU(3)_{flavor} \times SU(2)_{spin}$ multiplet structure, but other model choices are also possible.[131] [a]

We show in Fig. 7 the model predictions for the orbital excitation spectrum of baryons which follows from the boundary conditions $\psi_\pm\left(\zeta = 1/\Lambda_{\rm QCD}\right) = 0$ in a truncated-space model in the infrared region.[52] [a] The figure shows the predicted orbital spectrum of the nucleon and $\Delta$ orbital resonances for $n = 0$. The only parameter is the value of $\Lambda_{QCD}$ which we take as 0.25 GeV. Orbital excitations are approximately aligned along two trajectories corresponding to even and odd parity states, with exception of the $\Delta\frac{1}{2}^-(1620)$ and $\Delta\frac{3}{2}^-(1700)$ states which are in the same trajectory. The spectrum shows a clustering of states with the same orbital $L$, consistent with a strongly suppressed spin-orbit force. This remarkable prediction for the baryons is not a peculiarity of the hard-wall model, but is an important property of light-front holographic models.

In the quark-diquark model of Jaffe and Wilczek,[132] nucleon states with $S = 1/2$ in Fig. 7 (a) correspond to "good" diquarks, $S = 3/2$ nucleons and all the $\Delta$ states in Fig. 7 (b) to "bad" diquarks, with exception of the $\Delta(1930)$ which does not follow the simple $3q$ quark-diquark pattern. As for the case for mesons discussed in

---

[a] For the truncated-space model, (95) follows from the identity $\int_0^1 x dx \left[J_\alpha^2(x\beta) - J_{\alpha+1}^2(x\beta)\right] = J_\alpha(\beta)J_{\alpha+1}(\beta)/\beta$, independently of the component wavefunction chosen to fix the boundary conditions at $\zeta = \zeta_0$.

[a] A recent exploration of the properties of baryon resonances derived from a multichannel partial wave analysis[130] report additional resonances not included in the Review of Particle Properties.[50]

[a] In particular the $\Delta\frac{5}{2}^-(1930)$ state (not shown in Table 2) has been given the non-$SU(6)$ assignment $S = 3/2$, $L = 1$, $n = 1$ in Ref. [131] This assignment will be further discussed in the section below.

[a] The results shown here in Fig. 7 give better results for the lower mass baryons as compared with Ref.[52] where naive conformal dimensions were used instead.

| $L$ | $S$ | $n$ | Baryon State |
|---|---|---|---|
| 0 | $\frac{1}{2}$ | 0 | $N\frac{1}{2}^+(940)$ |
| 0 | $\frac{1}{2}$ | 1 | $N\frac{1}{2}^+(1440)$ |
| 0 | $\frac{1}{2}$ | 2 | $N\frac{1}{2}^+(1710)$ |
| 0 | $\frac{3}{2}$ | 0 | $\Delta\frac{3}{2}^+(1232)$ |
| 0 | $\frac{3}{2}$ | 1 | $\Delta\frac{3}{2}^+(1600)$ |
| 1 | $\frac{1}{2}$ | 0 | $N\frac{1}{2}^-(1535)$ $N\frac{3}{2}^-(1520)$ |
| 1 | $\frac{3}{2}$ | 0 | $N\frac{1}{2}^-(1650)$ $N\frac{3}{2}^-(1700)$ $N\frac{5}{2}^-(1675)$ |
| 1 | $\frac{1}{2}$ | 0 | $\Delta\frac{1}{2}^-(1620)$ $\Delta\frac{3}{2}^-(1700)$ |
| 2 | $\frac{1}{2}$ | 0 | $N\frac{3}{2}^+(1720)$ $N\frac{5}{2}^+(1680)$ |
| 2 | $\frac{1}{2}$ | 1 | $N\frac{5}{2}^+(1900)$ |
| 2 | $\frac{3}{2}$ | 0 | $\Delta\frac{1}{2}^+(1910)$ $\Delta\frac{3}{2}^+(1920)$ $\Delta\frac{5}{2}^+(1905)$ $\Delta\frac{7}{2}^+(1950)$ |
| 3 | $\frac{1}{2}$ | 0 | $N\frac{5}{2}^-$ $N\frac{7}{2}^-$ |
| 3 | $\frac{3}{2}$ | 0 | $N\frac{3}{2}^-$ $N\frac{5}{2}^-$ $N\frac{7}{2}^-(2190)$ $N\frac{9}{2}^-(2250)$ |
| 3 | $\frac{1}{2}$ | 0 | $\Delta\frac{5}{2}^-$ $\Delta\frac{7}{2}^-$ |
| 4 | $\frac{1}{2}$ | 0 | $N\frac{7}{2}^+$ $N\frac{9}{2}^+(2220)$ |
| 4 | $\frac{3}{2}$ | 0 | $\Delta\frac{5}{2}^+$ $\Delta\frac{7}{2}^+$ $\Delta\frac{9}{2}^+$ $\Delta\frac{11}{2}^+(2420)$ |
| 5 | $\frac{1}{2}$ | 0 | $N\frac{9}{2}^-$ $N\frac{11}{2}^-$ |
| 5 | $\frac{3}{2}$ | 0 | $N\frac{7}{2}^-$ $N\frac{9}{2}^-$ $N\frac{11}{2}^-(2600)$ $N\frac{13}{2}^-$ |

Sec. 3.1, the hard-wall model predicts $\mathcal{M} \sim 2n + L$, in contrast to the usual Regge behavior $\mathcal{M}^2 \sim n + L$ found in experiment.[51] The radial modes are also not well described in the truncated-space model. For example, the first AdS radial state has a mass 1.85 GeV, which is thus difficult to identify with the Roper $N(1440)$ resonance. This problem is not present in the soft wall model for baryons discussed below.

### 5.2. *A soft-wall model for baryons*

For fermion fields in AdS one cannot break conformality with the introduction of a dilaton in the action since it can be rotated away leaving the action conformally invariant. [a] As a result, one must introduce an effective confining potential $V(z)$ in the action of a Dirac field propagating in AdS$_{d+1}$ space to break the conformal invariance of the theory and generate a baryon spectrum

$$S_F = \int d^d x\, dz \sqrt{g} \left(\frac{i}{2}\bar{\Psi} e^M_A \Gamma^A D_M \Psi - \frac{i}{2}(D_M \bar{\Psi}) e^M_A \Gamma^A \Psi - \mu \bar{\Psi}\Psi - V(z)\bar{\Psi}\Psi\right). \tag{96}$$

The variation of the action (96) leads to the Dirac equation in AdS

$$\left[i\left(z\eta^{MN}\Gamma_M \partial_N + \frac{d}{2}\Gamma_z\right) - \mu R - RV(z)\right]\Psi = 0. \tag{97}$$

As in the case for the hard wall model described in the previous section, the corresponding light-front wave equation in physical space-time follows from identifying the transverse LF coordinate $\zeta$ with the AdS

[a]This remarkable property was first pointed out in Ref.,[133] and later derived independently in Ref.[134]

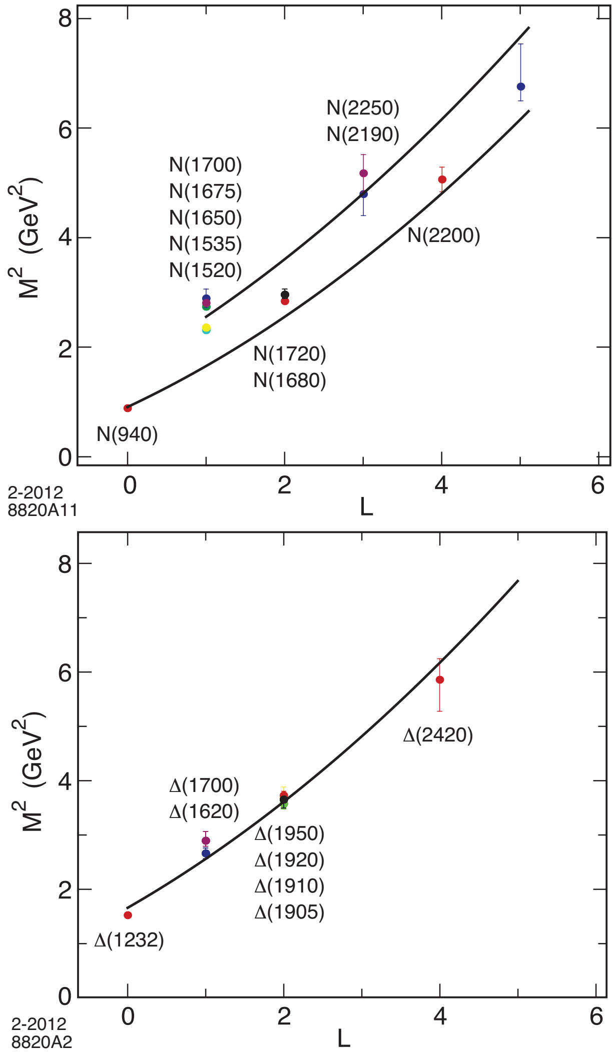


Fig. 7. Light baryon orbital spectrum ($n = 0$) for $\Lambda_{\rm QCD} = 0.25$ GeV. Predictions for the nucleons (left) and for the $\Delta$ trajectories (right).

holographic variable $z$, $z \to \zeta$, and the substitution (88) in (97). For d = 4 we find the matrix eigenvalue equation in the $2 \times 2$ spinor component representation

$$\frac{d}{d\zeta}\psi_+ + \frac{\nu + \frac{1}{2}}{\zeta}\psi_+ + U(\zeta)\psi_+ = \mathcal{M}\psi_-,$$
$$-\frac{d}{d\zeta}\psi_- + \frac{\nu + \frac{1}{2}}{\zeta}\psi_- + U(\zeta)\psi_- = \mathcal{M}\psi_+, \qquad (98)$$

where $U(\zeta) = \frac{R}{\zeta} V(\zeta)$ is the effective confining potential in the light-front Dirac equation.

Instead of choosing a dilaton profile to reproduce linear Regge behavior, as described in Sec. 3.2 for the case of mesons, we choose the confining interaction $V$ in (96) to reproduce linear Regge trajectories for the baryon mass spectrum $\mathcal{M}^2$. This "soft-wall" model for baryons in a higher dimensional AdS space, has also a LF analogue; it corresponds to a Dirac equation in physical space-time in presence of an effective linear confining potential $U$ defined at equal LF time. For the potential $U = \kappa^2\zeta$ equation (98) is equivalent to the system of second order equations

$$\left(-\frac{d^2}{d\zeta^2} - \frac{1-4\nu^2}{4\zeta^2} + \kappa^4\zeta^2 + 2(\nu+1)\kappa^2\right)\psi_+(\zeta) = \mathcal{M}^2\psi_+(\zeta), \tag{99}$$

and

$$\left(-\frac{d^2}{d\zeta^2} - \frac{1-4(\nu+1)^2}{4\zeta^2} + \kappa^4\zeta^2 + 2\nu\kappa^2\right)\psi_-(\zeta) = \mathcal{M}^2\psi_-(\zeta). \tag{100}$$

As a consequence, when one squares the Dirac Equation with $U(\zeta)$, one generates a Klein-Gordon equation with the potential $\kappa^4 z^2$. This is consistent with the same confining potential which appears in the meson equations. The LF equation $H_{LF}\psi_\pm = \mathcal{M}^2\psi_\pm$ has thus the two-component solution

$$\psi_+(\zeta) \sim \zeta^{\frac{1}{2}+\nu} e^{-\kappa^2\zeta^2/2} L_n^\nu(\kappa^2\zeta^2), \qquad \psi_-(\zeta) \sim \zeta^{\frac{3}{2}+\nu} e^{-\kappa^2\zeta^2/2} L_n^{\nu+1}(\kappa^2\zeta^2), \tag{101}$$

with equal probability for the properly normalized components. The eigenvalues are

$$\mathcal{M}^2 = 4\kappa^2(n+\nu+1), \tag{102}$$

identical for both plus and minus eigenfunctions. Note that, as expected, the potential $\kappa^4\zeta^2$ in the second order equation matches the soft-wall potential for mesons discussed in Sec. 3.2. However, in contrast to the case for mesons, the dilaton modification of the action gives little guidance for finding an effective potential for baryons, since the dilaton can be scaled away by a field redefinition. Consequently the overall energy scale is left unspecified for the baryons.[122] The remarkable regularities observed in the nucleon spectrum and the analytical properties of the AdS/LF equations allows us, nonetheless, to built precise rules to describe the observed baryon spectrum and make predictions for, as yet undiscovered, new baryon excited states.

Before computing the baryon spectrum we must fix the overall mass scale and the parameter $\nu$. Since our starting point for finding the bound state equation of motion for baryons is the light-front method, we shall require the mass scale to be identical for mesons and baryons while maintaining chiral symmetry for the pion[122] in the LF Hamiltonian equations. In practice, these constraints require a subtraction of $-4\kappa^2$ from (102). [a]

As is the case for the truncated-space model, the value of $\nu$ is determined by the short distance scaling behavior, $\nu = L + 1$. Higher-spin fermionic modes $\Psi_{\mu_1\cdots\mu_{J-1/2}}$, $J > 1/2$, with all of its polarization indices along the 3 + 1 coordinates follow by shifting dimensions for the fields as shown for the case of mesons in Ref.[55] [a]. Therefore, as in the meson sector, the increase in the mass $\mathcal{M}^2$ for baryonic states for increased radial and orbital quantum numbers is $\Delta n = 4\kappa^2$, $\Delta L = 4\kappa^2$ and $\Delta S = 2\kappa^2$, relative to the lowest ground state, the proton; *i.e.*, the slope of the spectroscopic trajectories in $n$ and $L$ are identical. Thus for the positive-parity nucleon sector

$$\mathcal{M}^{2\,(+)}_{n,L,S} = 4\kappa^2\left(n + L + \frac{S}{2} + \frac{3}{4}\right), \tag{103}$$

where the internal spin $S = \frac{1}{2}$ or $\frac{3}{2}$.

---

[a]This subtraction to the mass scale may be understood as the displacement required to describe nucleons with $N_C = 3$ as a composite system with leading twist $3 + L$; i.e., a quark-diquark bound state with a twist-2 composite diquark rather than an elementary twist-1 diquark.

[a]The detailed study of higher fermionic spin wave equations in modified AdS spaces is based on our collaboration with Hans Guenter Dosch.[32] See also the discussion in Ref.[37]

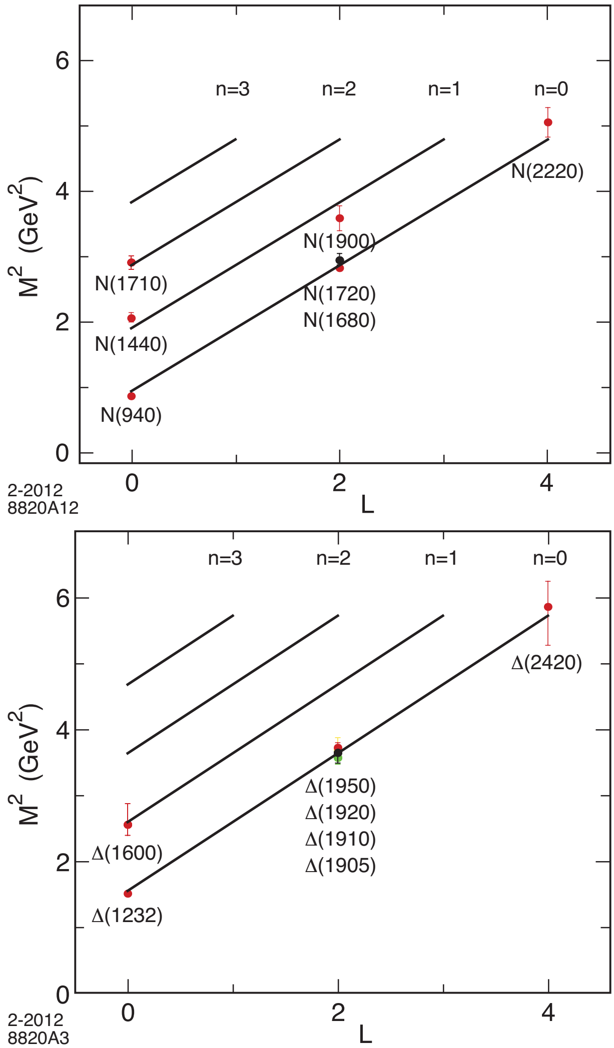


Fig. 8. Orbital and radial baryon excitations for the positive-parity Regge trajectories for the $N$ (left) and $\Delta$ (right) families for $\kappa = 0.49 - 0.51$ GeV.

The resulting predictions for the spectroscopy of positive-parity light baryons are shown in Fig. 8. Only confirmed PDG[50] states are shown. The Roper state $N(1440)$ and the $N(1710)$ are well accounted for in this model as the first and second radial states of the proton. Likewise, the $\Delta(1660)$ corresponds to the first radial state of the $\Delta(1232)$ as shown in in Fig. 8. The model is successful in explaining the parity degeneracy observed in the light baryon spectrum, such as the $L = 2$, $N(1680) - N(1720)$ degenerate pair and the $L = 2$, $\Delta(1905)$, $\Delta(1910)$, $\Delta(1920)$, $\Delta(1950)$ states which are degenerate within error bars. The parity degeneracy of baryons shown in Fig. 8 is also a property of the hard-wall model described in the previous section, but in that case the radial states are not well described.[52]

In order to have a comprehensive description of the baryon spectrum, we need to extend (103) to the negative-parity baryon sector. In the case of the hard-wall model, this was realized by choosing the boundary conditions for the plus or minus components of the AdS wave function $\Psi^{\pm}$. In practice, this amounts to allowing the negative-parity spin baryons to have a larger spatial extent, a point also raised in.[135] In the soft-wall model there are no boundary conditions to set in the infrared since the wave function vanishes exponentially for large values of $z$. We note, however, that setting boundary conditions on the wave functions, as done in Sec. 5.1, is equivalent to choosing the branch $\nu = \mu R - \frac{1}{2}$ for the negative-parity spin-$\frac{1}{2}$ baryons and $\nu = \mu R + \frac{1}{2}$ for the positive parity spin-$\frac{3}{2}$ baryons. This gives a factor $4\kappa^2$ between the lower-lying and the higher-lying nucleon trajectories as illustrated in Fig. 9, where we compare the lower nucleon trajectory corresponding to the $J = L + S$ spin-$\frac{1}{2}$ positive-parity nucleon family with the upper nucleon trajectory corresponding to the $J = L + S - 1$ spin-$\frac{3}{2}$ negative-parity nucleons. As is clearly shown in the figure, the gap is precisely the factor $4\kappa^2$.

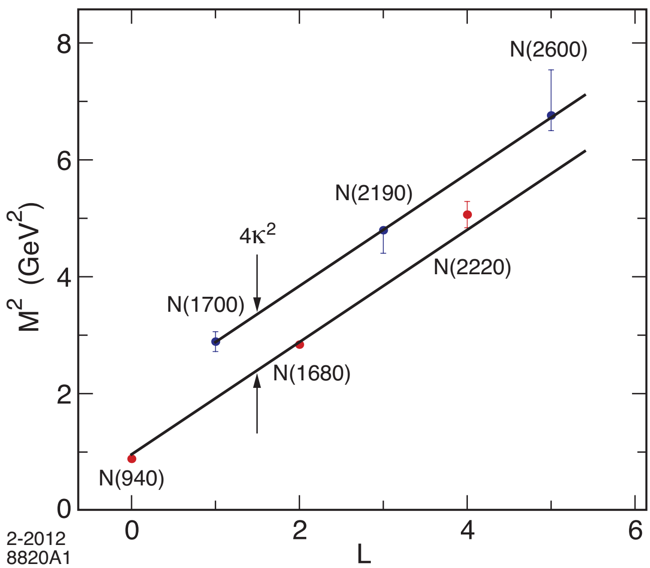


Fig. 9. Spectrum gap between the negative-parity spin-$\frac{3}{2}$ nucleons and the spin-$\frac{1}{2}$ positive-parity nucleon families for $\kappa = 0.49$ GeV.

If we apply the same spin-change rule previously discussed for the positive-parity nucleons, we would expect that the trajectory for the family of spin-$\frac{1}{2}$ negative-parity nucleons is lower by the factor $2\kappa^2$ compared to the spin-$\frac{3}{2}$ minus-parity nucleons according to the spin-change rule previously discussed. Thus the formula for the negative-parity baryons

$$\mathcal{M}^{2\,(-)}_{n,L,S} = 4\kappa^2\left(n + L + \frac{S}{2} + \frac{5}{4}\right), \tag{104}$$

where $S = \frac{1}{2}$ or $\frac{3}{2}$. It is important to recall that our formulas for the baryon spectrum are the result of an analytic inference, rather than formally derived.

The full baryon orbital excitation spectrum listed in Table 2 for $n = 0$ is shown in Fig. 10. We note that $\mathcal{M}^{2\,(+)}_{n,L,S=\frac{3}{2}} = \mathcal{M}^{2\,(-)}_{n,L,S=\frac{1}{2}}$ and consequently the positive and negative-parity $\Delta$ states lie in the same trajectory, consistent with the experimental results. Only the confirmed PDG[50] states listed in Table 2 are shown. Our results for the $\Delta$ states agree with those of Ref.[60] "Chiral partners" as the $N(1535)$ and the $N(940)$ with different

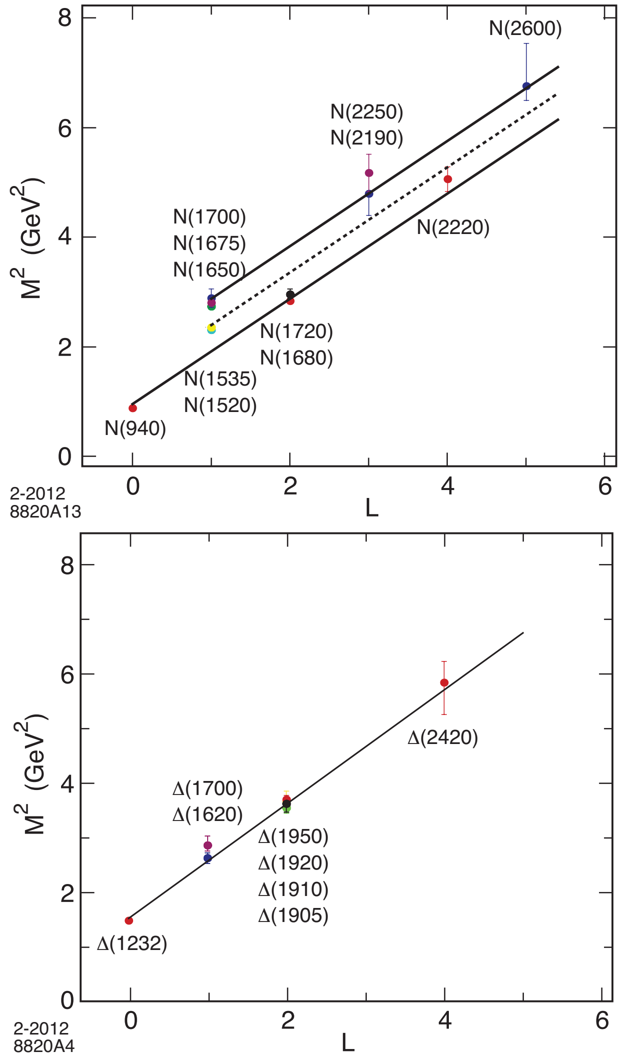


Fig. 10. Baryon orbital trajectories for the $N$ (left) and $\Delta$ families (right) for $n = 0$ and $\kappa = 0.49-0.51$ GeV. The lower and upper nucleon trajectories (left) correspond respectively to the the spin-$\frac{1}{2}$, positive-parity, and to the spin-$\frac{3}{2}$, negative-parity, families. The middle dotted trajectory (left) corresponds to spin-$\frac{1}{2}$ negative-parity nucleons. Plus and minus-parity states for the $\Delta$ states (right) are in the same Regge trajectory.

orbital angular momentum are non-degenerate from the onset. Using (103) and (104) we find the relation

$$\frac{\mathcal{M}_{N(1535)}}{\mathcal{M}_{N(940)}} = \sqrt{\frac{5}{2}}, \tag{105}$$

which is consistent with experiment to a good accuracy. One can in fact also build the entire negative-parity excitation spectrum starting from the proton partner, the $J = 1/2$ negative-parity nucleon state $N(1535)$, using the same rules *e.g.*, an increase in mass $\mathcal{M}^2$ of $4\kappa^2$ for a unit change in the radial quantum number, $4\kappa^2$ for a change in one unit in the orbital quantum number and $2\kappa^2$ for a change of one unit of spin relative to the lowest negative-parity state, the $N(1535)$.

With the exception of the $\Delta(1930)$ state (which is not included in Table 2), all the confirmed baryon excitations are well described by formulas (103) and and (104). If we follow the non-$SU(6)$ quantum number assignment for the $\Delta(1930)$ given in Ref.,[131] namely $S = 3/2$, $L = 1$, $n = 1$ we find from (104) the value $\mathcal{M}_{\Delta(1930)} = 4\kappa \simeq 2$ GeV, consistent with the experimental result 1.96 GeV.[50] Expected results from new experiments are important to find out if new baryonic excitations follow the simple pattern described by Eqs. (103) and (104).

An important feature of light-front holography is that it predicts a similar multiplicity of states for mesons and baryons, consistent with what is observed experimentally.[51] This remarkable property could have a simple explanation in the cluster decomposition of the holographic variable, which labels a system of partons as an active quark plus a system of $n-1$ spectators. From this perspective, a baryon with $n = 3$ looks in light-front holography as a quark–scalar-diquark system. It is also interesting to notice that in the hard wall model the proton mass is entirely due to the kinetic energy of the light quarks, whereas in the soft-wall model described here, half of the invariant mass squared $\mathcal{M}^2$ of the proton is due to the kinetic energy of the partons and half is due to the confinement potential.

## 6. Nucleon form factors

Proton and neutron electromagnetic form factors are among the most basic observables of the nucleon, and thus central for our understanding the nucleon's structure and dynamics. In general two form factors are required to describe the elastic scattering of electrons by spin-$\frac{1}{2}$ nucleons, the Dirac and Pauli form factors, $F_1$ and $F_2$

$$\langle P'|J^\mu(0)|P\rangle = u(P')\left[\gamma^\mu F_1(q^2) + \frac{i\sigma^{\mu\nu}q^\nu}{2\mathcal{M}}F_2(q^2)\right]u(P), \tag{106}$$

where $q = P' - P$. In the light-front formalism one can identify the Dirac and Pauli form factors from the LF spin-conserving and spin-flip current matrix elements of the $J^+$ current.[136]

On the higher dimensional gravity side the spin-non-flip amplitude for the EM transition corresponds to the non-local coupling of an external EM field $A^M(x,z)$ propagating in AdS with a fermionic mode $\Psi_P(x,z)$, given by the left-hand side of the equation below

$$\int d^4x\, dz\, \sqrt{g}\, \overline{\Psi}_{P'}(x,z)\, e^A_M\, \Gamma_A\, A^M(x,z)\Psi_P(x,z)$$
$$\sim (2\pi)^4\delta^4\,(P' - P - q)\,\epsilon_\mu u(P')\gamma^\mu F_1(q^2)u(P), \tag{107}$$

where $e^A_M = \left(\frac{R}{z}\right)\delta^A_M$ is the vielbein with curved space indices $M, N = 1, \cdots 5$ and tangent indices $A, B = 1, \cdots, 5$. The expression on the right-hand side represents the Dirac EM form factor in physical space-time. It is the EM matrix element (106) of the local quark current $J^\mu = e_q\bar{q}\gamma^\mu q$ with local coupling to the constituents. In this case one can also show that a precise mapping of the $J^+$ elements can be carried out at fixed LF time, providing an exact correspondence between the holographic variable $z$ and the LF impact variable $\zeta$ in ordinary space-time with the result[31]

$$G_\pm(Q^2) = g_\pm R^4 \int \frac{dz}{z^4}\, V(Q^2,z)\,\Psi^2_\pm(z), \tag{108}$$

for the components $\Psi_+$ and $\Psi_-$ with angular momentum $L^z = 0$ and $L^z = +1$ respectively. The effective charges $g_+$ and $g_-$ are determined from the spin-flavor structure of the theory.

A precise mapping for the Pauli form factor using light-front holographic methods has not been carried out. To study the spin-flip nucleon form factor $F_2$ using holographic methods, Abidin and Carlson[137] propose to introduce a non-minimal electromagnetic coupling with the 'anomalous' gauge invariant term

$$\int d^4x\, dz\, \sqrt{g}\, \bar{\Psi}\, e^A_M\, e^B_N\, [\Gamma_A, \Gamma_B]\, F^{MN} \Psi, \tag{109}$$

in the five-dimensional action, since the structure of (107) can only account for $F_1$. Although this is a practical avenue, the overall strength of the new term has to be fixed by the static quantities and thus some predictivity is lost.

Light-front holographic QCD methods have also been used to obtain generalized parton distributions (GPDs) of the nucleon in the zero skewness limit in Refs.[138] and[139] for the soft and hard-wall models respectively. GPDs are nonperturbative, and thus holographic methods are well suited to explore their analytical structure. [a] In the sections below we discuss elastic, transition and flavor-separated nucleon form factors using light-front holographic ideas. [b] [b]

## 6.1. *Computing nucleon elastic form factors in light-front holographic QCD*

In order to compute the individual features of the proton and neutron form factors one needs to incorporate the spin-flavor structure of the nucleons, properties which are absent in models of the gauge/gravity correspondence. The spin-isospin symmetry can be readily included in AdS/QCD by weighting the different Fock-state components by the charges and spin-projections of the quark constituents; e.g., as given by the $SU(6)$ spin-flavor symmetry. We label by $N_{q\uparrow}$ and $N_{q\downarrow}$ the probability to find the constituent $q$ in a nucleon with spin up or down respectively. For the $SU(6)$ wave function we have

$$N_{u\uparrow} = \frac{5}{3}, \qquad N_{u\downarrow} = \frac{1}{3}, \qquad N_{d\uparrow} = \frac{1}{3}, \qquad N_{d\downarrow} = \frac{2}{3}, \tag{110}$$

for the proton and

$$N_{u\uparrow} = \frac{1}{3}, \qquad N_{u\downarrow} = \frac{2}{3}, \qquad N_{d\uparrow} = \frac{5}{3}, \qquad N_{d\downarrow} = \frac{1}{3}, \tag{111}$$

for the neutron. The effective charges $g_+$ and $g_-$ in (108) are computed by the sum of the charges of the struck quark composed by the corresponding probability for the $L^z = 0$ and $L^z = +1$ components $\Psi_+$ and $\Psi_-$ respectively. We find $g_p^+ = 1$, $g_p^- = 0$, $g_+^n = -\frac{1}{3}$ and $g_-^n = \frac{1}{3}$. The nucleon Dirac form factors in the $SU(6)$ limit are thus given by

$$F_1^p(Q^2) = R^4 \int \frac{dz}{z^4}\, V(Q^2, z)\, \Psi_+^2(z), \tag{112}$$

$$F_1^n(Q^2) = -\frac{1}{3} R^4 \int \frac{dz}{z^4}\, V(Q^2, z) \left[\Psi_+^2(z) - \Psi_-^2(z)\right], \tag{113}$$

where $F_1^p(0) = 1$ and $F_1^n(0) = 0$.

In the soft-wall model the plus and minus components of the twist-3 nucleon wave function are

$$\Psi_+(z) = \frac{\sqrt{2}\kappa^2}{R^2} z^{7/2} e^{-\kappa^2 z^2/2}, \qquad \Psi_-(z) = \frac{\kappa^3}{R^2} z^{9/2} e^{-\kappa^2 z^2/2}, \tag{114}$$

---

[a] See also the discussion in Ref.[140]

[b] A study of the EM nucleon to $\Delta$ transition form factors has been carried out in the framework of the Sakai and Sugimoto model in Ref.[141]

[b] LF holographic methods can also be used to study the flavor separation of the elastic nucleon form factors which have been determined recently up to $Q^2 = 3.4\ \mathrm{GeV}^2$.[142] This will be described elsewhere. See also Ref.[143]

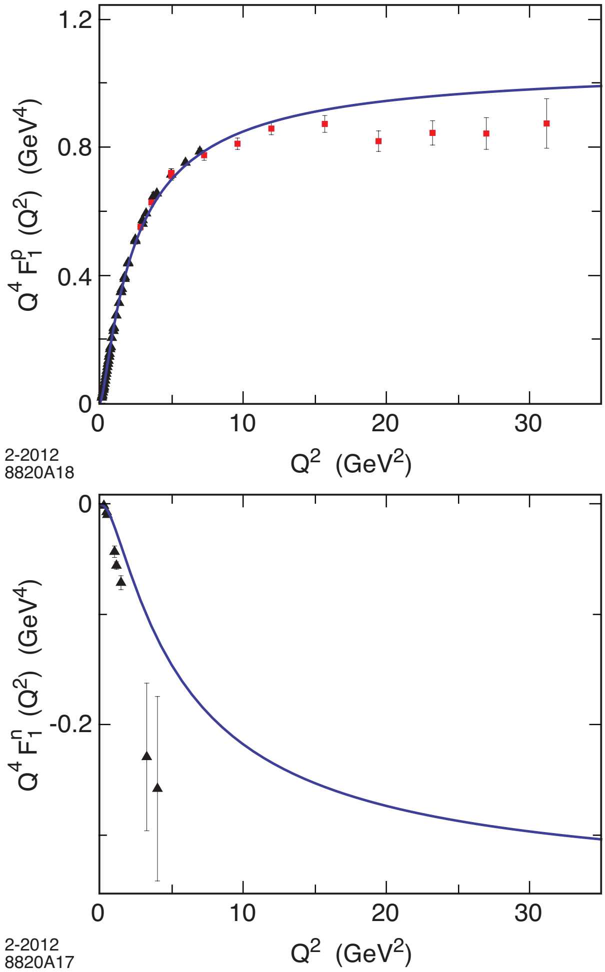


Fig. 11. Predictions for $Q^4 F_1^p(Q^2)$ (left) and $Q^4 F_1^n(Q^2)$ (right) in the soft wall model. Data compilation from Diehl.[144]

and $V(Q^2, z)$ is given by (60). The results for $F_1^{p,n}$ follow from the analytic form (63) for any twist $\tau$. We find

$$F_1^p(Q^2) = F_+(Q^2), \tag{115}$$

and

$$F_1^n(Q^2) = -\frac{1}{3}\Big(F_+(Q^2) - F_-(Q^2)\Big), \tag{116}$$

where we have, for convenience, defined the twist-2 and twist-3 form factors

$$F_+(Q^2) = \frac{1}{\Big(1 + \frac{Q^2}{\mathcal{M}_\rho^2}\Big)\Big(1 + \frac{Q^2}{\mathcal{M}_{\rho'}^2}\Big)}, \tag{117}$$

and

$$F_-(Q^2) = \frac{1}{\Big(1 + \frac{Q^2}{\mathcal{M}_\rho^2}\Big)\Big(1 + \frac{Q^2}{\mathcal{M}_{\rho'}^2}\Big)\Big(1 + \frac{Q^2}{\mathcal{M}_{\rho''}^2}\Big)}. \tag{118}$$

As discussed in Sec. 4.2, the multiple pole structure in (117) and (118) is derived from the dressed EM current propagating in AdS space.

The results for $Q^4 F_1^p(Q^2)$ and $Q^4 F_1^n(Q^2)$ are shown in Fig. 11. To compare with physical data we have shifted the poles in expression (63) to their physical values located at $M^2 = 4\kappa^2(n+1/2)$ following the discussion in Sec. 4.4. The value $\kappa = 0.545$ GeV is determined from the $\rho$ mass.

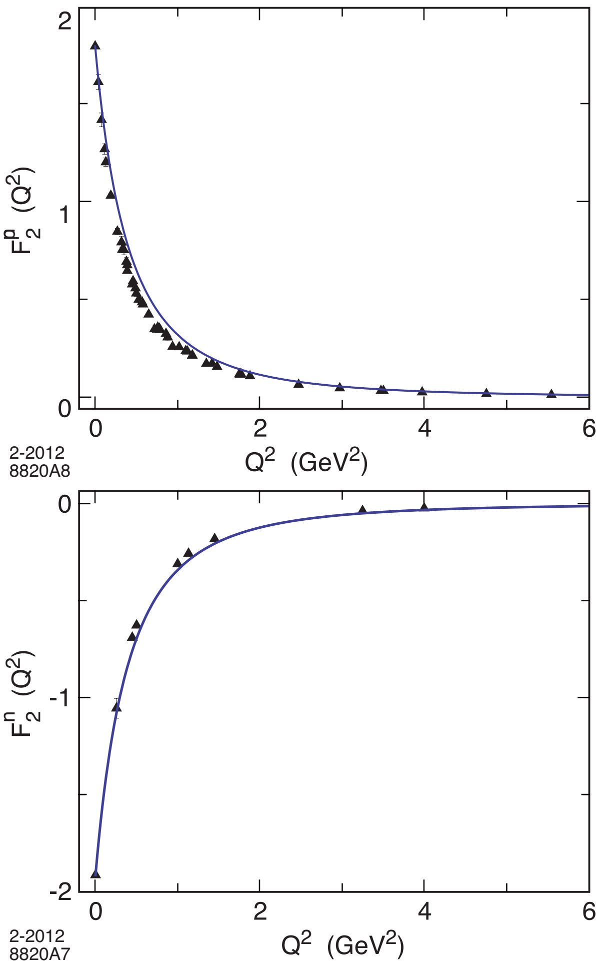


Fig. 12. Predictions for $F_2^p(Q^2)$ (left) and $F_2^n(Q^2)$ (right) in the soft wall model. Data compilation from Diehl.[144]

The expression for the elastic nucleon form factor $F_2^{p,n}$ follows from (106) and (109).

$$F_2^{p,n}(Q^2) \sim \int \frac{dz}{z^3} \Psi_+(z) V(Q^2, z) \Psi_-(z). \tag{119}$$

Using the twist-3 and twist-4 AdS soft-wall wavefunctions $\Psi_+$ and $\Psi_-$ (114) we find

$$F_2^{p,n}(Q^2) = \chi_{p,n} F_-(Q^2), \tag{120}$$

where the amplitude (119) has been normalized to the static quantities $\chi_p$ and $\chi_n$ and $F_-(Q^2)$ is given by (118). The experimental values $\chi_p = 1.793$ and $\chi_n = -1.913$ are consistent with the $SU(6)$ prediction[145] $\mu_P/\mu_N = -3/2$. In fact $(\mu_P/\mu_N)_{\text{exp}} = -1.46$ where $\mu_P = 1 + \chi_p$ and $\mu_N = \chi_n$. The results for $F_2^p(Q^2)$ and $F_2^n(Q^2)$ for $\kappa = 0.545$ GeV are shown in Fig. 12.

We compute the charge and magnetic root-mean-square (rms) radius from the usual electric and magnetic nucleon form factors

$$G_E(q^2) = F_1(q^2) + \frac{q^2}{4\mathcal{M}^2} F_2(q^2) \tag{121}$$

and

$$G_M(q^2) = F_1(q^2) + F_2(q^2). \tag{122}$$

Using the definition

$$\langle r^2 \rangle = -\frac{6}{F(0)} \frac{dF(Q^2)}{dQ^2}\Big|_{Q^2=0}, \tag{123}$$

we find the values $\sqrt{\langle r_E \rangle_p} = 0.802$ fm, $\sqrt{\langle r_M^2 \rangle_p} = 0.758$ fm, $\langle r_E^2 \rangle_n = -0.10$ fm$^2$ and $\sqrt{\langle r_M^2 \rangle_n} = 0.768$ fm, compared with the experimental values $\sqrt{\langle r_E \rangle_p} = (0.877 \pm 0.007)$ fm, $\sqrt{\langle r_M^2 \rangle_p} = (0.777 \pm 0.016)$ fm, $\langle r_E^2 \rangle_n = (-0.1161 \pm 0.0022)$ fm$^2$ and $\sqrt{\langle r_M^2 \rangle_n} = (0.862 \pm 0.009)$ fm from electron-proton scattering experiments.[50] [a] The muonic hydrogen measurement gives $\sqrt{\langle r_E \rangle_p} = 0.84184(67)$ fm from Lamb-shift measurements.[146] [b]

Chiral effective theory predicts that the slopes are singular for zero pion mass. For example, the slope of the Pauli form factor of the proton at $q^2 = 0$ computed by Beg and Zepeda diverges as $1/m_\pi$.[147] This comes from the simple triangle diagram $\gamma^* \to \pi^+\pi^- \to p\bar{p}$. One can also argue from dispersion theory that the singular behavior of the form factors as a function of the pion mass comes from the two-pion cut. Lattice theory computations of nucleon form factors require in fact the strong dependence at small pion mass to extrapolate the predictions to the physical pion mass.[148] The two-pion calculation[147] is a Born computation which probably does not exhibit vector dominance. To make a reliable computation in the hadronic basis of intermediate states one evidently has to include an infinite number of states. On the other hand, chiral divergences do not appear in AdS/QCD when we use the dressed current since, as shown is Sec. 4.2, the holographic analysis with a dressed EM current in AdS generates instead a nonperturbative multi-vector meson pole structure.[c]

## 6.2. *Computing nucleon transition form factors in light-front holographic QCD*

As an illustrative example we consider in this section the form factor for the $\gamma^* p \to N(1440)P_{11}$ transition measured recently at JLab. We shall weight the different Fock-state components by the charges and spin-projections of the quark constituents using the $SU(6)$ spin-flavor symmetry as in the previous section. The expression for the spin non-flip proton form factors for the transition $n, L \to n'L$ is[31]

$$F^p_{1\,n,L\to n',L}(Q^2) = R^4 \int \frac{dz}{z^4}\, \Psi_+^{n',L}(z) V(Q^2, z) \Psi_+^{n,L}(z), \tag{124}$$

[a] The neutron charge radius is defined by $\langle r_E^2 \rangle_n = -6 \frac{dG_E(Q^2)}{dQ^2}\Big|_{Q^2=0}$.

[b] Other soft and hard-wall model predictions of the nucleon rms radius are given in Refs.[137–139]

[c] In the limit of a free propagating current in AdS, we obtain logarithmic divergent results: $\langle r_p^2 \rangle_{F_1} = 3 \ln\left(\frac{4\kappa^2}{Q^2}\right)\Big|_{Q^2\to 0}$ and $\langle r_p^2 \rangle_{F_2} = \frac{9}{2} \ln\left(\frac{4\kappa^2}{Q^2}\right)\Big|_{Q^2\to 0}$.

where we have factored out the plane wave dependence of the AdS fields

$$\Psi_+(z) = \frac{\kappa^{2+L}}{R^2}\sqrt{\frac{2n!}{(n+L+1)!}}\, z^{7/2+L} L_n^{L+1}\left(\kappa^2 z^2\right) e^{-\kappa^2 z^2/2}. \tag{125}$$

The orthonormality of the Laguerre polynomials in (125) implies that the nucleon form factor at $Q^2 = 0$ is one if $n = n'$ and zero otherwise. Using the integral representation of the bulk-to-boundary propagator $V(Q^2, z)$ given by (62) we find the twist-3 spin non-flip transition form factor

$$F^p_{1\,N\to N^*}(Q^2) = \frac{\sqrt{2}}{3}\,\frac{\frac{Q^2}{\mathcal{M}_\rho^2}}{\left(1+\frac{Q^2}{\mathcal{M}_\rho^2}\right)\left(1+\frac{Q^2}{\mathcal{M}_{\rho'}^2}\right)\left(1+\frac{Q^2}{\mathcal{M}_{\rho''}^2}\right)}. \tag{126}$$

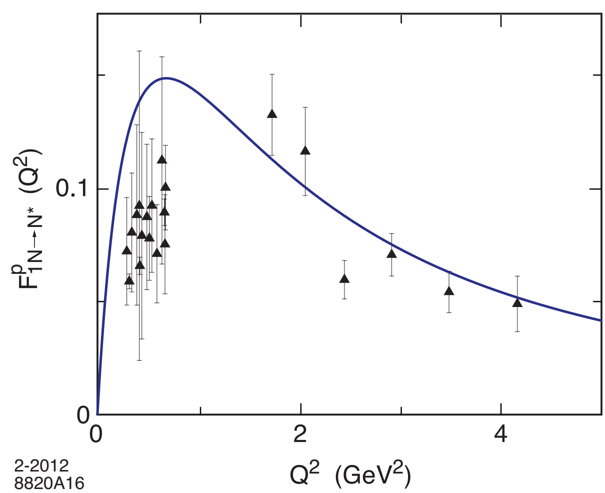


Fig. 13. Proton transition form factor $F^p_{1\,N\to N^*}(Q^2)$ to the first radial excited state. Data from JLAB.[149]

The result (126), compared with available data in Fig. 13, correspond to the valence approximation. The transition form factor (126) is expressed in terms of the mass of the $\rho$ vector meson and its first two radial excited states, with no additional parameters. The results in Fig. 13 are in good agreement with experimental data. The transition to the $N(1440)P_{11}$ state corresponds to the first radial excitation of the three-quark ground state of the nucleon. In fact, the Roper resonance $N(1440)P_{11}$ and the $N(1710)P_{11}$ are well accounted in the light-front holographic framework as the first and second radial states of the nucleon family as shown in Sec. 5.2 (See Fig. 8). It is certainly worth to extend the simple computations described here and perform a systematic study of the different transition form factors measured at JLab. This study will help to discriminate among models and compare with the new results expected from the JLab 12 GeV Upgrade Project, in particular at photon virtualities $Q^2 > 5\ \mathrm{GeV}^2$, which correspond to the experimental coverage of the CLAS12 detector at JLab.[150]

## 7. Higher Fock components in light-front holographic QCD

The light-front Hamiltonian eigenvalue equation (7) is a matrix in Fock space which represents an infinite number of coupled integral equations for the Fock components $\psi_n = \langle n|\psi\rangle$. The resulting potential in quantum field theory can be considered as an instantaneous four-point effective interaction in LF time, similar to the instantaneous gluon exchange in the light-cone gauge $A^+ = 0$, which leads to $qq \to qq$, $q\bar{q} \to q\bar{q}$, $q \to qq\bar{q}$ and $\bar{q} \to \bar{q}q\bar{q}$ as in QCD(1+1). Higher Fock states can have any number of extra $q\bar{q}$ pairs, but surprisingly no dynamical gluons. Thus in holographic QCD, gluons are absent in the confinement potential.[a] This unusual property of AdS/QCD may explain the dominance of quark interchange[153] over quark annihilation or gluon exchange contributions in large angle elastic scattering.[154 b]

In order to illustrate the relevance of higher Fock states and the absence of dynamical gluons at the hadronic scale, we will discuss a simple semi-phenomenological model of the elastic form factor of the pion where we include the first two components in a Fock expansion of the pion wave function $|\pi\rangle = \psi_{q\bar{q}/\pi}|q\bar{q}\rangle_{\tau=2} + \psi_{q\bar{q}q\bar{q}}|q\bar{q}q\bar{q}\rangle_{\tau=4} + \cdots$ , where the $J^{PC} = 0^{-+}$ twist-two and twist-4 states $|q\bar{q}\rangle$ and $|q\bar{q}q\bar{q}\rangle$ are created by the interpolating operators $\bar{q}\gamma^+\gamma_5 q$ and $\bar{q}\gamma^+\gamma_5 q\bar{q}q$ respectively.

Since the charge form factor is a diagonal operator, the final expression for the form factor corresponding to the truncation up to twist four is the sum of two terms, a monopole and a three-pole term. In the strongly coupled semiclassical gauge/gravity limit hadrons have zero widths and are stable. One can nonetheless modify the formula (63) by introducing a finite width: $q^2 \to q^2 + \sqrt{2}i\mathcal{M}\Gamma$. We choose the values $\Gamma_\rho = 140$ MeV, $\Gamma_{\rho'} = 360$ MeV and $\Gamma_{\rho''} = 120$ MeV. The results for the pion form factor with twist two and four Fock states are shown in Fig. 14. The results correspond to $P_{q\bar{q}q\bar{q}} = 13$ %, the admixture of the $|q\bar{q}q\bar{q}\rangle$ state. The value of $P_{q\bar{q}q\bar{q}}$ (and the widths) are input in the model. The value of $\kappa$ is determined from the $\rho$ mass and the masses of the radial excitations follow from setting the poles at their physical locations, $\mathcal{M}^2 \to 4\kappa^2(n+1/2)$, as discussed in Sec. 4.4. The time-like structure of the pion form factor displays a rich pole structure with constructive and destructive interfering phases; this is incompatible with the admixture of the twist-three state $|q\bar{q}g\rangle$ containing a dynamical gluon since the interference in this case is opposite in sign.

## 8. Conclusions

As we have shown, the exact light-front Hamiltonian $H_{LF}|\psi\rangle = \mathcal{M}^2|\psi\rangle$ for QCD can be systematically reduced to a relativistic frame-independent semiclassical wave equation[12]

$$\left(-\frac{d^2}{d\zeta^2} - \frac{1-4L^2}{4\zeta^2} + U(\zeta)\right)\phi(\zeta) = \mathcal{M}^2\phi(\zeta), \tag{127}$$

for the valence Fock state of mesons. The unmodified AdS equations correspond to the kinetic energy terms of the massless constituent quarks with relative orbital angular momentum $L = L^z$. The effective potential $U(\zeta)$ corresponds to the color-confining potential and follows from the truncation of AdS space, in a modified effective AdS action, and light-front holography. The variable $\zeta$ is the invariant separation of the constituents. This frame-independent light-front wave equation is comparable in simplicity to Schrödinger theory in atomic physics which is formulated at equal instant time. We have also derived an analogous light-front Dirac equation for holographic QCD which describes light-quark baryons with finite color $N_C = 3$.

Remarkably, these light-front equations are equivalent to the equations of motion in a higher dimensional warped space asymptotic to AdS space. The mapping of the gravity theory to the boundary quantum field theory, quantized at fixed light-front time, thus gives a precise relation between holographic wave functions and the light-front wave functions which describe the internal structure of the hadrons and their electromagnetic

[a]This result is consistent with the flux-tube interpretation of QCD[151] where soft gluons interact so strongly that they are sublimated into a color confinement potential for quarks. The absence of constituent glue in hadronic physics has been invoked also in Ref.,[152] where the role of the confining potential is attributed to an instanton induced interaction.
[b]In Ref.[155] we discuss a number of experimental results in hadron physics which support this picture.

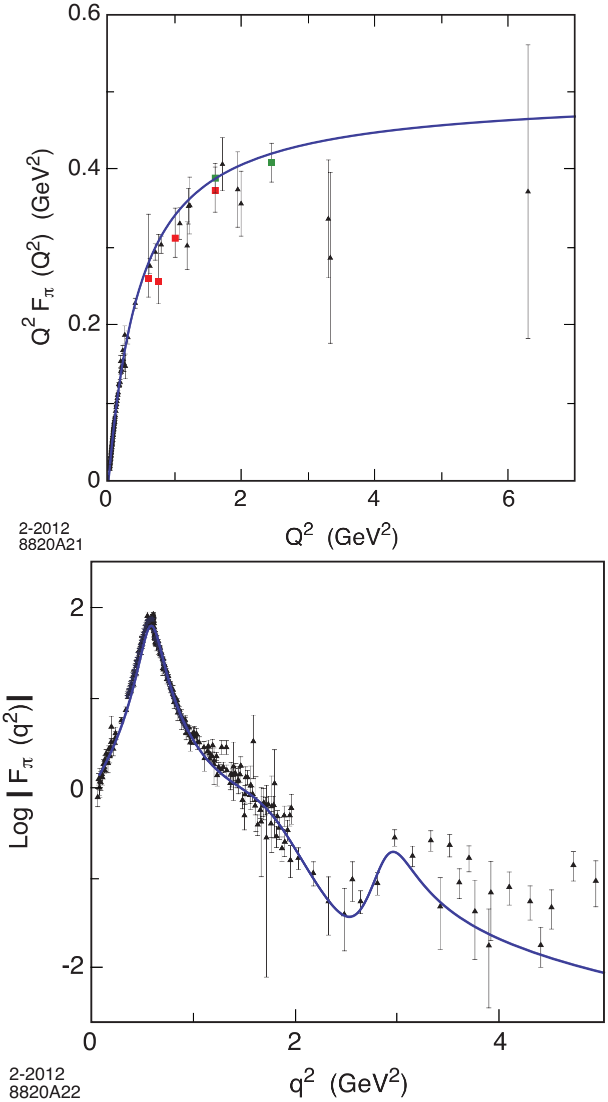


Fig. 14. Structure of the space-like (left) and time-like (right) pion form factor in light-front holography for a truncation of the pion wave function up to twist four. Triangles are the data compilation from Baldini *et al.*,[78] squares are JLAB data.[79]

couplings. This mapping provides the basis for a profound connection between physical QCD quantized in the light-front and the physics of hadronic modes in a higher dimensional AdS space. However, the derivation of the effective color-confining potential $U(\zeta)$ directly from QCD, remains an open question.

Despite some limitations of AdS/QCD,[156] the light-front holographic approach to the gauge/gravity duality, *Light-Front Holography*, has already provided significant physical insight into the strongly-coupled nature and internal structure of hadrons; in fact, it is one of the few tools available. As we have seen, the resulting model provides a simple and successful framework for describing nonperturbative hadron dynamics: the systematics of the excitation spectrum of hadrons: the mass eigenspectrum, observed multiplicities and degeneracies. It also provides powerful new analytical tools for computing hadronic transition amplitudes, incorporating the scaling behavior and the transition from the hard-scattering perturbative domain, where quark and gluons are the relevant degrees of freedom, to the long range confining hadronic region.

The dressed current in AdS includes the nonperturbative pole structure. Consequenly, the approach incorporates both the long-range confining hadronic domain and the constituent conformal short-distance quark particle limit in a single framework. The results display a simple analytical structure which allows us to explore dynamical properties in Minkowski space-time; in many cases these studies are not amenable to Euclidean lattice gauge theory computations. In particular, the excitation dynamics of nucleon resonances encoded in the nucleon transition form factors can provide fundamental insight into the strong-coupling dynamics of QCD. New theoretical tools are thus of primary interest for the interpretation of the results expected at the new mass scale and kinematic regions accessible to the JLab 12 GeV Upgrade Project.

The semiclassical approximation to light-front QCD described in this article is expected to break down at short distances where gluons become dynamical degrees of freedom and hard gluon exchange and quantum corrections become important. One can systematically improve the semiclassical approximation, for example, by introducing nonzero quark masses and short-range Coulomb-like gluonic corrections, thus extending the predictions of the model to the dynamics and spectra of heavy and heavy-light quark systems. The model can also be improved by applying Lippmann-Schwinger methods to systematically improve the light-front Hamiltonian of the semiclassical holographic approximation. One can also use the holographic LFWFs as basis functions for diagonalizing the full light-front QCD Hamiltonian[157] as well as the input boundary functions to study the evolution of structure functions and distribution amplitudes at a low energy scale.

## Acknowledgements

Invited lectures presented by GdT at the Niccolò Cabeo International School of Hadronic Physics, Ferrara, Italy, May 2011. GdT is grateful to the organizers and especially to Paola Ferretti Dalpiaz for her outstanding hospitality. We thank E. Klempt, V. E. Lyubovitskij and S. D. Glazek for helpful comments. We are grateful to F.-G. Cao, A. Deur, H. G. Dosch and J. Erlich for collaborations. This research was supported by the Department of Energy contract DE–AC02–76SF00515.

## Appendix A.

## 9. AdS boundary conditions and interpolating operators

The formal statement of the duality between a gravity theory on $(d+1)$-dimensional Anti-de Sitter $AdS_{d+1}$ space and the strong coupling limit of a conformal field theory (CFT) on the $d$-dimensional asymptotic boundary of $AdS_{d+1}$ at $z = 0$ is expressed in terms of the $d + 1$ partition function for a field $\Phi(x, z)$ propagating in the bulk

$$Z_{grav}[\Phi] = e^{iS_{eff}[\Phi]} = \int \mathcal{D}[\Phi] e^{iS[\Phi]}, \tag{A.1}$$

where $S_{eff}$ is the effective action of the $AdS_{d+1}$ theory, and the $d$-dimensional generating functional of correlation functions of the conformal field theory in presence of an external source $\Phi_0(x^\mu)$

$$Z_{CFT}[\Phi_0] = e^{iW_{CFT}[\Phi_0]} = \left\langle \exp\left(i \int d^d x\, \Phi_0(x) O(x)\right)\right\rangle. \tag{A.2}$$

The functional $W_{CFT}$ is the generator of connected Green's functions of the boundary theory and $O$ is a QCD local interpolating operator.

According to the AdS/CFT correspondence, to every operator in the conformal field theory there corresponds an AdS field. We use the isometries of AdS space to map the scaling dimensions of the local interpolating operators defined at the AdS boundary into the modes propagating inside AdS space. The precise relation of the gravity theory on AdS space to the conformal field theory at its boundary is[7]

$$Z_{grav}[\Phi(x, z)\big|_{z=0} = \Phi_0(x)] = Z_{CFT}\,[\Phi_0]\,, \tag{A.3}$$

where the partition function (A.1) on $AdS_{d+1}$ is integrated over all possible configurations $\Phi$ in the bulk which approach its boundary value $\Phi_0$. If we neglect the contributions from quantum fluctuations to the gravity partition function, then the generator $W_{CFT}$ of connected Green's functions of the four-dimensional gauge theory (A.2) is precisely equal to the classical (on-shell) gravity action (A.1)

$$W_{CFT}\,[\phi_0] = S_{eff}[\Phi(x, z)\big|_{z=0} = \Phi_0(x)]_{\text{on-shell}}, \tag{A.4}$$

evaluated in terms of the classical solution to the bulk equation of motion. This defines the semiclassical approximation to the conformal field theory. In the bottom-up phenomenological approach, the effective action in the bulk is usually modified for large values of $z$ to incorporate confinement and is truncated at the quadratic level.

In the limit $z \to 0$, the independent solutions behave as

$$\Phi(x, z) \to z^\tau\, \Phi_+(x) + z^{d-\tau}\, \Phi_-(x), \tag{A.5}$$

where $\tau$ is the scaling dimension. The non-normalizable solution $\Phi_-$ has the leading boundary behavior and is the boundary value of the bulk field $\Phi$ which couples to a QCD gauge invariant operator $O$ in the $z \to 0$ asymptotic boundary, thus $\Phi_- = \Phi_0$. The normalizable solution $\Phi_+$ is the response function and corresponds to the physical states.[158] The interpolating operators $O$ of the boundary conformal theory are constructed from local gauge-invariant products of quark and gluon fields and their covariant derivatives, taken at the same point in four-dimensional space-time in the $x^2 \to 0$ limit. According to (A.2) the scaling dimensions of $O$ are matched to the conformal scaling behavior of the AdS fields in the limit $z \to 0$ and are thus encoded into the propagation of the modes inside AdS space.

Integrating by parts, and using the equation of motion for the field in AdS, the bulk contribution to the action vanishes, and one is left with a non-vanishing surface term in the ultraviolet boundary

$$S = R^{d-1} \lim_{z\to 0} \int d^d x\, \frac{1}{z^{d-1}}\, \Phi \partial_z \Phi, \tag{A.6}$$

which can be identified with the boundary QFT functional $W_{CFT}$. Substituting the leading dependence (A.5) of $\Phi$ near $z = 0$ in the ultraviolet surface action (A.6) and using the functional relation

$$\frac{\delta W_{CFT}}{\delta \Phi_0} = \frac{\delta S_{\text{eff}}}{\delta \Phi_0}, \tag{A.7}$$

one finds that $\Phi_+(x)$ is related to the expectation values of $\mathcal{O}$ in the presence of the source $\Phi_0$[158]

$$\langle 0|\mathcal{O}(x)|0\rangle_{\Phi_0} \sim \Phi_+(x). \tag{A.8}$$

The exact relation depends on the normalization of the fields chosen.[159] The field $\Phi_+$ thus acts as a classical field, and it is the boundary limit of the normalizable string solution which propagates in the bulk.

## References


1. K. G. Wilson, "Confinement of quarks," http://prd.aps.org/abstract/PRD/v10/i8/p2445_1Phys. Rev. D **10**, 2445 (1974).
2. J. M. Cornwall, "Dynamical mass generation in continuum QCD," http://prd.aps.org/abstract/PRD/v26/i6/p1453_1Phys. Rev. D **26**, 1453 (1982).
3. P. A. M. Dirac, "Forms of relativistic dynamics," http://rmp.aps.org/abstract/RMP/v21/i3/p392_1 Rev. Mod. Phys. **21**, 392 (1949).
4. S. J. Brodsky, H. C. Pauli and S. S. Pinsky, "Quantum chromodynamics and other field theories on the light cone," http://www.sciencedirect.com/science?_ob=ArticleURL&_udi=B6TVP-3VWNH4V-2&_user=10&_coverDate=08%2F01%2F1998&_rdoc=1&_fmt=high&_orig=search&_sort=d&_docanchor=&view=c&_acct=C000050221&_version=1&_urlVersion=0&_userid=10&md5=ab0d459d9765d21676af7c1e4923025bPhys. Rept. **301**, 299 (1998) [http://arXiv.org/abs/hep-ph/9705477arXiv:hep-ph/9705477].
5. M. Burkardt, "Light front quantization," Adv. Nucl. Phys. **23**, 1 (1996) [http://arXiv.org/abs/hep-ph/9505259arXiv:hep-ph/9505259].
6. J. M. Maldacena, "The large N limit of superconformal field theories and supergravity," http://www.springerlink.com/content/q508214382421612/ Int. J. Theor. Phys. **38**, 1113 (1999) [http://arXiv.org/abs/hep-th/9711200arXiv:hep-th/9711200].
7. S. S. Gubser, I. R. Klebanov and A. M. Polyakov, "Gauge theory correlators from non-critical string theory," http://www.sciencedirect.com/science?_ob=ArticleURL&_udi=B6TVN-3TTKSGB-J&_user=10&_coverDate=05%2F28%2F1998&_rdoc=1&_fmt=high&_orig=search&_sort=d&_docanchor=&view=c&_acct=C000050221&_version=1&_urlVersion=0&_userid=10&md5=e703d335f1b9401dc4d10ce0ebb9562fPhys. Lett. B **428**, 105 (1998) [http://arXiv.org/abs/hep-th/9802109arXiv:hep-th/9802109].
8. E. Witten, "Anti-de Sitter space and holography," Adv. Theor. Math. Phys. **2**, 253 (1998) [http://arXiv.org/abs/hep-th/9802150arXiv:hep-th/9802150].
9. J. Polchinski and M. J. Strassler, "Hard scattering and gauge/string duality," http://prl.aps.org/abstract/PRL/v88/i3/e031601 Phys. Rev. Lett. **88**, 031601 (2002) [http://arXiv.org/abs/hep-th/0109174arXiv:hep-th/0109174].
10. S. J. Brodsky and G. R. Farrar, "Scaling laws at large transverse momentum," http://prl.aps.org/abstract/PRL/v31/i18/p1153_1 Phys. Rev. Lett. **31**, 1153 (1973).
11. V. A. Matveev, R. M. Muradian and A. N. Tavkhelidze, "Automodellism in the large-angle elastic scattering and structure of hadrons," http://www.springerlink.com/content/d272226535833524/ Lett. Nuovo Cim. **7**, 719 (1973).
12. G. F. de Teramond and S. J. Brodsky, "Light-front holography: a first approximation to QCD," http://prl.aps.org/abstract/PRL/v102/i8/e081601 Phys. Rev. Lett. **102**, 081601 (2009) [http://arXiv.org/abs/0809.4899arXiv:0809.4899 [hep-ph]].

13. S. J. Brodsky and G. F. de Teramond, "Hadronic spectra and light-front wavefunctions in holographic QCD," http://prl.aps.org/abstract/PRL/v96/i20/e201601 Phys. Rev. Lett. **96**, 201601 (2006) [http://arXiv.org/abs/hep-ph/0602252arXiv:hep-ph/0602252].
14. S. J. Brodsky and G. F. de Teramond, "Light-front dynamics and AdS/QCD correspondence: the pion form factor in the space- and timelike regions," http://prd.aps.org/abstract/PRD/v77/i5/e056007 Phys. Rev. D **77**, 056007 (2008) [http://arXiv.org/abs/0707.3859arXiv:0707.3859 [hep-ph]].
15. J. Polchinski and M. J. Strassler, "Deep inelastic scattering and gauge/string duality," http://iopscience.iop.org/1126-6708/2003/05/012/ JHEP **0305**, 012 (2003) [http://arXiv.org/abs/hepth/0209211arXiv:hep-th/0209211].
16. S. D. Drell and T. M. Yan, "Connection of elastic electromagnetic nucleon form-factors at large $Q^2$ and deep inelastic structure functions near threshold," http://prl.aps.org/abstract/PRL/v24/i4/p181_1 Phys. Rev. Lett. **24**, 181 (1970).
17. G. B. West, "Phenomenological model for the electromagnetic structure of the proton," http://prl.aps.org/abstract/PRL/v24/i21/p1206_1 Phys. Rev. Lett. **24**, 1206 (1970).
18. S. J. Brodsky and G. F. de Teramond, "Light-front dynamics and AdS/QCD correspondence: gravitational form factors of composite hadrons," http://prd.aps.org/abstract/PRD/v78/i2/e025032 Phys. Rev. D **78**, 025032 (2008) [http://arXiv.org/abs/0804.0452arXiv:0804.0452 [hep-ph]].
19. Z. Abidin and C. E. Carlson, "Gravitational form factors of vector mesons in an AdS/QCD model," http://prd.aps.org/abstract/PRD/v77/i9/e095007 Phys. Rev. D **77**, 095007 (2008) [http://arXiv.org/abs/0801.3839arXiv:0801.3839 [hep-ph]].
20. J. Erlich, E. Katz, D. T. Son and M. A. Stephanov, "QCD and a holographic model of hadrons," http://prl.aps.org/abstract/PRL/v95/i26/e261602Phys. Rev. Lett. **95**, 261602 (2005) [http://arXiv.org/abs/hep-ph/0501128arXiv:hep-ph/0501128].
21. L. Da Rold and A. Pomarol, "Chiral symmetry breaking from five dimensional spaces," http://www.sciencedirect.com/science?_ob=ArticleURL&_udi=B6TVC-4GBD5CF-1&_user=10&_coverDate=08%2F15%2F2005&_rdoc=1&_fmt=high&_orig=search&_sort=d&_docanchor=&view=c&_acct=C000050221&_version=1&_urlVersion=0&_userid=10&md5=631aa387ba048831c966f42fa3035b0dNucl. Phys. B **721**, 79 (2005) [http://arXiv.org/abs/hep-ph/0501218arXiv:hep-ph/0501218].
22. S. J. Brodsky and G. F. de Teramond, "Light-front hadron dynamics and AdS/CFT correspondence," http://www.sciencedirect.com/science/article/pii/S037026930400053XPhys. Lett. B **582**, 211 (2004) [http://arXiv.org/abs/hepth/0310227arXiv:hep-th/0310227].
23. A. Karch, E. Katz, D. T. Son and M. A. Stephanov, "Linear confinement and AdS/QCD," http://prd.aps.org/abstract/PRD/v74/i1/e015005Phys. Rev. D **74**, 015005 (2006) [http://arXiv.org/abs/hep-ph/0602229arXiv:hep-ph/0602229].
24. M. Shifman, "Highly excited hadrons in QCD and beyond," http://arXiv.org/abs/hepph/0507246arXiv:hep-ph/0507246.
25. S. D. Glazek and M. Schaden, "Gluon condensate induced confinement in mesons and baryons," http://www.sciencedirect.com/science/article/pii/0370269387901547Phys. Lett. B **198**, 42 (1987).
26. S. J. Brodsky and R. Shrock, "Maximum wavelength of confined quarks and gluons and properties of quantum chromodynamics," http://www.sciencedirect.com/science/article/pii/S0370269308007752Phys. Lett. B **666**, 95 (2008) [http://arXiv.org/abs/0806.1535arXiv:0806.1535 [hep-th]].
27. H. C. Pauli, "On the effective Hamiltonian for QCD: An overview and status report," http://www.sciencedirect.com/science?_ob=ArticleURL&_udi=B6TVD-45R34R8-1R&_user=10&_coverDate=04%2F30%2F2002&_rdoc=1&_fmt=high&_orig=search&_sort=d&_docanchor=&view=c&_acct=C000050221&_version=1&_urlVersion=0&_userid=10&md5=eac2da356bbfe271d5aeb5bbec76bdf3Nucl. Phys. Proc. Suppl. **108**, 273 (2002) [http://arXiv.org/abs/hep-ph/0202179arXiv:hep-ph/0202179].
28. G. 't Hooft, "A two-dimensional model for mesons," http://www.sciencedirect.com/science?_ob=ArticleURL&_udi=B6TVC-471YTMJ-14C&_user=10&_coverDate=06%2F25%2F1974&_rdoc=1&_fmt=high&_orig=search&_sort=d&_docanchor=&view=c&_acct=C000050221&_version=1&_urlVersion=0&_userid=10&md5=782d34f96ae8df8cda6096ead9646f59Nucl. Phys. B **75**, 461 (1974).
29. E. Katz and T. Okui, "The 't Hooft model as a hologram," http://iopscience.iop.org/1126-6708/2009/01/

013/JHEP **0901**, 113 (2009) [http://arXiv.org/abs/0710.3402arXiv:0710.3402 [hep-th]].
30. G. Parisi, "Conformal invariance in perturbation theory," http://www.sciencedirect.com/science?_ob=ArticleURL&_udi=B6TVN-46YKRPP-2K0&_user=10&_coverDate=05%2F29%2F1972&_rdoc=1&_fmt=high&_orig=search&_sort=d&_docanchor=&view=c&_acct=C000050221&_version=1&_urlVersion=0&_userid=10&md5=a3927623e39f0ffae2789d59490f19e8 Phys. Lett. B **39**, 643 (1972).
31. S. J. Brodsky and G. F. de Teramond, "AdS/CFT and light-front QCD," http://eproceedings.worldscinet.com/9789814293242/9789814293242_0008.html World Scientific Subnuclear Series, **45**, 139 (2007) [http://arXiv.org/abs/0802.0514arXiv:0802.0514 [hep-ph]].
32. S. J. Brodsky, H. G. Dosch and G. F. de Teramond *in preparation*.
33. C. Fronsdal, "Singletons and massless, integral spin fields on de Sitter space," http://prd.aps.org/abstract/PRD/v20/i4/p848_1Phys. Rev. **D20**, 848 (1979).
34. E. S. Fradkin, M. A. Vasiliev, "Cubic interaction in extended theories of massless higher spin fields," http://www.sciencedirect.com/science?_ob=ArticleURL&_udi=B6TVC-47318H9-Y7&_user=10&_coverDate=12%2F31%2F1987&_rdoc=1&_fmt=high&_orig=gateway&_origin=gateway&_sort=d&_docanchor=&view=c&_acct=C000050221&_version=1&_urlVersion=0&_userid=10&md5=1d987d2a91251609a0644f2cf9c4f651&searchtype=aNucl. Phys. **B291**, 141 (1987).
35. R. R. Metsaev, "Shadows, currents and AdS," http://prd.aps.org/abstract/PRD/v78/i10/e106010Phys. Rev. D **78**, 106010 (2008) [http://arXiv.org/abs/0805.3472arXiv:0805.3472 [hep-th]].
36. S. J. Brodsky, H. G. Dosch and G. F. de Teramond *in preparation*.
37. T. Gutsche, V. E. Lyubovitskij, I. Schmidt, A. Vega, "Dilaton in a soft-wall holographic approach to mesons and baryons," http://arXiv.org/abs/1108.0346arXiv:1108.0346 [hep-ph].
38. G. F. de Teramond and S. J. Brodsky, "Gauge/Gravity duality and hadron physics at the light-front," http://scitation.aip.org/getabs/servlet/GetabsServlet?prog=normal&id=APCPCS001296000001000128000001&idtype=cvips&gifs=yes&ref=no AIP Conf. Proc. **1296**, 128 (2010) [http://arXiv.org/abs/1006.2431arXiv:1006.2431 [hep-ph]].
39. J. Sonnenschein, "Stringy confining Wilson loops," http://arXiv.org/abs/hepth/0009146arXiv:hep-th/0009146.
40. S. S. Afonin, "No-wall holographic model for QCD," http://www.worldscinet.com/ijmpa/26/2621/S0217751X11053997.htmlInt. J. Mod. Phys. A **26**, 3615 (2011) [http://arxiv.org/abs/1012.5065arXiv:1012.5065 [hep-ph]].
41. C. Csaki and M. Reece, "Toward a systematic holographic QCD: a braneless approach," http://iopscience.iop.org/1126-6708/2007/05/062/JHEP **0705**, 062 (2007) [http://arXiv.org/abs/hepph/0608266hep-ph/0608266].
42. U. Gursoy, E. Kiritsis and F. Nitti, "Exploring improved holographic theories for QCD: Part II," http://iopscience.iop.org/1126-6708/2008/02/019/JHEP **0802**, 019 (2008) [http://arXiv.org/abs/0707.1349arXiv:0707.1349 [hep-th]].
43. W. de Paula, T. Frederico, H. Forkel and M. Beyer, "Dynamical AdS/QCD with area-law confinement and linear Regge trajectories," http://prd.aps.org/abstract/PRD/v79/i7/e075019 Phys. Rev. D **79**, 075019 (2009) [http://arXiv.org/abs/0806.3830arXiv:0806.3830 [hep-ph]].
44. T. Gherghetta, J. I. Kapusta and T. M. Kelley, "Chiral symmetry breaking in the soft-wall AdS/QCD model," http://prd.aps.org/abstract/PRD/v79/i7/e076003Phys. Rev. D **79**, 076003 (2009) [http://arXiv.org/abs/0902.1998arXiv:0902.1998 [hep-ph]].
45. Z. Abidin, H. J. Kwee and J. A. Tan, "Asymptotic freedom in holographic QCD," http://www.springerlink.com/content/r2635201h23k6588/JHEP **1112**, 026 (2011) [http://arXiv.org/abs/1110.2037arXiv:1110.2037 [hep-ph]].
46. L. D. Landau and E. M. Lifshitz, *Quantum Mechanics*, Pergamon, New York, 1958, Sec. 35.
47. P. Breitenlohner and D. Z. Freedman, "Stability in gauged extended supergravity," http://www.sciencedirect.com/science?_ob=ArticleURL&_udi=B6WB1-4DF4W12-66&_user=10&_coverDate=12%2F31%2F1982&_rdoc=1&_fmt=high&_orig=search&_sort=d&_docanchor=&view=c&_acct=C000050221&_version=1&_urlVersion=0&_userid=10&md5=48960c5f7d3f000d7336b5a6c774b92aAnnals Phys. **144**, 249 (1982).

48. J. J. Dudek, R. G. Edwards, K. Orginos and D. G. Richards, "Lattice QCD and the Jefferson Lab program," http://iopscience.iop.org/1742-6596/299/1/012007/pdf/1742-6596_299_1_012007.pdfJ. Phys. Conf. Ser. **299**, 012007 (2011).
49. A. Chodos, R. L. Jaffe, K. Johnson, C. B. Thorn and V. F. Weisskopf, "A new extended model of hadrons," http://prd.aps.org/abstract/PRD/v9/i12/p3471_1 Phys. Rev. D **9**, 3471 (1974).
50. K. Nakamura *et al.* [Particle Data Group Collaboration], "Review of particle physics," http://iopscience.iop.org/0954-3899/37/7A/075021/ J. Phys. GG **37**, 075021 (2010).
51. E. Klempt and A. Zaitsev, "Glueballs, hybrids, multiquarks. Experimental facts versus QCD inspired concepts," http://www.sciencedirect.com/science?_ob=ArticleURL&_udi=B6TVP-4PRYFV4-1&_user=10&_coverDate=12%2F31%2F2007&_rdoc=1&_fmt=high&_orig=search&_sort=d&_docanchor=&view=c&_acct=C000050221&_version=1&_urlVersion=0&_userid=10&md5=f4d99dc0a74105b5338b27c21ef0416cPhys. Rept. **454**, 1 (2007) [http://arXiv.org/abs/0708.4016arXiv:0708.4016 [hep-ph]].
52. G. F. de Teramond, S. J. Brodsky, "Hadronic spectrum of a holographic dual of QCD," http://prl.aps.org/abstract/PRL/v94/i20/e201601 Phys. Rev. Lett. **94**, 201601 (2005) [http://arXiv.org/abs/hep-th/0501022hep-th/0501022].
53. I. R. Klebanov and J. M. Maldacena, "Solving quantum field theories via curved spacetimes," http://dx.doi.org/10.1063/1.3074260Phys. Today **62**, 28 (2009).
54. O. Andreev, "$1/q^2$ corrections and gauge/string duality," http://prd.aps.org/abstract/PRD/v73/i10/e107901Phys. Rev. D **73**, 107901 (2006) [http://arXiv.org/abs/hep-th/0603170hep-th/0603170]; O. Andreev and V. I. Zakharov, "Heavy-quark potentials and AdS/QCD," http://prd.aps.org/abstract/PRD/v74/i2/e025023Phys. Rev. D **74**, 025023 (2006) [http://arXiv.org/abs/hep-ph/0604204arXiv:hep-ph/0604204].
55. G. F. de Teramond and S. J. Brodsky, "Light-front holography and gauge/gravity duality: the light meson and baryon spectra," http://www.sciencedirect.com/science?_ob=ArticleURL&_udi=B6TVD-4YV90X1-D&_user=10&_coverDate=02%2F28%2F2010&_rdoc=1&_fmt=high&_orig=search&_sort=d&_docanchor=&view=c&_acct=C000050221&_version=1&_urlVersion=0&_userid=10&md5=aaadaeb0126ca69a45f082bc078c5df4Nucl. Phys. B, Proc. Suppl. **199**, 89 (2010) [http://arXiv.org/abs/0909.3900arXiv:0909.3900 [hep-ph]]
56. H. Boschi-Filho, N. R. F. Braga and H. L. Carrion, "Glueball Regge trajectories from gauge/string duality and the Pomeron," http://prd.aps.org/abstract/PRD/v73/i4/e047901 Phys. Rev. D **73**, 047901 (2006) [http://arXiv.org/abs/hep-th/0507063arXiv:hep-th/0507063].
57. N. Evans and A. Tedder, "Perfecting the ultra-violet of holographic descriptions of QCD," http://www.sciencedirect.com/science?_ob=ArticleURL&_udi=B6TVN-4M57P31-3&_user=10&_coverDate=11%2F23%2F2006&_rdoc=1&_fmt=high&_orig=search&_sort=d&_docanchor=&view=c&_acct=C000050221&_version=1&_urlVersion=0&_userid=10&md5=f29e088070b179a0d5932dc1ff2ceb0c Phys. Lett. B **642**, 546 (2006) [http://arXiv.org/abs/hep-ph/0609112arXiv:hep-ph/0609112].
58. D. K. Hong, T. Inami and H. U. Yee, "Baryons in AdS/QCD," http://www.sciencedirect.com/science?_ob=ArticleURL&_udi=B6TVN-4MYVG5P-3&_user=10&_coverDate=03%2F15%2F2007&_rdoc=1&_fmt=high&_orig=search&_sort=d&_docanchor=&view=c&_acct=C000050221&_version=1&_urlVersion=0&_userid=10&md5=30e86a2e86751a26f988bca1f00b799d Phys. Lett. B **646**, 165 (2007) [http://arXiv.org/abs/hep-ph/0609270arXiv:hep-ph/0609270].
59. P. Colangelo, F. De Fazio, F. Jugeau and S. Nicotri, "On the light glueball spectrum in a holographic description of QCD," http://www.sciencedirect.com/science?_ob=ArticleURL&_udi=B6TVN-4P5R5W5-1&_user=10&_coverDate=08%2F23%2F2007&_rdoc=1&_fmt=high&_orig=search&_sort=d&_docanchor=&view=c&_acct=C000050221&_version=1&_urlVersion=0&_userid=10&md5=36f18b34bb053e1c9a7bde9ae56d7778 Phys. Lett. B **652**, 73 (2007) [http://arXiv.org/abs/hep-ph/0703316arXiv:hep-ph/0703316].
60. H. Forkel, M. Beyer, T. Frederico, "Linear square-mass trajectories of radially and orbitally excited hadrons in holographic QCD," http://iopscience.iop.org/1126-6708/2007/07/077/JHEP **0707**, 077 (2007) [http://arXiv.org/abs/0705.1857arXiv:0705.1857 [hep-ph]].
61. H. Forkel, "Holographic glueball structure," http://prd.aps.org/abstract/PRD/v78/i2/e025001 Phys. Rev. D **78**, 025001 (2008) [http://arXiv.org/abs/0711.1179arXiv:0711.1179 [hep-ph]].

62. A. Vega and I. Schmidt, "Scalar hadrons in $AdS_5 \times S^5$," http://prd.aps.org/abstract/PRD/v78/i1/e017703 Phys. Rev. D **78**, 017703 (2008) [http://arXiv.org/abs/0806.2267arXiv:0806.2267 [hep-ph]].
63. K. Nawa, H. Suganuma and T. Kojo, "Baryons with holography," http://www.worldscinet.com/mpla/23/2327n30/S0217732308029393.html Mod. Phys. Lett. A **23**, 2364 (2008) [http://arXiv.org/abs/0806.3040arXiv:0806.3040 [hep-th]].
64. P. Colangelo, F. De Fazio, F. Giannuzzi, F. Jugeau and S. Nicotri, "Light scalar mesons in the soft-wall model of AdS/QCD," http://prd.aps.org/abstract/PRD/v78/i5/e055009Phys. Rev. D **78**, 055009 (2008) [http://arXiv.org/abs/0807.1054arXiv:0807.1054 [hep-ph]].
65. H. Forkel and E. Klempt, "Diquark correlations in baryon spectroscopy and holographic QCD," http://www.sciencedirect.com/science?_ob=ArticleURL&_udi=B6TVN-4WRD3GS-1&_user=10&_coverDate=08%2F10%2F2009&_rdoc=1&_fmt=high&_orig=search&_sort=d&_docanchor=&view=c&_acct=C000050221&_version=1&_urlVersion=0&_userid=10&md5=64e77385c4b2a868f9344521b3f60118 Phys. Lett. B ğ**679**, 77 (2009) [http://arXiv.org/abs/0810.2959arXiv:0810.2959 [hep-ph]].
66. H. C. Ahn, D. K. Hong, C. Park and S. Siwach, "Spin 3/2 baryons and form factors in AdS/QCD," http://prd.aps.org/abstract/PRD/v80/i5/e054001 Phys. Rev. D **80**, 054001 (2009) [http://arXiv.org/abs/0904.3731arXiv:0904.3731 [hep-ph]].
67. Y. -Q. Sui, Y. -L. Wu, Z. -F. Xie and Y. -B. Yang, "Prediction for the mass spectra of resonance mesons in the soft-wall AdS/QCD with a modified 5D metric," http://arxiv.org/abs/0909.3887 Phys. Rev. D **81**, 014024 (2010) [http://arXiv.org/abs/0909.3887arXiv:0909.3887 [hep-ph]].
68. J. I. Kapusta and T. Springer, "Potentials for soft wall AdS/QCD," http://prd.aps.org/abstract/PRD/v81/i8/e086009 Phys. Rev. D **81**, 086009 (2010) [http://arXiv.org/abs/1001.4799arXiv:1001.4799 [hep-ph]].
69. P. Zhang, "Improving the excited nucleon spectrum in hard-wall AdS/QCD," http://prd.aps.org/abstract/PRD/v81/i11/e114029 Phys. Rev. D **81**, 114029 (2010) [http://arXiv.org/abs/1002.4352arXiv:1002.4352 [hep-ph]]; "Mesons and nucleons in soft-wall AdS/QCD," http://prd.aps.org/abstract/PRD/v82/i9/e094013 Phys. Rev. D **82**, 094013 (2010) http://arXiv.org/abs/1007.2163[arXiv:1007.2163 [hep-ph]].
70. I. Iatrakis, E. Kiritsis and A. Paredes, "An AdS/QCD model from Sen's tachyon action," http://prd.aps.org/abstract/PRD/v81/i11/e115004 Phys. Rev. D **81**, 115004 (2010) [http://arXiv.org/abs/1003.2377arXiv:1003.2377 [hep-ph]].
71. T. Branz, T. Gutsche, V. E. Lyubovitskij, I. Schmidt and A. Vega, "Light and heavy mesons in a soft-wall holographic approach," http://prd.aps.org/abstract/PRD/v82/i7/e074022 Phys. Rev. D **82**, 074022 (2010) [http://arXiv.org/abs/1008.0268arXiv:1008.0268 [hep-ph]].
72. M. Kirchbach, C. B. Compean, "Conformal symmetry and light flavor baryon spectra," http://prd.aps.org/abstract/PRD/v82/i3/e034008Phys. Rev. D **82**, 034008 (2010) [http://arXiv.org/abs/1003.1747arXiv:1003.1747 [hep-ph]].
73. Y. -Q. Sui, Y. -L. Wu and Y. -B. Yang, "Predictive AdS/QCD model for mass spectra of mesons with three flavors," http://prd.aps.org/abstract/PRD/v83/i6/e065030Phys. Rev. D **83**, 065030 (2011) [http://arXiv.org/abs/1012.3518arXiv:1012.3518 [hep-ph]].
74. J. Erlich, "How well does AdS/QCD describe QCD?," http://www.worldscinet.com/ijmpa/25/2502n03/S0217751X10048718.htmlInt. J. Mod. Phys. A **25**, 411 (2010) [http://arXiv.org/abs/0908.0312arXiv:0908.0312 [hep-ph]].
75. Y. Kim and D. Yi, "Holography at work for nuclear and hadron physics," http://www.hindawi.com/journals/ahep/2011/259025/Adv. High Energy Phys. **2011**, 259025 (2011) [http://arXiv.org/abs/1107.0155arXiv:1107.0155 [hep-ph]].
76. D. E. Soper, "The parton model and the Bethe-Salpeter wave function," http://prd.aps.org/abstract/PRD/v15/i4/p1141_1Phys. Rev. D **15**, 1141 (1977).
77. G. F. de Teramond, S. J. Brodsky, "Light-front quantization and AdS/QCD: an overview," http://iopscience.iop.org/1742-6596/287/1/012007/J. Phys. Conf. Ser. **287**, 012007 (2011) [http://arxiv.org/abs/1103.1100arXiv:1103.1100 [hep-ph]].
78. R. Baldini *et al.*, "Nucleon time-like form factors below the N anti-N threshold," http://www.springerlink.com/content/vmuvrt7x9vvq5fey/Eur. Phys. J. C **11**, 709 (1999).
79. V. Tadevosyan *et al.*, [Jefferson Lab $F_\pi$ Collaboration], "Determination of the pion charge form factor for $Q^2$=0.60–

1.60 GeV$^2$," http://prc.aps.org/abstract/PRC/v75/i5/e055205Phys. Rev. C **75**, 055205 (2007) [http://arXiv.org/abs/nucl-ex/0607007arXiv:nucl-ex/0607007]; T. Horn *et al.*, [Jefferson Lab $F_\pi$ Collaboration], "Determination of the charged pion form factor at $Q^2 = 1.60$ and 2.45 (GeV/c)$^2$," http://prl.aps.org/abstract/PRL/v97/i19/e192001Phys. Rev. Lett. **97**, 192001 (2006) [http://arXiv.org/abs/nucl-ex/0607005arXiv:nucl-ex/0607005].

80. H. R. Grigoryan, A. V. Radyushkin, "Structure of vector mesons in holographic model with linear confinement," http://prd.aps.org/abstract/PRD/v76/i9/e095007Phys. Rev. D **76**, 095007 (2007) [http://arxiv.org/abs/0706.1543arXiv:0706.1543 [hep-ph]].
81. H. J. Kwee and R. F. Lebed, "Pion form-factors in holographic QCD," http://iopscience.iop.org/1126-6708/2008/01/027/JHEP **0801**, 027 (2008) [http://arxiv.org/abs/0708.4054arXiv:0708.4054 [hep-ph]]. See also: H. J. Kwee and R. F. Lebed, "Pion form factor in improved holographic QCD backgrounds," http://prd.aps.org/abstract/PRD/v77/i11/e115007Phys. Rev. D **77**, 115007 (2008) [http://arxiv.org/abs/0712.1811arXiv:0712.1811 [hep-ph]].
82. H. R. Grigoryan and A. V. Radyushkin, "Pion form-factor in chiral limit of hard-wall AdS/QCD model," http://prd.aps.org/abstract/PRD/v76/i11/e115007Phys. Rev. D **76**, 115007 (2007) [http://arxiv.org/abs/0709.0500arXiv:0709.0500 [hep-ph]].
83. F. Zuo, "Improved soft-wall model with a negative dilaton," http://prd.aps.org/abstract/PRD/v82/i8/e086011Phys. Rev. D **82**, 086011 (2010) [http://arxiv.org/abs/0909.4240arXiv:0909.4240 [hep-ph]].
84. S. Nicotri, "Phenomenology of the holographic soft-wall model of QCD with 'reversed' dilaton," http://proceedings.aip.org/resource/2/apcpcs/1317/1/322_1?isAuthorized=noAIP Conf. Proc. **1317**, 322 (2011) [http://arxiv.org/abs/1009.4829arXiv:1009.4829 [hep-ph]].
85. A. Karch, E. Katz, D. T. Son and M. A. Stephanov, "On the sign of the dilaton in the soft wall models," http://www.springerlink.com/content/nr2283u37561qu45/JHEP **1104**, 066 (2011) [http://arxiv.org/abs/1012.4813arXiv:1012.4813 [hep-ph]].
86. G. F. de Teramond and S. J. Brodsky, "Excited baryons in holographic QCD," http://arxiv.org/abs/1108.0965arXiv:1108.0965 [hep-ph].
87. S. J. Brodsky, F.-G. Cao and G. F. de Teramond, "Evolved QCD predictions for the meson-photon transition form factors," http://prd.aps.org/abstract/PRD/v84/i3/e033001Phys. Rev. D **84**, 033001 (2011) [http://arXiv.org/abs/1104.3364arXiv:1104.3364 [hep-ph]].
88. S. J. Brodsky, F.-G. Cao and G. F. de Teramond, "Meson transition form factors in light-front holographic QCD," http://prd.aps.org/abstract/PRD/v84/i7/e075012Phys. Rev. D **84**, 075012 (2011) [http://arXiv.org/abs/1105.3999arXiv:1105.3999 [hep-ph]].
89. G. P. Lepage and S. J. Brodsky, "Exclusive processes in perturbative quantum chromodynamics," http://prd.aps.org/abstract/PRD/v22/i9/p2157_1 Phys. Rev. D **22**, 2157 (1980).
90. B. Aubert *et al.* [The BABAR Collaboration], "Measurement of the $\gamma\gamma^* \to \pi^0$ transition form factor," http://prd.aps.org/abstract/PRD/v80/i5/e052002Phys. Rev. **D80**, 052002 (2009) [http://arxiv.org/abs/0905.4778arXiv:0905.4778 [hep-ex]].
91. P. A. Sanchez *et al.* [The BABAR Collaboration], "Measurement of the $\gamma\gamma^* \to \eta$ and $\gamma\gamma^* \to \eta'$ transition form factors," http://arxiv.org/abs/1101.1142v1arXiv:1101.1142 [hep-ex].
92. V. P. Druzhinin *et al.* [The BABAR Collaboration], "Recent BABAR results on two-photon physics," http://pos.sissa.it/archive/conferences/120/144/ICHEP%202010_144.pdfPoS **ICHEP**, 144 (2010) [http://arxiv.org/abs/1011.6159arXiv:1011.6159 [hep-ex]].
93. H.-J. Behrend *et al.* [CELLO Collaboration], "A measurement of the $\pi^0$, $\eta$ and $\eta'$ electromagnetic form-factors," http://www.springerlink.com/content/l1313037817t1347/Z. Phys. C **49**, 401 (1991).
94. J. Gronberg *et al.* [CLEO Collaboration], "Measurements of the meson-photon transition form factors of light pseudoscalar mesons at large momentum transfer," http://prd.aps.org/abstract/PRD/v57/i1/p33_1Phys. Rev. D **57**, 33 (1998) [http://arXiv.org/abs/hep-ex/9707031arXiv:hep-ex/9707031].
95. H.-N. Li and S. Mishima, "Pion transition form factor in $k_T$ factorization," http://prd.aps.org/abstract/PRD/v80/i7/e074024Phys. Rev. D **80**, 074024 (2009) [http://arXiv.org/abs/0907.0166arXiv:0907.0166 [hep-ph]].
96. S. V. Mikhailov and N. G. Stefanis, "Pion transition form factor at the two-loop level vis-a-vis experimental data," http://www.worldscinet.com/mpla/24/2435n37/S0217732309001078.htmlMod. Phys. Lett. A **24**, 2858

(2009) [http://arXiv.org/abs/0910.3498arXiv:0910.3498 [hep-ph]].
97. X.-G. Wu and T. Huang, "An implication on the pion distribution amplitude from the pion-photon transition form factor with the new BABAR data," http://prd.aps.org/abstract/PRD/v82/i3/e034024Phys. Rev. D **82**, 034024 (2010) [http://arXiv.org/abs/1005.3359arXiv:1005.3359 [hep-ph]].
98. H. L. L. Roberts, C. D. Roberts, A. Bashir, L. X. Gutierrez-Guerrero, and P. C. Tandy, "Abelian anomaly and neutral pion production," http://prc.aps.org/abstract/PRC/v82/i6/e065202Phys. Rev. C **82**, 065202 (2010) [[http://arXiv.org/abs/1009.0067arXiv:1009.0067 [nucl-th]].
99. W. Broniowski and E. R. Arriola, "Pion transition form factor in the Regge approach," PoS **LC2010**, 062 (2010) [http://arXiv.org/abs/1008.2317arXiv:1008.2317 [hep-ph]].
100. P. Kroll, "The form factors for the photon to pseudoscalar meson transitions - an update" http://arxiv.org/abs/1012.3542arXiv:1012.3542 [hep-ph].
101. M. Gorchtein, P. Guo, and A. P. Szczepaniak, "Pion form factors" http://arxiv.org/abs/1102.5558arXiv:1102.5558 [nucl-th].
102. A. E. Dorokhov, "Photon-pion transition form factor: BABAR puzzle is cracked," http://arxiv.org/abs/1003.4693arXiv:1003.4693 [hep-ph]; "Photon-pion transition form factor at high photon virtualities within the nonlocal chiral quark model," http://www.springerlink.com/content/l6ng5pm2882768p5/JETP Lett. **92** 707 (2010).
103. S. S. Agaev, V. M. Braun, N. Offen, and F. A. Porkert, "Light cone sum rules for the $\pi^0\gamma^*\gamma$ form factor revisited," http://prd.aps.org/abstract/PRD/v83/i5/e054020Phys. Rev. D **83**, 054020 (2011) [http://arxiv.org/abs/1012.4671arXiv:1012.4671 [hep-ph]].
104. A. P. Bakulev, S. V. Mikhailov, A. V. Pimikov, and N. G. Stefanis "Pion-photon transition – the new QCD frontier," http://prd.aps.org/abstract/PRD/v84/i3/e034014Phys. Rev. D **84**, 034014 (2011) [http://arxiv.org/abs/1105.2753arXiv:1105.2753 [hep-ph]].
105. Y. N. Klopot, A. G. Oganesian and O. V. Teryaev, "Axial anomaly and mixing: from real to highly virtual photons," http://prd.aps.org/abstract/PRD/v84/i5/e051901Phys. Rev. D **84**, 051901 (2011) [http://arxiv.org/abs/1106.3855arXiv:1106.3855 [hep-ph]].
106. X. G. Wu and T. Huang, "Constraints on the light pseudoscalar meson distribution amplitudes from their meson-photon transition form factors," http://prd.aps.org/abstract/PRD/v84/i7/e074011Phys. Rev. D **84**, 074011 (2011) [http://arxiv.org/abs/1106.4365arXiv:1106.4365 [hep-ph]].
107. S. Noguera and S. Scopetta, "Eta-photon transition form factor," http://prd.aps.org/abstract/PRD/v85/i5/e054004Phys. Rev. D **85**, 054004 (2012) [http://arxiv.org/abs/1110.6402arXiv:1110.6402 [hep-ph]].
108. I. Balakireva, W. Lucha and D. Melikhov, "Pion elastic and $(\pi^0, \eta, \eta') \to \gamma\gamma^*$ transition form factors in a broad range of momentum transfers," http://prd.aps.org/abstract/PRD/v85/i3/e036006Phys. Rev. D **85**, 036006 (2012) [http://arxiv.org/abs/1110.6904arXiv:1110.6904 [hep-ph]]; "Elastic and transition form factors of light pseudoscalar mesons from QCD sum rules," http://arxiv.org/abs/1203.2599arXiv:1203.2599 [hep-ph].
109. D. McKeen, M. Pospelov and J. M. Roney, "Pion-photon transition form factor and new physics in the $\tau$ sector," http://prd.aps.org/abstract/PRD/v85/i5/e053002Phys. Rev. D **85**, 053002 (2012) [http://arxiv.org/abs/1112.2207arXiv:1112.2207 [hep-ph]].
110. C. -C. Lih and C. -Q. Geng, "$\pi^0 \to \gamma^*\gamma$ transition form factor within the light-front quark model," http://prc.aps.org/abstract/PRC/v85/i1/e018201Phys. Rev. C **85**, 018201 (2012) [http://arxiv.org/abs/arXiv:1201.2220arXiv:1201.2220 [hep-ph]].
111. H. Czyz, S. Ivashyn, A. Korchin and O. Shekhovtsova, "Two-photon form factors of the $\pi^0$, $\eta$ and $\eta'$ mesons in the chiral theory with resonances," http://arxiv.org/abs/1202.1171arXiv:1202.1171 [hep-ph].
112. A. Pomarol, A. Wulzer, "Baryon physics in holographic QCD," http://www.sciencedirect.com/science/article/pii/S0550321308005907Nucl. Phys. **B809**, 347-361 (2009), [http://arXiv.org/abs/0807.0316arXiv:0807.0316 [hep-ph].
113. H. R. Grigoryan, A. V. Radyushkin, "Anomalous form factor of the neutral pion in extended AdS/QCD model with Chern-Simons term," http://prd.aps.org/abstract/PRD/v77/i11/e115024Phys. Rev. **D77**, 115024 (2008) [http://arxiv.org/abs/0803.1143arXiv:0803.1143 [hep-ph]].
114. H. R. Grigoryan and A. V. Radyushkin, "Pion in the Holographic Model with 5D Yang-Mills Fields," http://prd.aps.org/abstract/PRD/v78/i11/e115008Phys. Rev. D **78**, 115008 (2008) [http://arxiv.org/abs/0808.

1243arXiv:0808.1243 [hep-ph]].

115. F. Zuo, Y. Jia, T. Huang, "$\gamma^*\rho^0 \rightarrow \pi^0$ transition form factor in extended AdS/QCD models," http://www.springerlink.com/content/7914350355476183/Eur. Phys. J. **C67**, 253-261 (2010) [http://arXiv.org/abs/arXiv:0910.3990arXiv:0910.3990 [hep-ph]].
116. T. Sakai, S. Sugimoto, "More on a holographic dual of QCD," http://ptp.ipap.jp/link?PTP/114/1083/Prog. Theor. Phys. **114**, 1083-1118 (2005) [http://arXiv.org/abs/hep-th/0507073hep-th/0507073].
117. C. T. Hill, C. K. Zachos, "Dimensional deconstruction and Wess-Zumino-Witten terms," http://prd.aps.org/abstract/PRD/v71/i4/e046002Phys. Rev. **D71**, 046002 (2005) [http://arXiv.org/abs/hep-th/0411157hep-th/0411157].
118. I. V. Musatov, A. V. Radyushkin, "Transverse momentum and Sudakov effects in exclusive QCD processes: $\gamma^*\gamma\pi^0$ form factor," http://prd.aps.org/abstract/PRD/v56/i5/p2713_1Phys. Rev. **D56**, 2713 (1997) [http://arxiv.org/abs/hep-ph/9702443hep-ph/9702443].
119. See, for example: R. G. Edwards, J. J. Dudek, D. G. Richards and S. J. Wallace, "Excited state baryon spectroscopy from lattice QCD," http://prd.aps.org/abstract/PRD/v84/i7/e074508Phys. Rev. D **84**, 074508 (2011) [http://arXiv.org/abs/1104.5152arXiv:1104.5152 [hep-ph]].
120. M. Henningson and K. Sfetsos, "Spinors and the AdS / CFT correspondence," http://www.sciencedirect.com/science/article/pii/S0370269398005590Phys. Lett. B **431**, 63 (1998) [http://arXiv.org/abs/hep-th/9803251arXiv:hep-th/9803251].
121. W. Mueck and K. S. Viswanathan, "Conformal field theory correlators from classical field theory on anti-de Sitter space. 2. Vector and spinor fields," http://prd.aps.org/abstract/PRD/v58/i10/e106006Phys. Rev. D **58**, 106006 (1998) [http://arXiv.org/abs/hep-th/9805145arXiv:hep-th/9805145].
122. G. F. de Teramond, S. J. Brodsky, "Light-front quantization approach to the gauge-gravity correspondence and hadron spectroscopy," http://scitation.aip.org/getabs/servlet/GetabsServlet?prog=normal&id=APCPCS001257000001000059000001&idtype=cvips&gifs=yes&bypassSSO=1AIP Conf. Proc. **1257**, 59 (2010) [http://arXiv.org/abs/1001.5193arXiv:1001.5193 [hep-ph]]; S. J. Brodsky and G. F. de Teramond, "AdS/CFT and light-front QCD," http://eproceedings.worldscinet.com/9789814293242/9789814293242_0008.html World Scientific Subnuclear Series, **45**, 139 (2007) [http://arXiv.org/abs/0802.0514arXiv:0802.0514 [hep-ph]].
123. A. Volovich, "Rarita-Schwinger field in the AdS / CFT correspondence," http://iopscience.iop.org/1126-6708/1998/09/022/JHEP **9809**, 022 (1998) [http://arXiv.org/abs/hep-th/9809009arXiv:hep-th/9809009].
124. P. Matlock and K. S. Viswanathan, "The AdS / CFT correspondence for the massive Rarita-Schwinger field," http://prd.aps.org/abstract/PRD/v61/i2/e026002Phys. Rev. D **61**, 026002 (2000) [http://arXiv.org/abs/hep-th/9906077arXiv:hep-th/9906077].
125. E. Witten, "Baryons and branes in anti-de Sitter space," http://iopscience.iop.org/1126-6708/1998/07/006/JHEP **9807**, 006 (1998) [http://arXiv.org/abs/hep-th/9805112arXiv:hep-th/9805112].
126. D. J. Gross and H. Ooguri, "Aspects of large N gauge theory dynamics as seen by string theory," http://prd.aps.org/abstract/PRD/v58/i10/e106002Phys. Rev. D **58**, 106002 (1998) [http://arXiv.org/abs/hep-th/9805129arXiv:hep-th/9805129].
127. D. K. Hong, M. Rho, H. -U. Yee and P. Yi, "Chiral dynamics of baryons from string theory," http://prd.aps.org/abstract/PRD/v76/i6/e061901Phys. Rev. D **76**, 061901 (2007) [http://arXiv.org/abs/hep-th/0701276arXiv:hep-th/0701276].
128. H. Hata, T. Sakai, S. Sugimoto and S. Yamato, "Baryons from instantons in holographic QCD," http://ptp.ipap.jp/link?PTP/117/1157/Prog. Theor. Phys. **117**, 1157 (2007) [http://arXiv.org/abs/hep-th/0701280arXiv:hep-th/0701280].
129. S. J. Brodsky and G. F. de Teramond, "Applications of AdS/QCD and light-front holography to baryon physics," http://proceedings.aip.org/resource/2/apcpcs/1388/1/22_1?isAuthorized=noAIP Conf. Proc. **1388**, 22 (2011) [http://arXiv.org/abs/1103.1186arXiv:1103.1186 [hep-ph]].
130. A. V. Anisovich, R. Beck, E. Klempt, V. A. Nikonov, A. V. Sarantsev and U. Thoma, "Properties of baryon resonances from a multichannel partial wave analysis," http://arXiv.org/abs/1112.4937arXiv:1112.4937 [hep-ph].
131. E. Klempt and J. M. Richard, "Baryon spectroscopy," http://rmp.aps.org/abstract/RMP/v82/i2/p1095_1Rev. Mod. Phys. **82**, 1095 (2010) [http://arXiv.org/abs/0901.2055arXiv:0901.205 [hep-ph]].

132. F. Wilczek, “Diquarks as inspiration and as objects,” http://arXiv.org/abs/hep-ph/0409168arXiv:hep-ph/0409168; A. Selem and F. Wilczek, “Hadron systematics and emergent diquarks,” http://arXiv.org/abs/hep-ph/0602128arXiv:hep-ph/0602128.
133. I. Kirsch, “Spectroscopy of fermionic operators in AdS/CFT,” http://iopscience.iop.org/1126-6708/2006/09/052/JHEP **0609**, 052 (2006) [http://arXiv.org/abs/hep-th/0607205arXiv:hep-th/0607205].
134. H. G. Dosch, “A practical guide to AdS/CFT,” Lectures given at the School of Physics and Technology, Wuhan University, March-April (2009), http://www.thphys.uni-heidelberg.de/~dosch/wuhantot.pdf.
135. E. Klempt, “Is chiral symmetry broken and or restored in high-mass light baryons?,” http://arXiv.org/abs/1011.3644arXiv:1011.3644 [hep-ph].
136. S. J. Brodsky and S. D. Drell, “The anomalous magnetic moment and limits on fermion substructure,” http://prd.aps.org/abstract/PRD/v22/i9/p2236_1Phys. Rev. D **22**, 2236 (1980).
137. Z. Abidin, C. E. Carlson, “Nucleon electromagnetic and gravitational form factors from holography,” http://prd.aps.org/abstract/PRD/v79/i11/e115003Phys. Rev. **D79**, 115003 (2009) [[http://arXiv.org/abs/0903.4818arXiv:0903.4818 [hep-ph]].
138. A. Vega, I. Schmidt, T. Gutsche, V. E. Lyubovitskij, “Generalized parton distributions in AdS/QCD,” http://prd.aps.org/abstract/PRD/v83/i3/e036001Phys. Rev. **D83**, 036001 (2011) [http://arXiv.org/abs/1010.2815arXiv:1010.2815 [hep-ph]].
139. A. Vega, I. Schmidt, T. Gutsche and V. E. Lyubovitskij, “Generalized parton distributions in an AdS/QCD hard-wall model,” http://arXiv.org/abs/1202.4806arXiv:1202.4806 [hep-ph].
140. R. Nishio, T. Watari, “Investigating generalized parton distribution in gravity dual,” http://arXiv.org/abs/1105.2907arXiv:1105.2907 [hep-ph].
141. H. R. Grigoryan, T.-S. H. Lee, H.-U. Yee, “Electromagnetic nucleon-to-delta transition in holographic QCD,” http://prd.aps.org/abstract/PRD/v80/i5/e055006Phys. Rev. **D80**, 055006 (2009) [http://arXiv.org/abs/0904.3710arXiv:0904.3710[hep-ph]].
142. G. D. Cates, C. W. de Jager, S. Riordan and B. Wojtsekhowski, “Flavor decomposition of the elastic nucleon electromagnetic form factors,” http://prl.aps.org/abstract/PRL/v106/i25/e252003Phys. Rev. Lett. **106**, 252003 (2011) [http://arXiv.org/abs/1103.1808arXiv:1103.1808 [nucl-ex]].
143. M. Rohrmoser, K. -S. Choi and W. Plessas, “Flavor analysis of nucleon electromagnetic form factors,” http://arXiv.org/abs/1103.1808arXiv:1110.3665 [hep-ph].
144. M. Diehl, “Generalized parton distributions from form factors,” http://www.sciencedirect.com/science/article/pii/S0920563206004798Nucl. Phys. Proc. Suppl. **161**, 49 (2006) [http://arXiv.org/abs/hep-ph/0510221arXiv:hep-ph/0510221].
145. M. A. B. Beg, B. W. Lee and A. Pais, “SU(6) and electromagnetic interactions,” http://prl.aps.org/abstract/PRL/v13/i16/p514_1Phys. Rev. Lett. **13**, 514 (1964).
146. R. Pohl, A. Antognini, F. Nez *et al.*, “The size of the proton,” http://www.nature.com/nature/journal/v466/n7303/full/nature09250.htmlNature **466**, 213 (2010).
147. M. A. B. Beg and A. Zepeda, “Pion radius and isovector nucleon radii in the limit of small pion mass,” http://prd.aps.org/abstract/PRD/v6/i10/p2912_1Phys. Rev. D **6**, 2912 (1972).
148. S. Collins, M. Gockeler, P. Hagler *et al.*, “Dirac and Pauli form factors from lattice QCD,” http://prd.aps.org/abstract/PRD/v84/i7/e074507Phys. Rev. D **84**, 074507 (2011) [http://arXiv.org/abs/1106.3580arXiv:1106.3580 [hep-lat]].
149. I. G. Aznauryan *et al.* [CLAS Collaboration], “Electroexcitation of nucleon resonances from CLAS data on single pion electroproduction,” http://prc.aps.org/abstract/PRC/v80/i5/e055203Phys. Rev. **C80**, 055203 (2009) [http://arXiv.org/abs/0909.2349arXiv:0909.2349 [nucl-ex]].
150. I. G. Aznauryan and V. D. Burkert, “Electroexcitation of nucleon resonances,” http://www.sciencedirect.com/science/article/pii/S0146641011001086Prog. Part. Nucl. Phys. **67**, 1 (2012) [http://arXiv.org/abs/1109.1720arXiv:1109.1720 [hep-ph]].
151. N. Isgur and J. E. Paton, “A flux tube model for hadrons in QCD,” http://prd.aps.org/abstract/PRD/v31/i11/p2910_1Phys. Rev. D **31**, 2910 (1985).
152. E. Klempt, “Hadron spectroscopy without constituent glue,” http://www.worldscinet.com/ijmpa/20/2008n09/S0217751X05023232.htmlInt. J. Mod. Phys. A **20**, 1720 (2005) [http://arXiv.org/abs/hep-ph/0409164arXiv:hep-ph/0409164].

153. J. F. Gunion, S. J. Brodsky, R. Blankenbecler, "Composite theory of inclusive scattering at large transverse momenta," `http://prd.aps.org/abstract/PRD/v6/i9/p2652_1`Phys. Rev. **D6**, 2652 (1972).
154. B. R. Baller, G. C. Blazey, H. Courant *et al.*, "Comparison of exclusive reactions at Large *t*," `http://prl.aps.org/abstract/PRL/v60/i12/p1118_1`Phys. Rev. Lett. **60**, 1118 (1988).
155. S. J. Brodsky and G. F. de Teramond, "AdS/QCD, Light-Front Holography, and Sublimated Gluons," PoS QCD **-TNT-II**, 008 (2011) [`http://arXiv.org/abs/1112.4212arXiv:1112.4212 [hep-th]`].
156. C. Csaki, M. Reece and J. Terning, "The AdS/QCD correspondence: still undelivered," `http://iopscience.iop.org/1126-6708/2009/05/067/`JHEP **0905**, 067 (2009) [`http://arXiv.org/abs/0811.3001arXiv:0811.3001 [hep-ph]`].
157. J. P. Vary, H. Honkanen, J. Li, P. Maris, S. J. Brodsky, A. Harindranath, G. F. de Teramond, P. Sternberg *et al.*, "Hamiltonian light-front field theory in a basis function approach," `http://prc.aps.org/abstract/PRC/v81/i3/e035205`Phys. Rev. C **81**, 035205 (2010) [`http://arXiv.org/abs/0905.1411arXiv:0905.1411 [nucl-th]`].
158. V. Balasubramanian, P. Kraus and A. E. Lawrence, "Bulk vs. boundary dynamics in anti-de Sitter spacetime," `http://prd.aps.org/abstract/PRD/v59/i4/e046003`Phys. Rev. D **59**, 046003 (1999) [`http://arXiv.org/abs/hep-th/9805171arXiv:hep-th/9805171`].
159. I. R. Klebanov and E. Witten, "AdS/CFT correspondence and symmetry breaking," `http://www.sciencedirect.com/science/article/pii/S0550321399003879`Nucl. Phys. B **556**, 89 (1999) [`http://arXiv.org/abs/hep-th/9905104arXiv:hep-th/9905104`].

# Phenomenology of Nucleon Form Factors

Egle Tomasi-Gustafsson

*CEA,IRFU,SPhN, Saclay, and*
*Univ Paris-Sud, CNRS/IN2P3, IPN Orsay, UMR 8608, France*

The most simple reaction that can be studied theoretically and experimentally is the process involving electrons and protons. In spite of its elementarity, electron-proton elastic scattering and the crossed channels as nucleon-antinucleon to (or created by) an electron positron pair are actively studied since decades. Assuming that the colliding particles interact by exchange of one virtual photon, the transferred momentum squared (the mass of the virtual photon) probes the dynamical structure of the nucleon at the corresponding internal scale.

The differential cross section and the polarization observables in these reactions are expressed in terms of form factors, which contain unique information on the nucleon structure: form factors parametrize the internal structure of a composite particle and describe its dynamical properties. The knowledge of form factors constitutes a stringent test for any model which, after the static properties of a particle, like masses or magnetic moments, should be able to reproduce charge and magnetic distributions.

The experimental achievements: high energy accelerators, high intensity beams, high resolution spectrometers, polarized targets, hadron polarimeters, full coverage detectors.. open the possibility of very precise measurements in an unexplored kinematical region. A wide program is ongoing or is planned at facilities in the GeV range: electron accelerators, such as Jefferson Lab (Newport News), electron-positron colliders such as VEPPIII (Novosibirk), BEPCII (Beijing), proton-antiproton colliders such as FermiLab and the future FAIR facility, at Darmstadt.

From the theoretical point of view, the precise knowledge of the form factors in a wide kinematical range gives the best insight in the transition region, between the non perturbative domain where the nucleon is best described by constituent quarks and meson cloud, and the perturbative region where QCD can be applied and the nucleon appears as a confined system of quarks and gluons. Analytical and model independent properties of form factors are a guide for modelization of the nucleon structure.

After an historical and pedagogical introduction into this field, a formal derivation of electromagnetic form factors for the scattering and the annihilation channels, as well as discussion of the recent data, and of new ideas in the understanding of the reaction mechanism, is given.

## 1. Introduction

The experimental determination of the elastic proton electromagnetic form factors (FFs) at large momentum transfer is presently of large interest, due to experimental developments which open the possibility to achieve new kinematical regions and very high precision. In particular, polarization experiments have been made possible by polarized electron beams at high intensity and proton polarimetry in the GeV energy region, as suggested many years ago.[1–3]

Hadron FFs are considered fundamental quantities, as they characterize the internal structure of a non pointlike particle. They contain dynamical information on the electric and magnetic currents of hadrons, and are experimentally accessible through differential cross section and polarization observables. Theoretically FFs enter in the expression of the electromagnetic current. Any hadron theory, that reproduces the static properties such as masses and magnetic moments, should be able to describe also the dynamics of the charge and magnetic distributions, i.e., the electromagnetic FFs.

In a P and T invariant theory, the structure of any particle of spin $S$ is parametrized in terms of $(2S + 1)$ FFs. Protons and neutrons are described by two FFs, electric $G_E$ and magnetic $G_M$, which are functions of one kinematical variable, physically representing the internal scale. The deuteron (spin one particle) is described by three form factors, charge, electric, and quadrupole. The $\alpha$ particle, spin zero, has one form factor.

The normalization of these FFs is related to the charge and the magnetic moment of the hadron and corresponds to the static value which can be observed through low energy electron elastic scattering on hadrons, at the photon point. Schematically, one can say that at small momenta (large internal distances) FFs probe the size of the nucleus. At high energies (short distances) they probe the quark and gluon structure. Their behavior should follow scaling laws, predicted by perturbative quantum-chromodynamics (pQCD). In this respect, the precise knowledge of FFs in a wide kinematical region should probe the transition region, from non perturbative to perturbative QCD.

The traditional way to measure proton electromagnetic FFs consists in the measurement of electron-proton elastic scattering, assuming that the interaction occurs through the exchange of a virtual photon, of four momentum squared $Q^2 = -q^2$. The differential cross section at a fixed value of $Q^2$ is depends linearly on $\cot^2(\theta/2)$ (where $\theta$ is the electron scattering angle). The slope and the intercept allow to determine $G_E$ and $G_M$. This is a specific characteristic of the one photon exchange mechanism. This method was proposed first by N. M. Rosenbluth.[4]

Polarization phenomena play a major role (except for spin zero particles), as they contain unique information on the imaginary part of amplitudes (amplitudes are, in general, complex functions). Being related to interference of amplitudes, they are very sensitive to small contributions. Elastic electron hadron scattering has been the privileged reaction to access FFs. Assuming one photon exchange, a simple and elegant formalism, which will be illustrated in these lectures, relates all observables, cross section and polarization phenomena, to hadron FFs.

The idea that double spin polarization observables in elastic electron proton ($ep$) scattering (with longitudinally polarized electrons on a polarized target, or on an unpolarized target, measuring the transverse polarization of the scattered proton) carry the information on the product $G_E G_M$ was firstly suggested by A. I. Akhiezer and M. P. Rekalo[1] but was only recently applied. Besides the expected large precision achieved, the surprising fact, was that the data revealed a $Q^2$-dependence of the ratio $\mathcal{R} = \mu G_E/G_M$ ($\mu$ is the proton magnetic moment) which deviates from unity, as was previously commonly assumed.

In case of the neutron, the measurements are even more difficult, as the electric FF is small (the static value is zero). As there is no free neutron target, one has to use either a deuteron or an $^3He$ target, and then correct for nuclear effects. In the neutron case, too, the polarization method allows to extend the measurements in the scattering region at larger $Q^2$ values with higher precision.

Inconsistencies appeared among the results from polarized and unpolarized experiments. The ratio $\mu G_E/G_M$ measured from the ratio $P_\ell/P_t$ (the longitudinal and transverse polarization of the recoil proton in $ep$ scattering induced by longitudinally polarized electrons) shows a monotone decreasing with $Q^2$, whereas the individual determination of $G_E$ and $G_M$ from the Rosenbluth separation suggests a constant behavior. No shortcoming has been found neither in the experiments or in the data analysis, which are based on the same theoretical background (the lowest order diagrams for $ep$ elastic scattering). Therefore, the attention has been focused to higher order corrections in the power of $\alpha$, radiative corrections in $\alpha^n$ including the interference between one and two photon exchange. This puzzle has given rise to many speculations and different interpretations, suggesting further experiments (for a review, see[5]).

Applying crossing symmetry considerations, the same physical information can be extracted from the annihilation reactions: $\bar{p} + p \leftrightarrow e^+ + e^-$ through the measurement of a precise angular distribution. However, the kinematical variables scan a different region, called the time-like (TL) region, because the momentum transfer squared is positive here (i.e, the time component of the four momentum transfer squared, $q^2$, is larger than the space component). The region accessible through the scattering channel is therefore denoted as space-like (SL) region.

FFs are assumed to be analytical functions of $q^2$.[6] In the general case, reaction amplitudes are complex functions of the relevant kinematical variables. Analyticity and unitarity constrain FFs to be real in SL region, and complex in TL region. Up to now, no individual determination of FFs has been done in TL region, due to the low statistics. FFs have been determined under the assumption $G_E = G_M$ or $G_E$=0.[7] Attempts of measuring the FF ratio were done by PS170[8] and BABAR[9] collaborations.

The possibility of better measurements has inspired experimental programs to measure hadron form factors at JLab, Frascati and at future machines, such as FAIR, both in SL and in TL regions. Electron beams in the GeV range are available at MAMI and JLab, with high intensity and high polarization, large acceptance spectrometers, hadron polarized targets, and hadron polarimeters. In colliding mode, the VEPP2 facility at Novosibirsk and the BES facility at BEPC provide $4\pi$ detection with high luminosity $e^+e^-$ collisions. High intensity hadron and particularly antiproton beams will be available at PANDA (FAIR) in near future.

From a theoretical point of view, the new results obtained with the polarization method have stimulated a revision of the nucleon models. The interpretation of FFs as the Fourier transforms of charge and magnetization densities is exact only in non relativistic approximation or in the Breit frame, where the four components of the momentum can be reduced to three. Recent model dependent pictures of the proton structure have been derived. In particular, form factors are specific integrals of generalized parton distributions, and they constitute, in this respect, an experimental constraint for theses functions. Different classes of models have been developed in the non perturbative region: soliton models, constituent quarks, di-quark models, vector meson dominance, dispersion relations ... (for a review, see[5]). However, not all of them are able to describe the existing data on the four nucleon FFs (electric, magnetic, neutron and proton) and not all of them contain the necessary analytical properties to describe both the SL and TL regions.[10]

## 2. History

In 1961 R. Hofstadter got the Nobel prize, "for his pioneering studies of electron scattering in atomic nuclei and for his thereby achieved discoveries concerning the structure of the nucleons". In his Nobel lecture one can read *"Over a period of time lasting at least two thousand years, Man has puzzled over and sought an understanding of the composition of matter. It is no wonder that his interest has been aroused in this deep question because all objects he experiences, including, even his own body, are in a most basic sense special configurations of matter. The history of physics shows that whenever experimental techniques advance to an extent that matter, as then known, can be analyzed by reliable and proved methods into its "elemental" parts, newer and more powerful studies subsequently show that the "elementary particles" have a structure themselves. Indeed this structure may be quite complex, so that the elegant idea of elementarity must be abandoned."*

The first experimental evidence for a composite structure of the proton, arising from charge and magnetization currents, dynamically changing with the distance (probed by the virtual photon in $ep$ elastic scattering), was given in a series of experiments at the Stanford accelerator SLAC, based on the Rosenbluth separation.[11]

In this chapter we recall the milestones of our present knowledge on FFs.

- Rutherford scattering

- 1909: Experiments of Geiger and Marsden. The cross section for the scattering of electrons in the Coulomb field of a nucleus of charge $Z$, is given by the Rutherford formula (1911).[12] It applies to non relativistic, spin zero, pointlike particle scattering. It was used to measure the 'size' of the target and to introduce the concept of atomic nucleus*.
- 1968: DIS "deep inelastic scattering" experiments in which very energetic electrons were scattered off protons showed that all the mass and charge of the proton is concentrated in smaller components, then called "partons". Partons were later identified with quarks (Friedman, Kendall and Taylor, Nobel Prize 1991).
- 1967: First order extension of the Rutherford formula, valid at high energy.[13]
- 1975-79: Extension to higher orders (eikonal approximation).[14,15]
- >1980: Extension to heavy ions/ polarization observables.[16,17]

- Beyond the Rutherford formula
  - 1929: N.F. Mott derives a formula for relativistic nuclei, that holds for scattering of spin 1/2 pointlike particles.[18]
  - 1950: M.N. Rosenbluth extends the formalism to composite targets.[4]
  - 1961: R. Hofstadter receives the Nobel Prize, for experiments at SLAC, on unpolarized $ep$ scattering, at fixed $Q^2$, doing the first experimental determination of $G_E$ and $G_M$.[11]
  - 1958-1967: Polarization in ep scattering (Kharkov school,[19] and[20]). A.I Akhiezer and M.P. Rekalo give the explicit derivation of polarization observables for elastic $ep$ scattering in terms of form factors.[1,2]
  - later, after 1997: Polarization experiment at MIT, JLab[21] and Refs. therein.
    - *better precision* (large sensitivity to the small $G_E$ contribution)
    - *determination of the sign of FFs*.

- Time-like region
  - 1962: Cross section and single polarization in terms of FFs in the annihilation process $p+\bar{p} \to e^+ + e^-$ (A. Zichichi, S. M. Berman, N. Cabibbo, R Gatto[22]).
  - 1983-1994: First TL measurements with antiprotons at LEAR(CERN): PS170.[8]
  - 1998: First TL measurements at FENICE (Frascati), with $e^+e^-$ collisions for proton and neutron FFs.[23]
  - 1997-2003: E760,[24] E835[7] with antiprotons at FermiLab.
  - 2002: Threshold measurements at BES.[25]
  - 2005: ISR in BABAR $e^+e^-$ colliders.[9]
  - after 2010: Experiments at BESIII.

- Reaction mechanism
  - 1970-73: Experimental and theoretical studies of two photon exchange.[26–30]
  - 1999-2006: Model independent properties of unpolarized and polarized scattering[31,32] and annihilation[33] in presence of two photon exchange.
  - 2006-today: Model calculations including proton structure[34] and revision of nucleon models.

- Radiative corrections:

---

*Different sites have been built to play with.
For example, see http://waowen.screaming.net/revision/nuclear/rssim.htm

– 1949: J.S. Schwinger calculates photon emission in pure QED scattering[35]
– 1969: L.W. Mo and Y.S. Tsai calculate at first order the radiative corrections for electron hadron scattering.[36]
– 1985: E.A. Kuraev and V.S. Fadin include higher orders using the electron structure function method, and apply those to elastic and deep inelastic scattering.[37]
– 2000: L.C. Maximon and J.A. Tjon revise the work of Ref.[36] on $ep$ scattering including (partly) the structure of the proton.[38]
– $>$ 2000: Radiative corrections to polarization phenomena in $ep$ elastic scattering.[39–41]

## 3. Basic concepts

As a first exercise, we consider here the elastic scattering of *structureless* particles,

$$a(p_a) + b(p_b) \to c(p_c) + d(p_d), \tag{1}$$

(the four momenta are indicated in parenthesis) which interact through the Coulomb potential $H_1 = U(\vec{r})$. The Coulomb potential between the target and the projectile $U(r)$ is spherically symmetric, directly proportional to the charges and inversely to the distance:

$$U(r) = \frac{Z_a Z_b e^2}{r}. \tag{2}$$

In order to take into account the screening effects of the electrons surrounding the atomic nucleus (and also to avoid divergences), a damping function is added and the Coulomb potential is usually as:

$$U(r) = \frac{Z_a Z_b e^2}{r} e^{-r/\lambda}, \tag{3}$$

where $\lambda \sim 10^{-8}$ cm $\sim 10^5$ fm is of the order of the dimensions of the atom.

### 3.1. *Reminder on perturbation theory*

The elements of the scattering matrix, $S_{fi}$ are the probability amplitudes for the reaction $i \to f$. The initial state of the system, $|i>$, after an interaction can be written as a superposition of possible final free particle states $|f>$:

$$|\Psi_i>= \sum_f |f>< f|S|i>= \sum_f |f> S_{fi} \tag{4}$$

where $|S_{fi}|^2$ is the probability of the transition $i \to f$. $S \equiv U(-\infty, \infty)$, $U(t, t_0)$ is the time evolution operator.

The scattering amplitude $T$ is defined as:

$$S_{fi} = \delta_{fi} + i(2\pi)^4 \delta^4(p_f - p_i) T_{fi}, \tag{5}$$

where $\delta_{fi}$ is the Kronecker symbol, which gives the superposition $< f|i >$ in the absence of interaction. The Dirac function

$$\delta^4(p_f - p_i) = \delta^3(\vec{p}_f - \vec{p}_i)\delta(E_f - E_i), \tag{6}$$

insures that each component of the four vector energy-momentum has to be conserved.

In a scattering process, the matrix element can be expressed using the perturbation theory. The Hamiltonian which describes the evolution of the system can be decomposed as:

$$H = H_0 + H_1, \tag{7}$$

where $H_0$ is the free particle Hamiltonian and $H_1$ is the interaction Hamiltonian. The time evolution is given in the Heisenberg representation by

$$H_I'(t) = e^{iH_0(t-t_0)}H'e^{-iH_0(t-t_0)}. \tag{8}$$

Assuming that $H'(t)$ can be treated as a perturbation, it is convenient to develop the $S$ matrix in a series of terms which contain the product of operators $H_I'$:

$$S = U(-\infty, \infty) = \sum_{n=1}^{\infty} S^n = 1 + \sum_{n=1}^{\infty} \frac{(-i)^n}{n!} \int_{\infty}^{\infty} dt_n..dt_1 T[H_I'(t_n)...[H_I'(t_1)] \tag{9}$$

where $T$ is the time ordering operator, particularly important when $H_I'(t)$ and $H_I'(t')$ do not commute.

The first terms of the development (9) are:

$$\begin{aligned} S^1 &= -i\int_{\infty}^{\infty} H_I'(t_1)dt_1, \\ S^2 &= -\frac{1}{2}\int_{\infty}^{\infty} dt_1 \int_{\infty}^{\infty} dt_2 T\left[H_I'(t_2)H_I'(t_1)\right]. \end{aligned} \tag{10}$$

There is of course a one to one correspondence with the matrix $T$: a corresponding term of the same order and corresponding elements $T_{fi} = \sum_{n=0}^{\infty} T_{fi}^n$. **The Born approximation consists in keeping only the term** $n = 1$. For our interest here, it is applied to processes which involve electromagnetic and weak interactions.

### 3.2. *Derivation of the Rutherford formula: analogy with optics*

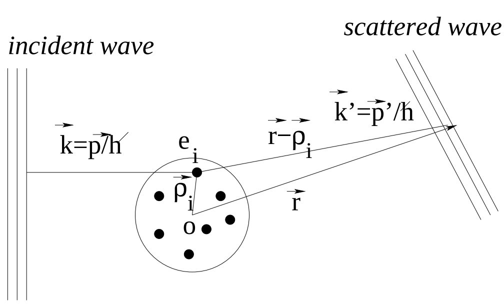


Fig. 1. Schematic view of elastic scattering on a composite object.

In quantum mechanics, the particle-wave duality requires that a particle of three momentum $\vec{p}$ is associated to a plane wave vector $\vec{k} = \vec{p}/\hbar$. If a plane wave scatters off a charge $e_i$ at a position $\rho_i$, it generates a spherical wave, that can be observed at large distances as a plane wave $\vec{k}' = \vec{p}\,'/\hbar$. The amplitude of the scattered wave in the point defined by $\vec{r}$ is:

$$A_i = fe_ie^{i\vec{k}\cdot\vec{\rho}_i}e^{i\vec{k}'\cdot(\vec{r}-\vec{\rho}_i)} = fe^{i\vec{k}'\cdot\vec{r}}e_ie^{iq\cdot\vec{\rho}_i} \tag{11}$$

where $f$ is the amplitude on the unit charge, $f = Z_ae$, which is the same for all constituent particles, $\vec{r} - \vec{\rho}_i$ is the vector from the observation point to the charge $i$, and $\vec{q} = \vec{p}_i - \vec{p}_f$ is the momentum transfer. The factor $e^{i\vec{k}\cdot\vec{\rho}_i}$ defines the phase of the incident plane wave at the interaction point, and $e^{i\vec{k}'\cdot(\vec{r}-\vec{\rho}_i)}$ determines the phase of the scattered wave at the observation point. Similarly to optics, the total scattered amplitude on the nucleus can be taken as the sum of the amplitudes on the individual charges:

$$A = \sum_i A_i = f e^{i\vec{k}'\cdot\vec{r}} \sum_i e_i e^{iq\cdot\vec{\rho}_i}. \tag{12}$$

However, in quantum mechanics, $\vec{\rho}_i$ represent the position operators of the internal motion in the target. Therefore the last term should be replaced by the corresponding mean value in the ground state of the target. We define the form factor:

$$F(\vec{q}) = \frac{1}{Z_b e} < i| \sum_i e_i e^{i\vec{q}\cdot\vec{\rho}_i} |i >, \tag{13}$$

and then the cross section on an extended nucleus becomes

$$\left(\frac{d\sigma}{d\Omega}\right) = \left(\frac{d\sigma}{d\Omega}\right)_{pl} |F(\vec{q})|^2, \tag{14}$$

where we identified the cross section on a pointlike particle as:

$$\left(\frac{d\sigma}{d\Omega}\right)_{pl} = (Z_b e)^2 |f|^2 \propto (Z_a Z_b e^2)^2. \tag{15}$$

The detailed and rigorous derivation of charge and magnetic FFs in a relativistic formalism is given in Section 4.

### 3.3. *The charge form factor*

Form factors are fundamental quantities, as they allow a direct comparison between the theory and the experiment. In order to determine $|F(\vec{q})|^2$ one has to measure the differential cross section, for different values of $q$. This can be done by varying the scattering angle and the energy of the projectile. If one wants to deduce the mean value of the charge density, in principle one can invert Eq. (13):

$$\rho(\vec{x}) =< \Psi_i|\hat{\rho}(\vec{x})|\Psi_i >= \frac{Z_b e}{(2\pi)^3} \int d^3q F(\vec{q}) e^{-i\vec{q}\cdot\vec{x}}. \tag{16}$$

However, in practice, $F(\vec{q})$ can not be determined for all values of $\vec{q}$, due to the limits of the kinematically accessible region. Moreover, at large $q$, cross sections are very small and difficult to measure. Furthermore, the cross section is sensitive to the FF modulus squared, and does not give access to the phase. Therefore, in general, one assumes a specific mathematical function for $\rho(\vec{x})$, and free parameters that are fitted to the experimental data.

For small values of $q^2$ one can develop $F(q^2)$ in a Taylor series expansion on $\vec{q}\cdot\vec{x}$:

$$\begin{aligned}
F(\vec{q}) &= \frac{1}{Z_b e} \int d^3\vec{x} e^{i\vec{q}\cdot\vec{x}} \rho(\vec{x}) \\
&= \frac{1}{Z_b e} \int d^3\vec{x} \left[1 + i\vec{q}\cdot\vec{x} - \frac{1}{2}(\vec{q}\cdot\vec{x})^2 + ...\right] \rho(\vec{x}) \\
&\simeq \frac{1}{Z_b e} \int_0^\infty x^2 dx \int_0^{2\pi} d\varphi \\
&\quad \int_{-1}^1 d\cos\theta \left[1 + iqx\cos\theta - \frac{1}{2} q^2 x^2 \cos^2\theta\right] \rho(\vec{x}).
\end{aligned}$$

The normalization is $\int_\Omega d^3\vec{x}\rho(\vec{x}) = Z_b e$. The second term does not give any contribution, as $\vec{q}\cdot\vec{x} = qx\cos\theta$ and $\int_{-1}^{1}\cos\theta d\cos\theta = 0$. This is a general fact, as $x$ is a odd quantity, whereas $\rho(\vec{x})$, which contains the square of the wave function, is an even quantity with respect to space parity.

In case of spherical symmetry,

$$F(q) \sim 1 - \frac{1}{6}q^2 < r_c^2 > +O(q^2), \tag{17}$$

where we define the mean square root charge radius of the target, $< r_c^2 >$, as

$$< r_c^2 >= \frac{\int_0^\infty x^4\rho(x)dx}{\int_0^\infty x^2\rho(x)dx}.$$

3.3.1. *Application to different charge distributions*

Let us calculate $F(q)$ normalized to the full volume and charge:

$$F(q) = \frac{\int_\Omega d^3\vec{x}e^{i\vec{q}\cdot\vec{x}}\rho(\vec{x})}{\displaystyle\int_\Omega d^3\vec{x}\rho(\vec{x})}.$$

In case of spherical symmetry the denominator is:

$$D = 4\pi\int_0^\infty x^2\rho(x)dx$$

and the numerator:

$$N(q) = 2\pi\int_0^\infty x^2\rho(x)dx\int_{-1}^{1} d\cos\theta e^{iqx\cos\theta} = 2\pi\int_0^\infty x^2\rho(x)dx\frac{e^{iqx} - e^{-iqx}}{iqx}$$

Therefore:

$$F(q) = \frac{4\pi\int \dfrac{x}{q}\sin(qx)\rho(x)dx}{4\pi\int_0^\infty x^2\rho(x)dx}. \tag{18}$$

The typical shapes of charge density, with spherical symmetry, and the corresponding form factors and radii are shown in Table 1.

As an example, let us calculate the radius corresponding to an exponential charge density, $\rho(x) = e^{-ax}$. First, we recall the following integrals:

$$\Gamma(\frac{1}{2}) = \int_0^\infty dze^{-z}z^{-1/2} = \sqrt{\pi}, \tag{19}$$

$$\Gamma(x) = \int_0^\infty dze^{-z}z^{x-1},\ \Gamma(x+1) = x\Gamma(x), \tag{20}$$

$$n! = \int_0^\infty dxx^n e^{-x}dx. \tag{21}$$

The radius is given by:

$$< r_c^2 >= \frac{\int_0^\infty x^4e^{-ax}dx}{\int_0^\infty x^2e^{-ax}dx} = \frac{a^{-5}\int_0^\infty(ax)^4e^{-ax}d(ax)}{a^{-3}\int_0^\infty(ax)e^{-ax}d(ax)}$$

| density $\rho(r)$ | Form factor $F(q^2)$ | r.m.s. $< r_c^2 >$ | comments |
|---|---|---|---|
| $\delta$ | 1 | 0 | pointlike |
| $e^{-ar}$ | $\frac{a^4}{(q^2+a^2)^2}$ | $\frac{12}{a^2}$ | dipole |
| $\frac{e^{-ar}}{r}$ | $\frac{a^2}{q^2+a^2}$ | $\frac{6}{a^2}$ | monopole |
| $\frac{e^{-ar^2}}{r^2}$ | $e^{-q^2/(4a^2)}$ | $\frac{1}{2a}$ | gaussian |
| $\rho_0$ for $x \le R$<br>0 for $r \ge R$ | $\frac{3(\sin X - X\cos X)}{X^3}$<br>$X = qR$ | $\frac{3}{5}R^2$ | square well |

and the form factor:

$$F(q) = \frac{\frac{1}{q}\int_0^\infty x\sin(qx)e^{-ax}dx}{\int_0^\infty x^2 e^{-ax}dx}. \tag{22}$$

Applying (21), the denominator in Eq. (22) is:

$$D = \int_0^\infty x^2 e^{-ax}dx = \frac{2}{a^3}.$$

The numerator:

$$\begin{aligned} N &= \frac{1}{2iq}\int_0^\infty x(e^{iqx} - e^{-iqx})e^{-ax}dx \\ &= \frac{1}{2iq}\int_0^\infty x\left[e^{-(-iq+a)x} - e^{-(iq+a)x}\right]dx \\ &= \frac{1}{2iq}\left[\frac{1}{(a-iq)^2}\int_0^\infty ye^{-y}dy - \frac{1}{(a+iq)^2}\int_0^\infty ye^{-y}dy\right]. \end{aligned}$$

Integrating per parts:

$$\Gamma(2) = \int ye^{-y}dy = -\int yd(e^{-y}) = -ye^{-y} + \int e^{-y}dy = -ye^{-y} - e^{-y}|_0^\infty = +1.$$

one finds:

$$N = \frac{1}{2iq}\left[\frac{1}{(a-iq)^2} - \frac{1}{(a+iq)^2}\right] = \frac{4aiq}{2iq(a^2+q^2)^2} = \frac{2a}{(a^2+q^2)^2}.$$

Finally:

$$F(q) = \frac{a^4}{(a^2+q^2)^2}.$$

Similarly one can verify all the results of Table 1.

### 3.3.2. *Units and orders of magnitudes*

The amplitude of the scattered wave is the sum of the amplitudes of the waves scattered from the individual constituents. An observer far from the target can see that the intensity of the scattered wave shows minima and maxima, as a function of the scattered angle, which correspond to interference among the different amplitudes $A_i$ of the scattered waves. As in optics, one can introduce a resolving power $\delta$:

$$\delta[fm] = \frac{\hbar}{|\vec{q}|} \sim \frac{200}{c|\vec{q}|}, \tag{23}$$

The quantity $\delta$ defines the spatial region that can be accessed in an experiment where the transferred momentum is $|\vec{q}|$. For example $|\vec{q}|$= 1 GeV (in center of mass system) in $ep$ scattering corresponds to $\delta$ = 0.2 fm.

Let us compare $\hbar c$ to the Bohr radius: $\lambda \sim 10^5$[fm]:

$$\frac{\hbar c}{\lambda} \simeq \frac{200[\text{Mev}]\ [\text{fm}]}{10^5[\text{fm}]} \simeq 2 \cdot 10^{-3}\text{MeV}. \tag{24}$$

## 3.4. *Extensions of the Rutherford Formula*

Let us summarize the assumptions under which the Rutherford formula holds:

- $U(r) = Z_1Z_2e^2/r$: coulomb interaction between target and projectile;
- validity of the Born approximation (lowest order/one photon exchange);
- non relativistic approximation;
- structureless and spinless particles.

The non relativistic approach is justified if the momenta of the particles are smaller than their masses ($p/m\Lambda\overline{\Lambda}1$). The differential cross section for spinless and pointlike+-*****- particles, in the relativistic case and in the Born approximation, was derived by N. F. Mott, including recoil effects of the target nucleus of mass $M$:[18]

$$\left(\frac{d\sigma}{d\Omega}\right)^{Lab}_{Mott} = \frac{e^2}{4E^2}\frac{\cos^2(\theta/2)}{\sin^4(\theta/2)}\frac{1}{1+\dfrac{2E}{M}\sin^2(\theta/2)}. \tag{25}$$

In the language of Feynman diagrams, it is easy to verify the main features of the Mott cross section. The transition amplitude is proportional to $Z_ie$, the vertices contribution, which does not depend on the particle momenta for pointlike particles, and to the photon propagator $1/q^2$:

$$T_{fi} \propto \frac{Z_1Z_2e^2}{|\vec{q}|^2}, \quad \left(\frac{d\sigma}{d\Omega}\right)^{Lab}_{Mott} \propto T^2_{fi}. \tag{26}$$

Further developments were given several years later. The extension of the Rutherford formula at the next order $\sim (Z\alpha)^3$[13] showed that the scattering of electrons and positrons is no more equivalent, because the correction depends on the charge:

$$\frac{d\sigma^{\pm}}{d\Omega} = \frac{d\sigma_R}{d\Omega}\left[1 \pm \pi\alpha Z\sin(\theta/2)\right], \quad \frac{d\sigma_R}{dd\Omega} = \frac{(Z\alpha)^2}{4E^2\sin^4(\theta/2)}, \tag{27}$$

which leads to a charge asymmetry. Higher order corrections $\sim (Z\alpha)^n$ have been calculated more recently in the eikonal approximation[14,15,17] for charge asymmetry and polarization phenomena. A non trivial universal angular dependence is predicted, whose sign depends on the charge, observable in electron and positron scattering. The Rutherford cross section results modified by a factor:

$$\left(\frac{d\sigma}{d\Omega}\right)^{\pm} \sim \left(\frac{d\sigma}{d\Omega}\right)_R [1 \pm \pi x \sin(\theta/2)\cos\varphi(x)]\,,\ x = \frac{Z\alpha}{\beta}, \tag{28}$$

with

$$\Phi(x) = \cos\varphi(x) + i\sin\varphi(x) = \frac{\Gamma(\frac{1}{2}+ix)\Gamma(1-ix)}{\Gamma(\frac{1}{2}-ix)\Gamma(1+ix)}, \tag{29}$$

where $\beta$ is the velocity $v$ of the initial particle of mass $m$, in the Laboratory system, in units of $c$: $\beta = v/c = \sqrt{1-(4m^2)/E^2}$. Using the properties of Euler gamma function one obtains:

$$\varphi(x) = -4\sum_{n=0}^{\infty}(-1)^n \frac{x^{2n+1}}{2n+1}c_n,$$
$$c_0 = \ln 2;\ c_1 = 3\xi_3;\ c_2 = 15\xi_5, ...,\ c_n = (2^{2n}-1)\xi_{2n+1},\ n \geq 1. \tag{30}$$

Applying the Stirling formula one can write

$$\cos(\varphi(x))|_{x>>1} \sim \frac{1}{4x}. \tag{31}$$

One can apply this formalism to the strong interaction, through the replacement $x = Z\alpha \to x_c = N\alpha_s$, proton and antiproton peripheral collisions on heavy nuclei may show a measurable multiphoton effect.

Further developments of the Rutherford formula include also high energy scattering on heavy targets (also in the eikonal approximation).[16]

### 3.5. *Cross section for a binary process*

The cross section $\sigma$ for a binary process

$$a(p_1) + b(p_2) \to c(p_3) + d(p_4), \tag{32}$$

(where the momenta of the particles are indicated in parenthesis) characterizes the probability that a given process occurs. The number of events issued from a definite reaction is proportional to the number of incident particles $N_B$, the number of the target particles $N_T$ and the constant of proportionality is the cross section:

$$N_F = \sigma N_a \times N_b. \tag{33}$$

The cross section can be viewed as an "effective area" over which the incident particle reacts. Therefore, its dimension is cm$^2$, but more often barn (1 barn=$10^{-28}$ m$^2$), or fm$^2$ (1 fm=$10^{-15}$ m) are used.

A useful quantity is the luminosity $\mathcal{L}$, defined as $\mathcal{L} = N_B$ [s$^{-1}$] $N_T$ [cm$^{-2}$]. For simple counting estimations, $N_f = \sigma\mathcal{L}$. This is an operative definition, which is used in experimental physics.

On the other hand $\sigma$ needs to be calculated theoretically for every type of process. The present derivation is done in a relativistic approach. This means that :

- The kinematics is relativistic,
- The matrix element $\mathcal{M}$, which contains the dynamics of the reaction is a relativistic invariant. In general it is function of kinematical variables, also relativistic $\mathcal{M} = f(s,t,u)$,
- $\sigma$ has to be written in a relativistic invariant form.

The starting point is the following expression for the cross section

$$d\sigma = \frac{|\mathcal{M}|^2}{\mathcal{I}}(2\pi)^4\delta^{(4)}(p_1 + p_2 - p_3 - p_4)d\mathcal{P}, \tag{34}$$

which is composed of four terms:

(1) The matrix element $\mathcal{M}$, which contains the dynamics of the reaction, and it is calculated following a model,
(2) The flux of colliding particles $\mathcal{I}$,
(3) The phase space for the final particles, $d\mathcal{P}$,
(4) A term which insures the conservation of the four-momentum $\delta^{(4)}(p_1 + p_2 - p_3 - p_4)$ which is the product of four $\delta$ functions, because each component has to be conserved separately.

Let us calculate in detail each term.

### 3.5.1. *Definition of flux $\mathcal{I}$*

The flux is defined through the relative velocity of incoming and target particles:

$$\mathcal{I} = n_B n_T v_{rel}, \tag{35a}$$

$$\mathcal{I} = 4\sqrt{(p_1 \cdot p_2)^2 - M_1^2 M_2^2}, \tag{35b}$$

where $M_1(M_2)$ is the mass of the beam (target) particle, $v_{rel}$ is the relative velocity between beam and target particles and the densities of the beam and target particles $n_B, n_T$ are proportional to their energies as $n_i = 2E_i$.

Let us prove that the two expressions (35a) and (35b) are equivalent. It is more convenient to calculate $\mathcal{I}$ (Eq. 35 ) in the laboratory frame where the target is at rest:

$$p_1 = (E_1, \vec{p}_1), \quad p_2 = (M_2, 0), \quad |\vec{v}_{rel}| = |\vec{v}_1 - \vec{v}_2| = \frac{|\vec{p}_1|}{E_1} \ \Rightarrow \ n_B = 2E_1, \ n_T = 2M_2. \tag{36}$$

Replacing the equalities (36) in Eq. (35a):

$$\mathcal{I} = 2E_1 2M_2 \frac{|\vec{p}_1|}{E_1} = 4M_2|\vec{p}_1|$$

and in Eq. (35b) :

$$(p_1 \cdot p_2)^2 - M_1^2 M_2^2 = M_2^2 E_1^2 - M_1^2 M_2^2 = M_2^2(E_1^2 - M_1^2) = M_2^2|\boldsymbol{p}_1|^2, \text{ thus } \mathcal{I} = 4M_2|\vec{p}_1|$$

and the equalities (35) are proved. Moreover, we prove also that the flux does not depend on the reference frame, because it can be written in a Lorentz invariant form.

Let us consider the center of mass system (CMS):

$$p_1 = (E_1, \vec{k}), \ p_2 = (E_2, -\vec{k}), \ p_1 \cdot p_2 = E_1 E_2 + |\vec{k}|^2, \ M_1^2 = E_1^2 - |\vec{k}|^2, \ M_2^2 = E_2^2 - |\vec{k}|^2$$

and

$$\begin{aligned}(p_1 \cdot p_2)^2 - M_1^2 M_2^2 &= E_1^2 E_2^2 + 2E_1 E_2|\vec{k}|^2 + |\vec{k}|^4 - E_1^2 E_2^2 + |\vec{k}|^2(E_1^2 + E_2^2) - |\vec{k}|^4 \\ &= |\vec{k}|^2(E_1 + E_2)^2 = |\vec{k}|^2 W^2.\end{aligned} \tag{37}$$

The flux, $\mathcal{I}$, can be written as

$$\mathcal{I} = 4|\vec{k}|W, \tag{38}$$

where $W = E_1 + E_2$ is the initial energy of the system in CMS.

### 3.5.2. *Phase space*

The phase space for a particle of energy $E$, mass $M$ and four–momentum $p$ (the number of states in the unit volume) can be written according to quantum mechanics in an invariant form:

$$d\mathcal{P} = \int \frac{d^4 p\, \delta(p^2 - M^2)}{(2\pi)^3} \Theta(E),$$

where the $\delta$ function insures that the particle is on mass shell and the step function $\Theta(E)$ insures that only the solution with positive energy is taken into account. Note that the wave functions of all particles entering in the matrix element must be normalized to one particle per unit volume. In this case all these wave functions contain the factor $1/\sqrt{2\varepsilon}$, where $\varepsilon$ is the particle energy. Usually these factors are explicitly taken into account in the expression for the cross section, we insert them into the phase space.

Extracting the term which depends on energy:

$$d^4 p\, \delta(p^2 - M^2) = \delta^3 \vec{p} dE \delta(E^2 - \vec{p}^2 - M^2),$$

and using the property of the $\delta$ function

$$\int \delta[f(x)]dx = \sum \frac{1}{|f'(x_i)|}, \tag{39}$$

($x_i$ are the roots of $f(x)$), with $f(E) = E^2 - \vec{p}^2 - M^2$, and $f'(E) = 2E$ one finds:

$$\int dE \delta(E^2 - \vec{p}^2 - M^2)\Theta(E) = \frac{1}{2E}.$$

For the reaction under consideration:

$$d\mathcal{P} = \frac{d^3 \vec{p}_3}{(2\pi)^3 2E_3} \frac{d^3 \vec{p}_4}{(2\pi)^3 2E_4}.$$

### 3.5.3. *Final formulas*

The total cross section can be written as:

$$\sigma = \frac{(2\pi)^4}{\mathcal{I}} \int |\mathcal{M}|^2 \delta^{(4)}(p_1 + p_2 - p_3 - p_4) \frac{d^3 \vec{p}_3}{(2\pi)^3 2E_3} \frac{d^3 \vec{p}_4}{(2\pi)^3 2E_4}. \tag{40}$$

One can see that it corresponds to a six-fold differential, but four $\delta$ functions are equivalent to four integrations. So finally, for a $2 \to 2$ process one is left with two independent variables, $(E, \theta)$ or $(s, t)$. For three particles, one has nine differentials, four integrations, *i.e.*, five independent variables.

The term $\delta^{(4)}(p_1 + p_2 - p_3 - p_4)$ can be split into an energy and a space part: $\delta^{(4)}(p_1 + p_2 - p_3 - p_4) = \delta(E_1 + E_2 - E_3 - E_4)\delta^{(3)}(\vec{p}_1 + \vec{p}_2 - \vec{p}_3 - \vec{p}_4)$.

Note that

$$\int \delta^{(3)}(\vec{p}_1 + \vec{p}_2 - \vec{p}_3 - \vec{p}_4) d^3 \vec{p}_4 = 1 \tag{41}$$

in any reference frame.

Let us use spherical coordinates in CMS ($p_3 = (E_3, \vec{p})$, $p_4 = (E_4, -\vec{p})$, $d^3 \vec{p} = |\vec{p}|^2 d\Omega dp$)and consider the quantity $\mathcal{J}$:

$$\mathcal{J} = \delta(E_1 + E_2 - E_3 - E_4) \frac{d^3 \vec{p}_3}{4E_3 E_4} = \delta(W - E_3 - E_4) \frac{|\vec{p}|^2 d\Omega dp}{4E_3 E_4}, \tag{42}$$

where

$$E_3^2 = M_3^2 + |\vec{p}|^2,\ E_4^2 = M_4^2 + |\vec{p}|^2 \to E_3 dE_3 = E_4 dE_4 = |\vec{p}| dp.$$

After integration, using the property (39):

$$\mathcal{J} = \int \delta(W - E_3 - E_4) \frac{dE_3 |\vec{p}| d\Omega}{4E_4} = \frac{|\vec{p}| d\Omega}{4E_4} \frac{1}{\left| \frac{d}{dE_3} (W - E_3 - E_4) \right|}, \tag{43}$$

where

$$\frac{d}{dE_3}(W - E_3 - E_4) = -1 - \frac{dE_4}{dE_3} = -1 - \frac{E_3}{E_4} = -\frac{W}{E_4} \tag{44}$$

and therefore

$$\mathcal{J} = \frac{|\vec{p}| d\Omega}{4W}. \tag{45}$$

Substituting Eqs. (38, 45) in Eq. (40) we find the general expression for the differential cross section of a binary process, in CMS:

$$\frac{d\sigma}{d\Omega} = \frac{\bar{|\mathcal{M}|^2} |\vec{p}|}{64\pi^2 W^2 |\vec{k}|}, \tag{46}$$

and for the total cross section:

$$\sigma = \int \frac{|\mathcal{M}|^2 |\vec{p}|}{64\pi^2 W^2 |\vec{k}|} d\Omega. \tag{47}$$

In case of elastic scattering, $|\vec{k}| = |\vec{p}|$, therefore:

$$\frac{d\sigma^{el}}{d\Omega} = \frac{|\mathcal{M}|^2}{64\pi^2 W^2} = |\mathcal{F}^{el}|^2,\ \mathcal{F}^{el} = \frac{|\mathcal{M}|}{8\pi W}, \tag{48}$$

where $\mathcal{F}^{el}$ is the elastic amplitude.

### 3.6. *Reminder on the Dirac formalism*

Spin 1/2 particles

The elastic $eN$ scattering involves four particles, with spin 1/2. The relativistic description of the spin properties of each of these particles is based on the Dirac equation:

$$(\hat{k} - m)u(k) = 0,\ \ \hat{k} = k_\mu \gamma_\mu = E\gamma_0 - \mathbf{k} \cdot \vec{\gamma},$$

where $k$ is the particle four momentum ($k = (E, \mathbf{k})$) and $u(k)$ is a four-component Dirac spinor. We shall use the following representation of the Dirac $4 \times 4$ matrices:

$$\gamma_0 = \begin{pmatrix} 1 & 0 \\ 0 & -1 \end{pmatrix},\ \vec{\gamma} = \begin{pmatrix} 0 & \vec{\sigma} \\ -\vec{\sigma} & 0 \end{pmatrix}, \tag{49}$$

where $\vec{\sigma}$ is the standard set of the Pauli $2 \times 2$ matrices. On the basis of the Dirac equation one can write:

$$u(k) = \sqrt{E + m} \begin{pmatrix} \chi \\ \frac{\vec{\sigma} \cdot \mathbf{k}}{E + m} \chi \end{pmatrix}, \tag{50}$$

where $\chi$ is a two-component spinor. We used here the relativistic invariant normalization for the four-component spinor: $u^\dagger u = 2E$.

Spin 1/2 antiparticles

An antiparticle is described by the following spinor

$$v(k) = \sqrt{E+m}\begin{pmatrix} \dfrac{\vec{\sigma}\cdot\mathbf{k}}{E+m}\chi \\ \chi \end{pmatrix}. \tag{51}$$

The Dirac equation for particles (nucleon with momentum $p_2$) and antiparticles (antinucleon with momentum $p_1$) is:

$$\overline{u}(p_2)(\hat{p}_2 - m) = 0 \Rightarrow \overline{u}(p_2)\hat{p}_2 = \overline{u}(p_2)m,$$
$$(\hat{p}_1 + m)u(-p_1) = 0 \Rightarrow \hat{p}_1 u(-p_1) = -u(-p_1)m.$$

The density matrices $\rho = u(p)\overline{u}(p)$ for polarized and unpolarized particles and antiparticles are given in the Table 2. Applying the Dirac equation to the four-component spinor $u(p)$, of an electron with mass $m_e$, one can find the expressions for the density matrix of polarized electrons $\rho_{\alpha\beta} = u_\alpha(p)u^\dagger_\beta(p)$ reported in Table 2, where $s_\alpha$ is the four vector of the electron spin.

| | particle | antiparticle |
|---|---|---|
| unpolarized | $\hat{p}+m$ | $\hat{p}-m$ |
| polarized | $(\hat{p}+m)\frac{1}{2}(1-\gamma_5\hat{s})$ | $(\hat{p}-m)\frac{1}{2}(1-\gamma_5\hat{s})$ |

### 3.6.1. *Useful properties of Dirac matrices*

Some useful properties of Dirac matrices :

- The anticommutator is: $\{\gamma_\mu, \gamma_\nu\} = 2g_{\mu\nu}$, where $g_{\mu\nu}$ is the metric tensor of the Minkowski space-time;
- $\hat{a}\hat{b} + \hat{b}\hat{a} = 2ab$, $\hat{a}\gamma_\mu + \gamma_\mu\hat{a} = 2a_\mu$, where $a$ and $b$ are four vectors;
- $Tr\ \gamma_\alpha\gamma_\beta = 4g_{\alpha\beta}$;
- $Tr\ \gamma_\alpha\gamma_\beta\gamma_\gamma = 0$;
- $Tr\ \gamma_\alpha\gamma_\beta\gamma_\gamma\gamma_\delta = 4\left(g_{\alpha\beta}\gamma_{\gamma\delta} + \gamma_{\beta\gamma}\gamma_{\delta\alpha} - \gamma_{\gamma\alpha}\gamma_{\delta\beta}\right)$.

### 3.6.2. *Relativistic formulation for the spin*

The four vector of the electron spin, $s_\alpha$, satisfies the following two conditions:

$$s\cdot p = 0,\quad s^2 = -1. \tag{52}$$

In terms of the three-vector $\vec{\chi}$ of the electron polarization at rest, i.e., with zero three-momentum, the four-vector $s$ can be written as:

$$s = \left(\frac{\vec{\chi}\cdot\mathbf{p}}{m_e}\right),\ \vec{\chi} + \frac{(\vec{\chi}\cdot\mathbf{p})\mathbf{p}}{m_e(\epsilon+m_e)}. \tag{53}$$

The condition $s^2 = -1$ corresponds to full electron polarization, so $s^2 = -|\vec{s}|^2 = -1$. Eq. (53) is simplified in case of relativistic electrons, $\epsilon \gg m_e$. In this case:

$$s_\alpha = \frac{\epsilon}{m}s_\ell(1, \mathbf{1}), \tag{54}$$

where **1** denotes the unit vector along **p** and $s_\ell = \vec{\chi} \cdot \mathbf{p}/|\mathbf{p}| \equiv \lambda$.

Taking into account that for relativistic electrons:

$$p_\alpha = \epsilon(1, \mathbf{1}), \tag{55}$$

it is possible to re-write Eq. (54) in the form:

$$s_\alpha = \frac{p_{1\alpha}}{m}\lambda. \tag{56}$$

One can find the following expression for the density matrix of a relativistic polarized electron:

$$\begin{aligned}
\rho &= \frac{1}{2}(\hat{p} + m_e)\left(1 - \gamma_5 \frac{\hat{p}}{m_e}\lambda\right) = \frac{1}{2}(\hat{p} + m_e) + \frac{\lambda}{2}(\hat{p} + m_e)\frac{\hat{p}}{m_e}\gamma_5 \\
&= \frac{1}{2}(\hat{p} + m_e) + \frac{\lambda}{2}\left(p^2 + m_e\hat{p}\right)\frac{1}{m_e}\gamma_5 \\
&= \frac{1}{2}(\hat{p} + m_e)(1 + \lambda\gamma_5) \equiv \frac{1}{2}\hat{p}(1 + \lambda\gamma_5),
\end{aligned} \tag{57}$$

where we used the following property of the $\gamma_5$-matrix: $\hat{p}\gamma_5 + \gamma_5\hat{p} = 0$, for any four-vector $p_\alpha$.

## 4. Relativistic formalism for ep elastic scattering

Let us derive step by step the elastic cross section and the polarization observables for electron proton scattering, in the Born approximation, in a fully relativistic formalism, taking into account that the proton has a spin and an internal structure. This derivation closely follows lecture notes earlier prepared with Prof. M. P. Rekalo.[42]

### 4.1. *Relativistic kinematics*

The Feynman diagram for elastic $eN$-scattering is shown in Fig. 2, assuming one-photon exchange. The notations of the particle four-momenta are also shown in the Fig. 2 and in Table 3 (we will use in our calculation the system where $\hbar$=c=1).

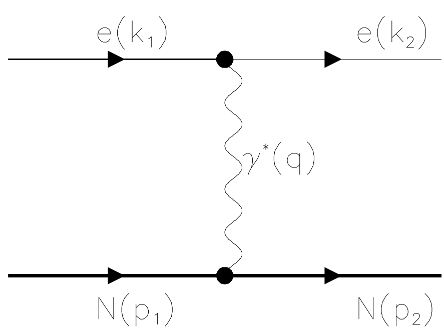


Fig. 2. One-photon exchange diagram for elastic scattering, $e + N \to e + N$.

The conservation of four-momenta at each vertex of the diagram can be written as:

$$q = k_1 - k_2 = p_2 - p_1, \tag{58}$$

which is valid in any reference frame. Using the relation (58) in the Lab-system, we derive the formula for the momentum transfer squared $q^2$, which is the basic kinematical variable for elastic $eN$ scattering:

$$q^2 = (p_2 - p_1)^2 = p_1^2 + p_2^2 - 2M_pE_2 = 2M_p^2 - 2M_pE_2 = -2M_pT,$$

where $E_2$ is the total energy of the final nucleon, $M_p$ is the nucleon mass, and $T = E_2 - M_p$ is the kinetic energy. This formula demonstrates that, for elastic scattering, the momentum transfer squared, $q^2$, is negative for all energies and scattering angles of the outgoing electron. As $q^2$ is a relativistic invariant, this is true in any reference system. The kinematical region for which $q^2 < 0$ is called the $Space-Like$ region.

| | Lab | CMS | Breit |
|---|---|---|---|
| $q$ | $(\omega, \mathbf{q})$ | $(\widetilde{\omega}, \widetilde{\mathbf{q}})$ | $(\omega_B = 0, \mathbf{q_B})$ |
| $k_1$ | $(\epsilon_1, \mathbf{k_1})$ | $(\widetilde{\epsilon_1}, \widetilde{\mathbf{k_1}})$ | $(\epsilon_{1B}, \mathbf{k_{1B}})$ |
| $p_1$ | $(M_p, 0)$ | $(\widetilde{E_1}, -\widetilde{\mathbf{k_1}})$ | $(E_{1B}, \mathbf{p_{1B}})$ |
| $k_2$ | $(\epsilon_2, \mathbf{k_2})$ | $(\widetilde{\epsilon_2}, \widetilde{\mathbf{k_2}})$ | $(\epsilon_{2B}, \mathbf{k_{2B}})$ |
| $p_2$ | $(E_2, \mathbf{p_2})$ | $(\widetilde{E_2}, -\widetilde{\mathbf{k_2}})$ | $(E_{2B}, -\mathbf{p_{1B}})$ |

### 4.1.1. *Proton kinematics in the Breit system*

The most convenient frame for the analysis of elastic $eN$-scattering is the Breit frame, which is defined as the system where the initial and final nucleon energies are the same. As a consequence, the energy of the virtual photon vanishes and its four-momentum squared, $q^2$, coincides with its three-momentum squared, $\mathbf{q_B}^2$, more exactly, $q^2 = -\mathbf{q_B}^2$. The derivation of the formalism in Breit system is therefore simpler and has some analogy with a non-relativistic description of the nucleon electromagnetic structure. From the energy conservation, and from the definition of the Breit system, one can find:

$$\omega_B = E_{1B} - E_{2B} = 0,$$

where all kinematical quantities in the Breit system are denoted with subscript $B$. The proton three-momentum can be found from the relation

$$E_{1B}^2 = E_{2B}^2 = \mathbf{p_{1B}}^2 + M_p^2 = \mathbf{p_{2B}}^2 + M_p^2, \; i.e., \; \mathbf{p_{1B}}^2 = \mathbf{p_{2B}}^2.$$

The physical solution of this quadratic relation is $\mathbf{p_{1B}} = -\mathbf{p_{2B}}$, as the Breit system moves in the direction of the outgoing proton. From the three-momentum conservation, in the Breit system $\mathbf{q_B} + \mathbf{p_{1B}} = \mathbf{p_{2B}}$, one can find:

$$\mathbf{p_{1B}} = -\frac{\mathbf{q_B}}{2}, \;\; \mathbf{p_{2B}} = \frac{\mathbf{q_B}}{2}.$$

The proton energy can be expressed as a function of $\mathbf{q_B}^2$, and therefore of $q^2$:

$$E_{1B}^2 = E_{2B}^2 = M_p^2 + \frac{\mathbf{q_B}^2}{4} = M_p^2 - \frac{q^2}{4} = M_p^2(1+\tau),$$

where we replaced the three-momentum in Breit system by the four-momentum and we introduced the dimensionless quantity $\tau = \dfrac{Q^2}{4M_p^2} = -\dfrac{q^2}{4M_p^2} \geq 0$.

### 4.1.2. *Electron kinematics in the Breit system*

The conservation of the four momentum, at the electron vertex, can be written, in any reference system, as: $k_1 = q + k_2$ (the virtual photon is radiated by the electron). In the Breit system, the energy and momentum conservation is:

$$\begin{cases} \epsilon_{1B} = \ \omega_B + \epsilon_{2B} = \epsilon_{2B}, \\ \mathbf{k_{1B}} = \mathbf{q_B} + \mathbf{k_{2B}}. \end{cases} \tag{59}$$

In order to proceed, we must define a reference (coordinate) system: we choose the $z$-axis parallel to the photon three-momentum in the Breit system: $z \parallel \mathbf{q_B}$, and the $xz$-plane as the scattering plane. So we can write:

$$\begin{cases} \epsilon_{1B}^2 = \epsilon_{2B}^2 = m_e^2 + (k_{1B}^x)^2 + (k_{1B}^z)^2 = m_e^2 + (k_{2B}^x)^2 + (k_{2B}^z)^2, \\ k_{1B}^x = k_{2B}^x, \\ k_{1B}^y = k_{2B}^y = 0, \\ k_{1B}^z = q_B + k_{2B}^z. \end{cases} \tag{60}$$

It follows $k_{1B}^z = -k_{2B}^z = \dfrac{q_B}{2}$ (the other possible solution $k_{1B}^z = k_{2B}^z$ would imply $q_B = 0$). A graphical representation for the conservation of three-momenta is given in Fig. 3.

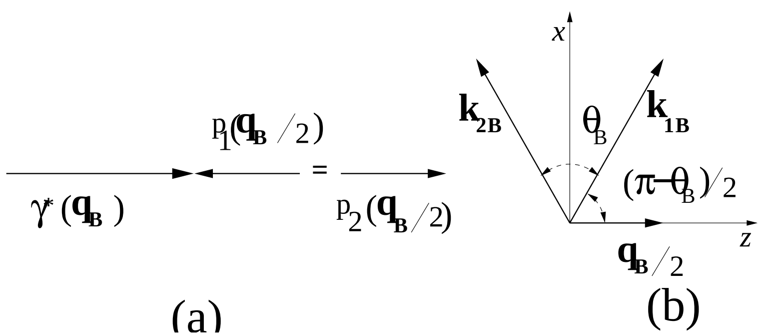


Fig. 3. Proton (a) and electron (b) three-momenta representation for elastic $eN$-scattering in the Breit system.

Then we can write, for the components of the initial and final electron three-momenta:

$$\mathbf{k_{1B}} = (k_{1B}^x, k_{1B}^y, k_{1B}^z) = \left(\frac{q_B}{2}\cot\frac{\theta_B}{2}, 0, \frac{q_B}{2}\right) = \frac{\sqrt{-q^2}}{2}\left(\cot\frac{\theta_B}{2}, 0, 1\right), \tag{61}$$

$$\mathbf{k_{2B}} = (k_{2B}^x, k_{2B}^y, k_{2B}^z) = \left(\frac{q_B}{2}\cot\frac{\theta_B}{2}, 0, -\frac{q_B}{2}\right) = \frac{\sqrt{-q^2}}{2}\left(\cot\frac{\theta_B}{2}, 0, -1\right). \tag{62}$$

The energy of the electron (neglecting the electron mass) is given by:

$$\epsilon_{1B}^2 = \mathbf{k_{1B}}^2 = (k_{1B}^x)^2 + (k_{1B}^z)^2 = \frac{-q^2}{4\sin^2\dfrac{\theta_B}{2}} \text{ and } \epsilon_{2B} = \epsilon_{1B}.$$

4.1.3. *Relation between the electron scattering angles in the Lab system, $\theta_e$ and in the Breit system, $\theta_B$*

As the Breit system is moving along the $z$-axis, the $x$ and $y$ components of the particle three-momenta do not change after transformation from the Lab to the Breit system:

$$\begin{cases} k^B_{1y} = k_{2y} = 0, \\ k^B_{1x} = k_{1x}. \end{cases} \tag{63}$$

From $\mathbf{k_1}^2 = k^2_{1x} + k^2_{1z}$ one can find:

$$k^2_{1x} = \mathbf{k_1}^2 - \frac{(\mathbf{k_1}\cdot\mathbf{q})^2}{\mathbf{q}^2} = \frac{\mathbf{k_1}^2\mathbf{q}^2 - (\mathbf{k_1}\cdot\mathbf{q})^2}{\mathbf{q}^2} = \frac{\epsilon_1^2\epsilon_2^2\sin^2\theta_e}{\mathbf{q}^2} = \frac{4\epsilon_1^2\epsilon_2^2}{\mathbf{q}^2}\sin^2\frac{\theta_e}{2}\cos^2\frac{\theta_e}{2}, \tag{64}$$

where we replaced $\mathbf{q} = \mathbf{k_1} - \mathbf{k_2}$, $\mathbf{k_1}^2 = \epsilon_1^2$, $\mathbf{k_2}^2 = \epsilon_2^2$ after setting $m_e = 0$. On the other hand we find for $q^2$ the following expression in the Lab system (in terms of the energies of the initial and final electron and of the electron scattering angle):

$$\begin{aligned} q^2 &= (k_1 - k_2)^2 = 2m_e^2 - 2k_1\cdot k_2 \overset{m_e=0}{\simeq} -2\epsilon_1\epsilon_2 + 2\mathbf{k_1}\cdot\mathbf{k_2} = -2\epsilon_1\epsilon_2(1-\cos\theta_e) \\ &= -4\epsilon_1\epsilon_2\sin^2\frac{\theta_e}{2}. \end{aligned} \tag{65}$$

Comparing Eqs. (64) and (65), we find:

$$k^2_{1x} = \frac{(q^2)^2}{4\mathbf{q}^2}\cot^2\frac{\theta_e}{2}.$$

Using the relations: $\mathbf{q}^2 = \omega^2 - q^2$ and $q^2 + 2q\cdot p_1 + p_1^2 = p_2^2$, we have, in the Lab system, $\omega = -\dfrac{q^2}{2m}$ and $\mathbf{q}^2 = -q^2(1+\tau)$. Finally:

$$k^2_{1x} = -\frac{q^2}{4(1+\tau)}\cot^2\frac{\theta_e}{2}.$$

So, from the relation $k^2_{1x} = (k^x_{1B})^2$, we find the following relation between the electron scattering angle in the Lab system and in the Breit system:

$$\boxed{\cot^2\frac{\theta_B}{2} = \frac{\cot^2\theta_e/2}{1+\tau}.} \tag{66}$$

4.1.4. *Expression of* $\sin\dfrac{\theta_B}{2}$ *in terms of energies in the Lab system*

Let us find the expression for $\sin\dfrac{\theta_B}{2}$ in terms of the kinematical variables in the Lab-system.

Using the relation (66), one finds:

$$\frac{1}{\sin^2\frac{\theta_B}{2}} = 1 + \frac{\cot^2\frac{\theta_e}{2}}{1+\tau} = \frac{1}{1+\tau}\left[\tau + \frac{1}{\sin^2\frac{\theta_e}{2}}\right] = \frac{1}{1+\tau}\frac{1+\tau\sin^2\frac{\theta_e}{2}}{\sin^2\frac{\theta_e}{2}} \tag{67}$$

So

$$1+\tau\sin^2\frac{\theta_e}{2} = 1 + \frac{\frac{\epsilon_1^2}{M_p^2}\sin^4\frac{\theta_e}{2}}{1+2\frac{\epsilon_1}{M_p}\sin^2\frac{\theta_e}{2}} = \frac{(1+\frac{\epsilon_1}{M_p}\sin^2\frac{\theta_e}{2})^2}{1+2\frac{\epsilon_1}{M_p}\sin^2\frac{\theta_e}{2}}. \tag{68}$$

Using the relation (87) between the initial and final electron energy, we have:

$$1 + \frac{\epsilon_1}{M_p}\sin^2\frac{\theta_e}{2} = \frac{1}{2}\frac{\epsilon_1 + \epsilon_2}{\epsilon_2}. \tag{69}$$

Substituting (69) in (67), one finally finds:

$$\frac{1}{\sin^2\frac{\theta_B}{2}} = \frac{(\epsilon_1 + \epsilon_2)^2}{(-q^2)(1+\tau)}. \tag{70}$$

### 4.2. *Dynamics*

Electron proton scattering through one photon exchange is illustrated by the Feynman diagram in Fig. 2, which includes two vertexes: (1) the electron vertex, which is described by QED-rules, (2) the proton vertex described by QCD and hadron electrodynamics, connected by the virtual photon line. The matrix element corresponding to this diagram, is written as:

$$\mathcal{M} = \frac{e^2}{q^2}\ell_\mu \mathcal{J}_\mu = \frac{e^2}{q^2}\ell \cdot \mathcal{J}, \tag{71}$$

where $\ell_\mu = \overline{u}(k_2)\gamma_\mu u(k_1)$ is the electromagnetic current of electron. The nucleon electromagnetic current, $\mathcal{J}_\mu$ describes the proton vertex and is generally written in terms of Pauli and Dirac FFs $F_1$ and $F_2$:

$$\mathcal{J}_\mu = \overline{u}(p_2)\left[F_1(q^2)\gamma_\mu - \frac{\sigma_{\mu\nu}q_\nu}{2m}F_2(q^2)\right]u(p_1), \tag{72}$$

with

$$\sigma_{\mu\nu} = \frac{\gamma_\mu\gamma_\nu - \gamma_\nu\gamma_\mu}{2}.$$

Note that $\mathcal{J} \cdot q = 0$, for any values of $F_1$ and $F_2$, i.e., the current $\mathcal{J}_\mu$ is conserved†.

Using the Dirac equation for the four-component spinors of the initial and final nucleon, Eq. (72) can be rewritten in a simpler form, using:

$$\overline{u}(p_2)\frac{\sigma_{\mu\nu}q_\nu}{2M_p}u(p_1) = \overline{u}(p_2)\left[\gamma_\mu - \frac{(p_1 + p_2)_\mu}{2M_p}\right]u(p_1). \tag{73}$$

which is also conserved.

†This can be easily proved as follows. The term $\sigma_{\mu\nu}q_\mu q_\nu$ vanishes, because it is the product of a symmetrical and antisymmetrical tensors, and $\overline{u}(p_2)\hat{q}u(p_1) = \overline{u}(p_2)(\hat{p}_2 - \hat{p}_1)u(p_1) = \overline{u}(p_2)(M_p - M_p)u(p_1) = 0$, as a result of the Dirac equation for both four-component spinors, $u(p_1)$ and $u(p_2)$. Note that the current (72) is conserved only when both nucleons (in initial and final states) are real, the form factor $F_1$ violates the current conservation, if one nucleon is virtual.

Let us prove Eq. (73).
Using the definition for $\sigma_{\mu\nu}$, one can write:

$$\overline{u}(p_2)\frac{\gamma_\mu\gamma_\nu-\gamma_\nu\gamma_\mu}{4M_p}q_\nu u(p_1)=\overline{u}(p_2)\frac{\gamma_\mu\hat{q}-\hat{q}\gamma_\mu}{4M_p}u(p_1).$$

Recalling that $q=p_2-p_1$ with $\hat{a}=a_\mu\gamma_\mu$:

$$\overline{u}(p_2)\frac{\gamma_\mu(\hat{p}_2-\hat{p}_1)-(\hat{p}_2-\hat{p}_1)\gamma_\mu}{4M_p}u(p_1).$$

Applying the Dirac equation:

$$(\hat{p}-M_p)u(p)=0\rightarrow\hat{p}u(p)=M_pu(p),$$
$$\overline{u}(p)(\hat{p}-M_p)=0\rightarrow\overline{u}(p)\hat{p}=\overline{u}(p)M_p,$$

we find:

$$\overline{u}(p_2)\frac{\gamma_\mu(\hat{p}_2-M_p)-(M_p-\hat{p}_1)\gamma_\mu}{4M_p}u(p_1)=-\frac{1}{2}\overline{u}(p_2)\gamma_\mu u(p_1)+\frac{1}{4M_p}\overline{u}(p_2)\left[\gamma_\mu\hat{p}_2+\hat{p}_1\gamma_\mu\right]u(p_1). \tag{74}$$

Using the properties: $\gamma_\mu\gamma_\nu+\gamma_\nu\gamma_\mu=2g_{\mu\nu}$, $\hat{a}\hat{b}+\hat{b}\hat{a}=2ab$, $\hat{a}\gamma_\mu+\gamma_\mu\hat{a}=2a_\mu$ we have $\hat{p}_1\gamma_\mu=-\gamma_\mu\hat{p}_1+2p_{1\mu}$, so that:

$$\begin{aligned}\frac{1}{4M_p}\overline{u}(p_2)\left[\gamma_\mu\hat{p}_2+\hat{p}_1\gamma_\mu\right]u(p_1)&=\frac{1}{4M_p}\overline{u}(p_2)\left[-\hat{p}_2\gamma_\mu+2p_{2\mu}-\gamma_\mu\hat{p}_1+2p_{1\mu}\right]u(p_1)\\&=\frac{1}{4M_p}\overline{u}(p_2)\left[-2\gamma_\mu M_p+2(p_{2\mu}+p_{1\mu})\right]u(p_1)\\&=\frac{1}{2}\overline{u}(p_2)\left[-\gamma_\mu+\frac{(p_{2\mu}+p_{1\mu})}{M_p}\right]u(p_1).\end{aligned} \tag{75}$$

Inserting Eq. (75) in (74), we find Eq. (73).

Note that the relation (73) is correct only when both nucleons are on mass shell, i.e; they are described by the four-component spinors $u(p)$, satisfying the Dirac equation. It is not the case for the quasi-elastic scattering of electrons by atomic nuclei, $e+A\rightarrow e+p+X$, which contains as subprocess the scattering $e+N^*\rightarrow e+N$, where $N^*$ is a virtual nucleon.

Eq. (73) is an expression of the nucleon electromagnetic current, which holds in any reference system. However, for the analysis of polarization phenomena, the Breit system is the most preferable. First of all, the explicit expression of the current $\mathcal{J}_\mu=(\mathcal{J}_0,\vec{\mathcal{J}})$ is simplified in the Breit system:

$$\begin{cases}\mathcal{J}_0\ =\overline{u}(p_2)\left[(F_1+F_2)\gamma_0-\dfrac{(E_{1B}+E_{2B})}{2M_p}F_2\right]u(p_1),\ E_{1B}=E_{2B}=E,\\ \vec{\mathcal{J}}=\overline{u}(p_2)\left[(F_1+F_2)\vec{\gamma}-\dfrac{(\mathbf{p_{1B}}+\mathbf{p_{2B}})}{2M_p}F_2\right]u(p_1)=(F_1+F_2)\overline{u}(p_2)\vec{\gamma}u(p_1).\end{cases} \tag{76}$$

With $u(p_1)$ and $u(p_2)$ defined according to (50) we find, for the time component $\mathcal{J}_0$ of the current $\mathcal{J}_\mu$:

$$\begin{aligned}\mathcal{J}_0 &= (F_1+F_2)\,u^\dagger(p_2)u(p_1) - F_2\frac{E}{M_p}u^\dagger(p_2)\gamma_0 u(p_1)\\ &= (E+M_p)\left\{(F_1+F_2)\chi_2^\dagger\left(1\,,\ \frac{\vec\sigma\cdot\mathbf{q_B}}{2(E+M_p)}\right)\begin{pmatrix}\chi_1\\ \dfrac{-\vec\sigma\cdot\mathbf{q_B}}{2(E+M_p)}\chi_1\end{pmatrix}\right.\\ &\left.-F_2\frac{E}{M_p}\chi_2^\dagger\left(1\,,\ \frac{\vec\sigma\cdot\mathbf{q_B}}{2(E+M_p)}\right)\begin{bmatrix}1&0\\0&-1\end{bmatrix}\begin{pmatrix}\chi_1\\ \dfrac{-\vec\sigma\cdot\mathbf{q_B}}{2(E+M_p)}\chi_1\end{pmatrix}\right\} =\\ &= 2M_p\chi_2^\dagger\chi_1\,(F_1-\tau F_2)\,,\end{aligned} \tag{77}$$

where we used the definition:

$$\mathbf{p_{2B}}^2 = E^2 - M_p^2 = \frac{\mathbf{q_B}^2}{4},\ \text{so that}\ \frac{\mathbf{q_B}^2}{4(E+M_p)^2} = \frac{E-M_p}{E+M_p},$$

and

$$\overline{u}(p_2) = u^\dagger(p_2)\gamma_0,\ \gamma_0^2 = 1 \text{ and } (\vec\sigma\cdot\mathbf{q})(\vec\sigma\cdot\mathbf{q}) = \mathbf{q}^2.$$

For the vector part $\vec{\mathcal{J}}$ of the nucleon electromagnetic current we can find similarly:

$$\begin{aligned}\vec{\mathcal{J}} &= (F_1+F_2)\,(E+M_p)\chi_2^\dagger\left(1\,,\ -\frac{\vec\sigma\cdot\mathbf{q_B}}{2(E+M_p)}\right)\begin{bmatrix}0&\vec\sigma\\-\vec\sigma&0\end{bmatrix}\begin{pmatrix}\chi_1\\ \dfrac{-\vec\sigma\cdot\mathbf{q_B}}{2(E+M_p)}\chi_1\end{pmatrix}\\ &= -\frac{1}{2}\,(F_1+F_2)\chi_2^\dagger\,(\vec\sigma\vec\sigma\cdot\mathbf{q_B} - \vec\sigma\cdot\mathbf{q_B}\vec\sigma)\chi_1\end{aligned}$$

Multiplying the left and right side by $\vec a$:

$$\begin{aligned}\vec{\mathcal{J}}\cdot\vec a &= \vec\sigma\cdot\vec a\vec\sigma\cdot\mathbf{q_B} - \vec\sigma\cdot\mathbf{q_B}\vec\sigma\cdot\vec a\\ &= \vec a\cdot\mathbf{q_B} + i\vec\sigma\cdot(\vec a\times\mathbf{q_B}) - (\mathbf{q_B}\cdot\vec a + i\vec\sigma\cdot\mathbf{q_B}\times\vec a) = -2i\vec a\cdot\vec\sigma\times\mathbf{q_B}.\end{aligned}$$

Finally:

$$\boxed{\begin{aligned}\mathcal{J}_0 &= 2M_p\chi_2^\dagger\chi_1\,(F_1-\tau F_2)\,,\\ \vec{\mathcal{J}} &= i\chi_2^\dagger\vec\sigma\times\mathbf{q_B}\chi_1\,(F_1+F_2)\,.\end{aligned}}$$

These expressions for the different components of the current $\mathcal{J}_\mu$ are valid in the Breit frame only, and allow to introduce in a straightforward way the Sachs nucleon electromagnetic FFs,[43] electric and magnetic, which are related to $F_1$ and $F_2$ as in Table 4. Note that, by convention, $\tau > 0$ is chosen to be always positive. In TL region, these relations are correct after replacement $\tau \to -\tau$.

| | |
|---|---|
| $G_M = F_1 + F_2$ | $F_1 = \dfrac{G_E + \tau G_M}{1+\tau}$ |
| $G_E = F_1 - \tau F_2$ | $F_2 = \dfrac{G_M - G_E}{1+\tau}$ |

Such identification can be easily understood, if one takes into account that the time component of the current, $\mathcal{J}_0$, describes the interaction of the nucleon electric charge with the Coulomb potential. Correspondingly, the space component $\vec{\mathcal{J}}$ describes the interaction of the nucleon spin with the magnetic field.

### 4.3. *The unpolarized cross section*

The starting point is the expression (34) for the cross section. From Eq.(71) we can find the following representation for $\overline{|\mathcal{M}|}$ (the bar denotes the averaging over the polarizations of the initial electron and the summing over the polarizations of the final electrons):

$$\overline{|\mathcal{M}|^2} = \left(\frac{e^2}{q^2}\right)^2 \overline{|\ell \cdot \mathcal{J}|^2} = \left(\frac{e^2}{q^2}\right)^2 L_{\mu\nu} W_{\mu\nu}, \tag{78}$$

where:

$L_{\mu\nu} = \overline{\ell_\mu \ell_\nu^*}$ is the leptonic tensor,

$W_{\mu\nu} = \overline{\mathcal{J}_\mu \mathcal{J}_\nu^*}$ is the hadronic tensor.

The product of the tensors $L_{\mu\nu}$ and $W_{\mu\nu}$ is a relativistic invariant, therefore it can be calculated in any reference system. The differential cross section, in any coordinate system, can be expressed in terms of the matrix element as:

$$d\sigma = \frac{(2\pi)^4 \overline{|\mathcal{M}|^2}}{4\sqrt{(k_1 \cdot p_1)^2 - m_e^2 M_p^2}} \delta^4(k_1 + p_1 - k_2 - p_2) \frac{d^3\mathbf{k_2}}{(2\pi)^3 2\epsilon_2} \frac{d^3\mathbf{p_2}}{(2\pi)^3 2E_2}. \tag{79}$$

To compare with experiments, it is more convenient to use the differential cross section in Lab system, $d\sigma/d\Omega_e$, where $d\Omega_e$ is the element of the electron solid angle in the Lab system. This can be done, integrating Eq. (79), using the properties of the $\delta^4$ function.

First of all, let us integrate over the three-momentum $\mathbf{p_2}$, applying the three momentum conservation for the considered process:

$$\int d^3\mathbf{p_2} \delta^3(\mathbf{k_1} - \mathbf{k_2} - \mathbf{p_2}) = 1, \text{ with the condition } \mathbf{p_2} = \mathbf{k_1} - \mathbf{k_2}.$$

Using the definition $d^3\mathbf{k_2} \overset{m_e=0}{=} d\Omega_e \mathbf{k_2}^2 d|\mathbf{k_2}| \simeq d\Omega_e \epsilon_2^2 d\epsilon_2$, we can integrate over the electron energy, taking into account the conservation of energy:

$$\delta(\epsilon_1 + M_p - \epsilon_2 - E_2) d\epsilon_2 = \delta\left(\epsilon_1 + M_p - \epsilon_2 - \sqrt{M_p^2 + \mathbf{p_2}^2}\right) d\epsilon_2 =$$

$$\delta\left(\epsilon_1 + M_p - \epsilon_2 - \sqrt{M_p^2 + (\mathbf{k_1} - \mathbf{k_2})^2}\right) d\epsilon_2.$$

Let us recall that:

$$\int \delta\left[f(\epsilon_2)\right] d\epsilon_2 = \frac{1}{|f'(\epsilon_2)|},$$

where $f(\epsilon_2) = \epsilon_1 + M_p - \epsilon_2 - \sqrt{M_p^2 + \epsilon_1^2 + \epsilon_2^2 - 2\epsilon_1\epsilon_2 \cos\theta_e}$. Therefore:

$$|f'(\epsilon_2)| = 1 + \frac{\epsilon_2 - \epsilon_1 \cos\theta_e}{E_2} = 1 + \frac{\epsilon_2^2 - \mathbf{k_1} \cdot \mathbf{k_2}}{\epsilon_2 E_2} = \frac{k_2 \cdot (k_1 + p_1)}{\epsilon_2 E_2},$$

where we multiplied by $\epsilon_2$ the numerator and denominator, and we used the conservation of energy $\epsilon_2 + E_2 = \epsilon_1 + M_p$. But from the conservation of four-momentum, in the following form $k_1 + p_1 - k_2 = p_2$, we have:

$$(k_1 + p_1)^2 + k_2^2 - 2(k_1 + p_1) \cdot k_2 = M_p^2.$$

So $2(k_1 + p_1) \cdot k_2 = (k_1 + p_1)^2 - M_p^2 = 2k_1 \cdot p_1 = 2\epsilon_1 M_p$ (in Lab system). Finally

$$|f'(\epsilon_2)| = \frac{\epsilon_1}{\epsilon_2}\frac{M_p}{E_2}.$$

After substituting in Eq. (79), one finds the following relation between $\overline{|\mathcal{M}|^2}$ and the differential cross section in Lab system:

$$\frac{d\sigma}{d\Omega_e} = \frac{\overline{|\mathcal{M}|^2}}{64\pi^2}\left(\frac{\epsilon_2}{\epsilon_1}\right)^2 \frac{1}{M_p^2}. \tag{80}$$

#### 4.3.1. *Hadronic tensor $W_{\mu\nu}$*

Let us calculate the hadronic tensor $W_{\mu\nu}$ in the Breit system, where there is a simple expression of the nucleon current. Let us write this current as: $\mathcal{J}_\mu = \chi_2^\dagger F_\mu \chi_1$, with $F_\mu = 2M_p G_E$, for $\mu = 0$ and $F_\mu = i\vec{\sigma} \times \mathbf{q_B} G_M$, for $\mu = x, y, z$. So the the four components of $F_\mu$, in terms of FFs $G_E$ and $G_E$, can be written as:

$$F_\mu = \begin{cases} 2M_p G_E & ,\mu = 0 \\ i\sqrt{-q^2} G_M \sigma_y & ,\mu = x \\ -i\sqrt{-q^2} G_M \sigma_x & ,\mu = y \\ 0 & ,\mu = z. \end{cases} \tag{81}$$

Therefore, the hadronic tensor $W_{\mu\nu}$ can be written as follows:

$$W_{\mu\nu} = \overline{(\chi_2^\dagger F_\mu \chi_1)(\chi_1^\dagger F_\nu^\dagger \chi_2)} = \frac{1}{2} Tr F_\mu \rho_1 F_\nu^\dagger \rho_2,$$

where the averaging (summing) acts only on the two-component spinors, and we introduced density matrix for the nucleon: $\rho = \chi\chi^\dagger$, $\rho_{ab} = \chi_a \chi_b^*$, and $a, b = 1, 2$ are the spinor indexes. We included the statistical factor $1/(2s + 1) = 1/2$, for the initial nucleon.

In case of unpolarized particles $\rho = 1/2$, and

$$W_{\mu\nu} = \frac{1}{2} Tr F_\mu F_\nu^\dagger.$$

#### 4.3.2. *Leptonic tensor $L_{\mu\nu}$*

The leptonic tensor, which describes the electron vertex, is written as:

$$L_{\mu\nu} = \overline{\ell_\mu \ell_\nu^*} = \overline{\overline{u}(k_2)\gamma_\mu u(k_1)\,[\overline{u}(k_2)\gamma_\nu u(k_1)]^*}.$$

Recalling that

$$\overline{u} = u^\dagger \gamma_0,\ \ \overline{u}^\dagger = (u^\dagger \gamma_0)^\dagger = \gamma_0^\dagger u = \gamma_0 u,\ \ \gamma_0\gamma_0 = 1,\ \gamma_0^\dagger = \gamma_0,$$

we can write:

$$\begin{aligned} L_{\mu\nu} &= \overline{\overline{u}(k_2)\gamma_\mu u(k_1) u^\dagger(k_1)\gamma_\nu^\dagger \overline{u}(k_2)} = \overline{\overline{u}(k_2)\gamma_\mu u(k_1) u^\dagger(k_1)\gamma_0\gamma_0\gamma_\nu^\dagger \gamma_0 u(k_2)} \\ &= \overline{\overline{u}(k_2)\gamma_\mu u(k_1)\overline{u}(k_1)\gamma_0\gamma_\nu^\dagger\gamma_0 u(k_2)} = \frac{1}{2} Tr \gamma_\mu \rho_e^1 \gamma_\nu \rho_e^2. \end{aligned} \tag{82}$$

From the Dirac theory we can write: $u(k)\overline{u}(k) = \hat{k} + m_e = \rho$:

$$L_{\mu\nu} = \frac{1}{2} Tr\gamma_\mu(\hat{k_1} + m_e)\gamma_\nu(\hat{k_2} + m_e) = Tr\gamma_\mu\hat{k_1}\gamma_\nu\hat{k_2} + m_e^2 Tr\gamma_\mu\gamma_\nu.$$

Recalling that $Tr\gamma_a\gamma_b = 4g_{ab}$ ($g_{ab} = 1$, for $a, b = 0$, $g_{ab} = -1$, for $a, b = x, y$, or $z$; and $Tr\gamma_a\gamma_b\gamma_c\gamma_d = 4(g_{ab}g_{cd} + g_{bc}g_{da} - g_{ac}g_{bd})$ we derive :

$$L_{\mu\nu} = 2k_{1\mu}k_{2\nu} + 2k_{1\nu}k_{2\mu} + 2g_{\mu\nu}(m_e^2 - k_1 \cdot k_2).$$

Using that $k_1 = q + k_2$; $q^2 = 2(m_e^2 - k_1 \cdot k_2)$ we find:

$$L_{\mu\nu} = 2k_{1\mu}k_{2\nu} + 2k_{1\nu}k_{2\mu} + g_{\mu\nu}q^2. \tag{83}$$

Neglecting the electron mass:

$$\boxed{L_{\mu\nu} = 2k_{1\mu}k_{2\nu} + 2k_{1\nu}k_{2\mu} - 2g_{\mu\nu}k_1 \cdot k_2.}$$

From this expression we see that the leptonic tensor which describes unpolarized electrons is symmetrical.

### 4.4. *The Rosenbluth formula*

Let us calculate explicitly the components for the hadronic tensor $W_{\mu\nu}$, in terms of FFs $G_E$ and $G_M$. Recalling the property that $Tr\vec{\sigma} \cdot \mathbf{A} = 0$, for any vector $\mathbf{A}$, we see that all terms for the components $W_{\mu\nu}$ which contain the product $G_E G_M$ vanish: this means that the unpolarized cross section of $eN-$scattering does not contain this interference term. The non-zero components of $W_{\mu\nu}$ are determined only by $G_E^2$ and $G_M^2$:

$$W_{00} = 4M_p^2 G_E^2,$$

$$W_{xx} = -q^2 G_M^2,$$

$$W_{yy} = -q^2 G_M^2.$$

Substituting these expressions in Eq. (78), one can find for the matrix element squared:

$$\left(\frac{q^2}{e^2}\right)^2 \overline{|\mathcal{M}|^2} = L_{00}W_{00} + (L_{xx} + L_{yy})W_{xx} = L_{00}4M_p^2 G_E^2 + (L_{xx} + L_{yy})(-q^2)G_M^2. \tag{84}$$

The necessary components of the leptonic tensor $L_{\mu\nu}$, calculated in the Breit system, are:

$$L_{00} = 4\epsilon_{1B}^2 + q^2 = -q^2 \cot^2 \frac{\theta_B}{2},$$

$$L_{yy} = -q^2,$$

$$L_{xx} = 4k_{1x}^2 - q^2 = -q^2 \left(1 + \cot^2 \frac{\theta_B}{2}\right).$$

Substituting the corresponding terms in Eq. (84) we have:

$$\overline{|\mathcal{M}|^2} = \left(\frac{e^2}{q^2}\right)^2 \left[-q^2 \cot^2 \frac{\theta_B}{2} 4M_p^2 G_E^2 + (-2q^2 - q^2 \cot^2 \frac{\theta_B}{2})(-q^2 G_M^2)\right],$$

which becomes in the Lab system:

$$\overline{|\mathcal{M}|^2} = \left(\frac{e^2}{q^2}\right)^2 4M_p^2(-q^2)\left[2\tau G_M^2 + \frac{\cot^2 \frac{\theta_e}{2}}{1 + \tau}(G_E^2 + \tau G_M^2)\right]. \tag{85}$$

We can then find the following formula for the cross section, $d\sigma/d\Omega_e$, in the Lab system, in terms of the electromagnetic FFs $G_E$ and $G_M$ (Rosenbluth formula[4]) $^{\ddagger}$:

$$\frac{d\sigma}{d\Omega_e} = \frac{\alpha^2}{-q^2}\left(\frac{\epsilon_2}{\epsilon_1}\right)^2\left[2\tau G_M^2 + \frac{\cot^2\frac{\theta_e}{2}}{1+\tau}\left(G_E^2+\tau G_M^2\right)\right], \tag{86}$$

where $\alpha = e^2/4\pi \simeq 1/137$ is the fine structure constant.

Taking into account Eq. (65) and the following relation between the energy $\epsilon_2$ and the angle $\theta_e$ of the scattered electron:

$$\epsilon_2 = \frac{\epsilon_1}{1+2\dfrac{\epsilon_1}{M_p}\sin^2\dfrac{\theta_e}{2}}, \tag{87}$$

the differential cross section can be written in the following form:

$$\frac{d\sigma}{d\Omega_e} = \sigma_M\left[2\tau G_M^2\tan^2\frac{\theta_e}{2} + \frac{G_E^2+\tau G_M^2}{1+\tau}\right], \tag{88}$$

with

$$\sigma_M = \frac{\alpha^2}{-q^2}\left(\frac{\epsilon_2}{\epsilon_1}\right)^2\frac{\cos^2\dfrac{\theta_e}{2}}{\sin^2\dfrac{\theta_e}{2}} = \left(\frac{\alpha}{2\epsilon_1}\right)^2\frac{\cos^2\dfrac{\theta_e}{2}}{\sin^4\dfrac{\theta_e}{2}}\frac{1}{\left(1+2\dfrac{\epsilon_1}{M_p}\sin^2\dfrac{\theta_e}{2}\right)},$$

where $\sigma_M$ is the Mott cross section, for the scattering of unpolarized electrons by a point charge particle (with spin 1/2).

Note that the very specific $\cot^2\dfrac{\theta_e}{2}$-dependence of the cross section for $eN$-scattering results from the assumption of one-photon mechanism for the considered reaction. This can be easily proved,[31] by crossing symmetry considerations, looking to the annihilation channel, $e^+ + e^- \to \bar{p} + p$. In the CMS of such reaction, the one-photon mechanism induces a simple and evident $\cos^2\theta$-dependence of the corresponding differential cross section, due to the C-invariance of the hadron electromagnetic interaction, and unit value of the photon spin.

The particular $\cot^2\dfrac{\theta_e}{2}$-dependence of the differential $eN$-cross section is at the basis of the method to determine both nucleon electromagnetic FFs, $G_E$ and $G_M$, using the linearity of the *reduced* cross section:

$$\sigma_{red} = \frac{\dfrac{d\sigma}{d\Omega_e}}{\dfrac{\alpha^2}{-q^2}\left(\dfrac{\epsilon_2}{\epsilon_1}\right)^2},$$

as a function of $\cot^2\frac{\theta_e}{2}$ (Rosenbluth fit or Rosenbluth separation). One can see that the backward $eN$-scattering ($\theta_e = \pi, \cot^2\frac{\theta_e}{2} = 0$) is determined by the magnetic FF only, and that the slope for $\sigma_{red}$ is sensitive to $G_E^2$ (Fig. 4).

At large $q^2$, for $\tau \gg 1$, the differential cross-section $d\sigma/d\Omega_e$ (with unpolarized particles) is insensitive to $G_E$: the corresponding combination of the nucleon FFs, $G_E^2 + \tau G_M^2$ is dominated by the $G_M$ contribution, due to the following reasons:

- $G_M/G_E \simeq \mu_p$, where $\mu_p$ is the proton magnetic moment, so $G_M^2/G_E^2 \simeq 2.79^2 \simeq 8$;

$^{\ddagger}$More exactly, the original formula has been written in terms of the Dirac ($F_1$) and Pauli ($F_2$) form factors.

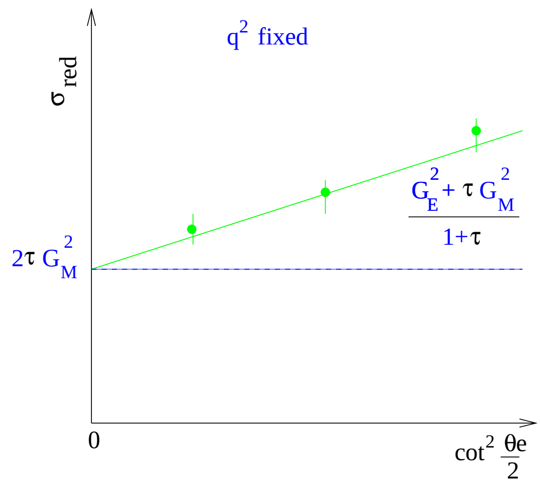


Fig. 4. Illustration of the Rosenbluth separation for the elastic differential cross section for $eN$-scattering.

- The factor $\tau$ increases the $G_M^2$ contribution at large momentum transfer, where $\tau \gg 1$.

Therefore $ep-$scattering (with unpolarized particles) is dominated by the magnetic term, at large values of momentum transfer. The same holds for $en-$scattering, even at relatively small values of $q^2$, due to the smaller values of the neutron electric FF.

As a result, for the exact determination of the proton electric FF, in the region of large momentum transfer, and for the neutron electric FF - at any value of $q^2$, polarization measurements are required and in particular those polarization observables which are determined by the product $G_E G_M$, and are, therefore, more sensitive to $G_E$.

There are at least two different classes of polarization experiments of such type: the scattering of longitudinally polarized electrons by polarized target (with polarization in the reaction plane, but perpendicular to the direction of the three-momentum transfer) $\vec{e} + \vec{p} \to e + p$, or the measurement of the ratio of transversal to longitudinal proton polarization (in the reaction plane) for the scattering of longitudinally polarized electrons by unpolarized target, $\vec{e} + p \to e + \vec{p}$.

In principle, there are some components of the depolarization tensor (characterizing the dependence of the final proton polarization on the target polarization (for the scattering of unpolarized electrons, $e + \vec{p} \to e + \vec{p}$) which are also proportional to $G_E G_M$, and therefore can be used for the determination of the nucleon electric FF.[1,2,44]

Both experiments (with polarized electron beam) have been realized: $p(\vec{e}, \vec{p})e$ for the determination of the proton electric FF, $G_{Ep}$[21] and, for the determination of the neutron electric FF, $G_{En}$, $d(\vec{e}, e'\vec{n})p$ and $d(\vec{e}, e'n)\vec{p}$.[46]

### 4.5. *Polarization observables*

In general the hadronic tensor $W_{\mu\nu}$, for $ep$ elastic scattering, contains four terms, related to the four possibilities of polarizing the initial and final protons:

$$W_{\mu\nu} = W_{\mu\nu}^{(0)} + W_{\mu\nu}(\vec{P}_1) + W_{\mu\nu}(\vec{P}_2) + W_{\mu\nu}(\vec{P}_1, \vec{P}_2),$$

where $\vec{P}_1$, $(\vec{P}_2)$ is the polarization vector of the initial (final) proton. The first term corresponds to the unpolarized case, the second (third) term corresponds to the case when the initial (final) proton is polarized, and the last term describes the reaction when both protons (initial and final) are polarized. The $2 \times 2$ density matrix for a nucleon with polarization $\vec{P}$ can be written as: $\rho = \frac{1}{2}\left(1 + \vec{\sigma} \cdot \vec{P}\right)$.

Let us consider the case when only the final proton is polarized ($\vec{P} = \vec{P}_2$):

$$W_{\mu\nu}(\vec{P}) = \frac{1}{2} Tr F_\mu F_\nu^\dagger \vec{\sigma} \cdot \mathbf{P}.$$

For the scattering of longitudinally polarized electrons (by unpolarized target), only the $x$ and $z$ components of the polarization vector $\mathbf{P}$ do not vanish. To find these components, let us calculate the tensors $W_{\mu\nu}(P_x)$ and $W_{\mu\nu}(P_z)$.

$$W_{\mu\nu}(P_x) = \frac{1}{2} Tr F_\mu F_\nu^\dagger \sigma_x.$$

Let us start [§] from the calculation of the components $F_\nu^\dagger$:

$$F_\nu^\dagger = \begin{cases} 2M_p G_E & , \nu = 0, \\ -i\sqrt{-q^2} G_M \sigma_y & , \nu = x, \\ i\sqrt{-q^2} G_M \sigma_x & , \nu = y, \\ 0 & , \nu = z. \end{cases} \tag{89}$$

Therefore, one can find easily (using $\sigma_x \sigma_y = i\sigma_z,\ \sigma_y \sigma_z = i\sigma_x, \sigma_z \sigma_x = i\sigma_y$):

$$F_\nu^\dagger \sigma_x = \begin{cases} 2M_p G_E \sigma_x & , \nu = 0, \\ -\sqrt{-q^2} G_M \sigma_z & , \nu = x, \\ i\sqrt{-q^2} G_M & , \nu = y, \\ 0 & , \nu = z. \end{cases} \tag{90}$$

This allows to write:

$$F_\mu F_\nu^\dagger \sigma_x = \begin{cases} 2M_p G_E & , \mu = 0, \\ i\sqrt{-q^2} G_M \sigma_y & , \mu = x, \\ -i\sqrt{-q^2} G_M \sigma_x & , \mu = y, \\ 0 & , \mu = z, \end{cases} \bigotimes \begin{cases} 2M_p G_E \sigma_x & , \nu = 0, \\ -\sqrt{-q^2} G_M \sigma_z & , \nu = x, \\ i\sqrt{-q^2} G_M & , \nu = y, \\ 0 & , \nu = z. \end{cases} \tag{91}$$

As we have to calculate the trace, recalling that $Tr\sigma_{x,y,z} = 0$, we can see that the non-zero components of the hadronic tensor $W_{\mu\nu}(P_x)$ are:

$$\begin{aligned} W_{0y}(P_x) &= i\sqrt{-q^2}\ 2M_p G_E G_M, \\ W_{y0}(P_x) &= -i\sqrt{-q^2}\ 2M_p G_E G_M. \end{aligned} \tag{92}$$

So we proved here that only two components of $W_{\mu\nu}(P_x)$ are different from zero: they are equal in absolute value and opposite in sign: it follows that $W_{\mu\nu}(P_x)$ is an antisymmetrical tensor. Therefore, the product $L_{\mu\nu} W_{\mu\nu}(P_x)$ vanishes: the product of a symmetrical tensor and an asymmetrical tensor is zero. This means that the polarization of the final proton vanishes, if the electron is unpolarized: **unpolarized electrons can not induce polarization of the scattered proton**. This is a property of the one-photon mechanism $for\ any\ elastic\ electron - hadron\ scattering$ and of the hermiticity of the Hamiltonian for the hadron electromagnetic interaction. Namely the hermiticity condition allows to prove that the hadron electromagnetic FFs are real functions of the momentum transfer squared in the space-like region. On the other hand, in the time-like

[§] We will take into account the fact that $G_E(q^2)$ and $G_M(q^2)$ are real functions of $(q^2)$ in the space-like region.

region, which is scanned by the annihilation processes, $e^- + e^+ \leftrightarrow \overline{p} + p$, the nucleon electromagnetic FFs are complex functions of $q^2$, if $q^2 \geq 4m_\pi^2$, where $m_\pi$ is the pion mass. This is due to the unitarity condition, which can be illustrated as in Fig. 5.

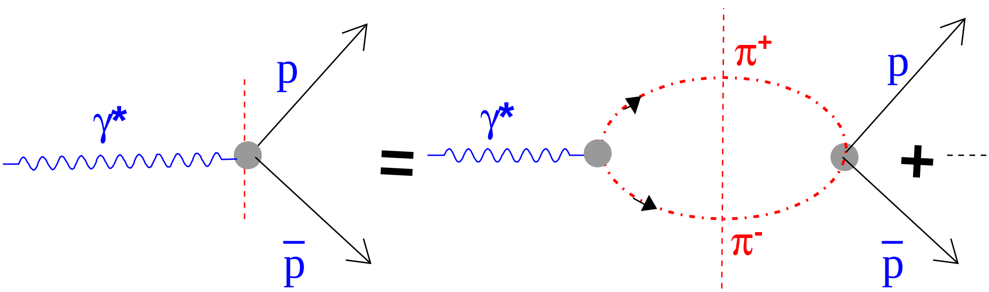


Fig. 5. The unitarity condition for proton electromagnetic FFs in the time-like region of momentum transfer squared. Vertical line on the right side crosses the pion lines, describing real particles (on mass shell). The dotted line denotes other possible multi-pion states, in the chain of the following transitions: $\gamma^* \to n\pi \to p\overline{p}$, where $n$ is the number of pions in the intermediate state.

The complexity of nucleon FFs (in the time-like region) results in specific polarization phenomena, for the annihilation processes $e^+ + e^- \leftrightarrow \overline{p} + p$, which are different from the case of elastic $ep$–scattering. For example, the polarization of the final proton (or antiproton) is different from zero, even in the case of collisions of unpolarized leptons: this polarization is determined by the product $\mathcal{I}mG_EG_M^*$ (and, therefore, vanishes in the case of elastic $ep$-scattering, where FFs are real). Note that two-photon exchange in $ep$-elastic scattering is also generating complex amplitudes. So the interference between one and two-photon amplitudes induces nonzero proton polarization, but small in absolute value, as it is proportional to $\alpha$.

Numerous experiments[47] have been done with the aim to detect such polarization at small momentum transfer $|q^2| \leq 1$ GeV$^2$, but with negative result, at a percent level. Only recently the above mentioned interference was experimentally detected, measuring the asymmetry in the scattering of transversally polarized electrons by an unpolarized proton target.[48,49]

Note that at very large momentum transfer, the relative role of two-photon amplitudes may be increased (violating the counting in $\alpha$), due to the steep $q^2$-decreasing of hadronic electromagnetic FFs.

Note also that the analytical properties of the nucleon FFs, considered as functions of the complex variable $z = q^2$, result in a specific asymptotic behavior, as they obey to the Phragmèn-Lindelöf theorem:[50]

$$\lim_{q^2\to-\infty} F^{(SL)}(q^2) = \lim_{q^2\to\infty} F^{(TL)}(q^2). \tag{93}$$

The existing experimental data about the proton FFs in the time-like region up to 15 GeV$^2$, seem to contradict this theorem.[51] More exactly, one can prove that, if one FF, electric or magnetic; satisfies the relation (93), then the other one violates this theorem, i.e., the asymptotic condition does not apply.

Let us consider now the proton polarization in the $z$-direction:

$$W_{\mu\nu}(P_z) = \frac{1}{2} Tr F_\mu F_\nu^\dagger \sigma_z.$$

First, we calculate the components of $F_\nu^\dagger \sigma_z$:

$$F_\nu^\dagger \sigma_z = \begin{cases} 2M_p G_E \sigma_z & , \nu = 0, \\ \sqrt{-q^2} G_M \sigma_x & , \nu = x, \\ \sqrt{-q^2} G_M \sigma_y & , \nu = y, \\ 0 & , \nu = z. \end{cases} \tag{94}$$

Therefore we find:

$$F_\mu F_\nu^\dagger \sigma_z = \begin{cases} 2M_p G_E & , \mu = 0, \\ i\sqrt{-q^2} G_M \sigma_y & , \mu = x, \\ -i\sqrt{-q^2} G_M \sigma_x & , \mu = y, \\ 0 & , \mu = z, \end{cases} \bigotimes \begin{cases} 2M_p G_E \sigma_z & , \nu = 0, \\ \sqrt{-q^2} G_M \sigma_x & , \nu = x, \\ \sqrt{-q^2} G_M \sigma_y & , \nu = y, \\ 0 & , \nu = z. \end{cases} \tag{95}$$

We see that $W_{0\nu}(P_z) = W_{\nu 0}(P_z) = 0$, for any $\nu$, and no interference term $G_E G_M$ is present. The nonzero components of $W_{\mu\nu}(P_z)$ are:

$$\begin{aligned} W_{xy}(P_z) &= -iq^2 G_M^2, \\ W_{yx}(P_z) &= iq^2 G_M^2, \end{aligned} \tag{96}$$

from where we see that $W_{\mu\nu}(P_z)$ is an antisymmetrical tensor, which depends on $G_M^2$ and that $P_x/P_z \propto G_E/G_M$.

#### 4.5.1. *Polarized electron*

The leptonic tensor, $L_{\mu\nu}$, in case of unpolarized particles, contains only one term. For longitudinally polarized electrons, the polarization is characterized by the helicity $\lambda$, which takes values $\pm 1$, corresponding to the direction of spin parallel or antiparallel to the electron three-momentum.

**Relativistic description of the electron polarization**

Using the expression 57 for the density matrix $\rho$, let us calculate the leptonic tensor $L_{\mu\nu}(\lambda)$, corresponding to the scattering of longitudinally polarized electrons (neglecting the electron mass):

$$L_{\mu\nu}(\lambda) = \frac{1}{2}Tr\gamma_\mu\hat{k}_1(1+\lambda\gamma_5)\gamma_\nu\hat{k}_2 = \frac{1}{2}Tr\gamma_\nu\hat{k}_1\gamma_\nu\hat{k}_2 + \frac{\lambda}{2}Tr\gamma_\nu\hat{k}_1\gamma_5\gamma_\nu\hat{k}_2 = L^{(0)}_{\mu\nu} + \lambda L^{(1)}_{\mu\nu}. \tag{97}$$

The tensor $L^{(0)}_{\mu\nu}$ corresponds to the scattering of unpolarized electrons:

$$L^{(0)}_{\mu\nu} = 2k_{1\mu}k_{2\nu} + k_{1\nu}k_{2\mu} - g_{\mu\nu}k_1\cdot k_2. \tag{98}$$

The tensor $L^{(1)}_{\mu\nu}$, describing the dependence on the longitudinal electron polarization can be written in the following form:

$$L^{(1)}_{\mu\nu} = \frac{1}{2}Tr\gamma_\mu\hat{k}_1\gamma_\nu\hat{k}_2\gamma_5 = -\frac{1}{2}Tr\gamma_\mu\gamma_\nu\hat{k}_1\hat{k}_2\gamma_5 = 2i\epsilon_{\mu\nu\rho\sigma}k_{1\rho}k_{2\sigma}. \tag{99}$$

We applied another property of $\gamma_5$, that is:

$$Tr\gamma_\mu\gamma_\nu\gamma_\rho\gamma_\sigma\gamma_5 = -4i\epsilon_{\mu\nu\rho\sigma}.$$

Taking into account the conservation of four-momentum in the electron vertex: $k_1 = k_2 + q$, we can rewrite the tensor $L^{(1)}_{\mu\nu}$ in the following form, which is more convenient in this frame:

$$L^{(1)}_{\mu\nu} = 2i\epsilon_{\mu\nu\rho\sigma}q_\rho k_{1\sigma}. \tag{100}$$

The three-vector $\mathbf{q}$ has only nonzero $z-$component, in the Breit system. The tensor $\epsilon_{\mu\nu\rho\sigma}$ is defined in such way that $\epsilon_{xyz0} = +1$.

The general expression for the leptonic tensor in case of longitudinally polarized electrons is:

$$L_{\mu\nu} = L^{(0)}_{\mu\nu} + L_{\mu\nu}(\lambda_1) + L_{\mu\nu}(\lambda_2) + L_{\mu\nu}(\lambda_1,\lambda_2), \tag{101}$$

where the first term, considered previously, describes the collision where the initial and final electrons are unpolarized, the second (third) term describes the case when the initial (final) electron is longitudinally polarized, and the last terms holds when both electrons are longitudinally polarized.

If only the initial electron is polarized, $\lambda_1 = \lambda$, one can write for $L_{\mu\nu}$:

$$L_{\mu\nu}(\lambda) = 2i\lambda\epsilon_{\mu\nu\alpha\beta}k_{1\alpha}k_{2\beta}. \tag{102}$$

The effect of the electron polarization is described by an antisymmetrical tensor $L_{\mu\nu}(\lambda)$. If the initial proton is unpolarized, again, being described by symmetrical tensor, the total result will be zero. This result holds because FFs are real, so it does not apply to the time-like region.

Let us consider the $x$ and $z$ components.

$x$-component

Let us consider the product of the leptonic $L_{\mu\nu}(\lambda)$ and hadronic $W_{\mu\nu}(P_x)$ tensors, for the $x$ component of the final proton polarization:

$$L_{\mu\nu}(\lambda)W_{\mu\nu}(P_x) = L_{0y}(\lambda)W_{0y}(P_x) + L_{y0}(\lambda)W_{y0}(P_x) \\ = L_{0y}(\lambda)\left[W_{0y}(P_x) - W_{y0}(P_x)\right] = 2L_{0y}(\lambda)W_{0y}(P_x). \tag{103}$$

Taking into account that: $L_{0y} = 2i\lambda\epsilon_{0y\alpha\beta}k_{1\alpha}k_{2\beta}$ the only non-zero terms correspond to $\alpha = x$ and $\beta = z$ or $\alpha = z$ and $\beta = x$. Therefore:

$$L_{0y}(\lambda) = 2i\lambda\left(\epsilon_{0yxz}k_{1x}k_{2z} + \epsilon_{0yzx}k_{1z}k_{2x}\right) = 2i\lambda\epsilon_{0yxz}(k_{1x}k_{2z} - k_{1z}k_{2x}) = i\lambda q^2 \cot\frac{\theta_B}{2},$$

with $\epsilon_{0yxz} = 1$, and using Eqs. (61) and (62).

We finally find:

$$L_{\mu\nu}(\lambda)W_{\mu\nu}(P_x) = -4\lambda M_p q^2\sqrt{-q^2}\cot\frac{\theta_B}{2}G_E G_M. \tag{104}$$

$z$-component

Similarly, considering the antisymmetry of both tensors $L_{\mu\nu}(\lambda)$ and $W_{\mu\nu}(P_z)$, one can find:

$$L_{\mu\nu}(\lambda)W_{\mu\nu}(P_z) = 2i\lambda\epsilon_{\mu\nu\alpha\beta}k_{1\alpha}k_{2\beta}W_{\mu\nu}(P_z) = 4\epsilon_{xy0z}W_{xy}(P_z)\left(\epsilon_{1B}k^z_{2B} - \epsilon_{2B}k^z_{1B}\right) \\ = 4\lambda q^2\frac{G_M^2}{\sin\theta_B/2}. \tag{105}$$

### 4.6. *Final formulas*

The polarization **P** of the scattered proton can be written as:

$$\mathbf{P}\frac{d\sigma}{d\Omega_e} = \frac{\alpha^2}{4\pi^2}\left(\frac{\epsilon_2}{\epsilon_1}\right)^2\frac{L_{\mu\nu}}{M_p^2}\vec{P}_{\mu\nu},$$

with $\vec{P}_{\mu\nu} = \frac{1}{2}(\mathcal{T}r\mathcal{F}_\mu\mathcal{F}_\nu^\dagger\vec{\sigma})$, so that $P^{(z)}_{\mu\nu} = W_{\mu\nu}(P_z)$ and $P^{(x)}_{\mu\nu} = W_{\mu\nu}(P_x)$.

Using Eq. (66) one can find the following expressions for the components $P_x$ and $P_z$ of the proton polarization vector (in the scattering plane) - in terms of the proton electromagnetic FFs:

$$\begin{aligned} DP_x &= -2\lambda\cot\frac{\theta_e}{2}\sqrt{\frac{\tau}{1+\tau}}G_E G_M, \\ DP_z &= \lambda\frac{\epsilon_1+\epsilon_2}{M_p}\sqrt{\frac{\tau}{1+\tau}}G_M^2, \end{aligned} \tag{106}$$

where D is proportional to the differential cross section with unpolarized particles:

$$D = 2\tau G_M^2 + \cot^2\frac{\theta_e}{2}\frac{G_E^2 + \tau G_M^2}{1+\tau}. \tag{107}$$

So, for the ratio of these components one can find the following formula:

$$\frac{P_x}{P_z} = \frac{P_t}{P_\ell} = -2\cot\frac{\theta_e}{2}\frac{M_p}{\epsilon_1+\epsilon_2}\frac{G_E(q^2)}{G_M(q^2)} \tag{108}$$

which clearly shows that a measurement of the ratio of transverse and longitudinal polarization of the recoil proton gives a direct measurement of the ratio of electric and magnetic FFs, $G_E(q^2)/G_M(q^2)$.

In the same way it is possible to calculate the dependence of the differential cross section for the elastic scattering of the longitudinally polarized electrons by a **polarized** proton target, with polarization $\mathcal{P}$, in the above defined coordinate system:

$$\frac{d\sigma}{d\Omega_e}(\mathcal{P}) = \left(\frac{d\sigma}{d\Omega_e}\right)_0 (1 + \lambda\mathcal{P}_x A_x + \lambda\mathcal{P}_z A_z), \tag{109}$$

where the asymmetries $A_x$ and $A_z$ (or the corresponding analyzing powers) are related in a simple and direct way, to the components of the final proton polarization:

$$\begin{aligned} A_x &= P_x, \\ A_z &= -P_z. \end{aligned} \tag{110}$$

This holds in the framework of the one-photon mechanism for elastic $ep-$scattering. Note that the quantities $A_x$ and $P_x$ have the same sign and absolute value, but the components $A_z$ and $P_z$, being equal in absolute value, have opposite sign.

These two different polarization experiments in elastic electron-proton scattering, namely the scattering with longitudinally polarized electrons by a polarized proton target (with polarization in the reaction plane) from one side and the measurement of the components of the final proton polarization (again in the reaction plane) in the scattering of longitudinally polarized electrons by an unpolarized proton target, from another side, bring the same physical information, concerning the electromagnetic FFs of proton.

Note that the $P_y$-component of the proton polarization vanishes in the scattering of polarized and unpolarized electrons, as well. This results from the one-photon mechanism and the fact that $G_E$ and $G_M$ are real. For the same reasons, the corresponding analyzing power, $A_y$, also vanishes.

### 4.7. *Discussion*

The expressions of the unpolarized cross section and of the polarization observables in terms of FFs given above for elastic $ep$-scattering, hold in the framework of the one-photon mechanism.

There are at least two different sources of corrections to these relations:

- the standard radiative corrections;
- the electroweak corrections.

These last corrections arise from the interference of amplitudes, corresponding to the exchange of $\gamma$ and $Z-$boson. The relative value of these contributions is characterized by the following dimensionless parameter:

$$G_{eff} = \frac{G_F}{2\sqrt{2}\alpha\pi}|q^2| \simeq 10^{-4}\frac{|q^2|}{\mathrm{GeV}^2},$$

where $G_F$ is the standard Fermi constant of the weak interaction, $G_F \simeq 10^{-5}/M_p^2$.

So, for $|q^2| \leq 10$ GeV$^2$, the electroweak corrections are negligible, for the polarization phenomena considered above. However, note that the $\gamma \otimes Z$-interference is not only inducing (small) corrections to the results of the one-photon considerations, but it induces also a new class of polarization observables of P-odd nature, i.e., with violation of the $P$-invariance. The simplest of them is the P-odd asymmetry of the scattering of longitudinally polarized electrons by an unpolarized proton target $\vec{e} + p \to e + p$ (the detection of the polarization of the scattered particles is not required). As this asymmetry vanishes in the one-photon mechanism, it is proportional to $G_{eff}$, at relatively small momentum transfer squared.

Let us turn to the QED radiative corrections. They appear essentially in the differential cross section, and they have been discussed, for example, in[36] and more recently by.[38]

For polarization phenomena, it can be proved[38] that, in case of soft photons, the contribution of radiative corrections can be explicitly factorized. Therefore, this contribution, which is important for the differential cross section, cancels in polarization effects. Radiation of non-soft photons by electrons (in initial and final states) results in corrections, which are different for the components $P_x$ and $P_z$. Such corrections can be calculated in a model independent way, in the framework of the standard QED, inducing effects of a few percent.[39]

Model dependent radiative corrections can not be uniquely calculated. This concerns, first of all, the virtual Compton scattering on nucleons, which is driven by the amplitude of the process $\gamma^* + p \to \gamma + p$, with very complicated spin structure and with different mechanisms, as, for example, pion exchange in $t$-channel and $\Delta$-exchange in $s$-channel. These contributions can be estimated to give corrections of 1-3 %.

The most intriguing part of the radiative corrections is due to the two-photon exchange at large momentum transfer, with comparable virtuality of the two photons. Polarization phenomena for elastic positron scattering and for elastic scattering of positive and negative muons are the same as in case of electron scattering, only in case of one photon exchange.

Radiative corrections modify not only the absolute value, but also the dependence of the observables on the relevant kinematical variables and, in case of unpolarized cross section, at large momentum transfer they can reach 30-40%.[52] Therefore, it appears necessary to introduce high order corrections,[41] what can be done in frame of the lepton structure functions (LSF) method.[37,53]

This formalism equally applies to *en*-elastic scattering, in the case of free neutron. As typically a target like $d$ or $^3He$ is used, specific considerations apply, which are outside the present notes (see Ref.[54]). The present formalism is valid in case of elastic $e +^3 He$ and $e +^3 H$ scattering, and, in general, for elastic scattering of electrons on any spin 1/2 target.

## 5. Symmetries and two photon exchange

The discrepancy of recent experimental results on *ed* and *ep* elastic scattering obtained in different experimental set-ups and/or with different methods, lead to the suggestion that, beyond possible systematic effects not taken properly into account, they could result from the presence of a different reaction mechanism, the exchange of two photons.[31] This is not a new idea: in the 70's much theoretical and experimental work was devoted to this problem. More than 25 years ago it was observed[27–30] that the simple rule of $\alpha$-counting for the estimation of the relative role of two-photon contribution to the amplitude of elastic $ed-$scattering, does not hold at large momentum transfer. Using a Glauber approach for the calculation of multiple scattering contributions,[26] it was shown that the relative role of two-photon exchange can be essentially increased in the region of high momentum transfer. It was also shown that this effect can be observed in particular in *ed*-elastic scattering , due to the steep decreasing of the deuteron form factors. Moreover the relative role of two-photon contributions has to be even larger for heavy nuclei (like $^3He$ or $^4He$) in comparison with deuteron. This effect would then manifest at relatively small momentum transfer - of the order of 1 GeV$^2$ - especially in the region of diffractive minima. The argument for the possible increase of the relative role of two-photon exchange at large momentum transfer follows from the fact that this momentum has to be shared between the two photons, which results in a non negligible two-photon amplitude. However, in[27] the two-photon amplitude is purely imaginary, at least at very small scattering angles, so it cannot interfere with the one-photon exchange amplitude. The experiments in the 70's were mainly focused on the difference between electron and positron elastic scattering on the proton (for a review, see[55]). The precision of the data does not allow to see the evidence of an effect lower than a few percent. Note that this is also the size of those radiative corrections which contain odd terms. Presently, many efforts are devoted to precise measurements of the difference between $e^{\pm}p$ elastic scattering at Novosibirsk, JLab and DESY.

One should also note that no experimental evidence of $2\gamma$ echange (more exactly, of the real part of the $1\gamma \bigotimes 2\gamma$ interference) has been found in the experimental data, searching for non linearities in the Rosenbluth plots for electron elastic scattering on particles with spin zero,[56] one half,[57] and one.[31] An analysis of asymmetry in the angular distributions for the BABAR data[9] also does not show evidence of two photon contribution, in the limit of the uncertainty of the data.[58]

Let us stress that the main advantage of the search of $2\gamma$ in TL region is that the information is fully contained in the angular distribution (which is equivalent to the charge asymmetry). In the same measurement, the odd terms corresponding to two photon exchange can be singled out (whereas in SL region, in case of two photon exchange it is necessary to measure electron and positron scattering, in the same kinematical conditions). Two photon exchange effects cancel if one does not measure the charge of the outgoing lepton, or in the sum of the cross section at complementary angles, allowing to extract the moduli of the true FFs.[33]

### 5.1. *Helicity amplitudes for binary reactions with spins* $1/2 + 1/2 \to 1/2 + 1/2$

| N | 1/2 | 1/2 | → | 1/2 | 1/2 | N | 1/2 | 1/2 | → | 1/2 | 1/2 |
|---|---|---|---|---|---|---|---|---|---|---|---|
| 1) | + | + | → | + | + | 9) | - | + | → | + | + |
| 2) | + | + | → | + | - | 10) | - | + | → | + | - |
| 3) | + | + | → | - | + | 11) | - | + | → | - | + |
| 4) | + | + | → | - | - | 12) | - | + | → | - | - |
| 5) | + | - | → | + | + | 13) | - | - | → | + | + |
| 6) | + | - | → | + | - | 14) | - | - | → | + | - |
| 7) | + | - | → | - | + | 15) | - | - | → | - | + |
| 8) | + | - | → | - | - | 16) | - | - | → | - | - |

The total number of amplitudes for a binary reaction is $(2S_1+1)(2S_2+1)(2S_3+1)(2S_4+1)$, where $S_i$, $i = 1-4$, is the spin of the $i$- particle involved, see Table 5. However, not all of them are independent, but they are related by symmetry properties:

- Parity conservation: it implies the identity of the amplitudes obtained when reversing all spins: it reduces the number of amplitudes from $16 \to 8$.
- Identity of initial and final states: it gives two more conditions: 2=5, 3=9=8 (9 was already equal to 8).

We are left with 16/2-2=6 amplitudes. In Table 6, they are classified with, in the right column, the ones which require a spin-flip of the projectile.

In case of high energy electrons (where $m_e/E\Lambda\overline{\Lambda}1$), helicity conservation strongly suppress the amplitudes 4-6. The amplitudes 1 and 3 correspond to $\Delta S = 0$, the amplitudes 2,4-6 correspond to $\Delta S = 1$. This require $L = 0$ and $L = 1$, respectively, in order to conserve parity.

This analysis is better done in the annihilation channel. For illustration, let us consider firstly the one-photon mechanism for $e^+ + e^- \to p + \overline{p}$. The conservation of the total angular momentum $\mathcal{J}$ allows only one value, $\mathcal{J} = 1$, and the quantum numbers of the photon.

The selection rules with respect to the C- and P invariances allow two states for $e^+e^-$ (and $p\overline{p}$):

$$S = 1,\ \ell = 0 \text{ and } S = 1,\ \ell = 2 \text{ with } \mathcal{J}^P = 1^-, \tag{111}$$

| N | e | p | → | e | p | N | e | p | → | e | p |
|---|---|---|---|---|---|---|---|---|---|---|---|
| 1) | + | + | → | + | + | 4) | + | + | → | - | + |
| 2) | + | + | → | + | - | 5) | + | + | → | - | - |
| 3) | + | - | → | + | - | 6) | + | - | → | - | + |

where $S$ is the total spin and $\ell$ is the orbital angular momentum of the $e^+ + e^-$ system. As a result the $\theta$ dependence of the cross section for $e^+ + e^- \to \overline{p} + p$, in the one-photon exchange mechanism must have the following general form:

$$\frac{d\sigma}{d\Omega}(e^+ + e^- \to \overline{p} + p) \simeq a(t) + b(t)\cos^2\theta, \tag{112}$$

where $a(t)$ and $b(t)$ are definite quadratic contributions of $G_E(t)$ and $G_M(t)$, $a(t)$ and $b(t) \geq 0$ at $t \geq 4M_p^2$.

Using the kinematical relation (see below):

$$\cos^2\theta = \frac{1+\epsilon}{1-\epsilon} = \frac{\cot^2\theta_e/2}{1+\tau} + 1 \tag{113}$$

between the variables in the CMS of $e^+ + e^- \to \overline{p} + p$ and in the LAB system for $e^- + p \to e^- + p$, it appears clearly that the one-photon mechanism generates a linear $\epsilon$ dependence (or $\cot^2\theta_e/2$) of the Rosenbluth differential cross section for elastic $ep$-scattering in Lab system.

Similarly, let us consider the $\cos\theta$ dependence of the $1\gamma \bigotimes 2\gamma$-interference contribution to the differential cross section of $e^+ + e^- \to \overline{p} + p$. The spin and parity of the $2\gamma$-states is not fixed, in general, but only a positive value of C-parity, $C(2\gamma) = +1$, is allowed. An infinite number of states with different quantum numbers (for $e^+ + e^-$ and $\overline{p} + p$) can contribute, and their relative role is determined by the dynamics of the process $\gamma^* + \gamma^* \to \overline{p} + p$, with both virtual photons.

But the $\cos\theta$ dependence of the $1\gamma \otimes 2\gamma$ interference contribution to the differential cross section can be predicted on the basis of its C-odd nature:

$$\frac{d\sigma^{(int)}}{d\Omega}(e^+ + e^- \to \overline{p} + p) = \cos\theta[c_0(t) + c_1(t)\cos^2\theta + c_2(t)\cos^4\theta + ...], \tag{114}$$

where $c_i(t)$, $i = 0, 1..$ are real coefficients, which are functions of $t$, only. This odd $\cos\theta$ dependence is essentially different from the even $\cos\theta$ dependence of the cross section for the one-photon approximation.

#### 5.1.1. *Kinematical relation between Lab electron-scattering angle in $e + p \to e + p$ and CMS antiproton angle in $\overline{p} + p \to e^+ + e^-$*

Let us prove the following relation

$$\cos^2\theta = \frac{1+\epsilon}{1-\epsilon} = \frac{\cot^2\theta_e/2}{1+\tau} + 1, \tag{115}$$

where $\theta_e$ is the laboratory scattering angle of the electron in elastic $ep$ scattering and $\theta$ is the CMS angle of the antiproton produced in the annihilation: $e^- + e^+ \to \overline{p} + p$ with respect to the beam direction.

This kinematical relation shows clearly the physical link between the linear $\epsilon$ dependence of the Rosenbluth differential cross section for elastic $ep$-scattering in Lab system (or $\cot^2\theta_e/2$) and the even distribution in $\cos^2\theta$ for the differential annihilation cross section in $\overline{p} + p \leftrightarrow e^+ + e^-$.

Crossing symmetry allows to connect scattering and annihilation channels (change a particle into antiparticle, change sign to the momenta):

$$e^-(k_1) + p(p_1) \to e^-(k_2) + p(p_2),\ e^-(k_1) + e^+(-k_2) \to \overline{p}(-p_1) + p(p_2).$$

(1) Let us calculate $s$ and $t$ in the scattering channel:

$$s = (p_1 + k_1)^2 = M_p^2 + 2\epsilon_1 M_p = M_p(M_p + 2\epsilon_1) \to \epsilon_1 = \frac{s - M_p^2}{2M_p}; \tag{116}$$

$$t = (k_1 - k_2)^2 = k_1^2 + k_2^2 - 2\epsilon_1\epsilon_2 + 2|\mathbf{k}_1||\mathbf{k}_2|\cos\theta_e = -4\epsilon_1\epsilon_2\sin^2\frac{\theta_e}{2}. \tag{117}$$

where we assumed $m_e = 0$ and we calculate $t$ as function of the electron variables.

(2) The energy and momentum conservation are: $\epsilon_1 + M_p = \epsilon_2 + E_2;\ \mathbf{k}_1 = \vec{k}_2 + \mathbf{p}_2;$

(3) Let us express $t$ from the hadron variables:

$$t = (p_2 - p_1)^2 = 2M_p^2 - 2M_pE_2 = 2M_p^2 - 2M_p(\epsilon_1 + M_p - \epsilon_2) = 2M_p(\epsilon_2 - \epsilon_1). \tag{118}$$

From the equality of Eqs. (117) and (118):

$$t = 2M_p(\epsilon_2 - \epsilon_1) = -4\epsilon_1\epsilon_2\sin^2\frac{\theta}{2}. \tag{119}$$

Hence

$$\epsilon_2 = \frac{\epsilon_1}{1 + 2\dfrac{\epsilon_1}{M_p}\sin^2\dfrac{\theta}{2}} = \frac{M_p(s - M_p^2)}{2\left[M_p^2 + (s - M_p^2)\sin^2\dfrac{\theta}{2}\right]}. \tag{120}$$

(4) Inserting the expression of $\epsilon_1$ and $\epsilon_2$ as a functions of $s$ in Eq. 118:

$$\frac{1}{t} = -\frac{M_p^2}{(s - M_p^2)^2\sin^2\dfrac{\theta}{2}} - \frac{1}{s - M_p^2}. \tag{121}$$

(5) In the annihilation channel (CMS) one has $\tilde{\epsilon}_1 = \tilde{\epsilon}_2 = \tilde{E}_1 = \tilde{E}_2 = \epsilon$; $\mathbf{k}_1 = -\mathbf{k}_2 = \mathbf{k}$, $\mathbf{p}_1 = -\mathbf{p}_2 = \mathbf{p} \neq \mathbf{k}$:

$$s = (k_1 - p_2)^2 = M_p^2 - 2\tilde{\epsilon}_1^2 + 2\tilde{\epsilon}_2\vec{p}_2\cos\tilde{\theta} \tag{122}$$

$$t = (k_1 + k_2)^2 = 2\tilde{\epsilon}_1^2 - 2\tilde{\epsilon}_1\tilde{\epsilon}_2\cos\widehat{k_1k_2} = 4\tilde{\epsilon}_1^2, \tag{123}$$

from where we find the expression of $\cos\tilde{\theta}$ as a function of the invariants $s$ and $t$:

$$\cos\tilde{\theta} = \frac{s - M_p^2 + 2\tilde{\epsilon}^2}{2\tilde{\epsilon}\sqrt{\tilde{\epsilon}^2 - M_p^2}} \ \to\ \cos^2\tilde{\theta} = \frac{(s - M_p^2)^2 + ts}{t\left(\dfrac{t}{4} - M_p^2\right)} + 1. \tag{124}$$

Reminding that $\tau = -t/(4M_p^2)$, one finds

$$t\left(\frac{t}{4} - M_p^2\right) = -M_p^2 t(\tau + 1). \tag{125}$$

Inserting the relation $\left(\sin^2\dfrac{\theta}{2}\right)^{-1} = \cot^2\dfrac{\theta}{2} + 1$ in Eq. (121), one finds

$$\cot^2\frac{\theta}{2} = \frac{(s - M_p^2)^2 + ts}{-M_p^2 t}. \tag{126}$$

(6) Comparing Eqs. (126) and (124) with the help of (125) one verifies the relation Eq. (115).

## 5.2. *Two photon exchange for ep scattering*

The exact calculation of the $2\gamma$-contribution to the amplitude of the $e^{\pm}p \to e^{\pm}p$-process requires the knowledge of the matrix element for the double virtual Compton scattering, $\gamma^* + p \to \gamma^* + p$, in a large kinematical region of colliding energy and virtuality of both photons, and can not be done in a model independent form. However general properties of the hadron electromagnetic interaction, as C-invariance and crossing symmetry, give rigorous prescriptions for different observables for the elastic scattering of electrons and positrons by nucleons, in particular for the differential cross section and for the proton polarization, induced by polarized electrons. These concrete prescriptions help in identifying a possible manifestation of the two-photon exchange mechanism. For example, assuming a linear $\epsilon$ dependence of the elastic cross section in presence of $2\gamma$-corrections is in contradiction with the C-invariance of the electromagnetic interaction ($\epsilon$ is the degree of polarization of the virtual photon).

If one takes into account the two-photon mechanism, the expressions of the matrix element and of the differential cross section, are essentially modified.

It is required, first of all, a generalization of the spin structure of the matrix element, which can be done, in analogy with elastic $np$-scattering,[59] using the general properties of the electron-hadron interaction, such as P-invariance and relativistic invariance.

Taking into account the identity of the initial and final states and the T-invariance of the electromagnetic interaction, we showed above that the processes $e^{\pm}N \to e^{\pm}N$, in which four particles with spin 1/2 participate, are characterized by six independent products of four-spinors, describing the initial and final fermions. The corresponding (model independent) parametrization of the matrix element can be done in many different but equivalent forms, in terms of six invariant complex amplitudes, $\mathcal{A}_i(s, Q^2)$, $i = 1-6$, which are functions of two independent variables, and $s = (k_1 + p_1)^2$ is the square of the total energy of the colliding particles. In the physical region of the reaction $e^{\pm}N \to e^{\pm}N$ the conditions: $Q^2 \geq 0$ and $s \geq (M_p + m_e)^2 \simeq M_p^2$, apply.

Previously, another set of variables, $\epsilon$ and $Q^2$, which is equivalent to $s$ and $Q^2$ (in Lab system) was considered. The variables $\epsilon$ and $Q^2$ are well adapted to the description of the properties of one-photon exchange for elastic $eN$-scattering, because, in this case, only the $Q^2$ dependence of the form factors has a dynamical origin, whereas the linear $\epsilon$ dependence in Eq. (88) is a trivial consequence of the one-photon mechanism. On the other hand, the variables $s$ and $Q^2$ are better suited to the analysis of the implications from crossing symmetry.

The conservation of the lepton helicity, which is a general property of the electromagnetic interaction in electron-hadron scattering at high energy, reduces the number of invariant amplitudes for elastic $eN$-scattering, in general complex functions of $s$ and $Q^2$, from six to three.

Therefore, we can write the following general parametrization of the spin structure of the matrix element for elastic $eN$-scattering, following the formalism of:[59]

$$\mathcal{M} = \frac{e^2}{Q^2}\overline{u}(k_2)\gamma_\mu u(k_1)\overline{u}(p_2)$$

$$\left[\mathcal{A}_1(s,Q^2)\gamma_\mu - \mathcal{A}_2(s,Q^2)\frac{\sigma_{\mu\nu}q_\nu}{2M_p} + \mathcal{A}_3(s,Q^2)\hat{K}\mathcal{P}_\mu\right]u(p_1), \tag{127}$$

$$K = \frac{k_1+k_2}{2},\ \mathcal{P} = \frac{p_1+p_2}{2},$$

where $\mathcal{A}_1 - \mathcal{A}_3$ are the corresponding invariant amplitudes.

In case of one-photon exchange these amplitudes are related to the nucleon form factors:

$$\mathcal{A}_1(s,Q^2) \to F_1(Q^2),\ \mathcal{A}_2(s,Q^2) \to F_2(Q^2),\ \mathcal{A}_3(s,Q^2) \to 0.$$

But in the general case (with multi-photon exchanges) the situation is more complicated, because:

- The amplitudes $\mathcal{A}_i(s,Q^2)$, $i=1-3$, are complex functions of two independent variables, $s$ and $Q^2$.
- The set of amplitudes $\mathcal{A}_i^{(-)}(s,Q^2)$ for the process $e^-+N\to e^-+N$ is different from the set $\mathcal{A}_i^{(+)}(s,Q^2)$ of corresponding amplitudes for positron scattering, $e^++N\to e^++N$, which means that the properties of positron scattering can not be derived from $\mathcal{A}_i^{(-)}(s,Q^2)$, as in case of the one-photon mechanism.
- The connection of the amplitudes $\mathcal{A}_i(s,Q^2)$ with the nucleon electromagnetic form factors, $F_{iN}(Q^2)$, is non-trivial, because these amplitudes depend on a large number of different quantities, as, for example, the form factors of the $\Delta$-excitation - through the amplitudes of the virtual Compton scattering.

In this framework, the simple and transparent phenomenology of electron-hadron physics does not hold anymore, and in particular, it would be very difficult to extract information on the internal structure of a hadron in terms of electromagnetic form factors, which are real functions of one variable, from electron scattering experiments.

It has been proved that even in case of two-photon exchange, one can still use the formalism of form factors, taking into account the C-invariance of the electromagnetic interaction of hadrons.

The spin structure of the amplitudes $\mathcal{A}_1$ and $\mathcal{A}_2$ corresponds to exchange by vector particle (in $t$-channel), whereas the spin structure for the amplitude $\mathcal{A}_3$ corresponds to tensor exchange. Therefore, in case of $e^\pm N$–elastic scattering, in the $1\gamma+2\gamma$ approximation, one can write the amplitudes $\mathcal{A}_{1,2}^{(\pm)}(s,Q^2)$ in the following form:

$$\mathcal{A}_{1,2}^{(\pm)}(s,Q^2)=\mp F_{1,2N}(Q^2)+\Delta\mathcal{A}_{1,2}^{(\pm)}(s,Q^2),$$

$$\Delta\mathcal{A}_{1,2}^{(+)}(s,Q^2)=\Delta\mathcal{A}_{1,2}^{(-)}(s,Q^2)\equiv\Delta\mathcal{A}_{1,2}(s,Q^2),$$

$$\mathcal{A}_{3}^{(+)}(s,Q^2)=\mathcal{A}_{3}^{(-)}(s,Q^2)\equiv\mathcal{A}_{3}(s,Q^2),$$

where the superscript $(\pm)$ corresponds to $e^{(\pm)}$ scattering. The amplitudes $\Delta\mathcal{A}_{1,2}(s,Q^2)$ and $\mathcal{A}_3(s,Q^2)$ contain only the $2\gamma$-contribution, and are equal for $e^{(\pm)}$ scattering; $\Delta\mathcal{A}_{1,2}$ and $\mathcal{A}_3$ are of the order of $\alpha$, $\alpha=e^2/(4\pi)=1/137$.

Note that the difference in the spin structure of these amplitudes, Eq. (127), results in specific symmetry properties with respect to the change $x\to -x$ $\left(x=\sqrt{\dfrac{1+\epsilon}{1-\epsilon}}\right)$:

$$\Delta\mathcal{A}_{1,2}(s,-x)=-\Delta\mathcal{A}_{1,2}(s,x),\mathcal{A}_3(s,-x)=+\mathcal{A}_3(s,x). \tag{128}$$

The $x$–odd behavior of $\Delta\mathcal{A}_{1,2}(s,x)$–contributions, corresponding to $2\gamma$-exchange with $C=+1$, results from the C-odd character of the two vector-like spin structures, $\gamma_\mu$ and $\sigma_{\mu\nu}q_\nu$.

To prove this, let us consider, in addition to C-invariance, crossing symmetry, which allows to connect the matrix elements for the cross-channels: $e^-+p\to e^-+p$, $s$–channel, and $e^++e^-\to\overline{p}+p$, $t$–channel. The transformation from $s$- to $t$-channel can be realized by the following substitution:

$$k_2\to -k_2,\ p_1\to -p_1,$$

and for the invariant variables:

$$s=(k_1+p_1)^2\to(k_1-p_1)^2,\ Q^2=-(k_1-k_2)^2\to-(k_1+k_2)^2=-t.$$

The crossing symmetry states that the same amplitudes $\mathcal{A}_i(s,Q^2)$ describe the two channels, when the variables $s$ and $Q^2$ scan the physical region of the corresponding channels. So, if $t\ge 4M_p^2$ and $-1\le\cos\theta\le 1$ ($\theta$ is the angle of the proton production with respect to the electron three-momentum, in the center of mass (CMS) for $e^+ + e^- \to \bar{p} + p$), the amplitudes $\mathcal{A}_i(t, \cos\theta)$, $i = 1 - 3$, describe the process $e^+ + e^- \to \bar{p} + p$.

From C-invariance it follows that:

$$\mathcal{A}_3(t, -\cos\theta) = \mathcal{A}_3(t, +\cos\theta), \Delta A_{1,2}(t, -\cos\theta) = -\Delta A_{1,2}(t, +\cos\theta), \tag{129}$$

which is equivalent to the symmetry relations (128).

Therefore, it is incorrect to approximate the $1\gamma \bigotimes 2\gamma$ interference contribution to the differential cross section, Eq. (114) by a linear function in $\cos^2\theta$ (what may be found in recent literature), because it is in contradiction with the C-invariance of hadronic electromagnetic interaction.

## 6. The annihilation channel $\bar{p} + p \to e^+ + e^-$

The measurement of the differential cross section for the process $\bar{p} + p \to \ell^+ + \ell^-$ at a fixed value of the total energy $s$, and for two different angles $\theta$, allows the separation of the two FFs, $|G_M|^2$ and $|G_E|^2$, and is equivalent to the Rosenbluth separation for the elastic $ep$-scattering. In TL region, this procedure is simpler, as it requires to change only one kinematical variable, $\cos\theta$, whereas, in SL region it is necessary to change simultaneously two kinematical variables: the energy of the initial electron and the electron scattering angle, fixing the momentum transfer squared, $Q^2$. Due to the limited statistics, the individual determination of the $|G_E|^2$ and $|G_M|^2$ contributions has not yet been realized in TL region.

In the TL region, the determination of a generalized FF requires to integrate the differential cross section over a wide angular range. One typically assumes that the $G_E$ contribution plays a minor role in the cross section at large $q^2$ and the experimental results are usually given in terms of $|G_M|$, under the hypothesis that $G_E = 0$ or $|G_E| = |G_M|$. The first hypothesis is an arbitrary one. The second hypothesis is strictly valid at threshold only, i.e., for $\tau = q^2/(4M_p^2) = 1$, but there is no theoretical argument which justifies its validity at any other momentum transfer, where $q^2 \neq 4M_N^2$ ($M_N$ is the nucleon mass, $N = p(n)$ for proton(neutron)). The $|G_M|$ values depend, in principle, on the kinematics where the measurement was performed and the angular range of integration. However, it turns out that these two assumptions for $G_E$ lead to comparable values for $|G_M|$.

In annihilation channel, it is more convenient to perform the calculatations in CMS.

### 6.1. *Observables for $\bar{p} + p \to e^+ + e^-$*

The derivation given below is simplified by the use of $2 \times 2$ Pauli matrix, and 2-rank spinors, instead of $4 \times 4$ Dirac matrices and 4-rank spinors. It is a rigorous and simple derivation. The full derivation in the Dirac formalism can be found in Ref.[60]

Let us consider the annihilation reaction

$$\bar{p}(p_1) + p(p_2) \to e^-(k_1) + e^+(k_2) \tag{130}$$

in the CMS system, where an antiproton with three-momentum $\mathbf{p_1} = \mathbf{p}$ annihilates with a proton with three-momentum $\mathbf{p}_2 = -\mathbf{p}$. The transferred momentum is $t = s = (k_1 + k_2)^2 = 4E^2$ and (assuming $m_e = 0$) one has $\mathbf{k} = \mathbf{k_1} = -\mathbf{k_2}$; $E = |\mathbf{k}|$. We choose a reference system with the $z$ axis along the beam momentum, and $xz$ is the scattering plane. In this system the unit vectors are: $\mathbf{p} = (0, 0, 1)$ and $\mathbf{k} = (\sin\theta, 0, \cos\theta)$, with $\mathbf{p} \cdot \mathbf{k} = \cos\theta$.

The following relation holds (neglecting the electron mass):

$$\frac{\vec{\sigma} \cdot \mathbf{k}}{E + m_e} = \frac{\vec{\sigma} \cdot \mathbf{k}}{|\mathbf{k}|} = \vec{\sigma} \cdot \mathbf{k} \tag{131}$$

The starting point of the analysis of the reaction $\bar{p} + p \to e^+ + e^-$ is the standard expression of the matrix element in framework of one-photon exchange mechanism:

$$\mathcal{M} = \frac{e^2}{q^2}\bar{v}(k_2)\gamma_\mu u(k_1)\bar{u}(p_2)J_\mu v(p_1), \tag{132}$$

with

$$J_\mu = \left[F_1(q^2)\gamma_\mu - \frac{\sigma_{\mu\nu}q_\nu}{2M_p}F_2(q^2)\right] = \left[F_1(q^2) + F_2(q^2)\right]\gamma_\mu - \frac{(-p_1+p_2)_\mu}{2M_p}F_2(q^2),$$

where $p_1$, $p_2$, $k_1$ and $k_2$ are the four-momenta of initial antiproton and proton and the final electron and positron respectively, $q^2 > 4M_p^2$, $q = k_1 + k_2 = p_1 + p_2$. $F_1$ and $F_2$ are the Dirac and Pauli nucleon electromagnetic FFs, which are complex functions of the variable $q^2$ - in the TL region of momentum transfer.

In framework of one-photon exchange, the matrix element is written as the product of the leptonic and hadronic currents:

$$\mathcal{M} = \frac{e^2}{q^2}L_\mu J_\mu = \frac{e^2}{q^2}(L_0 J_0 - \vec{L}\cdot\vec{J}) = -\frac{e^2}{q^2}\vec{L}\cdot\vec{J}, \tag{133}$$

where $L_0 J_0 = 0$, due to the conservation of the leptonic and hadronic currents. The conservation of the current implies that $L \cdot q = 0$, i.e., $L_0 q_0 - \vec{L}\cdot\vec{q} = 0$, but $\mathbf{q} = \mathbf{k_1} + \mathbf{k_2} = 0$ in CMS. Therefore, $L_0 q_0 = 0$ for any energy $q_0$, i.e., $L_0 = 0$.

Let us reduce the expressions of the current in terms of $\sigma$ (Pauli) matrices instead of Dirac $\gamma$ matrices $J_\mu \to \varphi_2 \tilde{J}_\mu \varphi_1$ (we keep in mind a global factor $(E + M_p)$).

$$\begin{aligned}
J_\mu &= (F_1+F_2)\left(\varphi_2,\ -\frac{\vec{\sigma}\cdot(-\mathbf{p})}{E+M_p}\varphi_2\right)\begin{pmatrix}1 & 0\\ 0 & -1\end{pmatrix}\begin{pmatrix}0 & \vec{\sigma}\\ -\vec{\sigma} & 0\end{pmatrix}\begin{pmatrix}\dfrac{\vec{\sigma}\cdot\mathbf{p}}{E+M_p}\varphi_1\\ \varphi_1\end{pmatrix}\\
&\quad+\left(\varphi_2,\ \frac{\vec{\sigma}\cdot(-\mathbf{p})}{E_1+M_p}\varphi_2\right)\begin{pmatrix}1 & 0\\ 0 & -1\end{pmatrix}\frac{2\mathbf{p}}{2M_p}F_2\begin{pmatrix}\dfrac{\vec{\sigma}\cdot\mathbf{p}}{E_1+M_p}\varphi_1\\ \varphi_1\end{pmatrix}\\
&= (F_1+F_2)\left(\varphi_2,\ \frac{\vec{\sigma}\cdot\mathbf{p}}{E+M_p}\varphi_2\right)\begin{pmatrix}\vec{\sigma}\varphi_1\\ -\vec{\sigma}\dfrac{\vec{\sigma}\cdot\mathbf{p}}{E+M_p}\varphi_1\end{pmatrix}\\
&\quad+\frac{\mathbf{p}}{M_p}F_2\varphi_2\left(\frac{\vec{\sigma}\cdot\mathbf{p}}{E+m}+\frac{\vec{\sigma}\cdot\mathbf{p}}{E+M_p}\right)\varphi_1\\
&= (F_1+F_2)\left[\vec{\sigma} - \frac{1}{(E+M_p)^2}\vec{\sigma}\cdot\mathbf{p}\vec{\sigma}\vec{\sigma}\cdot\mathbf{p}\right] + \frac{2\mathbf{p}}{M_p}F_2\varphi_2\frac{\vec{\sigma}\cdot\mathbf{p}}{E+M_p}\varphi_1.
\end{aligned} \tag{134}$$

Using the relation $p^2 = E^2 - M_p^2$, introducing the unit vectors $\hat{\mathbf{p}}$ and applying the following properties of $\sigma$ matrices:

$$(2\hat{\mathbf{p}} - \vec{\sigma}\vec{\sigma}\cdot\hat{\mathbf{p}})\vec{\sigma}\cdot\hat{\mathbf{p}} = 2\hat{\mathbf{p}}\vec{\sigma}\cdot\hat{\mathbf{p}} - \vec{\sigma},$$

one finds

$$
\begin{aligned}
J_\mu &= (F_1+F_2)\left(\vec{\sigma} - 2\frac{E-M_p}{E+M_p}\hat{\mathbf{p}}\vec{\sigma}\cdot\hat{\mathbf{p}} + \frac{E-M_p}{E+M_p}\vec{\sigma}\right) + \frac{2(E-M_p)}{M_p}F_2\hat{\mathbf{p}}\vec{\sigma}\cdot\hat{\mathbf{p}} \\
&= (F_1+F_2)\left(\vec{\sigma} + \frac{E-M_p}{E+M_p}\vec{\sigma}\right) - 2\left[(F_1+F_2)\frac{E-M_p}{E+M_p} - \frac{E-M_p}{M_p}F_2\right]\hat{\mathbf{p}}\vec{\sigma}\cdot\hat{\mathbf{p}} \\
&= \frac{2E}{E+M_p}(F_1+F_2)\vec{\sigma} - \frac{2(E-M_p)}{M_p(E+M_p)}[M_pF_1+M_pF_2-EF_2-M_pF_2]\hat{\mathbf{p}}\vec{\sigma}\cdot\hat{\mathbf{p}} \\
&= \frac{2E}{E+M_p}(F_1+F_2)\vec{\sigma} - 2E(F_1+F_2)\hat{\mathbf{p}}\vec{\sigma}\cdot\hat{\mathbf{p}} + 2M_p\left(F_1+\frac{E^2}{M_p^2}F_2\right) \\
&= \frac{2E}{E+M_p}\left[G_M(\vec{\sigma}-\hat{\mathbf{p}}\vec{\sigma}\cdot\hat{\mathbf{p}})\right] + 2M_pG_E\hat{\mathbf{p}}\vec{\sigma}\cdot\hat{\mathbf{p}}.
\end{aligned}
$$

Finally (reminding the global factor) we find for the hadronic current:

$$\vec{J} = \sqrt{q^2}\varphi_2^\dagger\left[G_M(q^2)(\vec{\sigma}-\hat{\mathbf{p}}\vec{\sigma}\cdot\hat{\mathbf{p}}) + \frac{1}{\sqrt{\tau}}G_E(q^2)\hat{\mathbf{p}}\vec{\sigma}\cdot\hat{\mathbf{p}}\right]\varphi_1, \tag{135}$$

where $\varphi_1$ and $\varphi_2$ are the two-component spinors of the antiproton and the proton, $\hat{\mathbf{p}}$ is the unit vector along the three momentum of the antiproton in CMS. The expression for the leptonic current is:

$$\vec{L} = \sqrt{q^2}\varphi_2^\dagger(\vec{\sigma}-\hat{\mathbf{k}}\vec{\sigma}\cdot\hat{\mathbf{k}})\varphi_1, \tag{136}$$

where $\varphi_1(\varphi_2)$ is the two-component spinor of the electron (positron), $\hat{\mathbf{k}}$ is the unit vector along the final electron three-momentum.

Note that Eq. (136) holds for the production of unpolarized lepton (sum over the lepton polarization). From this expression one can see the physical meaning of the particular relation between the nucleon electromagnetic FFs at threshold:

$$G_E(q^2) = G_M(q^2),\ q^2 = 4M_p^2.$$

The structure $\hat{\mathbf{p}}\vec{\sigma}\cdot\hat{\mathbf{p}}$ describes the $\overline{p}+p$ annihilation from $D$-wave, i.e., with angular momentum $\ell$=2. At threshold, where $\tau \to 1$, the finite radius of the strong interaction allows only the S-state, and $G_M(q^2) - \frac{1}{\sqrt{\tau}}G_E(q^2) = 0$.

From Eqs. (133), (136), and (135) one can find the formulas for the unpolarized cross section, the angular asymmetry and all the polarization observables.

### 6.2. *The cross section*

To calculate the cross section when all particles are unpolarized, one has to sum over the polarization of the final particles and to average over the polarization of initial particles:

$$\left(\frac{d\sigma}{d\Omega}\right)_0 = \frac{|\overline{\mathcal{M}}|^2}{64\pi^2q^2}\frac{|\mathbf{k}|}{|\mathbf{p}|},\ |\mathbf{k}| = \frac{\sqrt{q^2}}{2},\ |\mathbf{p}| = \sqrt{\frac{q^2}{4}-M_p^2},$$

$$
\begin{aligned}
|\overline{\mathcal{M}}|^2 &= \frac{1}{4}\frac{e^4}{q^4}L_{ab}J_{ab},\ L_{ab} = L_aL_b^*,\ J_{ab} = J_aJ_b^*. \\
\overline{L_{ab}} &= \overline{L_aL_b^*} \sim Tr(\sigma_a - \hat{k}_a\vec{\sigma}\cdot\mathbf{k})(\sigma_b-\hat{k}_b\vec{\sigma}\cdot\mathbf{k}) = 2(\delta_{ab}-k_ak_b).
\end{aligned} \tag{137}
$$

Let us decompose the contribution to $\mathcal{M}$ in four terms classifying along FFs:
1) - $|G_M|^2$:

$$\frac{1}{2}Tr(\sigma_a - p_a\vec{\sigma}\cdot\mathbf{p})(\sigma_b - p_b\sigma\cdot p) =$$
$$\delta_{ab} - \sigma_a p_a p_b\vec{\sigma}\cdot\mathbf{p} - p_a\vec{\sigma}\cdot\mathbf{p}\sigma_b + p_a p_b\vec{\sigma}\cdot\mathbf{p}\vec{\sigma}\cdot\mathbf{p} = \delta_{ab} - p_a p_b. \tag{138}$$

Therefore $|G_M|^2$ contributes to the cross section with:

$$(\delta_{ab} - p_a p_b)(\delta_{ab} - k_a k_b) = \delta_{ab}\delta_{ab} - p^2 - k^2 - (\mathbf{p}\cdot\mathbf{k}) = 3 - 1 - 1 + \cos^2\theta. \tag{139}$$

2) - The term $G_E G_M^*$ vanishes:

$$\frac{1}{2}Tr(p_a\vec{\sigma}\cdot\mathbf{p}\sigma_b - p_a p_b\vec{\sigma}\cdot\mathbf{p}\vec{\sigma}\cdot\mathbf{p}) = \frac{1}{2}(p_a p_b - p_a p_b) = 0. \tag{140}$$

3) - The term $G_M G_E^*$ similarly vanishes:

$$\frac{1}{\tau}p_a\vec{\sigma}\cdot\mathbf{p}(\sigma_b - p_b\vec{\sigma}\cdot\mathbf{p}). \tag{141}$$

This shows that no interference term will be present in the cross section.
4) - $|G_E|^2$:

$$(\sigma_a - p_a\sigma\cdot p)(\sigma_b - p_b\sigma\cdot p) = \frac{1}{\sqrt{\tau}}\vec{\sigma}\cdot\mathbf{p}\frac{1}{\sqrt{\tau}}\vec{\sigma}\cdot\mathbf{p} = \frac{1}{\sqrt{\tau}}p_a p_b \tag{142}$$

Therefore $|G_E|^2$ contributes to the cross section with:

$$\frac{1}{\sqrt{\tau}}p_a p_b(\delta_{ab} - k_a k_b) = \frac{1}{\sqrt{\tau}}[1 - (\mathbf{p}\cdot\mathbf{k})^2] = \frac{1}{\tau}(1 - \cos^2\theta) = \frac{1}{\tau}\sin^2\theta. \tag{143}$$

We took into account the properties of $\sigma$ matrices: $\vec{\sigma}\cdot\mathbf{p}\vec{\sigma}\cdot\mathbf{p} = p^2 = 1$, and $Tr\vec{\sigma}\cdot\vec{a}\vec{\sigma}\cdot\vec{b}\vec{\sigma}\cdot\vec{c} = i\vec{a}\cdot\vec{b}\times\vec{c}$.

Using the expressions (136) and (135), the formula for the cross section in CMS is:

$$\left(\frac{d\sigma}{d\Omega}\right)_0 = \mathcal{N}\left[(1 + \cos^2\theta)|G_M|^2 + \frac{1}{\tau}\sin^2\theta|G_E|^2\right], \tag{144}$$

where $\mathcal{N} = \dfrac{\alpha^2}{4\sqrt{q^2(q^2 - 4M_p^2)}}$, $\alpha = e^2/(4\pi) \simeq 1/137$, is a kinematical factor. This formula was firstly obtained in Ref.[22] Note that the normalization factor is inessential for the calculation of the polarization phenomena.

The angular dependence of the cross section, Eq. (144), results directly from the assumption of one-photon exchange, where the photon has spin 1 and the electromagnetic hadron interaction satisfies the $P-$invariance. Therefore, the measurement of the differential cross section at three angles (or more) would also allow to test the presence of $2\gamma$ exchange.

The electric and the magnetic FFs are weighted by different angular termss in the cross section, Eq. (144). One can define an angular asymmetry, $\mathcal{R}$, with respect to the differential cross section measured at $\theta = \pi/2$ :

$$\left(\frac{d\sigma}{d\Omega}\right)_0 = \sigma(\theta = \pi/2)\left[1 + \mathcal{R}\cos^2\theta\right], \tag{145}$$

where $\mathcal{R}$ can be expressed as a function of FFs:

$$\mathcal{R} = \frac{\tau|G_M|^2 - |G_E|^2}{\tau|G_M|^2 + |G_E|^2}. \tag{146}$$

This observable should be very sensitive to the different underlying assumptions on FFs, therefore, a precise measurement of this quantity, which does not require polarized particles, would be very interesting. A deviation of the differential cross section from a linearity in $\cos^2\theta$ would be the signature of mechanisms beyond one photon exchange (similarly to a deviation form linearity in the Rosenbluth plot).

The $q^2$ dependence of the total cross section can be presented as follows:

$$\sigma(q^2) = \mathcal{N}\frac{8}{3}\pi\left[2|G_M|^2 + \frac{1}{\tau}|G_E|^2\right]. \tag{147}$$

### 6.3. *Polarization observables*

Polarization phenomena will be especially important in $\bar{p} + p \to \ell^+ + \ell^-$.

The dependence of the cross section on the polarizations $\vec{P}_1$ and $\vec{P}_2$ of the colliding antiproton and proton can be written as follows:

$$\begin{aligned}\left(\frac{d\sigma}{d\Omega}\right)(\vec{P}_1, \vec{P}_2) = \left(\frac{d\sigma}{d\Omega}\right)_0 & [1 + A_y(P_{1y} + P_{2y}) + \\ & A_{xx}P_{1x}P_{2x} + A_{yy}P_{1y}P_{2y} + \\ & A_{zz}P_{1z}P_{2z} + A_{xz}(P_{1x}P_{2z} + P_{1z}P_{2x})],\end{aligned} \tag{148}$$

where the coefficients $A_i$ and $A_{ij}$ $(i, j = x, y, z)$, analyzing powers and correlation coefficients, depend on the nucleon FFs. Their explicit form is given below. The dependence (148) results from the P-invariance of hadron electrodynamics. The polarized hadronic tensor reads:

$$W_{ab}(\vec{P}_1, \vec{P}_2) = \frac{1}{2}TrJ_a\vec{\sigma}\cdot\vec{P}_1 J_b^*\vec{\sigma}\cdot\vec{P}_2$$

and the cross section with unpolarized electrons is proportional to $L_{ab}\overline{W_{ab}}$.

### 6.4. *Single spin polarization observables*

In case of polarized antiproton beam with polarization $\vec{P}_1$, the contribution to the cross section can be calculated as:

$$\begin{aligned}&\left(\frac{d\sigma}{d\Omega}\right)_0 \vec{A}_1 \sim -L_{ab}\frac{1}{4}TrJ_a\vec{\sigma}J_b^* = \\ &[(\sigma_a - p_a\vec{\sigma}\cdot\mathbf{p})G_M + \frac{1}{\tau}G_E p_a\vec{\sigma}\cdot\mathbf{p}](-\vec{\sigma}\cdot\vec{P}_1) \\ &[(\sigma_b - p_b\vec{\sigma}\cdot\mathbf{p})G_M^* + \frac{1}{\tau}G_E^* p_b\vec{\sigma}\cdot\mathbf{p}](\delta_{ab} - k_a K_b).\end{aligned} \tag{149}$$

(1) The term in $|G_M|^2$:

$$[1]: \ (\sigma_a - p_a\vec{\sigma}\cdot\mathbf{p})\vec{\sigma}\cdot\vec{P}_1(\sigma_b - p_b\vec{\sigma}\cdot\mathbf{p})\delta_{ab} - \tag{150}$$

$$[2]: \ (\sigma_a - p_a\vec{\sigma}\cdot\mathbf{p})\vec{\sigma}\cdot\vec{P}_1(\sigma_b - p_b\vec{\sigma}\cdot\mathbf{p})\hat{k}_a\hat{k}_b. \tag{151}$$

The first contribution (150) reduces to:

$$\begin{aligned}[1]: \quad & \sigma_a\vec{\sigma}\cdot\vec{P}_1\sigma_a - \sigma_a\vec{\sigma}\cdot\vec{P}_1 p_a\vec{\sigma}\cdot\mathbf{p} - p_a\vec{\sigma}\cdot\mathbf{p}\vec{\sigma}\cdot\vec{P}_1\sigma_a + p_a^2\vec{\sigma}\cdot\mathbf{p}\vec{\sigma}\cdot\vec{P}_1\vec{\sigma}\cdot\mathbf{p} \\ &= -p_a(a\cdot P_1\times\mathbf{p} + p\cdot P_1\times\vec{a}) + p_a^2\vec{\sigma}\cdot\vec{P}_1 = 0.\end{aligned}$$

The second contribution (151) becomes:

$$\begin{aligned}
[2]: \quad & (\vec\sigma\cdot\mathbf{k}-\mathbf{p}\cdot\mathbf{k}\vec\sigma\cdot\mathbf{p})\vec\sigma\cdot\vec P_1(\vec\sigma\cdot\mathbf{k}-\mathbf{p}\cdot\mathbf{k}\vec\sigma\cdot\mathbf{p})\\
& \vec\sigma\cdot\mathbf{k}\vec\sigma\cdot\vec P_1\vec\sigma\cdot\mathbf{k}-\vec\sigma\cdot\mathbf{k}\vec\sigma\cdot\vec P_1\mathbf{p}\cdot\mathbf{k}\vec\sigma\cdot\mathbf{p}-\\
& \mathbf{p}\cdot\mathbf{k}\vec\sigma\cdot\mathbf{p}\vec\sigma\cdot\vec P_1\vec\sigma\cdot\mathbf{k}+(\mathbf{p}\cdot\mathbf{k})^2\vec\sigma\cdot\mathbf{p}\vec\sigma\cdot\vec P_1\vec\sigma\cdot\mathbf{p}\\
& =-\cos\theta(\sigma\cdot\mathbf{k}\vec\sigma\cdot\vec P_1\vec\sigma\cdot\mathbf{p}+\sigma\cdot\mathbf{p}\sigma\cdot\vec P_1\sigma\cdot\mathbf{k}\\
& =-\cos\theta[(\mathbf{k}\cdot\vec P_1\times\mathbf{p}+\mathbf{p}\cdot\vec P_1\times\mathbf{k}]=0
\end{aligned}$$

due to the antisymmetric terms in first parenthesis and the fact that the $\sigma$ matrices have zero trace.

(2) The term $|G_E|^2$:

$$\frac{1}{\tau}\left[p_a\vec\sigma\cdot\mathbf{p}\vec\sigma\cdot\vec P_1p_a\vec\sigma\cdot\mathbf{p}-(\mathbf{p}\cdot\mathbf{k})^2\vec\sigma\cdot\mathbf{p}\vec\sigma\cdot\vec P_1\vec\sigma\cdot\mathbf{p}\right]=0.$$

(3) The term $G_MG_E^*$

$$\begin{aligned}
&\frac{1}{2}Tr\frac{1}{\tau}[(\sigma_a-p_a\vec\sigma\cdot\mathbf{p})\vec\sigma\cdot\vec P_1p_b\vec\sigma\cdot\mathbf{p}](\delta_{ab}-k_ak_b)\\
=&\frac{1}{\tau}[(\sigma_a-p_a\vec\sigma\cdot\mathbf{p})\vec\sigma\cdot\vec P_1p_a\vec\sigma\cdot\mathbf{p}-(\vec\sigma\cdot\mathbf{k}-\mathbf{p}\cdot\mathbf{k}\vec\sigma\cdot\mathbf{p}\vec\sigma\cdot\vec P_1\vec\sigma\cdot\mathbf{k}\vec\sigma\cdot\mathbf{p}].
\end{aligned}\tag{152}$$

Let us decompose explicitly the components:

$$\begin{aligned}
&\frac{1}{\tau}[(\sigma_x\vec\sigma\cdot\vec P_1p_x\sigma_z+\sigma_y\vec\sigma\cdot\vec P_1p_y\sigma_z)\\
&-(\sigma_x\sin\theta+\sigma_z\cos\theta-\sigma_z\cos\theta)\vec\sigma\cdot\vec P_1\cos\theta\sigma_z]\\
=&-\sigma_x\sin\theta\cos\theta\vec\sigma\cdot\vec P_1\sigma_z=-i\sin\theta\cos\theta P_{1y},
\end{aligned}$$

$$\boxed{G_MG_E^*\to-i\sin\theta\cos\theta P_{1y}}$$

(4) Similarly for the term in $G_EG_M^*$ one finds:

$$\begin{aligned}
&[p_a\vec\sigma\cdot\mathbf{p}\vec\sigma\cdot\vec P_1(\sigma_b-p_b\vec\sigma\cdot\mathbf{p})](\delta_{ab}-k_ak_b)\\
=&[p_a\vec\sigma\cdot\mathbf{p}\vec\sigma\cdot\vec P_1\vec\sigma_a-p_a\vec\sigma\cdot\mathbf{p}\vec\sigma\cdot\vec P_1p_a\vec\sigma\cdot\mathbf{p}-\\
&\mathbf{p}\cdot\mathbf{k}\vec\sigma\cdot\mathbf{p}\vec\sigma\cdot\vec P_1\vec\sigma\cdot\mathbf{k}-(\mathbf{p}\cdot\mathbf{k})^2\vec\sigma\cdot\mathbf{p}\vec\sigma\cdot\vec P_1\vec\sigma\cdot\mathbf{p}]\\
=&i[p_a\vec a\cdot\mathbf{p}\times\vec P_1-\cos\theta\mathbf{p}\cdot\vec P_1\times\mathbf{k}].
\end{aligned}$$

Let us calculate the mixte product:

$$\vec a\cdot\mathbf{p}\times\vec P_1\to p_x=p_y=0;zp_z\times P_1=0.$$

More explicitly:

$$\left(\begin{array}{c|ccc|}
p & 0 & 0 & 1\\
P & P_{1x} & P_{1y} & P_{1z}\\
k & \sin\theta & 0 & \cos\theta
\end{array}\right)$$

$$\boxed{G_EG_M^*\to\frac{i}{\sqrt{\tau}}\cos\theta\sin\theta P_{1y}}$$

In the calculation of the single spin polarization the terms related to $|G_E|^2$ and $|G_M|^2$ vanish. We add a global sign as the term for polarization of an antiparticle contains a "-" sign: $-\vec{\sigma}\cdot\mathbf{p}$.

For the interference terms, the only non zero analyzing power is related to the normal polarization $P_y$:

$$\left(\frac{d\sigma}{d\Omega}\right)_0 A_{1,y} = -\frac{i\mathcal{N}}{\sqrt{\tau}}\sin\theta\cos\theta[G_M G_E^* - G_E G_M^*] = \frac{\mathcal{N}}{\sqrt{\tau}}\sin 2\theta Im(G_M G_E^*). \tag{153}$$

Other observables can be obtained with some algebra in similar way. When the target is polarized, one writes:

$$\left(\frac{d\sigma}{d\Omega}\right)_0 \vec{A}_2 = L_{ab}\frac{1}{4}TrJ_aJ_b^*\vec{\sigma}.$$

Again the terms related to $|G_E|^2$ and $|G_M|^2$ vanish. Moreover, one can find $\vec{A}_2 = \vec{A}_1 = \vec{A}$.

Eq. (153) has been proved also in Ref.[22] One can see that this analyzing power, being T-odd, does not vanish in $\bar{p} + p \to \ell^+ + \ell^-$, even in one-photon approximation, due to the fact FFs are complex in time-like region. This is a principal difference with elastic $ep$ scattering. Let us note also that the assumption $G_E = G_M$ implies $A_y = 0$, independently from any model taken for the calculation of FFs.

### 6.5. *Double spin polarization observables*

The contribution to the cross section, when both colliding particles are polarized is calculated through the following expression:

$$\left(\frac{d\sigma}{d\Omega}\right)_0 A_{ab} = -\frac{1}{4}L_{mn}TrJ_m\sigma_a J_n^\dagger\sigma_b,$$

where $a$ and $b = x, y, z$ refer to the $a(b)$ component of the projectile (target) polarization. Among the nine possible terms, $A_{xy} = A_{yx} = A_{zy} = A_{yz} = 0$, and the nonzero components are:

$$\begin{aligned}
\left(\frac{d\sigma}{d\Omega}\right)_0 A_{xx} &= \sin^2\theta\left(|G_M|^2 + \frac{1}{\tau}|G_E|^2\right)\mathcal{N},\\
\left(\frac{d\sigma}{d\Omega}\right)_0 A_{yy} &= -\sin^2\theta\left(|G_M|^2 - \frac{1}{\tau}|G_E|^2\right)\mathcal{N},\\
\left(\frac{d\sigma}{d\Omega}\right)_0 A_{zz} &= \left[(1+\cos^2\theta)|G_M|^2 - \frac{1}{\tau}\sin^2\theta|G_E|^2\right]\mathcal{N},\\
\left(\frac{d\sigma}{d\Omega}\right)_0 A_{xz} &= \left(\frac{d\sigma}{d\Omega}\right)_0 A_{zx} = \frac{1}{\sqrt{\tau}}\sin 2\theta Re G_E G_M^*\mathcal{N}.
\end{aligned} \tag{154}$$

One can see that the double spin observables depend on the moduli squared of FFs, except $A_{xz}$ ($A_{zx}$). Therefore, in order to determine the relative phase of FFs, in TL region, the interesting observables are $A_y$, and $A_{xz}$, which contain respectively the imaginary and the real part of the product $G_E G_M^*$.

## 7. Conclusion

We have given here a formal derivation of unpolarized cross section and polarization observables for the case of $ep$ elastic scattering in the Breit system and $\bar{p}p$ annihilation into a (massless) lepton pair in CM system, where the calculation is simplified.

The results are model independent expressions of polarized and unpolarized experimental observables as functions of FFs, which hold in the assumption of one photon exchange mechanism taking into account the symmetries and the conservation laws of the electromagnetic and strong interactions.

Polarization observables play an important role as they are contain the interference of FFs, whereas only the moduli squared contribute to the unpolarized cross section.

The modelisation of the nucleon structure is contained in the parametrization of FFs. Different models have been developed in the recent years. In future, the interest will be focused on those models which can describe coherently all four nucleon FFs, proton and neutron, electric and magnetic, in SL and TL regions.

Precise data will strongly constrain nucleon models. Several experiments are planned or ongoing in electron accelerators as JLab, Mainz and colliders as Novosibirsk, BES, and Panda at FAIR. In SL region, the main purpose is to reach higher transferred momenta or better precisions. In TL region the individual determination of the electric and magnetic FFs at least in the region over threshold will be possible in next future. The measurements at the highest possible momentum transfer will allow to study asymptotic properties, where predictions exist from QCD and analyticity.

Search for effects beyond one photon exchange is object of a renewed experimental effort. The possibility to polarize antiprotons through spin filtering is also under investigation[61] opening the possibility to measure the relative phase of FFs in the time-like region.

## 8. Acknowledgments

Thanks are due to Paola Ferretti Dalpiaz, for a perfect organization of the School. All the participants are acknowledged for their stimulating remarks and discussions. These lectures are based on a work started in collaboration with M. P. Rekalo. Particular thanks are due to E.A. Kuraev for useful discussions when preparing these lectures. The author is grateful to G. I. Gakh, R. Kunne, J. Boucher, Binsong Ma for a patient work in reading the manuscript.

## References

1. A. I. Akhiezer and M. P. Rekalo, Dokl. Akad. Nauk USSR, **180**, 1081 (1968), [Soviet Physics - Doklady 13, 572 (1968)].
2. A. I. Akhiezer and M. P. Rekalo, Sov. J. Part. Nucl. **4**, 277 (1974)
3. N. Dombey, Phys. Lett. B **29**, 588 (1969).
4. M.N. Rosenbluth, Phys. Rev. **79**, 615 (1950).
5. C. F. Perdrisat, V. Punjabi, M. Vanderhaeghen, Prog. Part. Nucl. Phys. **59**, 694 (2007).
6. S. D. Drell and F. Zachariasen, *Oxford University Press, Belfast* (1961).
7. M. Ambrogiani *et al.* [E835 Collaboration], Phys. Rev. D **60**, 032002 (1999).
8. G. Bardin *et al.*, Nucl. Phys. B **411**, 3 (1994).
9. B. Aubert *et al.* [BABAR Collaboration], Phys. Rev. D **73**, 012005 (2006).
10. E. Tomasi-Gustafsson, F. Lacroix, C. Duterte and G. I. Gakh, Eur. Phys. J. A **24**, 419 (2005).
11. R. Hofstadter, Rev. Mod. Phys. **28**, 214-254 (1956).
12. E. Rutherford, Phil. Mag. **21**, 669-688 (1911).
13. W. A. McKinley and H. Feshbach, Phys. Rev. **74**, 1759 (1948);
14. V. N. Baier and V. M. Katkov, Dokl. Akad. Nauk Ser. Fiz. **227**, 325 (1976).
15. V. V. Bazanov, G. P. Pronko, L. D. Solovev and Yu. Ya. Yushin, Theor. Math. Fiz. **33**, 982 (1978) [Teor. Mat. Fiz. **33**, 218 (1977)]; V. V. Bazanov, G. P. Pronko, L. D. Solovev, Theor. Math. Fiz. **39**, 285 (1979) [Teor. Math. Fiz. **39**, 3 (1979)]
16. B. Z. Kopeliovich, A. V. Tarasov and O. O. Voskresenskaya, Eur. Phys. J. A **11**, 345 (2001).
17. E. A. Kuraev, M. Shatnev, E. Tomasi-Gustafsson, Phys. Rev. **C80**, 018201 (2009).
18. N. F. Mott: Proc. R. Soc. London, Ser. A **124**, (1929) 425.
19. A. I. Akhiezer, L. N. Rosenteig and I. M. Shmushkevich, Zh. Eksp. Teor. Fiz. **33**, 765 (1957) [Sov. Phys. JETP, **6**, 588 (1958)].
20. J. Scofield, Phys. Rev. **113**, 1599 (1959).

21. A.J.R. Puckett, *et al.*, the GEp collaboration, Phys. Rev. Lett. **104**, 242301 (2010).
22. A. Zichichi, S. M. Berman, N. Cabibbo, and R. Gatto, Nuovo Cim. **24**, 170 (1962).
23. A. Antonelli *et al.*, Nucl. Phys. B **517**, 3 (1998).
24. T. A. Armstrong *et al.* [Fermilab E760 Collaboration], Phys. Rev. D **56**, 2509 (1997).
25. M. Ablikim *et al.* [BES Collaboration], Phys. Lett. B **630**, (2005) 14.
26. R. Blankenbecker and J. Gunion, Phys. Rev. D **4**, 718 (1971).
27. J. Gunion and L. Stodolsky, Phys. Rev. Lett. **30**, 345 (1973);
28. V. Franco, Phys. Rev. D **8**, 826 (1973);
29. V. N. Boitsov, L.A. Kondratyuk and V.B. Kopeliovich, Sov. J. Nucl. Phys **16**, 287 (1973);
30. F. M. Lev, Sov. J. Nucl. Phys. **21**, 45 (1973);
31. M. P. Rekalo, E. Tomasi-Gustafsson and D. Prout, Phys. Rev. C **60**, 042202 (1999).
32. M. P. Rekalo and E. Tomasi-Gustafsson, Eur. Phys. J. A. **22**, 331 (2004); Nucl. Phys. A **740**, 271 (2004); Nucl. Phys. A **742**, 322 (2004).
33. G. I. Gakh and E. Tomasi-Gustafsson, Nucl. Phys. A **761**, 120 (2005). Nucl. Phys. A **771** (2006) 169;
34. P. A. M. Guichon and M. Vanderhaeghen, Phys. Rev. Lett. **91** (2003) 142303; A. V. Afanasev, S. J. Brodsky, C. E. Carlson, Y. C. Chen and M. Vanderhaeghen, Phys. Rev. D **72**, 013008 (2005); P. G. Blunden, W. Melnitchouk and J. A. Tjon, Phys. Rev. C **72**, 034612 (2005); D. Borisyuk and A. Kobushkin, Phys. Rev. C **74**, 065203 (2006).
35. J. S. Schwinger, Phys. Rev. **76**, 790(1949).
36. L. W. Mo and Y. S. Tsai, Rev. Mod. Phys. **41**, 205 (1969).
37. E. A. Kuraev and V. S. Fadin, Sov. J. Nucl. Phys. **41**, 466 (1985) [Yad. Fiz. **41**, 733 (1985)].
38. L. C. Maximon and J. A. Tjon, Phys. Rev. C **62**, 054320 (2000).
39. A. V. Afanasev, I. Akushevich, A. Ilyichev and N. P. Merenkov, Phys. Lett. B **514**, 269 (2001); 57].
40. L. C. Maximon, W. C. Parke, Phys. Rev. **C61**, 045502 (2000).
41. Yu. M. Bystritskiy, E. A. Kuraev and E. Tomasi-Gustafsson, Phys. Rev. C **75**, 015207 (2007).
42. M. P. Rekalo, E. Tomasi-Gustafsson, [nucl-th/0202025].
43. R. G. Sachs Phys. Rev. **126**, 2256 (1962).
44. R.G. Arnold, C. E. Carlson and F. Gross, Phys. Rev. **C23**, 366 (1981).
45. H. Zhu *et al.* [E93026 Collaboration ], Phys. Rev. Lett. **87**, 081801 (2001).
46. B. Plaster *et al.* [ Jefferson Laboratory E93-038 Collaboration ], Phys. Rev. **C73**, 025205 (2006).
47. G.V. DiGiorgio *et al.*, Il Nuovo Cimento **39**, 474 (1965);
J. C. Bizot, J. M. Buon, J. LeFrançois, J. Perez-y-Jorba, and P. Roy, Phys. Rev. **140**, B1387 (1965);
D. E. Lundquist, R. L. Anderson, J. V. Allaby, and D. M. Ritson, Phys. Rev. **168**, 1527 (1968);
R. Prepost, R. M. Simonds and B. H. Wiik, Phys. Rev. Lett. **21**, 1271 (1968).
48. S. P. Wells *et al.* [SAMPLE collaboration], Phys. Rev. C **63**, 064001 (2001).
49. F. E. Maas, K. Aulenbacher, S. Baunack, L. Capozza, J. Diefenbach, B. Glaser, Y. Imai, T. Hammel *et al.*, Phys. Rev. Lett. **94**, 082001 (2005).
50. E. C. Titchmarsh, *Theory of functions*, Oxford University Press, London, 1939.
51. M. P. Rekalo and E. Tomasi-Gustafsson, Phys. Lett. **504** (2001) 291.
52. E. Tomasi-Gustafsson, Phys. Part. Nucl. Lett. **4**, 281-288 (2007).
53. E. A. Kuraev, N. P. Merenkov and V. S. Fadin, Sov. J. Nucl. Phys. **47**, 1009 (1988) [Yad. Fiz. **47**, 1593 (1988)].
54. E. Tomasi-Gustafsson, G. I. Gakh, A. P. Rekalo, M. P. Rekalo, Phys. Rev. **C 70**, 025202 (2004).
55. E. Tomasi-Gustafsson, M.O. Osipenko, E.A. Kuraev, Yu. Bystritsky, V.V. Bytev, arXiv:0909.4736 [hep-ph] and references therein.
56. G. I. Gakh and E. Tomasi–Gustafsson, Nuclear Physics . **A 838**, 50 (2010).
57. E. Tomasi-Gustafsson, G. I. Gakh, Phys. Rev. **C72**, 015209 (2005).
58. E. Tomasi-Gustafsson, E. A. Kuraev, S. Bakmaev and S. Pacetti, Phys. Lett. B **659**, 197 (2008).
59. M. L. Goldberger, Y. Nambu and R. Oehme, Annals of Physics **2**, 226 (1957).
60. C. Adamuscin, G. I. Gakh, E. Tomasi-Gustafsson, [arXiv:0704.3375 [hep-ph]].
61. F. Rathmann, P. Lenisa, E. Steffens, M. Contalbrigo, P. F. Dalpiaz, A. Kacharava, A. Lehrach, B. Lorentz *et al.*, Phys. Rev. Lett. **94**, 014801 (2005).

# AUTHOR INDEX